LARS Information Note 072473

EMISSION AND REFLECTION FROM HEALTHY AND STRESSED NATURAL TARGETS WITH COMPUTER ANALYSIS OF SPECTRORADIOMETRIC AND MULTISPECTRAL SCANNER DATA*

Ravindra Kumar
LeRoy F. Silva
TR-EE 73-37
December, 1973

Published by the
Laboratory for Applications of Remote Sensing (LARS)
and the
School of Electrical Engineering
Purdue University
W. Lafayette, Indiana 47907

*This work was supported by the National Aeronautics and Space Administration under Grant No. NGL 15-005-112.

PRECEDING PAGE BLANK NOT FILMED

TABLE OF CONTENTS

Page

LIST OF TABLES

LIST OF FIGURES

LIST OF SYMBOLS

Symbol	Meaning	First Referred In
A	Area of the surface	eq. (2.2.2)
A_d	Projected area of the detector receiving radiation, normal to the direction of the sensor	eq. (4.2.1)
$A_{\ell S}$	Total projected area of the visible (from the sensor) sunlit leaves normal to the direction of the sensor	eq. (4.2.2)
$A_{\ell s}$	Total projected area of the visible (from the sensor) shaded leaves normal to the direction of the sensor	eq. (4.2.2)
A_s	Area of the spherical surface	eq. (2.2.2)
a	Dummy variable	eq. (2.2.3)
c	a. $-K_1(\lambda)K_2(\lambda)L_{\lambda, b\ ref}(\lambda,T_r)$ = constant	eq. (5.2.3)
	b. velocity of light	eq. (5.2.4)
$D(i,j/C_1,C_2 \ldots C_n)$	Divergence between blight class i and blight class j in n spectral channels - $C_1,C_2 \ldots C_n$	eq. (6.3.1)
D_T	Transformed divergence	eq. (6.3.2)
$D_T^n\ (i_k,j_\ell/C_1,C_2 \ldots C_n)$	Transformed divergence between k^{th} spectral class of blight level i and ℓ^{th} spectral class of blight level j in n spectral channels - $C_1,C_2 \ldots C_n$	eq. (6.3.3)
D_{TAVG}^n	Average transformed divergence in n spectral channels	Sec. 6.3
D_{TMAVG}^n	Denotes maximum of D_{TAVG}^n, maximized over a set of n spectral channels	eq. (6.3.3)

Symbol	Meaning	First Referred In
$\{D^n_{TMAVG}\}$	Denotes a vector whose p^{th} component represents D^n_{TMAG} in p^{th} flightline	Page 179
D^n_{TAVGij}	Average transformed divergence between spectral class pairs of blight level i and blight level j in n spectral channels $-C_1, C_2 \ldots C_n$	eq. (6.3.4)
$D^n_{TMAVGij}$	Maximum of D^n_{TAVGij}, maximized over a set of n spectral channels	Page 183
d	Distance of sun from the earth .	eq. (2.5.5)
E	Transpiration rate - energy gained or lost by transpiration or evaporation in mass area^{-1} time^{-1}	eq. (2.3.7)
E_S	Solar radiation reflected from the surroundings, incident on on the leaf	eq. (2.3.5)
E_s	Sky radiation reflected by the surroundings, incident on the leaf	eq. (2.3.5)
E_λ	Spectral irradiance	Page 11
$E_{\lambda,S}$	Spectral solar irradiance . . .	eq. (2.5.3)
F	Radiant flux density	eq. (2.2.5)
F_d	$F_o/f(T)$	eq. (2.6.5)
F_ℓ	Radiant flux density emitted by the leaf reaching the sensor	eq. (4.2.1)
F_o	Total apparent outward radiant flux density	eq. (2.6.3)
F_S	Environment integrated radiant flux density	eq. (2.6.3)
F^*_S	$\frac{f(T_S)}{f(T)} F_S$	eq. (2.6.7)
F_λ	Spectral radiant flux density . .	eq. (2.2.5)

Symbol	Meaning	First Referred In
$F_{\lambda,b}(T)$	Blackbody radiant flux density at temperature T and wavelength λ	eq. (2.6.4)
f	Fraction of the sunlit soil surface	eq. (2.3.8)
f(T)	Defined by eq. (2.6.4)	eq. (2.6.4)
$f(\lambda)$	Filter characteristics for the infrared radiometer	eq. (2.6.4)
$f[\epsilon(\lambda_k)]$	Known function of spectral emittance at wavelength λ_k	eq. (5.5.7)
h	a. enthalpy of a gas or liquid per unit mass	eq. (2.3.1)
	b. Planck's constant	eq. (5.2.4)
h_c	Convection coefficient of the leaf	eq. (2.4.1)
$I_{\parallel}$	Incident intensity of the ray parallel to the plane of incidence	eq. (3.3.2)
$I_{\perp}$	Incident intensity perpendicular to the plane of incidence	eq. (3.3.3)
i	Refers to integers 1,2,...N	Sec. 5.5
j	An integer lying between 1 and N	Sec. 5.5
K	$\frac{\sigma A_d}{r^2}$ = constant	eq. (4.2.2)
$K_1(\lambda)$	Instrument transfer function	eq. (5.2.1)
$K_2(\lambda)$	Constant for the reference blackbody	eq. (5.2.1)
k	a. Boltzmann constant	eq. (5.2.4)
	b. an integer lying between 1 and N	Sec. 5.5
k_{gS}	Absorptance of the soil to direct solar radiation	eq. (2.3.8)
k_{gs}	Absorptance of the soil to the sky radiation	eq. (2.3.8)
k_{gL}	Absorptance of the soil to the longwave thermal radiation (i.e., $\lambda>4\mu m$)	eq. (2.3.11)

Symbol	Meaning	First Referred In
k_ℓ	Absorptance of the leaf canopy to solar and sky radiation . . .	Page 20
$k_{\ell S}$	Absorptance of the leaf canopy to the direct solar radiation . . .	eq. (2.3.9)
$k_{\ell s}$	Absorptance of the leaf canopy to the sky radiation	eq. (2.3.9)
$k_{\ell t}$	Absorptance of the leaf canopy to longwave thermal radiation (i.e., $\lambda>4\mu m$)	eq. (2.3.10)
k_S	Absorptance to direct solar radiation	eq. (2.3.5)
k_s	Absorptance to scattered skylight	eq. (2.3.5)
k_t	Absorptance to longwave thermal radiation	eq. (2.3.5)
L	Latent heat of vaporization of water at the leaf temperature	eq. (2.3.7)
L_λ	Spectral radiance at a point P in the direction $\vec{s}$	eq. (2.2.4)
$L_{\lambda,b}(\lambda,T)$	Blackbody spectral radiance at temperature, T, and wavelength λ	eq. (2.2.7)
$L_{\lambda,b\ ref}(\lambda,T_r)$	Reference blackbody spectral radiance at temperature, T_r, and wavelength λ	eq. (5.2.1)
L_{λ_i}	Spectral radiance of radiation coming from the target at wavelength λ_i	eq. (5.5.2)
$L_{\lambda_i,b}(T_s(\lambda_i))$	Blackbody spectral radiance at wavelength λ_i and temperature $T_s(\lambda_i)$	eq. (5.5.4)
$L_{\lambda,i}(\vec{s}')$	Spectral radiance of incident radiation in the direction $\vec{s}'$	eq. (2.5.1)
$L_{\lambda,r}$	Spectral radiance of reflected radiation	eq. (2.5.8)

Symbol	Meaning	First Referred In
$L_{\lambda,r}(\vec{s}'\rightarrow\vec{s})$	Spectral radiance of reflected radiation from direction $\vec{s}'$ to direction $\vec{s}$	eq. (2.5.6)
m	$=K_1(\lambda)$=slope of the straight line	eq. (5.2.3)
m_1	a. Index of refraction of the first medium	eq. (3.3.1)
	b. Upper bound on the $\min \varepsilon(\lambda_i)$	eq. (5.5.9)
m_2	a. Refractive index of the second medium	eq. (3.3.1)
	b. Upper bound on the max. $\varepsilon(\lambda_i)$	eq. (5.5.9)
N	Total no. of spectral class pairs whose weights $W_{i_k j_\ell}$ were taken =1	eq. (6.3.3)
$\vec{n}$	Outward normal to the surface	Figure 2.2.2
n_i	No. of spectral classes in blight level i	eq. (6.3.3)
n_j	No. of spectral classes in blight level j	eq. (6.3.3)
Q_{CHEM}	Net heat added to the leaf per unit time by chemical processes taking place in the plant (excluding transpiration)	eq. (2.3.1)
Q_{COND}	Net heat added to the leaf per unit time by conduction	eq. (2.3.1)
Q_{CONV}	Net heat added to the leaf per unit time by convection	eq. (2.3.1)
$Q_{g\ abs}$	Net radiant energy absorbed by the sunlit soil surface	eq. (2.3.8)
$Q_{\overline{s}\ abs}$	Net radiant energy absorbed by the shaded soil surface	eq. (2.3.11)

Symbol	Meaning	First Referred In
Q_{TRAD}	Net heat radiated to the leaf per unit time	eq. (2.3.1)
Q_{TRANS}	Net heat added to the leaf per unit time by transpiration	eq. (2.3.2)
Q_{λ}	radiant energy in the wavelength interval λ and $\lambda+d\lambda$	eq. (2.2.4)
R	Total reflection	eq. (3.3.4)
R_a	Thermal radiation from the atmosphere as an extended source	eq. (2.3.5)
R_g	Thermal radiation from the ground as an extended source	eq. (2.3.5)
R_S	a. Radiant flux density emitted by the sunlit soil	eq. (2.3.8)
	b. Radius of the sun	eq. (2.5.5)
R_s	Longwave radiation emitted by the shaded soil surface	Page 20
$R_{\parallel}$	Reflection parallel to the plane of incidence	eq. (3.3.2)
$R_{\perp}$	Reflection perpendicular to the plane of incidence . . .	eq. (3.3.3)
r	a. Distance of the differential element of the surface from point P	eq. (2.2.2)
	b. Distance of the differential element of the leaf, da_{ℓ}, from the sensor	eq. (4.2.1)

Symbol	Meaning	First Referred In
r_{gS}	Reflectance of the sunlit soil to the incident direct sunlight	eq. (2.3.9)
r_{ℓ}	Reflectance of the leaf canopy to the solar and sky radiation	Page 20
$r(\lambda,\vec{s}'\rightarrow\vec{s})$	Reflection distribution function for the direction $\vec{s}'$ to $\vec{s}$ . . .	eq. (2.5.6)
S	a. Direct solar radiant flux density . . .	eq. (2.3.5)
	b. Output signal from the spectroradiometer	eq. (5.2.1)
s	Radiant flux density of scattered skylight	eq. (2.3.5)
$\vec{s}'$	denotes the direction of the incident radiation	eq. (2.5.1)
T	a. Temperature of the target	eq. (2.6.3)
	b. Total transmission	eq. (3.3.7)
T_1	Max $T_s(\lambda_i)$	eq. (5.5.10)
T_A	Temperature of the air	Page 149
T_{AVG}	Average temperature of a target	eq. (2.2.3)
T_B	Temperature of the blighted spot of the leaf	Page 149
T_H	Temperature of the healthy spot of the leaf	Page 149
$T_{h.l.b.}$	High lower bound of T	eq. (5.5.12)
T_{ℓ}	Leaf temperature in absolute scale	eq. (2.3.6)

Symbol	Meaning	First Referred In
$T_s(\lambda)_{AVG}$	Average spectral radiance temperature . . .	Page 144
$T_{\parallel}$	Transmission parallel to the plane of incidence .	eq. (3.3.5)
$T_{\perp}$	Transmission perpendicular to the plane of incidence	eq. (3.3.6)
t_{ℓ}	Transmittance of the leaf canopy to the solar and sky radiation . .	Page 20
$t_{\ell S}$	Transmittance of the leaf canopy to direct solar radiation	eq. (2.3.11)
$t_{\ell s}$	Transmittance of the leaf canopy to the sky radiation	eq. (2.3.11)
T	Temperature of the blackbody	eq. (5.2.1)
T_r	Temperature of the reference blackbody . . .	eq. (5.2.1)
T_s	Full radiator temperature	Page 9
T_s (8-14 μm)	Radiance temperature in the wavelength range 8 to 14 μm	eq. (5.7.2)
$T_s(\lambda)$	Spectral radiance temperature	Page 9
$T_s(\lambda_1-\lambda_2)$	Band radiance temperature	Page 9
$T_s(\lambda_i)$	Spectral radiance temperature at wavelength λ_i	eq. (5.5.2)
T'	Constant	eq. (5.5.8)
t	Denotes the time	eq. (2.2.4)
$W_{i_k j_\ell}$	Weight between k^{th} spectral class of blight level i and ℓ^{th} spectral class of blight level j	eq. (6.3.3)

Symbol	Meaning	First Referred In
w	Mass flow per unit time . .	eq. (2.3.1)
w(a)	Weight taken at area a . .	eq. (2.2.3)
y	=S	eq. (5.2.3)

GREEK SYMBOLS

Symbol	Meaning	First Referred In
$\alpha(\vec{s})$	Total directional absorptance in the direction $\vec{s}$	eq. (2.2.8)
$\alpha(\lambda)$	Spectral hemispherical absorptance	Page 13
$\alpha(\lambda,\vec{s})$	Spectral directional absorptance in the direction $\vec{s}$	eq. (2.2.8)
ΔT	Difference between leaf temperature and air temperature	eq. (2.4.1)
δF_d	Error in the measurement of F_d	eq. (2.6.9)
$\delta L_{\lambda,b}$	Error in the blackbody spectral radiance due to the stray radiation when the spectroradiometer is looking at the target blackbody	eq. (5.2.1)
$\delta L_{\lambda,b\ ref}$	Error in reference blackbody spectral radiance due to stray radiation when the spectroradiometer is looking at the reference blackbody	eq. (5.2.1)
δT	Error in the measurement of temperature	eq. (2.6.9)
$\delta\varepsilon$	Error in the determination of emittance	eq. (2.6.9)
ε	Total hemispherical emittance	eq. (2.6.1)

GREEK SYMBOLS (Continued)

Symbol	Meaning	First Referred In
$\varepsilon(\ell)$	Emittance of the leaf . . .	eq. (4.2.1)
$\varepsilon(\vec{s})$	Total directional emittance in the direction $\vec{s}$	Sec. 2.2
ε_{gt}	Emittance of the soil to longwave thermal radiation (i.e., $\lambda>4\mu m$) . .	Page 20
$\varepsilon_{\ell t}$	Emittance of the leaf canopy to longwave thermal radiation (i.e., $\lambda>\mu m$)	eq. (2.3.10)
ε_t	Emittance of the leaf to longwave thermal radiation (i.e., $\lambda>4\mu m$) . .	eq. (2.3.6)
$\varepsilon(\lambda)$	Spectral emittance at wavelength λ	Page 13
$\varepsilon(\lambda,\vec{s})$	Spectral directional emittance in direction $\vec{s}$	eq. (2.2.7)
$\varepsilon(\lambda_i)$	Spectral emittance of the target at wavelength λ_i	eq. (5.5.1)
$\varepsilon(\lambda_i)_{l.u.b.}$	Low upper bound on the spectral emittance $\varepsilon(\lambda_i)$	eq. (5.5.13)
$\varepsilon(8\text{-}14\mu m)$	Emittance in the wavelength region 8 to 14μm . .	eq. (5.7.2)
θ	Angle of normal n to the surface with the direction $\vec{s}$	eq. (2.2.4)
θ_i	Angle of incidence	eq. (3.3.1)
θ_r	Angle of refraction . . .	eq. (3.3.1)
θ_S	Angle subtended by the sun with the z axis . .	eq. (2.5.4)

GREEK SYMBOLS (continued)

Symbol	Meaning	First Referred In
λ	Refers to the wavelength of radiation	Sec. 2.2
λ_p	Predicted value of the wavelength by a straight line least square fit . . .	eq. (5.2.6)
μm	Denotes micrometers	Chapter I
$\rho(\lambda)$	Spectral hemispherical reflectance	Page 11
$\rho(\lambda,\vec{s})$	Spectral hemispherical directional reflectance in direction $\vec{s}$	Page 11
$\rho(\lambda,\vec{s}'\text{-}\vec{s})$	Spectral bidirectional reflection from direction $\vec{s}'$ to direction $\vec{s}$	eq. (2.5.7)
σ	Stefan-Boltzmann Constant	eq. (2.3.6)
$\tau_a(\lambda,\vec{s}')$	Spectral transmission characteristics of the atmosphere in the direction $\vec{s}'$	eq. (2.5.2)
ϕ	Azimuthal angle	Figure 2.2.1
Ω	Solid angle	eq. (2.2.1)
Ω_S	Solid angle subtended by the leaves, visible from the sunlit soil, at the sunlit soil	Page 20
Ω_s	Solid angle subtended by the leaves, visible from the shaded soil, at the shaded soil	Page 20
Ω'	Solid angle subtended by the sun at the earth's surface	eq. (2.5.3)

SUBSCRIPTS

Symbol	Meaning	First Referred In
λ	Refers to the wavelength . .	Sec. 2.2
g	Denotes the ground or soil	eq. (2.3.5)
a	Denotes the atmosphere . .	eq. (2.3.5)
ℓ	a. Denotes the leaf . . .	eq. (2.3.6)
	b. Denotes the leaf canopy	Sec. 2.3
t	Denotes thermal radiation (i.e., $\lambda>4\mu m$)	eq. (2.3.5)
s	Denotes the scattered skylight	eq. (2.3.5)
S	Denotes the direct sunlight	eq. (2.3.5)
*	Denotes the quantities for the stem corresponding to the quantities for the leaves with subscript ℓ . .	eq. (4.2.3)
g	Denotes the quantities for the soil corresponding to the quantities for the leaves with subscript ℓ . .	eq. (4.2.4)

SUPERSCRIPTS

Symbol	Meaning	First Referred In
n	Denotes the number of spectral channels	eq. (6.3.3)
*	Denotes the quantities for the stem corresponding to the quantities for the leaves with subscript ℓ . .	eq. (4.2.3)
'	Denotes the quantities for the incident radiation . .	Page 29

ABSTRACT

The purpose of this research is to study the emission and reflection from healthy and stressed (systemic-stress and non-systemic stress) natural targets, with special emphasis on corn plants, and to differentiate the healthy targets from stressed ones by remote sensing.

Infrared radiometry of plants is reviewed thoroughly with emphasis on agricultural crops. Theory and error analysis of the determination of emittance of a natural target by radiometer is discussed.

A light ray, incident at about 5° to the normal, is geometrically plotted through the drawing of the cross section of a soybean (Glycine max (L.) Merrill) leaf using Fresnel's Equations and Snell's Law. The optical mediums considered are: air, cell sap, chloroplast and cell wall. The values of the reflection and transmission found from ray tracing agree closely with the experimental results. Ray tracing, considering cell wall and air as the only optical mediums gives reflection considerably lower than the experimental results. A light ray, incident at about 60° to the normal, is also drawn through the palisade cells for illustrative purposes.

Thermal emission model of a plant canopy is proposed. Exotech Model 20C Spectroradiometer is described briefly. Wavelength calibration and the the spectral radiance calibration of the long wavelength spectroradiometer (wavelength ranges 2.8 to 5.6 μm and 7 to 14 μm)is done. Calibration of the Precision Thermistor Thermometer Probes and PRT-5 is described. Ground truth variables useful for experiments with long wavelength spectroradiometer are described. A spectroradiometric method for

determining the temperature and spectral emittance of a natural target is proposed and discussed.

Experiments were conducted on corn (Zea mays L.) plants with long wavelength spectroradiometer under field conditions. An α level of 0.05 was taken for statistical analysis. Average spectral radiance temperatures ($T_s(\lambda)_{AVG}$), average being taken over certain selected wavelength bands for the four healthy corn plant populations (15, 30, 60 and 90 thousand per hectare) were found to be statistically significantly different in 3.6 to 5.40 μm wavelength range. In corn blight experiment, $T_s(\lambda)_{AVG}$ of the corn plants increased with the increase of blight severity in 3.6 to 5.40 μm and 7.5 to 12.40 μm. The contact temperatures of the healthy spots and the blighted spots of corn leaves were not found to be statistically significantly different. A tentative conclusion is that the percentage of the soil, especially sunlit soil visible from the spectroradiometer, is the predominant factor causing differences between $T_s(\lambda)_{AVG}$ of the healthy and blighted corn plants. $T_s(\lambda)_{AVG}$ of the corn plants having different rates of nitrogen application (0 kg/hectare, 67 kg/hectare and 201 kg/hectare) were found to be statistically significantly different. Also, the difference between $T_s(\lambda)_{AVG}$ and the air temperature decreased with the increase of nitrogen dificiency.

Analysis of multispectral scanner data of ten selected flightlines of Corn Blight Watch Experiment of 1971 indicated:

1.) There was no regular pattern of the mean response of the higher level/levels blighted corn vs. lower level/levels blighted corn in any of the spectral channels.

2.) The greater the difference between the blight levels, the more statistically separable they usually were in subsets of one, two, three and four spectral channels.

CHAPTER I

INTRODUCTION

Remote multispectral sensing[62] may be defined as "the sensing, from a remote location, of electromagnetic radiation - either reflected or emitted - in many discrete, usually relatively narrow spectral bands between wavelengths of 0.3 μm and 15 μm and also in radar bands from about 0.86 to 3.0 centimeters."

The purpose of this research is to study the emission and reflection from healthy and stressed natural targets and to differentiate them (healthy and stressed ones) by remote sensing. A good part of the study is confined to corn plants for corn (Zea mays L.) is one of the major agricultural crops.

While doing the literature review of 'Infrared Radiometry of Plants', it was felt that the articles related to it were scattered in a number of different journals like Applied Optics, Agronomy Journal, American Journal of Botany, Plant Physiology, Bioscience, Science, American Scientist, Ecology, Journal of Applied Meteorology, Remote Sensing of Environment etc. Many biological scientists and a few physicists have contributed to the 'Infrared Radiometry of Plants'. Some of the statements in the literature are not true. For example, Monteith and Szeicz[70] (1962) estimate that assuming the emittance of the plant surfaces equal to one may cause errors of at most 0.2 C in the measurement of their temperature. The above statement is not consistent with the experiment. (Section 2.6). The need of review of 'Infrared Radiometry

of Plants' was felt and hence, an extensive literature review of the same is given in Chapter II.

Willstätter and Stoll[107] (W-S) in 1918 proposed a theory to explain reflectance from a leaf on the basis of critical reflection of visible light at spongy mesophyll cell wall - air interfaces. Their theory is commonly accepted even today. The pathway of light rays as envisioned by Willstätter and Stoll (Figure 3.3.3) shows that the light rays pass through the epidermis and palisade cells without any deviation, which is unrealistic. The author strongly felt the need for a better illustration to show the pathway of light through a leaf cross section than shown by Willstätter and Stoll and hence, reflectance model of a leaf is proposed in Chapter III.

In the analysis of multispectral scanner data of the Corn Blight Watch Experiment, almost all the analysts of the Laboratory for Applications of Remote Sensing (LARS) found thermal channel (9.30 to 11.70 μm) as one of the best four channels using feature selection algorithm. This created an interest among the staff members of LARS to find the reasons of thermal channel being as one of the best four channels. Prior to the summer of 1971, signal to noise ratio of the thermal channel of the multispectral scanner of Environmental Research Institute of Michigan (formerly called Willow Run Laboratory, University of Michigan) was relatively low and hence, the value of the thermal channel in differentiating various crop species was not known. Thus, it was decided to do field experiments with longwavelength (2.8 to 5.6 μm and 7 to 14 μm) spectroradiometer under field conditions. The spectral data under field conditions would help the proper interpretation of multispectral scanner data in the thermal channel. Three experiments were done with the longwavelength spectroradiometer: ground cover experiment, experiment on non-systemic stressed corn plants, and experiments on the systemic-stressed corn plants. The ground cover experiment was done to find the spectral response of the plants vs. percentage ground cover in the longwavelength thermal infrared wavelength region because percentage ground cover is likely to be an important factor causing differences between the healthy and non-systemic

stressed plants (Chapter VI). The experiments were done on the non-systemic stressed corn plants and systemic stressed corn plants because one of the major interests of LARS is to differentiate stressed plants from healthy ones by multispectral remote sensing. The expressions for the radiant flux density emitted by a plant canopy reaching the sensor (of aircraft or satellite or spectroradiometer) are given in Chapter IV to help explain the causes of spectral variability between the targets of interest in the longwavelength thermal infrared wavelength region.

The analysis of multispectral scanner data of selected flightlines of Corn Blight Watch Experiment of 1971 is done in Chapter VI to determine statistical separability of the spectral classes of blighted corn. The analysis presented has much practical application, for it gives the maximum average transformed divergence between the spectral class pairs of blight levels, from which hopefully in the near future, classification accuracy will be reasonably predicted.

CHAPTER II

INFRARED RADIOMETRY OF PLANTS

2.1 Introduction

A plant is exposed to electromagnetic radiation from surroundings such as soil, rocks, plants and so forth and from environment like sun, sky, clouds, atmosphere, etc. It is important to understand the interaction of a plant with its environment in order to properly and meaningfully interpret the data of plants secured by remote sensing. The radiation radiometer is a good and commonly used instrument for measuring the radiant temperature of plants. Infrared radiometry is quite useful in many fields.* .

It should be pointed out that thermocouples and thermistors attached to leaves for the purpose of measuring surface temperatures have certain disadvantages[19] . Their material usually has different spectral emittance than the leaf and thus experiences a different radiant energy regime. In addition, they have different heat dissipation mechanisms than the leaf material - having wire leads to carry heat but no evaporating surface. The extent to which these factors influence the temperature measured by these sensors must be considered in addition to other factors when judging the effectiveness of radiometrically determined temperatures.

---

* Infrared radiometry is quite useful in many fields like ecology, botany, zoology, forestry, agriculture, agronomy, hydrology, meteorology, climatology, atmospheric sciences, medical diagnosis, engineering, geology, etc.

The main purpose of this chapter is to review infrared radiometry of plants with emphasis on agricultural crops. This review is not completely exhaustive since the space is limited. For the same radiometric quantities, a number of different names and different symbols have been used in the literature which creates confusion for the readers. The author sought to use the nomenclature recommended by the International Commission on Illumination[50] throughout this thesis. As many references as possible are included, especially the recent ones.

2.2 Definitions

Definitions of the terms which will be commonly referred to in this thesis are given below for the convenience of the readers.

Spherical Co-ordinate System:

Spherical co-ordinate system is shown in Figure 2.2.1.

Direction Cosines:

Direction cosines of a direction are the projections of the unit direction on the co-ordinate axes.

Solid Angle:

Solid angle subtended by a differential element of a spherical surface of area dAs at point P is given by

$$d\Omega = \frac{dAs}{r^2} = \sin\theta\, d\theta\, d\phi \qquad \text{(Figure 2.2.2)} \qquad (2.2.1)$$

The solid angle subtended by a finite area, A, at point P is given by integrating the solid angle subtended by each differential element of the area over the entire area, A, i.e.,

$$\Omega = \int_A d\Omega = \int_A \frac{dAs}{r^2} \qquad (2.2.2)$$

where

A = area of the surface

Thermodynamic Equilibrium:

A thermodynamic system is said to be in thermodynamic equilibrium if it is simultaneously in thermal, mechanical and chemical equilibrium. In thermodynamic equilibrium, the properties of the system do not change either in space or time. Time does not enter as a fundamental notion in the classical science of thermodynamics.

Blackbody:

A blackbody is one which absorbs all of the radiation incident on it. There is no substance, which is perfectly black in this sense, but some substances approach this ideal closely. At a given wavelength and temperature, the spectral radiance of emitted radiation of a blackbody is maximum. Blackbody has an absorptivity and emissivity equal to one.

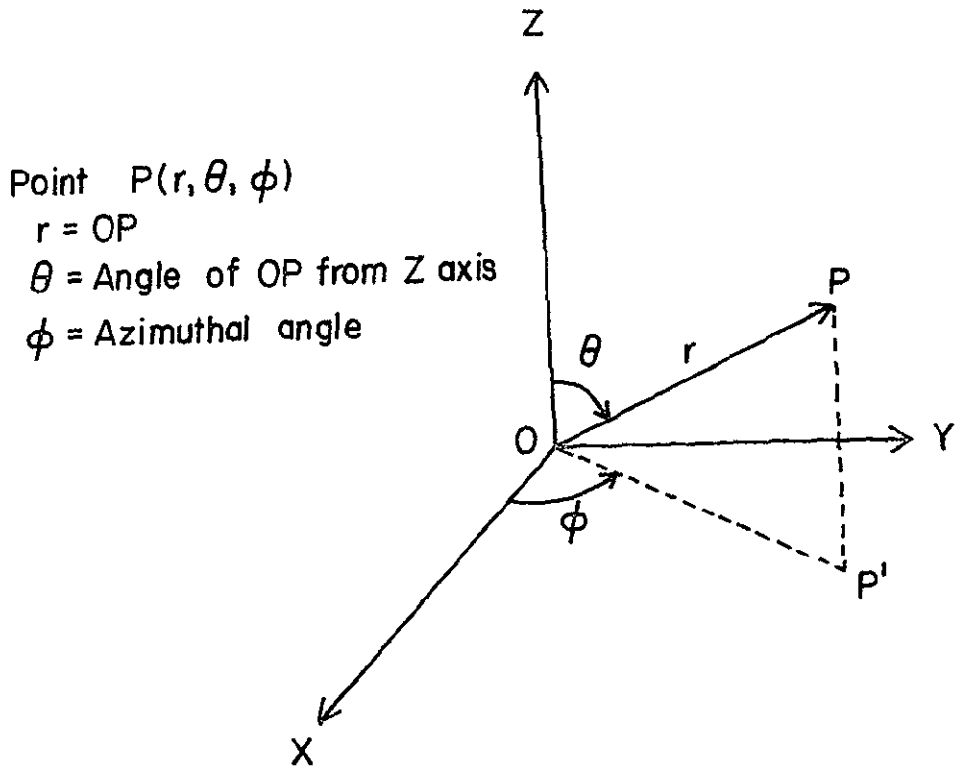

Figure 2.2.1 Spherical Co-ordinate System

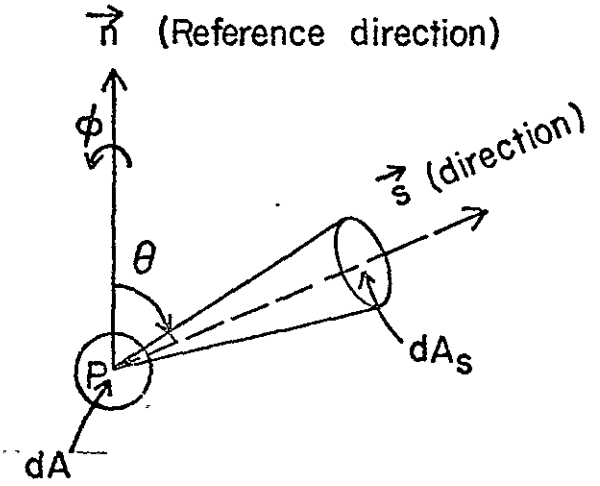

Figure 2.2.2 Definition of Solid Angle

Temperature T:

It is a measure of the average kinetic energy of the molecules. It is the quantity that would be measured by an ideal contact thermometer. It has also been called actual temperature, true temperature, real temperature, etc. in the literature.

Average Temperature T_{AVG}:

The temperature of a natural target is not uniform over the whole target, in general. So, a meaningful temperature, T_{AVG}, of a natural target can be defined as the weighted average of local temperature, T, of the target over its entire area, as follows.

$$T_{AVG} = \frac{{}_A\int w(a)T(a)da}{{}_A\int w(a)da} \qquad (2.2.3)$$

where

T(a) = temperature at area a

w(a) = weight taken at area a

A = total area of the target, ${}_A\int da$

If all the portions of the area of the target are given equal importance in determination of the temperature of the target, weight w(a) may be taken equal to one over the entire area.

Full Radiator Temperature T_s:

Full radiator temperature of a target is the temperature of a blackbody which emits the same amount of radiant energy as the target in entire range of wavelengths. It has also been called equivalent blackbody temperature, blackbody equivalent temperature, apparent temperature, radiant temperature, brightness temperature, etc.

Spectral Radiance Temperature $T_s(\lambda)$:

Spectral radiance temperature of a target at a specified wavelength, λ, is the temperature of a blackbody which emits the same amount of radiant energy as the target in the wavelength range λ to $\lambda+d\lambda$.

Band Radiance Temperature $T_s\ (\lambda_1 - \lambda_2)$:

Band radiance temperature of a target in wavelength range λ_1 to λ_2 is the temperature of a blackbody which emits the same amount of radiant energy as the target in the wavelength range λ_1 to λ_2.

Kirchhoff's Laws:

It was proved by Kirchhoff[87] that the cavity and the radiation inside it constitute a thermodynamic system which is independent of the particular physical processes of emission and absorption taking place in the walls. When the system is in thermodynamic equilibrium with its surroundings, then the spectral absorptivity $\alpha(\lambda)$ = spectral emissivity $\varepsilon(\lambda)$. This relation is also true on the directional as well as on the total basis.

Total Radiation Properties:

The designation 'total' is employed to describe radiation quantities that pertain to the entire range of wavelengths. When it is obvious that a radiation quantity pertains to the entire range of wavelengths, the designation 'total' may be omitted.

Spectral Radiation Properties:

The designation spectral is employed to describe radiation quantities for monochromatic radiation. When it is obvious that a radiation quantity pertains to the monochromatic radiation, the designation 'spectral' may be omitted.

In this Section, only spectral radiation quantities are defined. Total radiation quantities can be defined similar to the spectral radiation quantities as that pertaining to the entire range of wavelengths.

Spectral Radiance:

The fundamental quantity that governs the radiation field is the spectral radiance. It is defined as follows.

Let dQ_λ be the amount of radiant energy in the wavelength interval λ and $\lambda+d\lambda$ transported across an arbitrary oriented imaginary element of area dA at a point P (Figure 2.2.2) during a time interval dt and confined to an element of soild angle $d\Omega$ about the direction $\vec{s}$. The apex of the elementary cone is on the surface dA and the outward normal $\vec{n}$ to the surface makes an angle θ with the direction $\vec{s}$. Experiment shows that the ratio $dQ_\lambda/\cos\theta dA d\Omega d\lambda dt$ tends to a definite limit as dA, $d\Omega$, $d\lambda$, $dt \to 0$ in any manner provided that the point P and the direction $\vec{s}$ are kept fixed[99]. We denote this limit by L_λ and call it spectral radiance at point P in direction $\vec{s}$:

$$L_\lambda \equiv \lim_{dA,\, d\Omega,\, d\lambda,\, dt \to 0} \frac{dQ_\lambda}{\cos\theta\, dA\, d\Omega\, d\lambda\, dt} \tag{2.2.4}$$

Spectral Radiant Flux (surface) Density (at a point of a surface) F_λ:

Spectral radiant flux density is the amount of radiant energy in the wavelength interval λ and $\lambda+d\lambda$ transported across an arbitrary oriented imaginary element of area dA at a point P (Figure 2.2.2) during a time interval dt and confined to an element of soild angle $d\Omega$ about the direction $\vec{s}$.

$$F_\lambda = \frac{dQ_\lambda}{\cos\theta\, dA\, d\lambda\, dt} = L_\lambda d\Omega \tag{2.2.5}$$

$$\text{Radiant Flux Density } F = \int_0^\infty F_\lambda d\lambda = d\Omega \int_0^\infty L_\lambda d\lambda \tag{2.2.6}$$

Spectral Irradiance (at a point of a surface) E_λ:

It is the same as spectral radiant flux density except that it refers to the incident radiant energy.

Spectral Hemispherical Reflectance $\rho(\lambda)$:

Spectral hemispherical reflectance is defined as the ratio of radiant energy, in the wavelength interval λ and $\lambda+d\lambda$, reflected hemispherically by the surface to the radiant energy in the hemispherically incident beam.

Spectral Hemispherical Directional Reflectance $\rho(\lambda,\vec{s})$:

Spectral hemispherical directional reflectance in the direction $\vec{s}$ is defined as the ratio of radiant energy, in the wavelength interval λ and $\lambda+d\lambda$, reflected by the surface into direction $(\vec{s}, d\Omega)$ to the radiant energy in the hemispherically incident beam (Figure 2.2.3).

Directional Hemispherical Reflectance:

See Section 2.5(C), Equation (2.5.9).

Bidirectional Reflectance:

See Section 2.5(C), Equation (2.5.7).

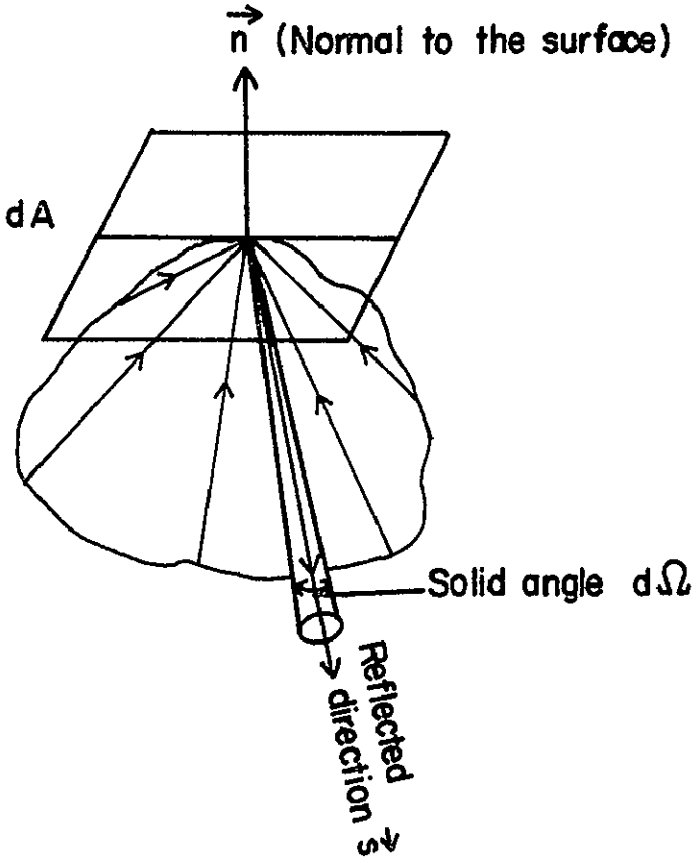

Figure 2.2.3 Definition of Hemispherical Directional Reflectance

Spectral Directional Emittance $\varepsilon(\lambda, \vec{s})$:

The spectral directional emittance $\varepsilon(\lambda, \vec{s})$ is the ratio of the emitted spectral radiance of the object in direction $\vec{s}$ to the emitted spectral radiance of the blackbody at the same temperature.

$$\varepsilon(\lambda, \vec{s}) = \frac{L_\lambda(T, \vec{s})}{L_{\lambda,b}(\lambda,T)} \tag{2.2.7}$$

where

$L_\lambda(T,\vec{s})$ = spectral emitted radiance of the object at wavelength λ and temperature T in direction $\vec{s}$

$L_{\lambda,b}(\lambda,T)$ = spectral radiance of the blackbody at wavelength λ and temperature T

Spectral Directional Absorptance $\alpha(\lambda, \vec{s})$:

Spectral absorptance in the direction $\vec{s}$ is the fraction of the radiant energy in the wavelength interval λ and $\lambda+d\lambda$, incident on the surface from direction $\vec{s}$ that is absorbed. In accordance with Kirchhoff's Law, the directional spectral absorptance and directional spectral emittance are equal provided that the incident beam is uniformly polarized -- that is,

$$\alpha(\lambda, \vec{s}) = \varepsilon(\lambda, \vec{s}) \tag{2.2.8}$$

The total directional absorptance, $\alpha(\vec{s})$, can be deduced from the total directional emittance $\varepsilon(\vec{s})$ in a simple manner for some of the cases enumerated in reference [87]

Spectral Hemispherical Absorptance $\alpha(\lambda)$:

The spectral hemispherical absorptance, $\alpha(\lambda)$, is the fraction of the hemispherically incident radiant energy in the wavelength interval λ and $\lambda+d\lambda$, that is absorbed by the surface.

Spectral Hemispherical Emittance $\varepsilon(\lambda)$:

Spectral hemispherical emittance, $\varepsilon(\lambda)$, of an object at temperature T is the ratio of the hemispherically emitted radiant energy by the object in the wavelength interval λ and $\lambda+d\lambda$ to the radiant energy emitted by

the blackbody at the same temperature and wavelength interval. The word 'emissivity' has also been used in the literature in place of 'emittance'. Actually, emissivity refers to the property of an ideal surface (i.e., free of dust, surface impurities, etc.), whereas emittance refers to the property of a real surface. The words 'emissivity' and 'emittance' have been used interchangeably in the literature.

2.3 Energy Balance

(A) Energy Balance on a Plant Leaf

The energy balance on a plant leaf is considered since a leaf constitutes a dominant energy exchange part of the plant. Conservation of energy exists on the leaf because it cannot store up energy indefinitely as it will get too hot, nor can it lose energy indefinitely for it will become too cold. However, a leaf may warm or cool, usually within a few seconds or, at most, a few minutes in the transient state. Aston et al.[5] (1969), from an experimental study of the energy balance of a dry artificial leaf under controlled radiative and convective heat loads, indicated the need for study of transient coupled exchange phenomenon; but this study shall be confined to the steady state only. A good part of this Section is reproduced from Cook[21] (1963) and Gates[34] (1964).

The equation of the energy balance on a leaflet, given by Cook[21] (1963) is partly reproduced here. Figure 2.3.1 shows the leaflet activity which must be taken into account, neglecting movement of the leaflet. Thus, taking an energy balance on the leaflet, the following equation results[21].

$$Q_{TRAD} + Q_{COND} + Q_{CONV} + Q_{CHEM} = (hw)\ O_2 \text{ gas} + (hw)\ H_2O \text{ gas} + (hw)\ CO_2 \text{ gas} + (hw) \text{ liquid out} - (hw) \text{ liquid in} - (hw)\ CO_2 \text{ in} - (hw)\ O_2 \text{ in} \qquad (2.3.1)$$

where

h = enthalpy of a gas or liquid per unit mass

w = mass flow per unit time

Q_{TRAD} = net heat radiated to the leaf per unit time

Q_{COND} = net heat added to the leaf per unit time by conduction

Q_{CONV} = net heat added to the leaf per unit time by convection

Q_{CHEM} = net heat added to the leaf per unit time by chemical processes taking place in the plant (excluding transpiration)

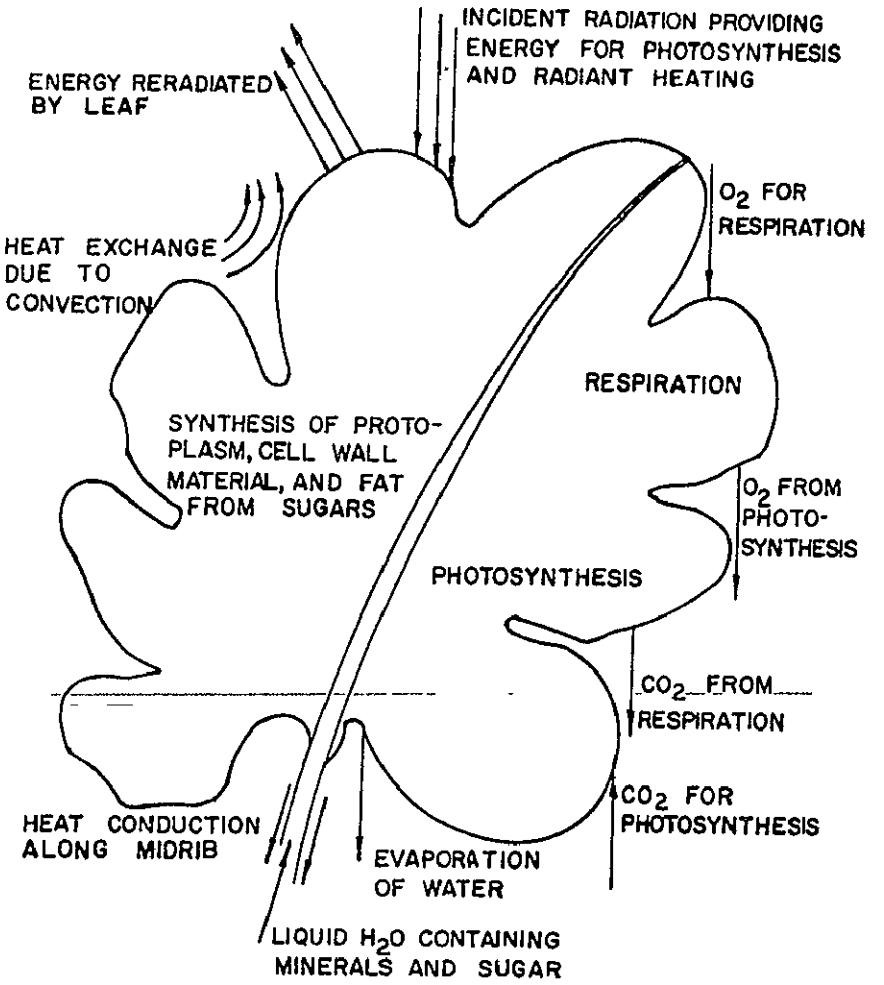

Figure 2.3.1 A Diagrammatic Representation of Leaf Activity Necessary for an Energy Balance on the Leaf (Taken from ref. 21, p. 56)

As can be seen, this equation takes into account not only the heat transfer modes of conduction, convection and radiation, but also the chemical energy due to photosynthesis and respiration, as well as the energy changes due to mass transfer. It turns out that the only significant energy change due to mass transfer is that due to the liquid (since this involves transpiration*), and the changes in energy due to mass transfer of oxygen and carbon dioxide can be neglected. It can also be assumed that the only significant part of energy change due to the mass transfer of the liquid is transpiration, i.e., the energy change due to the liquid moving through the mid rib to the leaf is negligible. Finally, it can be assumed that the heat transferred by conduction is very small as compared with the other energy terms. Making the above mentioned approximations, Equation 2.3.1 becomes:

$$Q_{TRAD} + Q_{CONV} + Q_{CHEM} = (hw)\ \text{liquid out} - (hw)\ \text{liquid in}$$

$$= Q_{TRANS} \qquad (2.3.2)$$

where

Q_{TRANS} = net heat added to the leaf per unit time by transpiration

Looking at the total heat radiated to the leaf, it can be said that this is equal to the heat radiated to the leaf from the surroundings, minus that reradiated by the leaf to the surroundings. Substituting this into the Equation (2.3.2) and rearranging:

$$Q_{TRAD} = Q_{INCIDENT} - Q_{LEAVING} = Q_{ABSORBED} - Q_{EMITTED}$$

$$= Q_{TRANS} - Q_{CONV} - Q_{CHEM} \qquad (2.3.3)$$

The above equation is the basic equation for calculating the net heat

* Transpiration converts the water in the leaves of a plant from the liquid to the gaseous state; the water vapor then passes from the leaf into the surrounding atmosphere.

k_S = absorptance to direct solar radiation
k_s = absorptance to scattered skylight
k_t = absorptance to longwave thermal radiation

ε_t = emittance of the leaf to longwave thermal radiation (i.e., $\lambda > 4$ μm)

E_s = sky radiation reflected by the surroundings, incident on the leaf

E_S = solar radiation reflected by the surroundings, incident on the leaf

S = direct solar radiation from a point source

s = scattered skylight from an extended source

R_a = thermal radiation from the atmosphere as an extended source

R_g = thermal radiation from the ground as an extended source

σ = Stefan-Boltzmann constant

T_ℓ = leaf temperature in absolute scale

L = latent heat of vaporization of water at the leaf temperature

E = transpiration rate - energy gained or lost by transpiration or evaporation in mass area^{-1} time^{-1}

Gates[34] (1964) took the typical values of these variables as follows:

$(S + s) = 1.20$ cal. cm^{-2} min^{-1}, $R_a = 0.48$ cal. cm^{-2}.min^{-1},
$R_S = 0.62$ cal. cm^{-2} min^{-1}, T_a (air temperature) = 30° C,
$k_S = 0.60$, $k_t = \varepsilon_t = 0.97$, relative humidity = 60%

(B) Energy Balance on a Plant Canopy

Gates[34] (1964) pointed out that one of the most difficult factors to evaluate, in terms of the energy budget of a plant, is the matter of plant geometry. It is not so difficult to evaluate the energy budget for a single isolated plant without other plants nearby, or to evaluate a dense, opaque canopy. When a plant produces only partial cover and some of the soil is exposed, the problem becomes more difficult. He[34] derived the following two relationships: a) the radiation absorbed by a plant as the function of the amount of plant cover; and b) the radiation reflected by

a plant as a function of the amount of plant cover. He assumed the emittance and absorptance of leaves and soil to be unity in the thermal long wavelength region, which is not always true, in general (Section 2.6). These relationships, taking into account absorptance and emittance of leaves and soil in the long wavelength region (i.e., $\lambda > 4$ μm), are derived below.

Let f be the fraction of the soil surface which is sunlit. Let k_{gS} and k_{gs} be the absorptance of the sunlit soil surface to the downward stream of solar and sky radiation, respectively, and let the absorptance and emittance of the soil to longwave radiation be k_{gt} and ε_{gt}, respectively; then the net radiant energy absorbed by the sunlit soil surface will be:

$$\text{Net } Q_{g \text{ abs}} = f[k_{gS}S + k_{gs}s + k_{gt}R_a - R_S] \qquad (2.3.8)$$

(see Equations (2.3.5) to (2.3.7) for symbols)

The leaf canopy will receive the downward solar flux, S + s; absorbing a fraction, k_ℓ; reflecting a fraction, r_ℓ; and transmitting a fraction, t_ℓ. It will also receive the longwave thermal flux, R_a, from the atmosphere and absorb it with an absorptance of $k_{\ell t}$. The underside of the leaves receive longwave thermal radiation from the sunlit soil surface, $\Omega_S R_S/\pi$, and from the shaded surface, $\Omega_s R_s/\pi$, where

Ω_S = solid angle subtended by the leaves, visible from the sunlit soil, at the sunlit soil. The solid angle is found at each small area of the sunlit soil and is averaged over the entire area of sunlit soil.

Ω_s = solid angle subtended by the leaves, visible from the shaded soil, at the shaded soil. The solid angle is found at each small area of the shaded soil and is averaged over the entire area of the shaded soil.

R_s = longwave radiation emitted by the shaded soil surface

Neglect the transmission of the leaf canopy in the long wavelength

(i.e., $\lambda > 4$ μm) region. Assume that the sunlit soil reflects diffusely, a fraction, r_{gS}, of the incident direct sunlight, S. The incident skylight, s, will also be reflected; however, the sunlit soil will only view a fraction of the sky, and this small term will be neglected in the formulation. Hence, the lower surface of the leaves will receive an amount of reflected sunlight, $\Omega_S r_{gS} S/\pi$. The leaf canopy will also radiate longwave radiation, $\varepsilon_{\ell t}\sigma T_\ell^4$, upward and downward. Hence, the net energy absorbed by the leaf canopy will be:

$$\text{Net } Q_{\ell \text{ abs}} = (1 - f)\,[k_{\ell S} S + k_{\ell s} s + \Omega_S r_{gS} k_{\ell S} S/\pi + k_{\ell t} (R_a + \Omega_S R_S/\pi + \Omega_s R_s/\pi) - 2\varepsilon_{\ell t}\sigma T_\ell^4] \qquad (2.3.9)$$

Also, we have

$$k_{\ell t} = \varepsilon_{\ell t} \qquad \text{(Kirchhoff's Law, see Section 2.2)} \qquad (2.3.10)$$

The shaded surface receives a fraction (1 - f) of the downward transmitted flux from the canopy, t_ℓ (S + s), and of the emitted downward longwave flux, $\varepsilon_{\ell t}\sigma T_\ell^4$. In turn, the shaded soil surface will emit on a unit area basis (1 - f) R_s, where R_s is the thermal radiation flux from the shaded soil surface. Hence, the net energy absorbed by the shaded soil surface will be:

$$\text{Net } Q_{s \text{ abs}} = (1 - f)\,[k_{gS} t_{\ell S} S + k_{gs} t_{\ell s} s + k_{gt} \varepsilon_{\ell t}\sigma T_\ell^4 - R_s] \qquad (2.3.11)$$

where

k_{gt} = the absorptance of the shaded soil to longwave radiation

The total energy absorbed by a vegetated soil surface, where the vegetation covers a fraction (1 - f) of the total surface, will be:

$$\text{Net } Q_{abs} = Q_{g\ abs} + Q_{\ell\ abs} + Q_{s\ abs} = Q_{TRANS} - Q_{CONV} \qquad (2.3.12)$$

(see Equation (2.3.4))

It should be pointed out that it is involved to derive an expression for absorption, reflection and transmission coefficients of a leaf canopy, in general because of its complex geometry.

2.4 Environmental Effects on the Plant Leaf Temperatures

(A) Introduction

Basic information regarding the relative temperatures of leaves has been available since the work of Askenasy[4] (1875). He observed that thin leaves in sunshine were 4 to 5° C warmer than air, while the thick leaves of succulent plants were about 20° C warmer than the surrounding air. Since his time there have been a large number of articles published in the general area of environmental effects on the plant leaf temperatures. Only a part of some of the relatively recently published articles will be summarized in this Section.

The temperature of a leaf depends on many environmental factors like air temperature, relative humidity, wind velocity, solar irradiance, intake water temperature, etc.[105, 100, 60] These are described briefly under the following headings.

(B) Temperature Variations Over Leaves

Cook[21] (1963) investigated the normal variation in tomato leaflet temperatures and found the extremities of the plant leaflet, where the veins are the smallest and fewest in number, to be the warmest. The maximum gradient of 1.8° F existed across the leaflet due to variation in transpiration. He found no significant temperature variation from leaflet to leaflet, from leaf to leaf, or from plant to plant (i.e., the maximum deviation was about 0.3° F). Of course, this result is somewhat limited, because all the plants used were young growing plants varying in height from about 3" to 12" and it is based on limited experiments of one author.

(C) Effect of Air Temperature

Under normal conditions one of the most important parameters in determining leaf temperature is the air temperature. Many measurements of leaf temperature have been made by Clum[18] (1926), Curtis[25] (1938), Ansari and Loomis[3] (1959), Cook[21] (1963), Gates[32] (1963), Wiegand and Namken[105]

(1966), Myers et al.[73] (1966), Gates[36] (1968), and others. These measurements have shown that the leaves in sunlight may have temperature up to 2° C[21], 8 to 9° C[105], or 10 to 15° C[31], but seldom more than 20° C[3,36,31] above air temperature. Gates[35] (1965) found that on overcast days, leaf temperatures in his yard shifted rapidly from 6 to 8° C above the air temperature to 2 to 4° C below it as the clouds alternately obscured the sun. Gates[36] has pointed out that in spite of the three primary mechanisms by which a plant leaf may prevent its temperature from rising too high above air temperature (i.e., low absorptance to incident radiation, free transpiration and free convection), there are many pieces of evidence to suggest that the plant leaves may get too warm to remain physiologically active, or indeed viable. Leaf temperatures often reach 50° C which is close to the denaturation temperature for most plant proteins; a few degrees higher will destroy the proteins. Thus, there is a need for determining temperature of leaves accurately.

The temperatures of leaves can also be lower than the air temperature. For example, Ansari and Loomis[3] (1959) found temperatures of leaves, sometimes at night, about 2° F below the air temperature, when the leaves were radiating to cold glass or clear sky. Readings of 5° F below air were obtained in one experiment when plants from a green house were rapidly moved to a dimly lighted laboratory with a relative humidity of 25%. Gates[36] (1968) found that shade leaves of Populus deltoides were at 30° C when the air temperature was 32° C.

(D) Effect of Sunshine

Ansari and Loomis[3] (1959) reported that the leaves, about 2 - 5° C above the air temperature could be heated by sunshine to about 20° C above the air temperature and finally cooled back to their original temperature by shading. The rate of cooling of leaves was found to be approximately linear. Leaves could also be heated 1 or 2° C by radiation from nearby heated surfaces. Gates[31] (1963) has given the temperature of Quercus macrocarpa leaves in the shade, sun and at cloudy times of the day. Loomis[65] (1965) found that leaves in direct sunlight heated rapidly to equilibrium temperature of 6 to 10° C above air for thin leaves and to

30° C or more for very thick leaves before reaching a steady temperature. The heating and cooling curves shown by wilted leaves were not significantly different from those of transpiring leaves. Dried leaves heated less and cooled faster than normal, transpiring leaves. Wiegand and Namken[105] (1966) found that a unit increase in solar radiation (from about 0.5 to 1.5 ly/min) resulted in 9 to 10° C increase in leaf temperature.

(E) Effect of Intake Water Temperature

Cook[21] (1963) lowered the water temperature taken up by the tomato plants at 76° F, to 34° F over the eight hour period, but it had no effect on the tomato leaflet temperature. This result is somewhat limited because it is based on the experiment of one author on one crop.

(F) Effect of Free and Forced Convection

Leaves lose or gain heat by convection to the air around them. Gates (1968) pointed out that air is only a fairly good insulator, and therefore, leaves are only partly decoupled from air temperature. The temperature gradient from the surface of the leaf to air occurs across a boundary layer of air adhering to its surface which causes the temperature of large leaves to be more decoupled from air temperature than the temperature of small leaves.

The energy exhange by convection can be expressed by

$$Q_{CONV} = h_c \Delta T \qquad (2.4.1)$$

where

h_c = convection coefficient which depends upon shape, orientation and size of a leaf

ΔT = difference between leaf temperature and air temperature

Gates[34] (1964) has given expressions of convection coefficient for a flat leaf for free and forced convection. He has also given the figures illustrating the energy transferred from a leaf by radiation, free and forced convection, and transpiration as a function of the departure of leaf temperature and angle of leaf from horizontal.

Ansari and Loomis[3] (1959) found that wind at 5 m.p.h. decreased the value of $T_L - T_A$ (leaf minus air temperature) to about half of its original value. Cook[21] (1963) found from wind tests on tomato leaflet, that transpiration was the dominant mode of heat transfer from velocities 0 to 350 feet per minute, that convection was the dominant mode from velocities 350 - 1100 feet per minute, and that velocities above 1100 feet per minute had no effect on leaf temperature. Loomis[65] (1965) reported that leaves in sunshine were cooled quickly toward air temperature by wind at 5 m.p.h. Aston[5] (1969) found that the exchange coefficients for free and forced convection of a vertical leaf agreed with the calculated value.

(G) Effect of Transpiration

Transpiration is a very important factor affecting the leaf temperature. Transpiration converts the water in the leaves to water vapor which is emitted through the stomates, which can be as many as 20,000 per sq. cm. of leaf surface[35]. On a hot sunny midday, when heat load is at its peak, transpiration rate is also at its highest and produces maximum cooling effect, and prevents or at least delays wilting. Gates[33] (1964) indicated that by the mechanism of transpiration, fully sunlit leaves may have their temperature depressed below air temperature. Gates[35] (1965) has given a remarkable example of temperature control by transpiration. It was found that the temperature of sunlit leaves of Mimulus cardinalis (monkey flowers) grown on well watered soil ranged from 30 to 35° C; whereas, the temperature of the leaves of a live oak, grown a few yards away from Mimulus cardinalis, in drier soil ranged from 40 to 43° C. The sky was clear and the air temperature was about 37° C. Monkey flower plants were also placed in a growth chamber under even and constant illumination. He found that when the air temperature was about 30° C or lower, the monkey flower leaves were warmer than the surrounding air, when the air temperature was raised above 30° C, the leaves remained cooler than air. Knoerr and Gay[57] (1965) found in a green house at air temperature of about 41° C that the non-transpiring leaves died almost immediately, and transpiring leaves died after a short period of exposure. Cook and Dixon (1964) reported that a definite and significant temperature gradient

existed over an area of a tomato leaflet which was apparently due to the variations in transpiration across the leaflet. Cook* (1967) reported an analytical and experimental study of heat transfer and transpiration from a leaf. He showed that the variations in the magnitude of the convective and stomatal resistances to diffusion were critical in determining the overall transpiration. Changes in the environmental conditions were shown to be mainly responsible for changes in the stomatal or pore resistance to diffusion rather than the convective resistance to diffusion. He pointed out that both resistances, however, must be accounted for in any determination of overall transpiration.

---

*G. D. Cook, Ph.D. Thesis, Purdue University, Indiana, 131., 1967.

2.5 Theoretical Aspects in Infrared Radiometry

(A) Atmospheric Interference

Atmosphere absorbs, scatters and emits radiation. The main atmospheric constituents which absorb and emit radiation in our usual wavelength region of interest -- 4 to 14 μm -- are: carbon dioxide, water vapor and ozone.

Strong absorption by CO_2 exists in the 2.7 μm region[98], the 4.3 μm region and the region between 11.4 and 20 μm. Weaker absorption bands are present at 1.4 μm, 2.0 μm, 4.8 μm, 5.2 μm, 9.4 μm and 10.4 μm. Major H_2O absorption bands[93] are at 1.87 μm, 2.70 μm and 6.27 μm. Minor water absorption bands are at 0.94 μm, 1.1 μm, 1.38 μm, and 3.2 μm. Ozone absorbs[97] in the narrow band in 9.35 to 9.90 μm; however, 95% of this absorption occurs above 11 km for most areas (see ref. 58 , p. 102). Lenschow and Dutton[64](1964) have pointed out that the effect of atmospheric absorption and emission is negligible if distance of the radiometer to the target is less than 100 meters. Bergstrom (Ph.D. Thesis, Purdue University, 1972) has done theoretical study of the thermal structure and dispersion in polluted urban atmospheres.

(B) Environment Radiation

The radiation incident on plant canopy comes from sun, sky, clouds, atmosphere and the surroundings. The solar radiation in the 4 to 14 μm thermal infrared region is negligible (Section 2.5(C)). The radiant temperature of the clear sky can be as low as -50° C but it usually lies between about -30° C to about -10° C; thus, the sky radiation can be neglected. Idso and Jackson[48] (1968) have reported that the absolute error in radiometrically determined surface temperatures caused by neglecting the fluctuations of sky radiant emittance over a diurnal period, can be as high as 0.55° C, for surfaces with temperatures between 0° C and 60° C and infrared emittances between 0.90 and 1.00. Jackson and Idso[53] (1969) have given the ambient temperature effects in infrared thermometry.

Thick cloud are good blackbodies (see ref.[98] p. 98). Because of the emission and absorption bands of the atmosphere at 6.3 μm and 15 μm, a cloud may not be visible in these regions and the radiation at these wavelengths is determined by the temperature of the atmosphere. Hovis et al.* (1967) have given the spectra of reflected solar and emitted

---

*W. A. Hovis, Jr., and M. Tobin, Appl. Opt. 6, p. 1399, 1967.

thermal radiation from natural surfaces and clouds in the wavelength range 1.6 μm to 5.4 μm. Measurements were made, from a jet aircraft, of characteristic spectra of a wide variety of surface and cloud conditions during day and night flights. It should be pointed out that when the sky is overcast with clouds, the radiant energy coming from the target can be significant or even of about the same magnitude as compared to the emitted radiant energy from the target, and thus, the infrared radiometer does not sense the true radiant temperature of the target.

Gates[34] (1964) gave the typical value of total atmospheric radiant flux density on a horizontal leaf to be equal to 0.48 cal. cm^{-2} min^{-1}, most part of which is in the thermal infrared region. The surroundings of the plant canopy may be plants, rocks, soil, buildings, etc. The radiation from surroundings of the target depends upon the type of surroundings.

(C) Contrast Between Reflected and Emitted Radiation from a Natural Target

It has been pointed out by several authors that for wavelengths shorter than 2 μm the reflected solar energy from a typical plant and/or soil predominates the radiant energy emitted by it; whereas, for wavelengths larger than 4 μm, the emitted energy predominates the relflected energy. The contrast between reflected and emitted radiant energy is low in the spectral region 2 to 4 μm (see ref.[62] pp. 84-85; ref.[27] pp. 11-14). It is important to note that we should compare the radiant flux density reflected from the target to the radiant flux density emitted by it. An expression for the solar radiant flux density reflected from an infintesimal area of the target is derived as follows, with the help of ref. [99].

Consider an element of a target shown in Figure 2.5.1. On a clear day (cloud free) most part of solar radiation comes directly from the sun. Let us consider only direct solar energy in this particular case. Let $L_{\lambda,i}(\vec{s}')$ be the spectral radiance of direct solar radiation incident on dA from direction $\vec{s}'$. the spectral irradiance or direct solar radiant energy incident per unit area, time, wavelength and confined within the solid angle $d\Omega'$ about the direction $\vec{s}'$ is

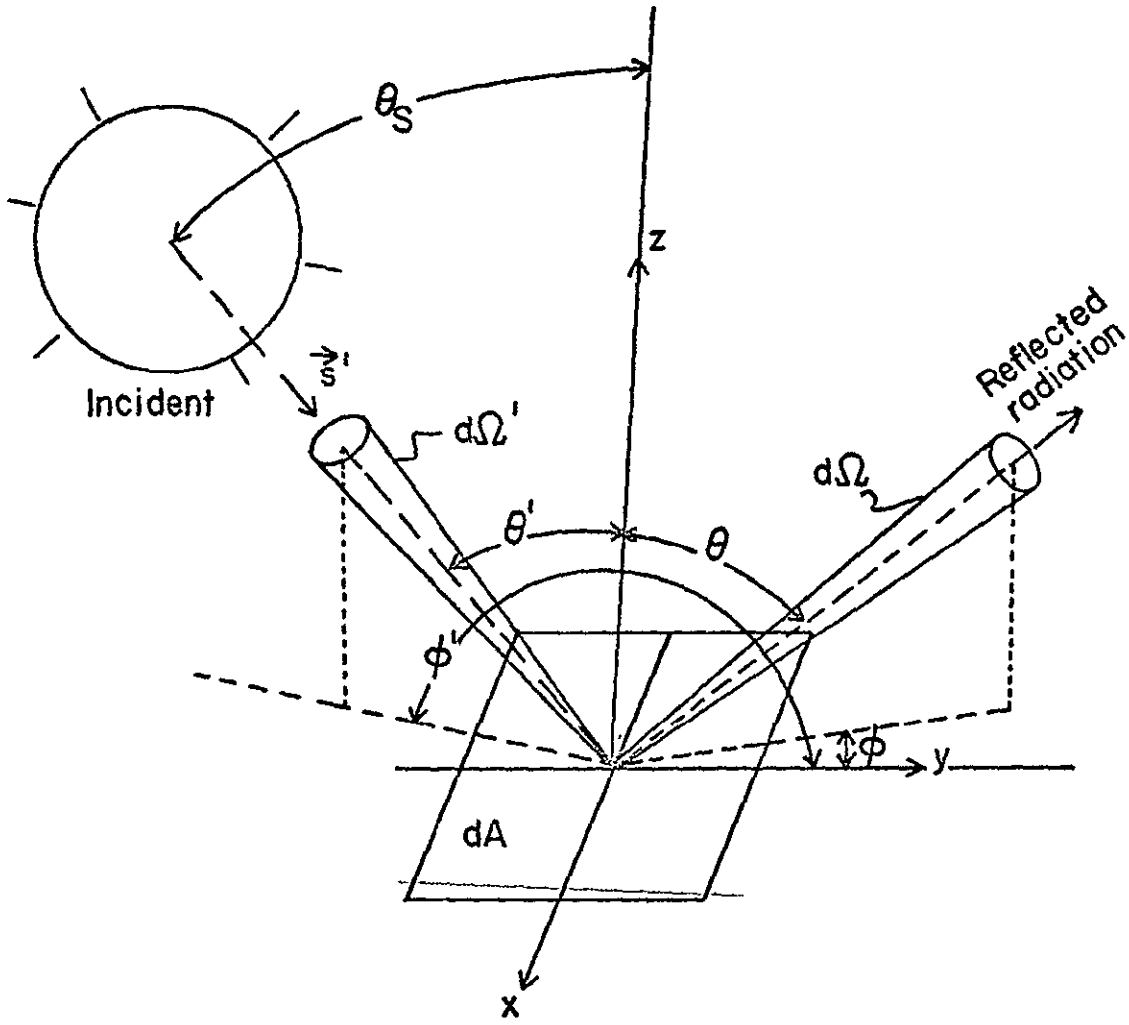

$\vec{s}'$ = Direction of incident solar radiation

$\vec{s}$ = Direction of reflected radiation

Figure 2.5.1 Diagram Showing Directions of Incident and Reflected Radiation

$$dE_\lambda(\vec{s}') = L_{\lambda,i}(\vec{s}')\cos\theta' d\Omega' \qquad \text{[Figure 2.5.1]} \qquad (2.5.1)$$

where

$$L_{\lambda,i}(\vec{s}') = \tau_a(\lambda, \vec{s}')L_{\lambda,\,b}(5500^\circ\,K) \qquad (2.5.2)$$

$\tau_a(\lambda, \vec{s}')$ = spectral transmission of the atmosphere in direction $\vec{s}'$.

$L_{\lambda,\,b}(5500^\circ\,K)$ = spectral blackbody radiance at 5500° K (sun's temperature).

$$\text{Spectral solar irradiance } E_{\lambda,\,S} = \int_{\Omega'} L_{\lambda,\,i}(\vec{s}')\cos\theta' d\Omega' \qquad (2.5.3)$$

where

Ω' = solid angle subtended by the sun at the earth's surface

subscript S = refers to <u>direct</u> solar radiation

or

$$E_{\lambda,\,S} \approx L_{\lambda,\,i}\cos\theta_S \Omega' \qquad (2.5.4)$$

where

θ_S = angle <u>subtended</u> by the sun with the z axis (Figure 2.5.1)

We have assumed that the radiation from the sun comes from a very small solid angle, Ω', and thus, $L_{\lambda,\,i}$ and $\cos\theta'$ have been considered to be constant within solid angle, Ω'.

or

$$E_{\lambda,\,S} = L_{\lambda,\,i}\left(\frac{\pi R_S^2}{d^2}\right)\cos\theta_S \qquad (2.5.5)$$

where

R_S = radius of sun

d = distance of sun from the earth

The spectral radiance of reflected radiation in the direction $\vec{s}$ within the solid angle $d\Omega$ is

$$dL_{\lambda,\, r}(\vec{s}' - \vec{s}) = r(\lambda, \vec{s}' - \vec{s})dE_{\lambda} \qquad \text{[by definition]} \qquad (2.5.6)$$

where

$r(\lambda, \vec{s}' - \vec{s})$ = reflection distribution function for the direction $\vec{s}'$ to $\vec{s}$.

The spectral bidirectional reflectance $\rho(\lambda, \vec{s}' - \vec{s})$ is defined as the ratio of radiant energy reflected by the surface into the beam $(\vec{s}, d\Omega)$ from the incident beam $(\vec{s}', d\Omega')$, to the radiant energy in the incident beam $(\vec{s}', d\Omega')$, and is given by

$$\rho(\lambda, \vec{s}' - \vec{s}) = r(\lambda, \vec{s}' - \vec{s})\cos\theta d\Omega \qquad (2.5.7)$$

The spectral radiance of reflected radiation in all directions is a result of contributions from the radiant energy reflected from the scene from all directions ($\Omega' = 2\pi$) and can be obtained by integrating Equation (2.5.6) over the hemisphere

$$L_{\lambda,\, r} = \int_{\Omega} dL_{\lambda,\, r}(\vec{s}' - \vec{s}) \cos\theta d\Omega \quad (\Omega \text{ denotes hemisphere}) \qquad (2.5.8)$$

Spectral directional hemispherical reflectance is defined as the ratio of radiant energy reflected by the surface into all directions from the incident beam $(\vec{s}', d\Omega')$ to the radiant energy in the incident beam. It is related to the bidirectional reflectance as

$$\rho(\lambda, \vec{s}') = \int_{\Delta} r(\lambda, \vec{s}' - \vec{s}) \cos\theta d\Omega \qquad (2.5.9)$$

or

$$\rho(\lambda, \vec{s}') = \int_{0}^{2\pi} d\phi \int_{0}^{\pi/2} r(\lambda; \theta', \phi'; \theta, \phi) \cos\theta \sin\theta d\theta \qquad (2.5.10)$$

The incident solar radiation comes hemispherically (from all directions) when the sky is overcast with clouds. Even when the sky is clear, there is some scattered solar radiation coming from all directions.

Spectral hemispherical reflectance is a useful quantity for computing reflected radiant flux density of hemispherical irradiance. Spectral hemispherical reflectance is given by

$$\rho(\lambda) = \int_{\Delta} \rho(\lambda, \vec{s}')L_{\lambda}(\vec{s}')\cos\theta' d\Omega' \qquad (2.5.11)$$

where

Δ = denotes integration over the hemisphere

The hemispherically incident solar (direct and scattered) irradiance is given by

$$E_{\lambda} = \int_{\Delta} L_{\lambda, i}(\vec{s}')\cos\theta' d\Omega' \qquad (2.5.12)$$

It turns out that for natural targets -- say plants and soils, hemispherically emitted radiant flux density $\varepsilon(\lambda, T)\pi L_{\lambda, b}$, can be usually neglected as compared to the hemispherically reflected radiant flux density, $\rho(\lambda)E_{\lambda,i}$, in the wavelength range: $0.35 \leq \lambda \leq 2$ μm

where

$\varepsilon(\lambda, T)$ = hemispherical spectral emittance of the natural target at temperature T and wavelength λ. (See Section 2.2 for definition of $\varepsilon(\lambda, T)$)

$L_{\lambda, b}(T)$ = blackbody spectral radiance at temperature T and wavelength λ.

$\rho(\lambda)E_{\lambda}$ can usually be neglected as compared to $\varepsilon(\lambda, T)\pi L_{\lambda,b}$ in the wavelength range: $4 \leq \lambda \leq 20$ μm. $\rho(\lambda)E_{\lambda}$ is of the same order as $\varepsilon(\lambda,T)\pi L_{\lambda,b}(T)$ in the wavelength range: $2 \leq \lambda \leq 4$ μm.

Hemispherical directional reflectance is quite useful for applications to machine analysis of remotely sensed data. The direct solar radiation comes in a relatively small solid angle but the scattered solar radiation comes from all directions. The radiation reflected from the target which reaches the detector of multispectral scanner of aircraft or satellite comes in a relatively small solid angle. Thus, the signal received by the

multispectral scanner in the spectral channel of wavelength range λ_1 to λ_2 is directly proportional to the solar irradiance in the wavelength range λ_1 to λ_2 and the band hemispherical directional reflectance of the target in the direction of remote sensing in the wavelength range λ_1 to λ_2. Reflection distribution function is useful because on a clear (cloud free) day, most part of the solar radiation comes directly from the sun and the reflection distribution function can convert direct solar spectral irradiance to the spectral reflected radiance of the target. Bidirectional reflectance can convert direct solar spectral radiance to the spectral reflected radiance of the target.

2.6 Emittance of Plants

(A) Introduction

All objects above absolute zero radiate energy by virtue of their temperature and emittance. At temperatures normally exhibited by natural objects at or near the earth's surface, this radiation is almost entirely in the infrared wavelength region from approximately 4 μm to 100 μm.

Planck's radiation law states that at any given temperature, T, and wavelength, λ, the maximum possible spectral radiance of emitted radiation is the blackbody spectral radiance at that temperature, T, and wavelength, λ.

No natural surface emits like a blackbody due to internal reflection of rays by the surface discontinuity. Therefore, spectral emittance has been defined in Section 2.2. Thus, no instruments can yield a correct estimate of surface temperature by remote sensing if the emittance of the surface is not taken into account. Gates and Tantraporn[40] (1952) have pointed out that accurate knowledge concerning the infrared reflectance, absorptance, and emittance of leaves in the 1.0 to 15.0 μm region is essential for a detailed understanding of the energy exchange in the biosphere. Accurate knowledge of the infrared emittance of plants is required in many diverse ecological applications. Most researchers recognized this problem, but have neglected to apply the needed corrections, arguing that all plant surfaces have a longwave emittance of 0.95 or greater, most leaf emittances being 0.97 to 0.98.

(B) Theory and Error Analysis of Measurement by Infrared Radiometer

Fuchs and Tanner[29] (1966) have discussed the theory of remote sensing of surface temperatures using infrared radiometer, a part of

which is summarized here. They made the following assumptions for remote sensing of plants.

1.) Gray emittance in the wavelength range sensed by the radiometer (i.e., 8 μm to 20 μm) or

$$\varepsilon(\lambda) = \varepsilon(8\ \mu m \leq \lambda \leq 20\ \mu m) \tag{2.6.1}$$

2.) $\varepsilon(\lambda)$ is independent of temperature.

3.) Kirchhoff's Law is valid.

$$\varepsilon(\lambda) = \alpha(\lambda) = 1 - \rho(\lambda) \tag{2.6.2}$$

(transmission ≈ 0 in 8 μm ≤ λ ≤ 20 μm)

where

$\rho(\lambda)$ = the reflectance at wavelength λ

Under these assumptions, the total apparent outward radiant flux density measured by the radiometer is given by F_o.

$$F_o = \varepsilon\ f(T)\ \sigma T^4 + (1 - \varepsilon)\ f(T_S)\ F_S \tag{2.6.3}$$

radiant flux density emitted by the plant	radiant flux density reflected from the plant

T = contact temperature of the plant

(See Section 5.5 for definition of plant temperature)

$$f(T) = \int_0^\infty f(\lambda)\ F_{\lambda,b}(T)\ d\lambda \ /\ \int_0^\infty F_{\lambda,b}(T)\ d\lambda \tag{2.6.4}$$

where

$F_{\lambda,b}(T)$ = the blackbody radiant flux density at temperature T and wavelength λ

F_S = environment integrated radiant flux density at temperature T_S

$f(\lambda)$ = filter characteristics for the infrared radiometer (for example, for Barnes infrared radiometer: $f(\lambda) \neq 0$, 8 μm ≤ λ ≤ 20 μm, $f(\lambda) = 0$, otherwise).

Equation (2.6.3) is the fundamental equation describing the quantity of radiation received at the detector of the radiometer. Since the absolute value of f(T) is not important, but only its form, an assumption is now made that f(T) is constant for the range of biological temperatures encountered. The radiometer is calibrated according to the quantity

$$F_d \equiv F_o \; / \; f(T) \tag{2.6.5}$$

where

$\equiv$ denotes that the quantity is defined.

Hence,

$$F_d = \varepsilon \, \sigma T^4 + (1 - \varepsilon) \, \frac{f(T_S)}{f(T)} \, F_S = \sigma T_s^{\,4} \tag{2.6.6}$$

where

T_s = full radiator surface temperature as sensed by the radiometer

The radiometer interprets the contact surface temperature, T, to be full radiator surface temperature T_s. If $\varepsilon = 1$, then $T_s = T$. Also, if the integrated full radiator temperature of the surroundings (T_S) is equal to the contact surface temperature (T), then $T_s = T$. If the surface has an emittance substantially less than unity, and if the surface images sun or cold sky, the full radiator surface temperature as measured with the IR radiometer may be quite different from the contact temperature. Hence, there is a need for determining emittance and the environment integrated full radiator temperature, T_S, accurately. Equation (2.6.6) can be rewritten as

$$F_d = \varepsilon \, \sigma T^4 + (1 - \varepsilon) \, F_S^* \tag{2.6.7}$$

where

$$F_S^* = \frac{f(T_S)}{f(T)} \, F_S$$

Fuchs and Tanner assumed that F_S^* is a constant (i.e., independent of temperature T), which in turn assumes that f(T) is constant. f(T) = constant is a good approximation for small variations of T. Equation (2.6.7) can be rearranged to give

$$\varepsilon = \frac{F_d - F_S^*}{\sigma T^4 - F_S^*} \tag{2.6.8}$$

F_d and T are experimentally measured values and contain measurement error. Let δF_d and δT be the measurement errors in F_d and T respectively. Then Equation (2.6.8) can be rewritten as

$$\varepsilon + \delta\varepsilon = \frac{F_d + \delta F_d - F_S^*}{\sigma(T + \delta T)^4 - F_S^*} \tag{2.6.9}$$

where

$\delta\varepsilon$ = error in the determination of emittance

From Equations (2.6.8) and (2.6.9), assuming $\frac{\delta T}{T} < 1$, $\frac{4\delta T}{T} \frac{\sigma T^4}{\sigma T^4 - F_S^*} < 1$ and neglecting second order and higher orders of $\frac{\delta T}{T}$ (i.e., $\left(\frac{\delta T}{T}\right)^2$, $\left(\frac{\delta T}{T}\right)^3$, etc.), we get

$$\delta\varepsilon = \delta F_d - \frac{4\delta T}{T} \frac{\sigma T^4 (F_d - F_S^*)}{\sigma T^4 - F_S^*} \tag{2.6.10}$$

It should be pointed out that Equation (2.6.7) is not an exact equation because of a number of assumptions made in deriving the equation. A complete error analysis should also include another term in δF_d, representing the error due to the assumptions made. Equation (2.6.10) can be rewritten as

$$|\delta\varepsilon| = \frac{1}{|\sigma T^4 - F_S^*|} \left| \delta F_d - \frac{4\delta T}{T} \frac{\sigma T^4}{(\sigma T^4 - F_S^*)} (F_d - F_S^*) \right| \tag{2.6.11}$$

where

$|\ \ |$ = denotes the absolute value

or

$$|\delta\varepsilon| \leq \frac{1}{|\ \sigma T^4 - F_S^*|} \left[|\delta F_d| + \frac{\left| \frac{4\delta T\, \varepsilon}{T} \right|}{|\ \sigma T^4 - F_S^*\ |} \right] \quad \begin{matrix} \text{(using triangle} \\ \text{inequality)} \end{matrix} \qquad (2.6.12)$$

It should be pointed out that when the environment integrated radiant flux density, $F_S^* = \sigma T^4$, the radiant flux density coming from the target is equal to σT^4 (blackbody radiant flux density) irrespective of the emittance of the target. Thus, the radiometer cannot be used to measure the emittance of the target in this particular case.

Using Equation (2.6.12), $|\delta\varepsilon|$ is plotted against F_S^* with the parameters ε, T, $|\delta T|$ and $|\delta F_d|$ in Figures 2.6.1 to 2.6.4. It is clear from Figures 2.6.1 to 2.6.4 that the upper bound of $|\delta\varepsilon|$ (absolute error in the determination of emittance) increases with the increase in F_S^*. Thus, for determination of emittance of the plant surfaces in the field accurately, the experiment should be conducted when the sky is relatively clear to have a small value of F_S^* and hence small $|\delta\varepsilon|$. Figure 2.6.1 shows that the emittance of the target, say a leaf, has a very little influence on $|\delta\varepsilon|$. Figure 2.6.2 shows that $|\delta\varepsilon|$ decreases with an increase in temperature. Figures 2.6.3 and 2.6.4 show that increasing the error in temperature measurements and radiometric measurements respectively, results in an increase in error in emittance

The previous investigators have assumed that the emittance of the natural targets to be equal to one for the interpretation of multispectral scanner data in the thermal channel. Neglecting the radiant flux density reflected from a target, Figure 2.6.5 shows the difference between temperature of the target and the band radiance temperature (i.e., temperature found by assuming the target to be a blackbody) vs. emittance for the thermal channels which have been used in multispectral

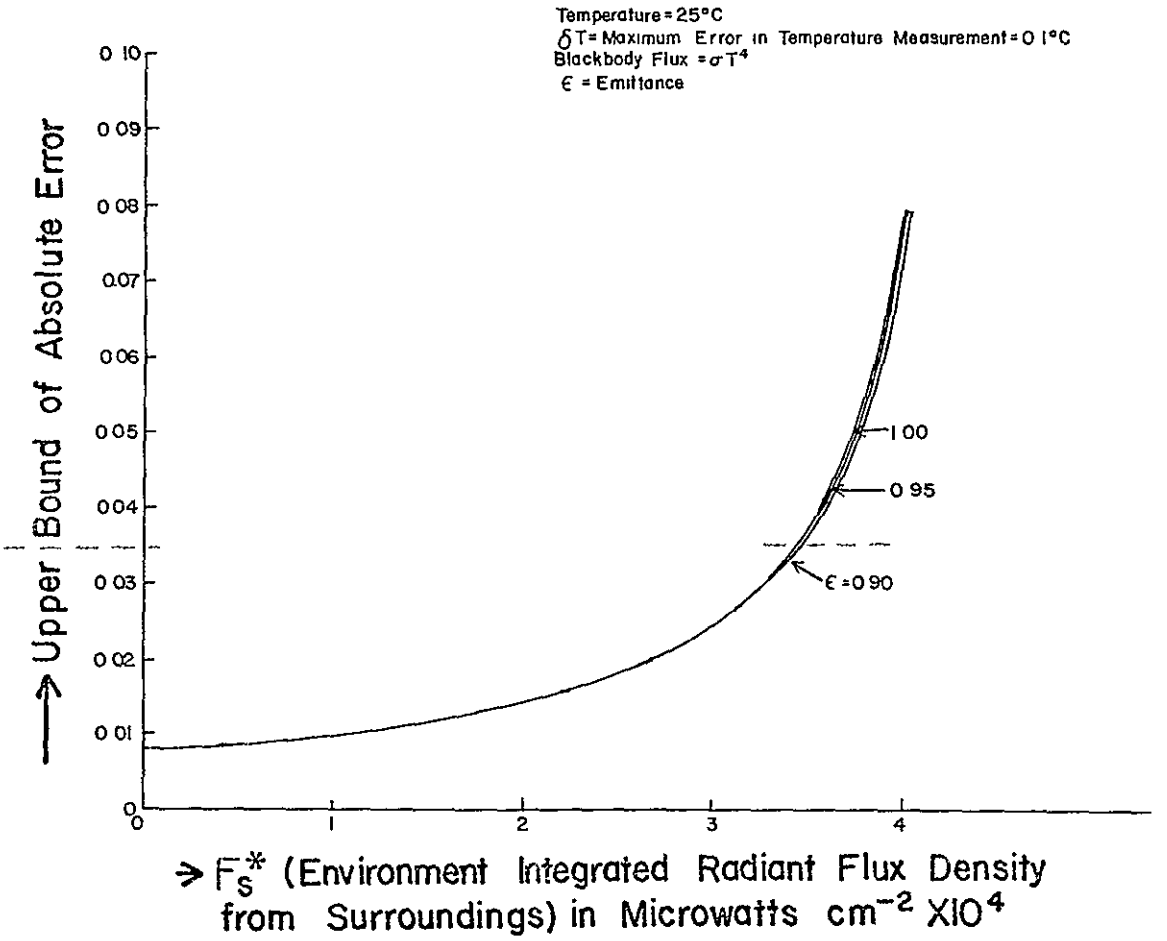

Figure 2.6.1 $|\delta\varepsilon|$ as a Function of F_s^* with ε as a Parameter

Temperature of the Target = 25° C

$\delta R_b = \sigma\{(273.16 + 25.5)^4 - (273.16 + 25)^4\}$

Emittance $\epsilon = 0.95$

Maximum Error in Temperature Measurement = 0.1° C

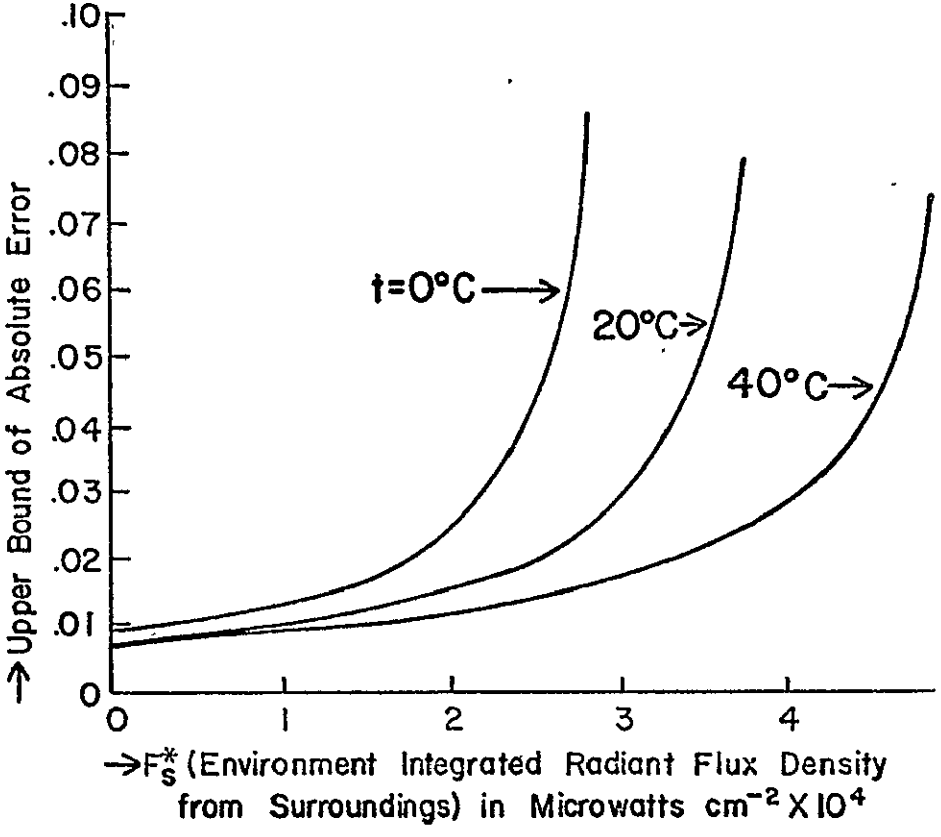

Figure 2.6.2 $|\delta\epsilon|$ as a Function of F_s^* with t as a Parameter

Temperature of the Target t = 25° C
Temperature T = 273.16 + 25 in °K
Emittance $\varepsilon = 0.95$
$|\delta T|$ = Maximum Error in Temperature Measurement in °C
$\delta R_b = \sigma\{(T + 0.5)^4 - T^4\}$

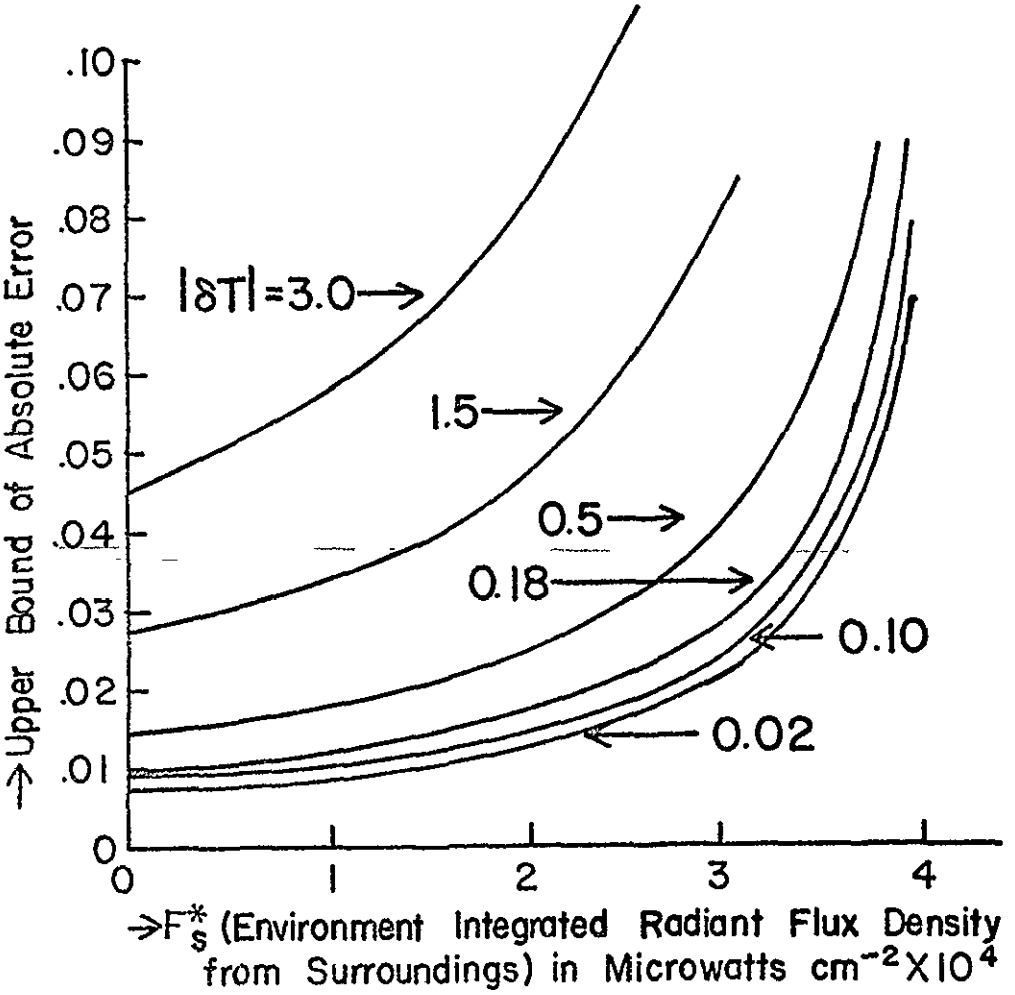

Figure 2.6.3 $|\delta\varepsilon|$ as a Function of F^*_s with $|\delta T|$ as a Parameter

Temperature t = 25° C
Emittance ε = 0.95
δT = Maximum Error in Temperature Measurement = 0.1° C
T = 273.16 + 25 in °K

δR_b = Maximum Measurement Error of Radiometer

$\delta R_{b1} = \sigma\{(T + 0.1)^4 - T^4\}$

$\delta R_{b2} = \sigma\{(T + 0.5)^4 - T^4\}$

$\delta R_{b3} = \sigma\{(T + 1.0)^4 - T^4\}$

$\delta R_{b4} = \sigma\{(T + 2.0)^4 - T^4\}$

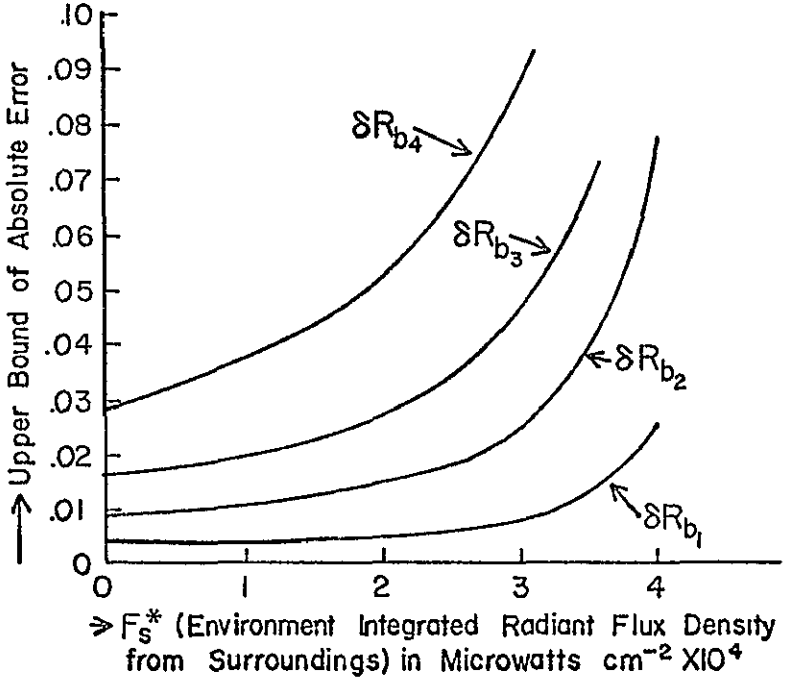

Figure 2.6.4 $|\delta\varepsilon|$ as a Function of F_s^* with $|\delta R_b|$ as a Parameter

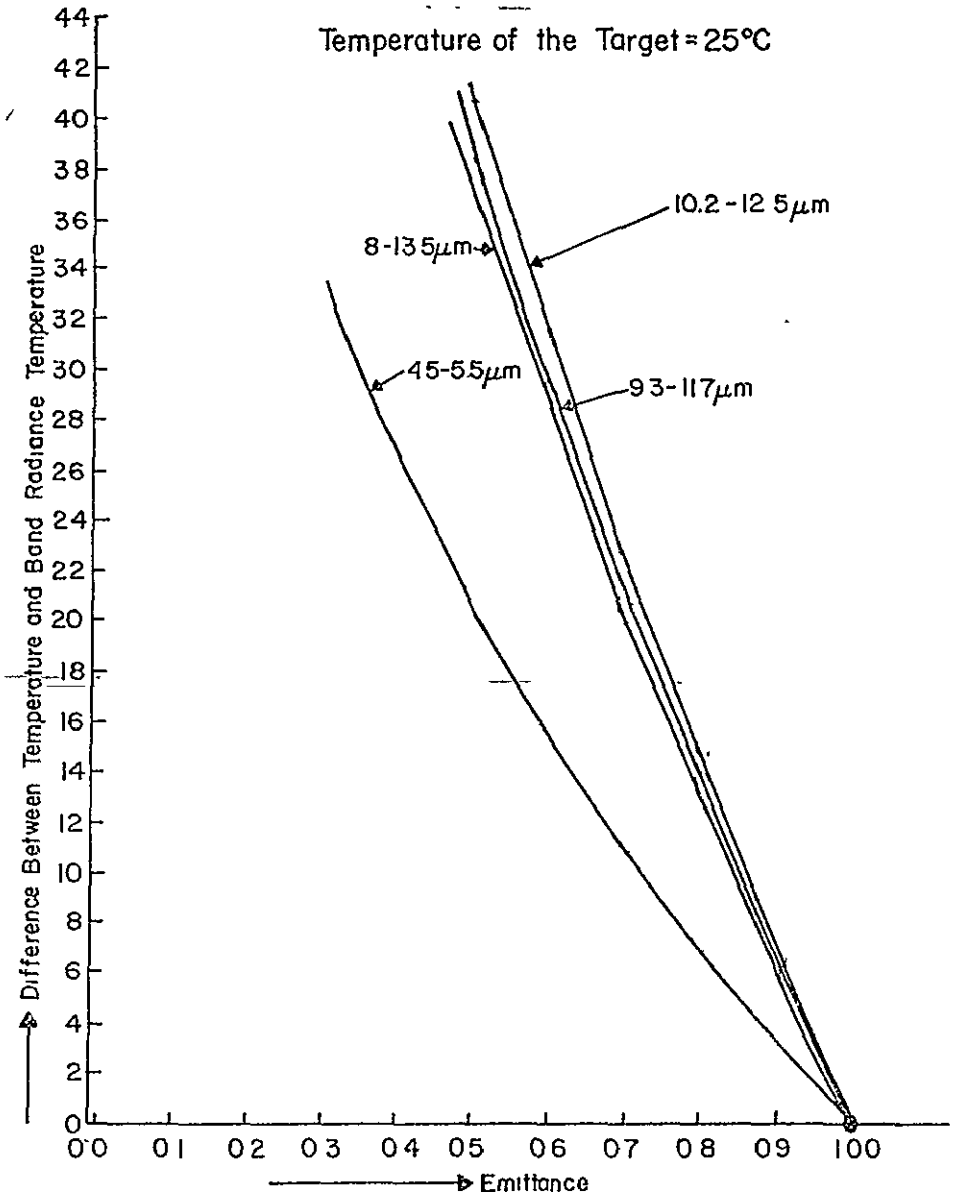

Figure 2.6.5 Difference Between Temperature and Band Radiance Temperature vs. Emittance

scanner of Environmental Research Institute of Michigan, formerly called Willow Run Laboratory, University of Michigan (4.5 to 5.5 μm, 8 to 13.5 μm and 9.3 to 11.7 μm), and Skylab (10.2 to 12.5 μm). Figure 2.6.5 shows that for a given value of the emittance, the difference between temperature and band radiance temperature (see Section 2.2 for the definition of band radiance temperature) is least in the 4.5 to 5.5 μm thermal channel, as compared to the band radiance temperature in the other thermal channels mentioned above. However, there are certain disadvantages of using 4.5 to 5.5 μm thermal channel, given as follows.

(i) Most natural targets have lower band emittance in the 4.5 to 5.5 μm thermal channel as compared to their band emittance in other thermal channels shown in Figure 2.6.5 (Sections 2.6(C) and 2.6(D)).

(ii) Atmosphere is less transparent in the 4.5 to 5.5 μm thermal channel as compared to its transmission in other thermal channels shown in Figure 2.6.5.

(iii) The band radiance of a natural target in the temperature range 0° C to 50° C (temperature range generally encountered in the natural targets) is considerably smaller in the 4.5 to 5.5 μm thermal channel as compared to its band radiance in other thermal channels shown in Figure 2.6.5.

Thus, signal to noise ratio in the thermal channel 4.5 to 5.5 μm is expected to be higher than in the other thermal channels shown in Figure 2.6.5 (Section 5.2).

(C) Emittance of Leaves

The emittance of a surface depends on its roughness as well as its temperature, in general. Emittance of leaves given by Falckenberg[28] (1928), Gates[34] (1964) and Gates et. al.[39] (1965) range from 0.95 to 0.98. Gubareff et. al.[43] (1960), p. 293, indicated the emittance of the leaves to be more than 0.90. Turrell and Austin[95] (1965) reported the emittance of citrus leaves to be about 0.87, using the data of Gates and Tantraporn[40] (1952). Gates and Tantraporn[40] measured the reflectance of upper and lower surfaces of leaves of deciduous trees

and herbaceous plants at 3, 5, 7.5, 10, 15 and 25 μm, at an angle of incidence of 20° and 65°. The infrared radiant source was the Globar, whose radiation was reflected off the leaf surface at the desired angle by means of spherical front-surface mirrors and then focussed upon the entrance slit of the infrared spectrometer. Neglecting the transmittance of plants in the infrared region, one can determine the emittance using Kirchhoff's Law, i.e.,

$$\varepsilon(\lambda) = 1 - \rho(\lambda)$$

where

$\varepsilon(\lambda)$ = spectral emittance

$\rho(\lambda)$ = spectral reflectance

It can be seen from their data that the reflectance of most leaves in the infrared beyond 2 μm lies between 0 and 10%, and its value varies from leaves of one plant to another. Plotting the spectral reflectance vs. wavelength from their data the following was concluded.

1. The shape and value of the spectral reflectance varied significantly from leaves of one plant to another. The reflection from a leaf beyond 2 μm is expected to be mainly from the surface because of strong water absorption bands. The author believes that the significant differences in spectral reflectance curves may be mainly due to differences in surface geometry rather than the differences in the index of refraction of the leaf constituents close to the leaf surface. Birth[11] (1971), pp. 13-29, has given diagrams illustrating the reflection of light rays from smooth and rough surfaces using Fresnel's equations and Snell's law.
2. The spectral reflectance variation from leaves of one plant to another was more significant for an angle of incidence of 65° as compared to an angle of incidence of 20°.
3. Almost all the spectral reflectance curves had a positive slope from 3 to 10 μm. A few of the spectral reflectance curves had

a negative slope from 10 to 15 μm.

4. The reflection of verbascum thapsus (Mullen, hairy surface) was found to be zero from 3 to 15 μm. This is probably because the light rays got trapped on the hairy leaf surface due to multiple surface reflections. The author believes, yet to be confirmed by experiments, that the reflection from a leaf in the thermal infrared region (i.e., 4-14 μm) is likely to be more specular as compared to the reflection in the visible and near infrared wavelength region, because a typical light ray has to pass through relatively a fewer number of interfaces in the leaf before it gets reflected in the thermal infrared region as compared to the visible or near infrared wavelength region (see Chapter III).

Gates and Tantraporn[40] also found that transmittance of leaves was zero in the infrared beyond 1.0 μm; whereas, Myers and Allen[71] (1968) found that the transmittance of a mature cotton leaf was similar and of the same order of magnitude, as its reflectance in the 0.5 to 2.5 μm region. This shows that the result of Gates and Tantraporn is not valid, in general, for all leaves.

Monteith and Szeicz[70] (1962) and Gates[32] (1963) estimate that assuming the emittance of the plant surfaces equal to one may cause errors of at most 0.2° C in the measurement of their temperature. Fuchs and Tanner[29] (1966) show from a simple calculation that if the incident thermal radiation from the sky and surroundings were 300 watts per square meter, corresponding to an apparent sky temperature of -4° C, and if the surface temperature were 25° C, a change of emittance from 0.95 to 0.98 would cause a measurement error of 2.2° C. For many detailed investigations, such discrepancies are intolerable[20].

Fuchs and Tanner[29] (1966) found the emittance of single leaves of snap beans and tobacco to be 0.96 and 0.97, respectively. They covered the temperature-controlled anodized surface by the base of a "skewed" aluminum cone with a highly polished reflecting surface. The leaf was placed at the base of the cone, and the apex of the cone was cut to fit the entrance pupil of the infrared thermometer, so that the leaf behaves

like a blackbody. Idso et al.[49] (1969) described a method for determining the infrared emittance of individual plant leaves which is relatively simpler than Fuchs and Tanner (F - T) method. Measurements on a wide variety of plant surfaces by this method indicated that significant differences of emittance exist among the various species. The emittance values ranged from about 0.94 to about 0.995. They pointed out that the values of emittance determined by infrared thermometers of different spectral sensitivity are not uniquely related, therby emphasizing the importance of emittance measurements.

The emittance of a single leaf is not representative of the emittance of a plant canopy because of the multiple internal reflections resulting from the plant geometry; therefore, the emittance of a plant canopy has to be determined separately[29] . For determining the emittance of a plant canopy, one has to define a meaningful temperature of a plant. For example, the temperature of a plant canopy can be defined as the average of the temperature of its leaves (Section 2.2). It is extremely difficult to measure the temperature of the plant surfaces in the field conditions because the surface temperature varies quite rapidly especially when the wind is blowing (Section 5.4). Fuchs and Tanner[29] determined the radiation emitted by the vegetal surface. Then, they covered the vegetal surface with a bottomless, hemispherical "pop tent"[14] covered on the inside with aluminum foil so that vegetal surface behaves approximately like a blackbody. They determined the emittance as the ratio of radiant flux density emitted by a vegetal surface to the radiant flux density emitted by it when it is covered with the pop tent. Covering the vegetal surface by the tent changes its energy balance and thus its surface temperature. During daytime, the tent cuts off the solar radiation and sky radiation. It affects the convective heat exchange and may also modify the transpiration pattern. They found the emittance of dense canopies of alfalfa and sudangrass to be between 0.97 and 0.98 on clear, calm nights when surface temperatures are more steady.

It is believed that the emittance of a wide variety of leaves has not been measured carefully in the natural environment in which the plants grow. The Laboratory for Applications of Remote Sensing (LARS)

at Purdue University has an extensive program to measure the spectral emittance of plant surfaces. LARS has the Exotech Model 20C Spectroradiometer which is capable of taking reliable spectral radiometric data under rigorous field conditions in the wavelength region 0.38 to 14 μm (Section 5.1). They have also recently acquired a Nernst Glower capable of operating at temperatures as high as 2800° K, providing spectral energy output over the entire spectroradiometer range. A spoked disc is used to chop the output beam. This is an ideal instrument for measuring the reflectance of the leaves and/or plant canopies in the field, because any radiation other than what is provided by the glower is averaged to zero and thus, the surrounding radiation has no effect on the measured reflectance. Knowing the spectral reflectance, spectral emittance can be calculated using Kirchhoff's Law on the spectral basis (Section 2.2). The effect of orientation, temperature, moisture content, plant diseases, nutrient deficiency, etc., on the leaf and plant spectral emittance shall be studied. This will help in interpreting the remotely sensed data of the thermal channel. For example, it was pointed out in a LARS report [63], p. 102, that no definite conclusions concerning the value of the thermal infrared data could be assessed.

(D) Emittance of Soils

With the advent of radiation data now available from the infrared measurements made by the satellite, there is an increasing need to know accurately the values of terrestrial surface emittance in order to interpret the data[13] . Most of the investigators (for example, Wark et. al.[101]) have assumed black earth in interpreting data of the satellite. Buettner et al.[13] (1964) have pointed out that the other data and literature are quite conflicting and confusing. For example, Falckenberg[28] (1928) shows that sand of the Baltic has an emittance of 0.89 at 300° K. While Kruse et al.[59] (1962) give a value for "terrain of 0.35 (it is not clear here whether this is the emittance of the whole spectrum or just a portion of it, but presumably the entire spectrum). Barnes[7] (1963) lists values of emittance of 0.28 to 0.44 for gravel, plowed field, and

granite. Falckenberg[28] (1928) also lists the value for snow emittance as 0.995, while Miller[69] (1963) lists the window value (water vapor window) as 0.35.

Buettner et al.[13] also reported that infrared signals received in the 8 to 12 μm water vapor window by weather satellites and aircraft are dependent on surface temperature, surface emittance and atmospheric interference. Nowhere can variations of surface emittance be neglected in order to evaluate the correct surface temperatures. They presented three methods of determining surface emittance: (1) reflection data from polished samples run on a spectrophotometer, (2) a device constructed by Buettner and Kern[13] called an emissivity box, and (3) emittance as inferred from the TIROS satellite data. They gave geological interpretations of the TIROS satellite data along with the values of emittance determined by the above three methods. Emittance of quartz, granite, feldspar, obsidian, basalt, dunite, dolomite, sand, water, etc., ranged from about 0.7 to 0.97.

In the emissivity box (Buettner and Kern (B - K) Method[13]), the radiosity of the soil is first measured when it is exposed to a highly reflecting enclosing surface. The soil is then exposed to a highly emitting surface. The emittance of the soil is determined as the ratio of the two measurements. Because of the large size of the B - K apparatus this method is used almost exclusively for determining infrared emittance of bare soils and rocks. On the other hand, the method presented by Fuchs and Tanner[29] (F - T Method, see Section 2.6(C)) is well adopted to this use and, in addition, is suitable for measuring the infrared emittance of plant leaves, but it requires that the base of the cone needed to create the blackbody cavity should be larger than the individual leaves of most plants. Fuchs and Tanner[30] (1968) recommended that aluminum cones with apex angles of 120° or larger, or shallow cylindrical cavities which have smaller apparent emissivities, be used to improve accuracy of the measurements. Idso et. al.[49] (1969) proposed a method for determining emittance of plants and soils which overcomes the dimensional limitations of the methods of Fuchs and Tanner as well as Buettner and Kern and it gives results in good agreement to both

of them.

Fuchs and Tanner[30] (1968) pointed out that the computation of background radiation implies constancy of the spectral emittance in the band pass of the infrared thermometer. In the case of quartz, which has a strong reflection band near 9 μm, this assumption fails. The resulting error can be minimized if background radiation is small, but in the "emissivity box" used by Buettner and Kern background radiation is large which results in an overestimate of emittance. Fuchs and Tanner have also found that emittance of Plainfield sand in the 8 to 13 μm decreased with moisture content. They have given a typical diurnal trend of temperature and emittance of the soil.

Hovis, Jr.[46] (1966) has given spectral reflectance of some common minerals like carbonates, sulfates, nitrates, salt, silica, etc. from 0.5 to 6 μm. He pointed out that the infrared reflectance spectra of these minerals exhibit spectral absorption band patterns that can be detected in reflection from surface minerals.

Hovis, Jr.[47] (1966) made the spectral reflectance measurements in the 0.5 to 22 μm, from a number of soils including some beach sands and some common surface minerals -- calcium carbonate, calcium sulfate or gypsum, sodium chloride, sodium carbonate, and sodium nitrate. He reported that if the measurements are restricted to the windows in the atmosphere of earth, the 10 μm to 12 μm interval seems to be the best choice for radiometry since, in this interval, minerals are most uniformly black. Lorenz[66] (1966) found the gray reflectances of some natural surfaces -- sand, concrete, coarse gravel, brick roof tile, fine basaltic gravel, asphalt and lawn to be in the range 0.027 to 0.062. Gray emittance can be found from gray reflectance using Kirchhoff's Law (Section 2.2).

(E) Emittance Changes

Gates[35] (1965) has pointed out that plants, like animals, must regulate their temperature in order to function at optimum physiological efficiency. This is accomplished through three mechanisms: radiation, transpiration and convection. The question arises: does a leaf adjust

its emittance in order to regulate its temperature? The emittance of a leaf can be changed by changing its surface geometry and/or its orientation. A change in environmental conditions can change the leaf moisture content, which in turn changes its surface geometry. The author believes, yet to be confirmed by experiments, that it is unlikely that a leaf adjusts its surface geometry in order to regulate its emittance and hence temperature, because it is much easier for a leaf to change its orientation in order to adjust its heat load and hence temperature. For example, on a hot sunny day, it can change its orientation with respect to direct sunlight to reduce solar radiation absorbed by it.

Conway and Van Bavel[19] (1966) reported that their radiometrically determined temperatures of the plant canopy could be explained by postulating a widely varying emittance of the plant canopy. They said that the possibility of widely varying emittance of the plant canopy exists since many changes occur in a plant canopy, as factors such as wind speed, solar radiation and water availability vary, but no attempt was made to study these.

(F) Stresses and Temperature of Plants

No important application of the infrared radiometry of plants has been discussed so far in this chapter. Do the stresses caused by insects, plant diseases, physiological disorders, nutrient deficiency and adverse environmental effects cause detectable temperature and/or emittance changes of the plants to be detected by remote means? This statement has not received much attention in the past, but it is a promising and a very useful field of research. Several authors [73, 105] have pointed out that the measurement of plant leaf temperatures is a technique for studying plant-water relations of agricultural crops, for estimating soil moisture, and detecting the occurrence and extent of soil salinity. It was pointed out in a paper by Myers and Allen [71] that the remote sensing of plant canopy temperatures appears feasible in assessing need for irrigation, or the extent and severity of drought; in determining distribution of precipitation on rangeland; in assessing the effect of slope on soil moisture distribution, etc.

It is well known that organisms have an optimum temperature for certain biological activity and that conditions are less favorable toward lower and higher temperatures[31]. These physiological processes are controlled by enzymes and other proteins in a complex manner; nevertheless certain definite reaction rates produce an end result which is temperature dependent. At very low temperatures all reactions may cease, and at too high a temperature, total destruction of organic complexes will occur and death will ensue. For example, soil temperatures too hot or too cold inhibit seed germination[8]. The tolerable temperature regimes for many plants is given by Gates[31] (1963).

Gates[38] (1970) has pointed out that the chemical status of plants determines normality or abnormality of growth. A chemical deficiency for a plant may cause chlorosis, premature yellowing and abscission of leaves, burning of leaf tips, bronzing, wilting, mottling, necrosis, water stress, cupping of leaves, flower-color changes, or other abnormalities. Abnormalities not only change the visual properties of the leaf surface (color, shape, size, pubescence), but also the leaf temperature relation to the incident energy absorbed and to the transpiration rate changes. An abnormality affecting the absorptance to incident sunlight will affect the energy budget and hence the leaf temperature. Changes in temperature are detected radiometrically. Thus, it is quite important to know the temperature of natural targets -- say plants -- to detect the subtle changes in temperature caused due to stresses.

Clum[18] (1926) and Curtis[24] (1936) noted that soil moisture stress could induce increases in plant leaf temperatures of 2° to 5° C. Gates (1963) found the temperature differences as great as 2° to 3° C in cotton as a result of moisture stress. Tanner[92] (1963) conducted studies which showed that the moisture stress of potatoes could increase their temperature up to 3° C. He concluded that the plant temperature may be a valuable qualitative index to differences in plant water regimes. Coupled with a better understanding of transfer processes at the plant surfaces, they may serve to provide quantitative data on plant-water status. The instrument used was a Barnes radiation thermometer which has an 8 to 13 μm spectral band pass filter. Cook and Dixon[22] (1964) found that a

definite and significant temperature gradient existed over an area of a tomato leaflet which was apparently due to the variations in transpiration across the leaflet. Leaves in which stomata were allowed to open naturally in response to light attained temperature about 5° C lower than leaves in which the stomata were forced to remain closed. Wiegand and Namken[105] (1966) found that a decrease in relative turgidity from 83% to 59% resulted in 3.6° C increase in $T_L - T_A$ (leaf minus air temperature). They also found that variations in plant moisture stress significantly altered leaf temperature and $(T_L - T_A)$.

They gave multiple regression equations and correlations of leaf temperature and $(T_L - T_A)$ with solar radiation, relative turgidity and air temperature, at a certain plant height, by moisture treatment. Cox and Boersma[23] (1967) observed a significant interaction between soil water stress and soil temperature for stomatal closures. Stomatal closure was observed even in the so-called wet range of soil water stress. Wear[102] (1966) and Wear et. al.[103] (1966) used infrared remote sensing successfully in studies of trees in the forest which were root rotted and attacked by insects. They found that the damaged trees without visible symptoms had a temperature up to 2° C higher than undamaged trees. Myers and Allen[71] (1968) gave four thermograms obtained with a Barnes infrared camera during a study of diurnal plant canopy temperature changes in small, differentially irrigated cotton plants. In each of the thermograms, the lighter tones indicated warmer targets. Results from two years of salinity -- plant temperature studies showed that the soil salinity at a particular site is highly correlated with cotton leaf temperature. A regression relationship was established between leaf minus ambient temperature and the average soil salinity level in the 1.6 meter profile[72].

Chang et al.* (1968) gave the relationship of temperature to the development of calcium deficiency symptoms in Nicotiana tabacum. Tabacco was grown in controlled environmental growth chambers at five different temperatures (21, 23, 26, 29 and 30° C). Plants grown at 21 and 23° C developed no Ca deficiency symptoms, and only a few plants of genetically susceptible varieties (Burley 21 and Ky Exp. 22) developed Ca deficiency symptoms when grown at 26° C. However, these varieties developed

---

* S. Y. Chang, R. H. Lowe and A. J. Hiatt, Ag. J., 60, p. 435, 1968.

very severe Ca deficiency symptoms when grown at either 29 or 30° C, because an increase in temperature resulted in Ca accumulation in the stems and failed to reach meristem and terminal leaves. Read and Ashford[79] (1968) studied the effects of varying levels of soil and fertilizer phosphorus and soil temperature on the growth and nutrient content of bromegrass and reed canarygrass. The study was conducted at three soil temperatures, on three soils, differing in levels of available phosphorus and applications of four rates of phosphatic fertilizer. Williamson and Splinter[106] (1969) reported that the survival and growth of Nicotiana tabacum L. to poor soil aeration was largely dependent on the ambient temperature and light intensity. Johannsen[55] (1969) did a detailed study on the detection of available soil moisture by remote sensing techniques. He found that available soil moisture in the root zone area did not show a definite relationship with reflective or thermal responses. It was determined that an interrelationship of plant cover, plant height and soil moisture exists, which is believed to show more positive relations to reflective and thermal response. Plant moisture samples taken during the September mission showed a progressively cooler thermal response with increasing plant moisture content.

Silva et al.[84] (1972) reported that a sulfur deficient corn plant in an ambient temperature of 24° C, and a nitrogen deficient corn plant in an ambient temperature of 23° C, was 1° C cooler and 2° C cooler, respectively, as compared to the healthy controlled plant when the surface located immediately behind the plants in both cases was 16.5° C. The preliminary conclusion made was that nutritionally stressed plants are not always hotter than a controlled plant, but apparently are influenced more strongly by environment.

Hagner[44] (1969) found that AGA thermovision thermal infrared camera proved to be well suited for the detection of differences in temperature among spruce seedlings (Picea abies (L) Karst) and within the crown of one seedling. Temperature varied with the water status of the seedlings, thus many types of pathological and physiological phenomena, which influence the water supply of the whole or parts of a seedling, could be detected by this method. Periferal parts of the seedling had different

temperatures from the rest of the foliage and succulent shoots, in particular. Characteristic temperatures of healthy seedlings indicated that variations in activity or vigor may result in measurable temperature differences. The apparatus had earlier been used in the field, carried by truck and helicopter, thus it may also be useful for the identification of insect and fungi attacks.

Gates [38] (1970) found that leaf temperature of alfalfa growing in saline soil to be 2° to 3° C warmer than the alfalfa grown in normal soil. He also found the temperatures of potassium-deficient sugercane leaves to be 0.5° C to 1.5° C warmer than normal leaves exposed simultaneously to the sunlight. Chapman [16] (1966) has given a thoroughly comprehensive compilation of information concerning diagnostic criteria for the chemical status of plants, but the book makes no references, whatsoever, to spectrophotometry or radiometry as useful diagnostic techniques. Carlson [15] (1971) has given a thorough discussion on the remote detection of moisture stress by field and laboratory experiments.

Bartholic et al. [8] (1972) used an airplane-mounted thermal scanner to measure irradiance in the 8 to 14 μm wavelength interval over an extensively instrumented agricultural area. The observed irradiances corresponded to cotton plant canopy temperature differences up to 6° C between the most and least water-stressed plots. They concluded that thermal imagery offers potential as a useful aid for delineating water-stressed and non-stressed fields, evaluating uniformity of irrigation, and evaluating surface soil water conditions.

The author made temperature measurements of healthy and blighted spots of the corn leaves alternately in the summer of 1972. These corn plants were grown at the Agronomy Farm of Purdue University. The temperature of blighted spots was higher than the healthy spot by an average (average of fifty readings) of 0.06° C (Section 5.7). Although the measurements were made on the healthy and blighted spots of the corn leaves only, the conclusions obtained from it may well be applicable to other non-systemic stresses. In conclusion, it must be said that the detection of stresses by thermal infrared remote sensing is an extremely useful and difficult task, and it requires considerable attention and research effort in the years to come.

CHAPTER III

REFLECTANCE MODEL OF A PLANT LEAF

3.1 Introduction

Willstätter and Stoll (W-S) in 1918 proposed a theory to explain[107] reflectance from a leaf on the basis of critical reflection of visible light at spongy mesophyll cell wall - air interfaces. According to several authors (i.e., Gates et al.[39] and Gausman et al.[42]) their experimental results on reflectance from leaves seem to have supported the W-S theory. Sinclair et al.[86] gave an excellent review of the reflectance and transmittance from the leaves. They critically examined the commonly accepted W-S theory and proposed a modification, termed the "diffuse reflectance hypothesis," which is based on diffusing reflecting qualities of cell walls oriented at near perpendicular angles. They pointed out that the microfibril structure of the cell wall presumably induces the scattering necessary to have diffuse reflectance. They presented experimental results on both the reflectance and transmittance from various species of leaves for both the visible (0.50 to 0.72 μm) and the reflective infrared (0.72 to 1.3 μm) wavelengths, which could not be satisfactorily explained by the W-S theory, but which they felt could be accounted for on the basis of their hypothesis.

Myers and Allen[71] explained the K-M (Kubelka - Munk) scattering coefficient (of diffuse reflectance) for a typical leaf by Fresnel reflections at normal incidence from 35 interfaces along the mean optical path through the leaf. Gausman et al.[41] noted that if oblique reflections are considered, fewer interfaces account for the results.

Knipling[56] emphasized that the air spaces within the palisade parenchyma layer of a leaf mesophyll may be more important in scattering light than air spaces in the spongy parenchyma layer. Allen et al.[1] have proposed that the complex structure of the leaf can be simulated by a pile of transparent plates with perfectly diffusing surfaces. Birth[11] has given an excellent critical review of existing concepts on the reflectance from a leaf. He pointed out that the work of Sinclair[86] is enlightening in that the diffuse character of light in the leaf is shown to start at the initial interface. Recently, Kumar[61] has reviewed much literature pertaining to reflection from leaves.

The purpose of this investigation is to compare the reflectance of a typical leaf found by tracing the ray of light through the leaf with the experimentally determined reflectance values of the same leaf. In addition, the authors would like to investigate if considering only cell wall and air as the optical mediums in ray tracing leads to good predictions of experimentally determined reflectance of the leaf; and if other optical mediums -- cell sap and chloroplasts -- should also be included in the ray tracing for significantly better prediction of the reflectance. Furthermore, the authors would like to create a more realistic illustration to show the pathway of a light ray through the leaf than shown by Willstatter and Stoll (Figures 3.1.1 to 3.1.3).

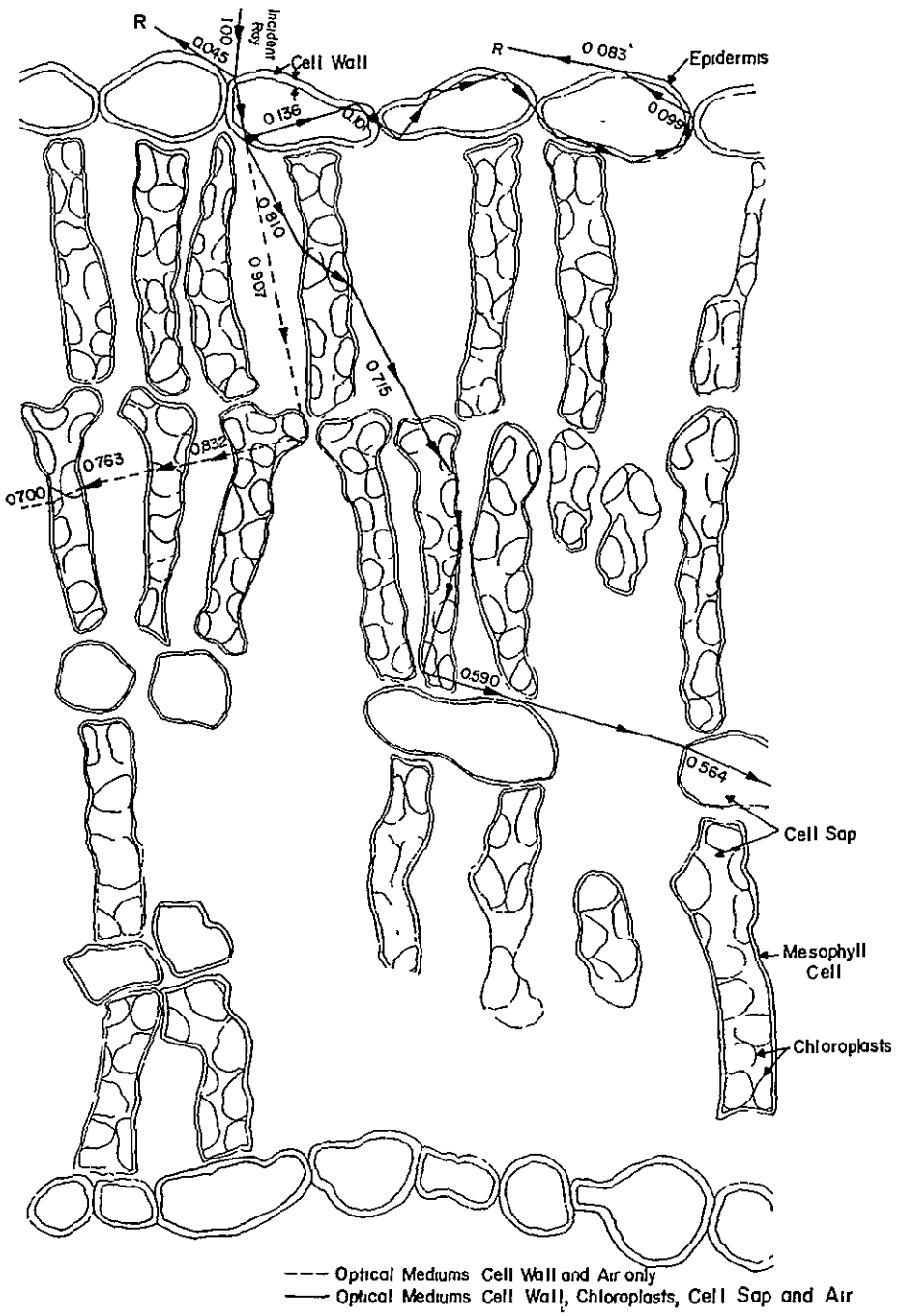

Figure 3.1.1 Pathway of Light Ray Through the Leaf Cross Section. R denotes the reflected ray. Solid lines show the pathway of light considering cell wall, chloroplasts, cell sap and air as the optical mediums. Dotted lines show the pathway of light considering only cell wall and air as the optical mediums. The numbers along the rays denote their total intensity. The rays whose total intensity is less than 0.05 are not shown.

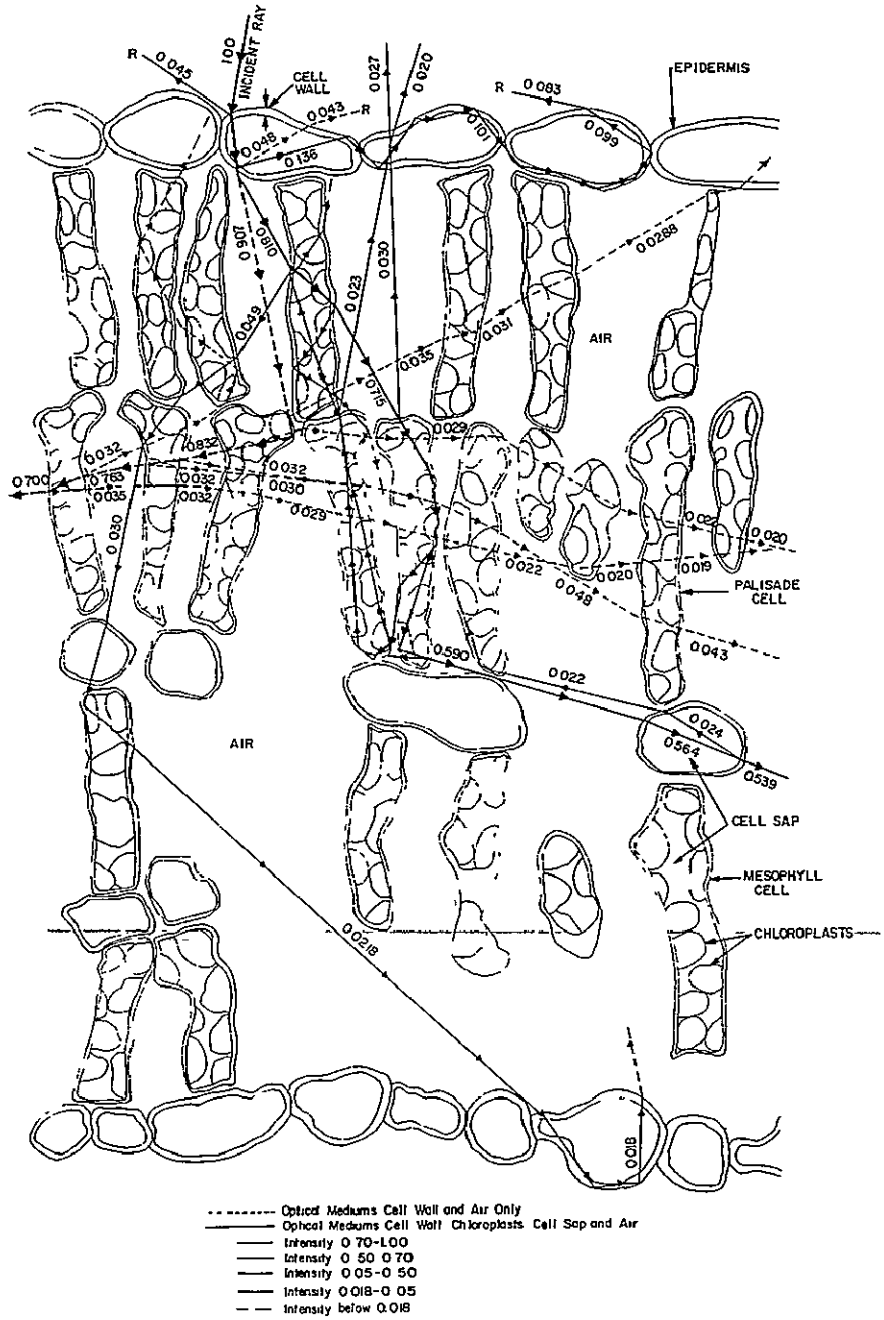

Figure 3.1.2 Pathway of Light Ray Through the Leaf Cross Section. R denotes the reflected ray. Solid lines show the pathway of light considering cell wall, chloroplasts, cell sap and air as the optical mediums. Dotted lines show the pathway of light considering only cell wall and air as the optical mediums. The numbers along the rays denote their total intensity. The rays whose total intensity is less than 0.018 are not shown.

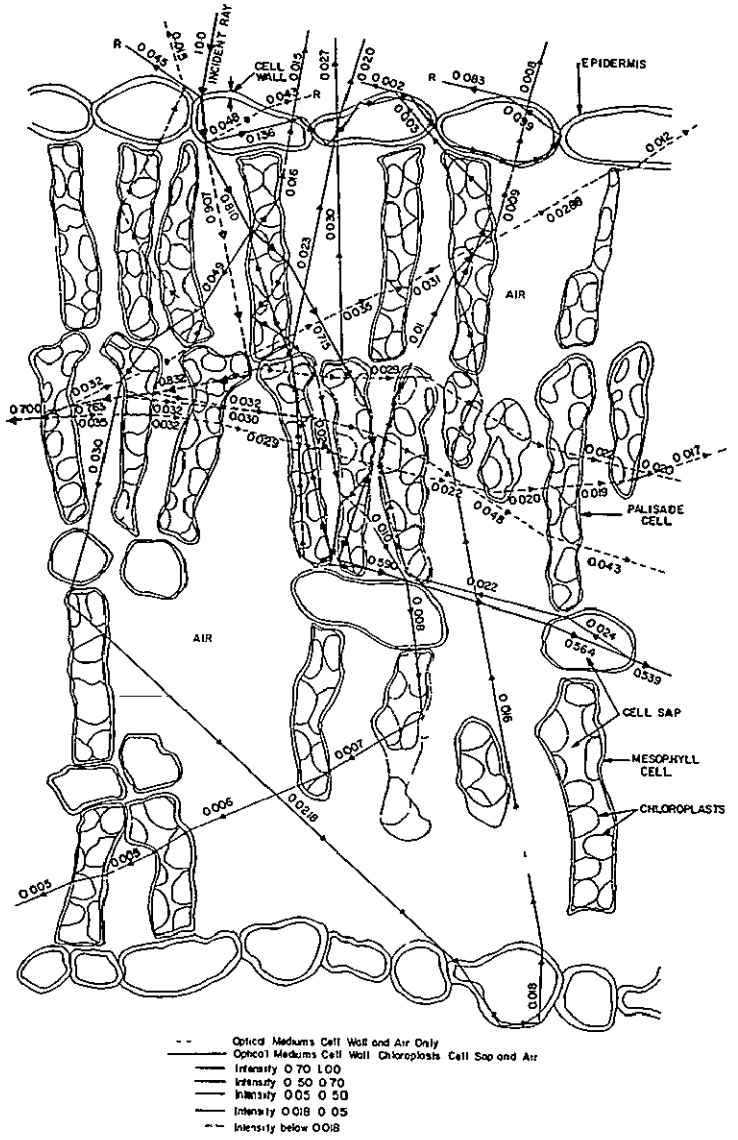

Figure 3.1.3 Pathway of Light Ray Through the Leaf Cross Section. R denotes the reflected ray. Solid lines show the pathway of light considering cell wall, chloroplasts, cell sap and air as the optical mediums. Dotted lines show the pathway of light considering only cell wall and air as the optical mediums. The numbers along the rays denote their total intensity. All the rays whose total intensity is more than or equal to 0.018 are shown. Some of the rays whose total intensity is less than 0.018 are also shown.

3.2 Cross Section of the Soybean Leaf

The cross section of the soybean (Glycine max (L.) Merrill) leaf was taken from Sinclair's thesis.[85] This cross section had been obtained by Sinclair by microtome cross-sectioning and a microscopic slide was prepared using the techniques outlined by Jensen.[54] This cross section was enlarged. An artist, well familiar with the cross section of leaves, drew the above mentioned cross section on a plain paper showing explicitly the cell walls, cell sap and chloroplasts, a part of which is shown in each of Figures 3.1.1 to 3.1.3. The cross section shown in these figures was enlarged in order to do ray tracing conveniently and accurately.

3.3 Reflectance From a Leaf

(A) Proposed Leaf Reflectance Model

The following assumptions are made in the reflectance model of a leaf:

1. The leaf is assumed to consist of homogeneous and isotropic media -- cell wall, chloroplasts, cell sap and air. This assumption is made for mathematical simplicity so that Fresnel's Equations can be applied at each interface.
2. Geometrical Optics is assumed to be valid for the media of the leaf mentioned above. This is not quite valid for chloroplasts (typical dimensions 5 μm to 8 μm in diameter and about 1 μm in width[39]) where diffraction is likely to be important.
3. The Rayleigh and Mie scattering by the leaf constituents (of the order of wavelength of light or smaller) is neglected. Gates[39] pointed out that cell dimensions of a leaf are generally too large for scattering; however, the chloroplasts and grana dimensions are such as to create some scattering (i.e., grana is about 0.5 μm in length and about 0.05 μm in diameter). Scattering could also be caused by mitochondria, ribosomes, nuclei, starch grains, and other plastids, etc. It is very hard to take scattering into account because the dimensions, distribution and refractive indices of these particles in the leaf cells are extremely complex and unknown.
4. The absorption of light by the leaf media is neglected. This is quite valid for most leaves in about 0.7 to 1.3 μm wavelength region. Since the leaf media absorb the light in the visible wavelengths, their indices of refraction are complex numbers. The model presented here can also be applied to the visible wavelengths for Fresnel's Equations and Snell's Law are also valid for absorbing media, if one

uses the appropriate complex index of refraction.[104] However, the ray tracing is not done in this chapter for the visible wavelengths since the complex indices of refraction of the leaf constituents in these wavelengths are not yet known. Also, the ray tracing in the visible wavelengths becomes quite involved because the index of refraction, angle of refraction, etc., are complex numbers.

5. The two dimensional cross section of a leaf (three dimensional leaf) is used for predicting the reflectance from a leaf.

(B) Basic Equations

Fresnel's Equations, Snell's Law and boundary conditions used for determining reflection and refraction at an interface are given below.[104]

$$m_1 \sin \theta_i = m_2 \sin \theta_r \qquad (3.3.1)$$

$$R_{\parallel} = \left[\frac{\left(\frac{m_2}{m_1}\right)^2 \cos \theta_i - \left[\left(\frac{m_2}{m_1}\right)^2 - \sin^2\theta_i\right]^{1/2}}{\left(\frac{m_2}{m_1}\right)^2 \cos \theta_i + \left[\left(\frac{m_2}{m_1}\right)^2 - \sin^2\theta_i\right]^{1/2}} \right]^2 I_{\parallel} \qquad (3.3.2)$$

$$R_{\perp} = \left[\frac{\cos \theta_i - \left[\left(\frac{m_2}{m_1}\right)^2 - \sin^2\theta_i\right]^{1/2}}{\cos \theta_i + \left[\left(\frac{m_2}{m_1}\right)^2 - \sin^2\theta_i\right]^{1/2}} \right]^2 I_{\perp} \qquad (3.3.3)$$

$$R = \frac{R_{\parallel} + R_{\perp}}{2} \qquad (3.3.4)$$

$$T_{||} = I_{||} - R_{||} \tag{3.3.5}$$

$$T_{\perp} = I_{\perp} - R_{\perp} \tag{3.3.6}$$

$$T = \frac{T_{||} + T_{\perp}}{2} \tag{3.3.7}$$

where

m_1 = refractive index of the first medium

m_2 = refractive index of the second medium

θ_i = angle of incidence

θ_r = angle of refraction

$R_{||}$ = reflection parallel to the plane of incidence

$R_{\perp}$ = reflection perpendicular to the plane of incidence

R = total reflection

$I_{||}$ = incident intensity parallel to the plane of incidence

$I_{\perp}$ = incident intensity perpendicular to the plane of incidence.

$T_{||}$ = transmission parallel to the plane of incidence

$T_{\perp}$ = transmission perpendicular to the plane of incidence

T = total transmission

(C) Indices of Refraction of Leaf Constituents

The index of refraction of the air spaces in the leaf cells is assumed to be one. The refractive index of a potato cell wall was found to be equal to 1.52 by Renck[80] in the visible wavelengths by Index Matching Technique (i.e., The cell wall was infiltrated with various liquids, mostly oils, having varying refractive indices. The minimum reflectance was noted visually with a medium having a refractive index of 1.52, which was taken to be the best approximation to the

refractive index of the potato cell wall.). The value of the index of refraction of the cell wall of the soybean leaf was assumed to be equal to 1.52 for the purpose of ray tracing, as it is likely to be close to the refractive index of the potato cell wall. The values of refractive indices for cell sap and chloroplasts were taken from Charney and Brackett[17] to be equal to 1.36 and 1.42, respectively. The values of the index of refraction of the leaf constituents in the 0.7 μm - 1.3 μm region are not available because it is quite difficult to measure the refractive indices of the leaf constituents by the Index Matching Technique in the infrared wavelength region as the human eye cannot see in that region. The value of the real part of the index of refraction of water is roughly the same in the near infrared region[52] (i.e., 0.7 μm to 1.3 μm) as in the visible wavelength region within .01. Since water is the main constituent of the cell wall, cell sap and chloroplasts, and since none of these absorb light strongly in the 0.7 μm - 1.3 μm region, the refractive indices of these constituents were assumed to be the same in the 0.7 μm - 1.3 μm region as in the visible wavelength region.

(D) Method of Ray Tracing

The four leaf constituents -- cell wall, chloroplasts, cell sap and air -- give rise to the following eight optical interfaces in the leaf all of which were considered in the ray tracing: 1) air to cell wall, 2) cell sap to cell wall, 3) chloroplasts to cell wall, 4) cell sap to chloroplasts, 5) chloroplasts to cell sap, 6) cell wall to chloroplasts, 7) cell wall to cell sap, and 8) cell wall to air.

In ray tracing, a ray of light of intensity $I_{||}$ (intensity parallel to the plane of incidence) = 1.000, and $I_{\perp}$ (intensity perpendicular to the plane of incidence) = 1.000 at about 5° to the normal was taken. The angle was taken 5° to the normal, because in the experimental setup with the DK-2A spectroreflectometer the light rays were incident at 5° to the leaf normal. A tangent and a normal were drawn at the interface. The angle of incidence of the ray was measured with a drafting set which can measure angles up to an accuracy of 5 minutes. Knowing the angle of incidence and relative index of refraction at the interface, the values of θ_r, $R_{||}$, $R_{\perp}$, $T_{||}$, and $T_{\perp}$ were found using equations given in

Section 3.3 "Basic Equations", and the refracted and reflected rays were drawn. Similar procedure was followed at the subsequent interfaces. Each ray was continued until it ended up as reflection or transmission from the leaf. The rays whose total intensity became less than 0.018 were discontinued to reduce the time and efforts required in ray tracing.

The light ray passed through a total of 253 interfaces out of which total internal reflection took place at 18 cell wall - air interfaces, two cell wall - chloroplast interfaces, and one cell wall - cell sap interface.

Table 3.3.1(A) shows the values of the reflected and transmitted intensity of the ray at the interfaces. Only the rays whose intensity is more than 0.05 are shown in Table 3.3.1(A). The pathway of the ray in a part of the leaf cross section, as given by this model, is shown by solid lines in Figure 3.1.1. The numbers along the rays represent their total intensity. Only the rays whose total intensity is more than 0.05 are shown in Figure 3.1.1. Figure 3.1.2 is a more complete version of Figure 3.1.1 in that the rays whose total intensity lie between 0.018 and 0.05 are also shown in Figure 3.1.2. Figure 3.1.3 is a more complete version of Figure 3.1.2 in that some of the rays whose total intensity is less than 0.018 are also shown in Figure 3.1.3.

Ray tracing was also done following the same procedure as the one mentioned above for the same original ray of light ($I_{||} = 1.000$ and $I_{\perp} = 1.000$) except that only the following two interfaces were considered: 1) air to cell wall and 2) cell wall to air. The light ray passed through a total of 144 interfaces out of which total internal reflection took place at 13 cell wall - air interfaces. Table 3.3.1(B) shows the values of the reflected and transmitted intensity of the ray at each interface. The pathway of the ray considering the above two interfaces, in a part of the leaf cross section, is shown in Figures 3.1.1 to 3.1.3 by dotted lines. It can be seen from Figures 3.1.1 to 3.1.3 that the light ray shown by dotted lines follows quite a different path than that shown by solid lines.

Ray tracing was also done through the palisade cells of a part of the cross section of a soybean leaf, following exactly the same procedure reported above. The light ray was taken at an angle of about

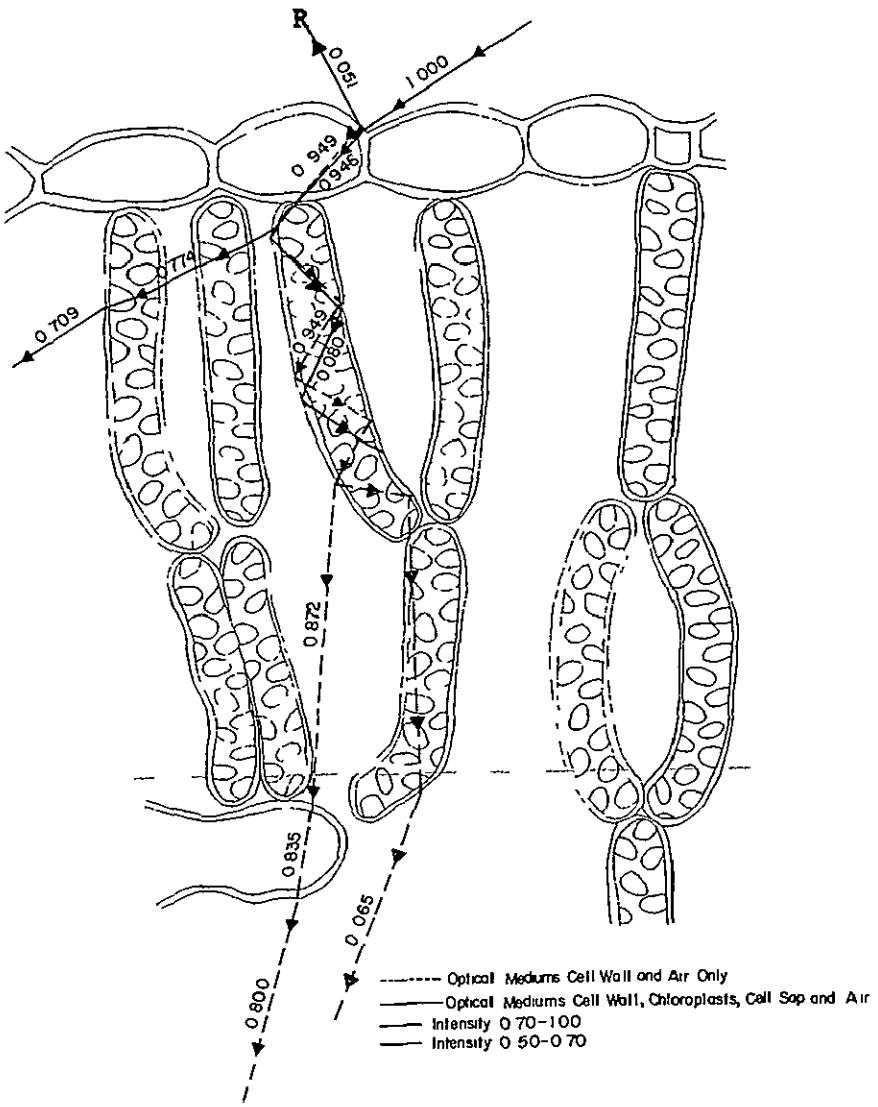

Figure 3.3.1 Pathway of Light Ray Through the Palisade Cells. R denotes the reflected ray. Solid lines show the pathway of light considering cell wall, chloroplasts, cell sap and air as the optical mediums. Dotted lines show the pathway of light considering only cell wall and air as the optical mediums. The numbers along the rays denote their total intensity. The rays whose total intensity is less than 0.05 are not shown.

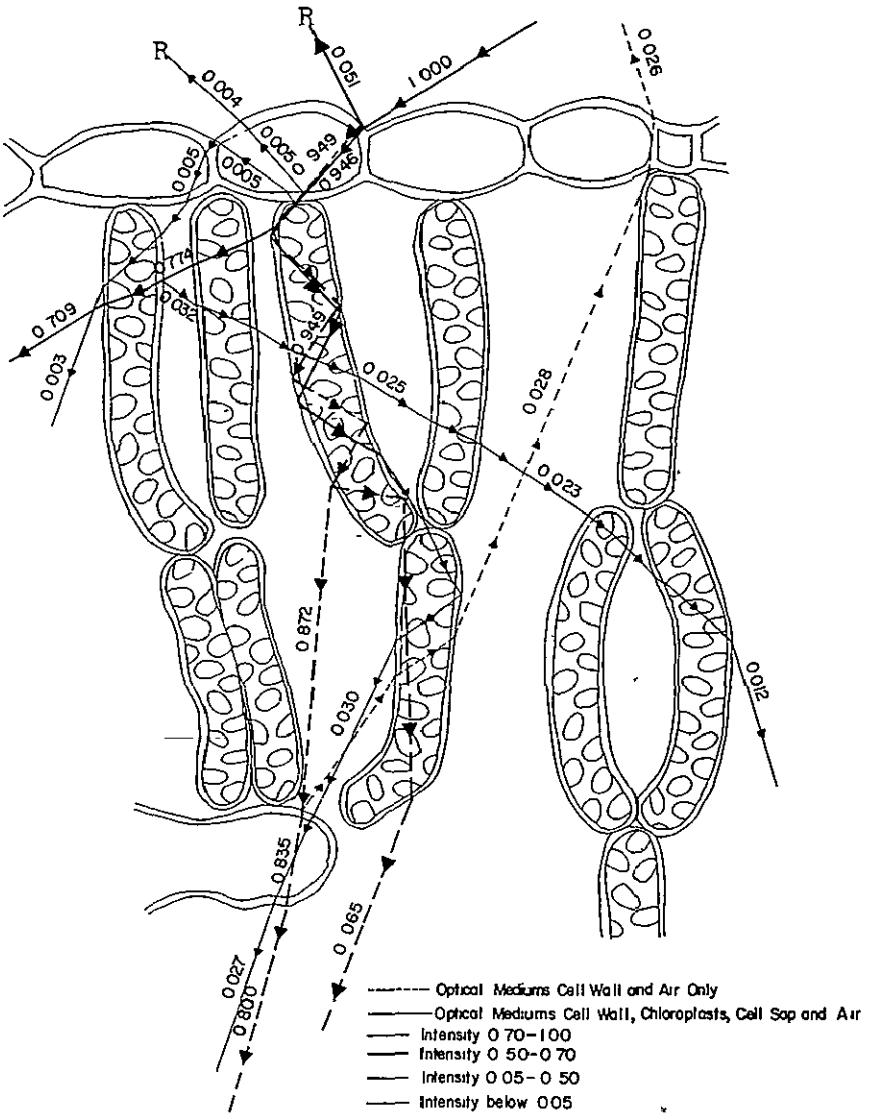

Figure 3.3.2 Pathway of Light Ray Through the Palisade Cells. R denotes the reflected ray. Solid lines show the pathway of light considering cell wall, chloroplasts, cell sap and air as the optical mediums. Dotted lines show the pathway of light considering only cell wall and air as the optical mediums. The numbers along the rays denote their total intensity. All the rays whose total intensity is more than or equal to 0.05 are shown. Some of the rays whose total intensity is less than 0.05 are also shown.

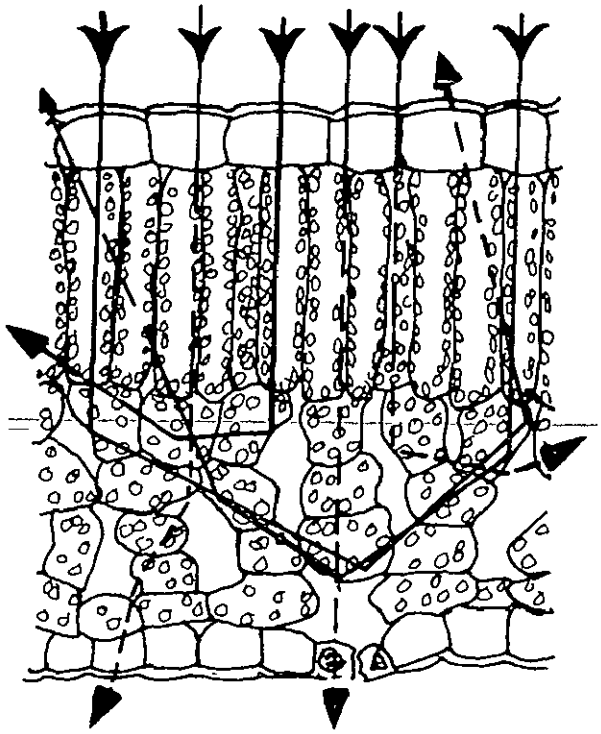

Figure 3.3.3 Pathway of Light Through a Leaf as Envisioned by Willstatter and Stoll Theory. (Taken From Sinclair[86])

60° to the leaf normal. The light ray was not drawn through the complete cross section because the only purpose of this ray tracing was to create a realistic illustration to show the pathway of a light ray, incident at an oblique angle to the leaf normal, through the palisade cells. Tables 3.3.1(C) and 3.3.1(D) show the values of the reflected and transmitted intensity of the ray at the interfaces in the palisade cells considering all the eight interfaces outlined in Section 3.3(D), and considering only cell wall - air and air- cell wall interfaces, respectively. Only those rays whose intensity is more than 0.05 are shown in the Tables 3.3.1(C) and 3.3.1(D).

Figure 3.3.1 shows the pathway of light through the palisade cells exactly similar to the Figure 3.1.1 (which shows the pathway of light through a leaf cross section). Only the rays whose total intensity is more than 0.05 are shown in Figure 3.3.1. Figure 3.3.2 is the same as Figure 3.3.1 except that some of the rays whose total intensity is less than 0.05 are also shown for illustration.

It can be understood from Figures 3.1.3 and 3.3.2 that if one takes a number of parallel rays incident on the leaf, each ray will encounter different geometrical internal surfaces and consequently will be reflected and transmitted in different directions. That is how a collimated beam of light incident on the leaf keeps on becoming diffuse slowly as it passes through the leaf. The greater the number of interfaces the light rays encounter in their path, the more diffuse the rays are likely to be. The pathway of light rays as envisioned by Willstatter and Stoll is shown in Figure 3.3.3. It can be seen from Figure 3.3.3 that the light rays pass through the epidermis and palisade cells without any deviation, which is unrealistic. Furthermore, Willstatter and Stoll did not show the reflection of light at air - cell wall interfaces, and cell wall - air interfaces at angles of incidence less than the critical angle. The author would like to emphasize that although cell wall - air interface causes more deviation of the ray than any other single interface for a given angle of incidence, and is perhaps the most important interface for contributing to the reflection from the leaf, the other interfaces can also contribute significantly to the reflection from a leaf (Figure 3.3.4).

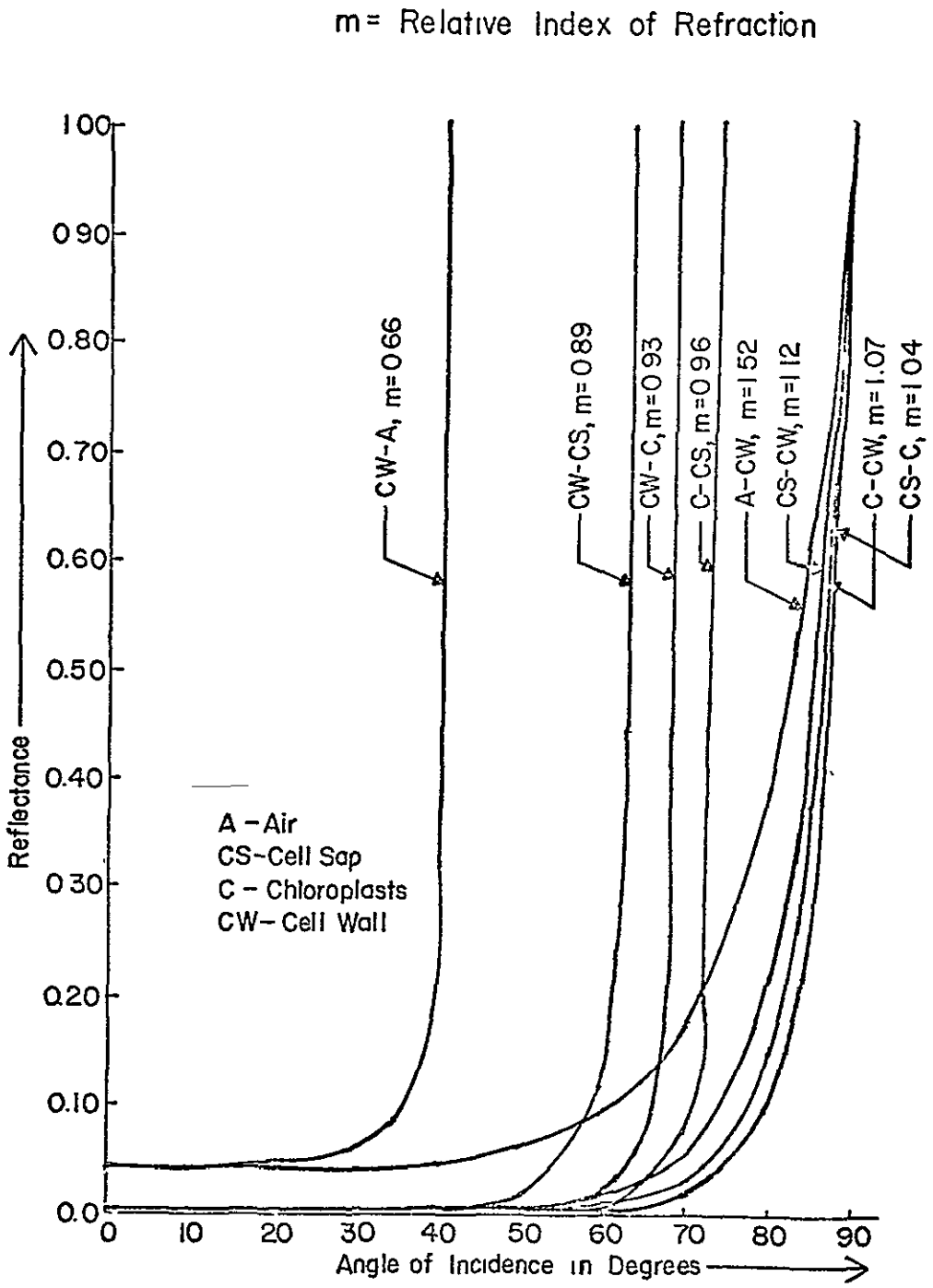

Figure 3.3.4 Reflectance vs. Angle of Incidence for Optical Interfaces of a Leaf

Nomenclature for Tables 3.3.1 (A) to 3.3.1 (D)

Tables 1(a) to 1(d) show the intensity of the reflected ray and the transmitted ray at each interface. The total intensity of the incident ray is taken to be 1.000. The rays whose total intensity (reflected and transmitted) is less than 0.05 are not shown in the tables.

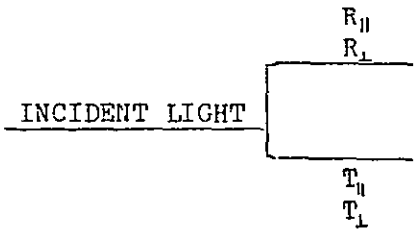

$R_{\parallel}$ = reflection $\parallel$ to the plane of incidence
$R_{\perp}$ = reflection $\perp$ to the plane of incidence
$T_{\parallel}$ = transmission $\parallel$ to the plane of incidence
$T_{\perp}$ = transmission $\perp$ to the plane of incidence

R = denotes that the ray has ended up as reflection
T = denotes that the ray has ended up as transmission
t = denotes total internal reflection
xx = denotes that the ray is discontinued in the table because its total intensity is less than 0.05.
--- = denotes that the value of intensity is less than 0.0005

AW Air to Cell Wall
SW Cell Sap to Cell Wall
CW Chloroplasts to Cell Wall
SC Cell Sap to Chloroplasts
CS Chloroplasts to Cell Sap
WC Cell Wall to Chloroplasts
WS Cell Wall to Cell Sap
WA Cell Wall to Air

Table 3.3.1(A) The Values of the Reflected and Transmitted Intensity of the Ray at Each Interface of the Leaf Cross Section. The rays whose total intensity (reflected + transmitted) is less than 0.05 are not shown in the table. The optical mediums considered are cell wall, chloroplasts, cell sap and air. The pathway of light rays whose intensity is given in this table is shown by the solid lines of Figure 3.1.1.

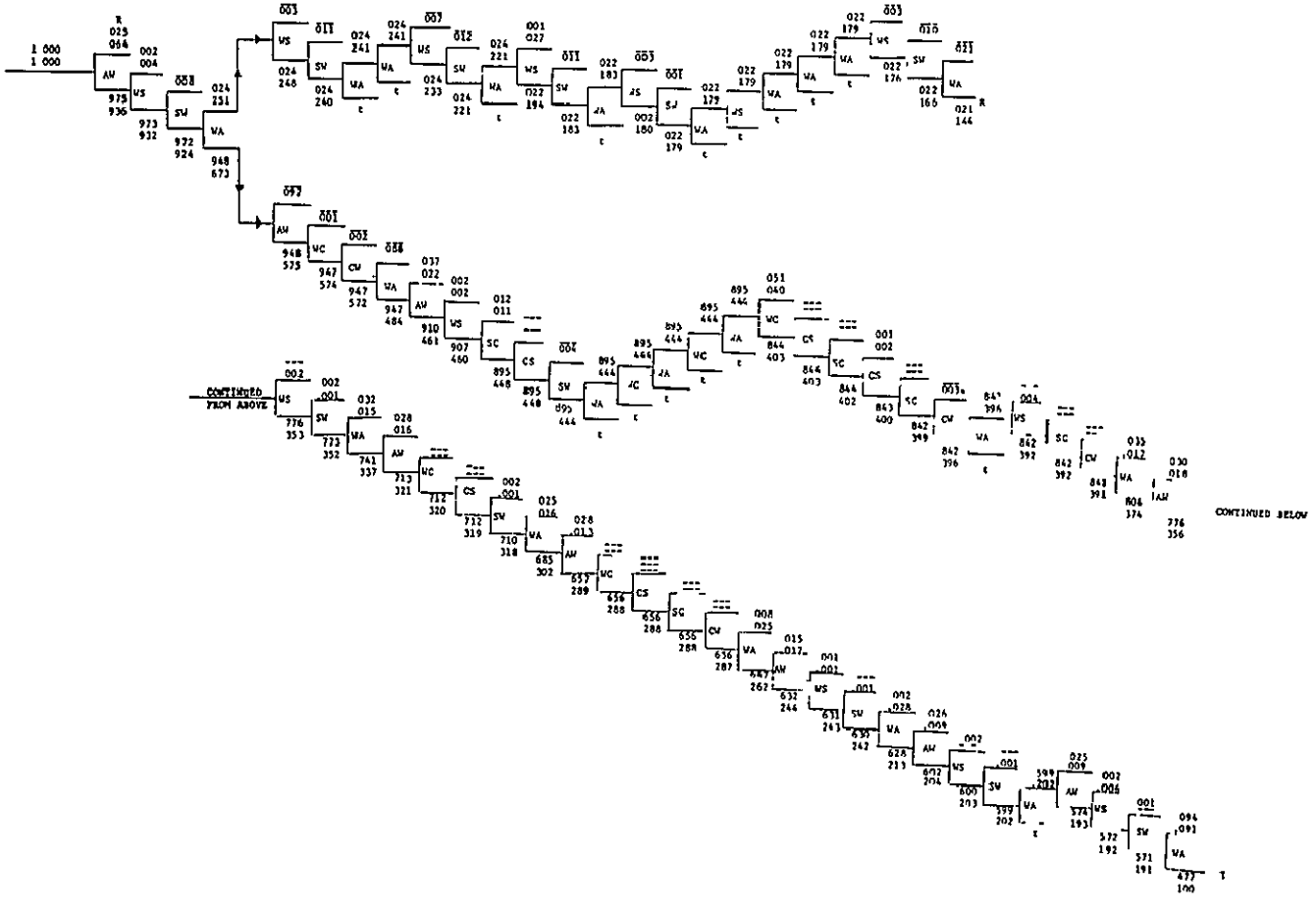

Table 3.3.1(B) The Values of the Reflected and Transmitted Intensity of the Ray at Each Interface of the Leaf Cross Section. The rays whose total intensity (reflected + transmitted) is less than 0.05 are not shown in the table. The optical mediums considered are cell wall and air. The pathway of light rays whose intensity is given in this table is shown by dotted lines of Figure 3.1.1.

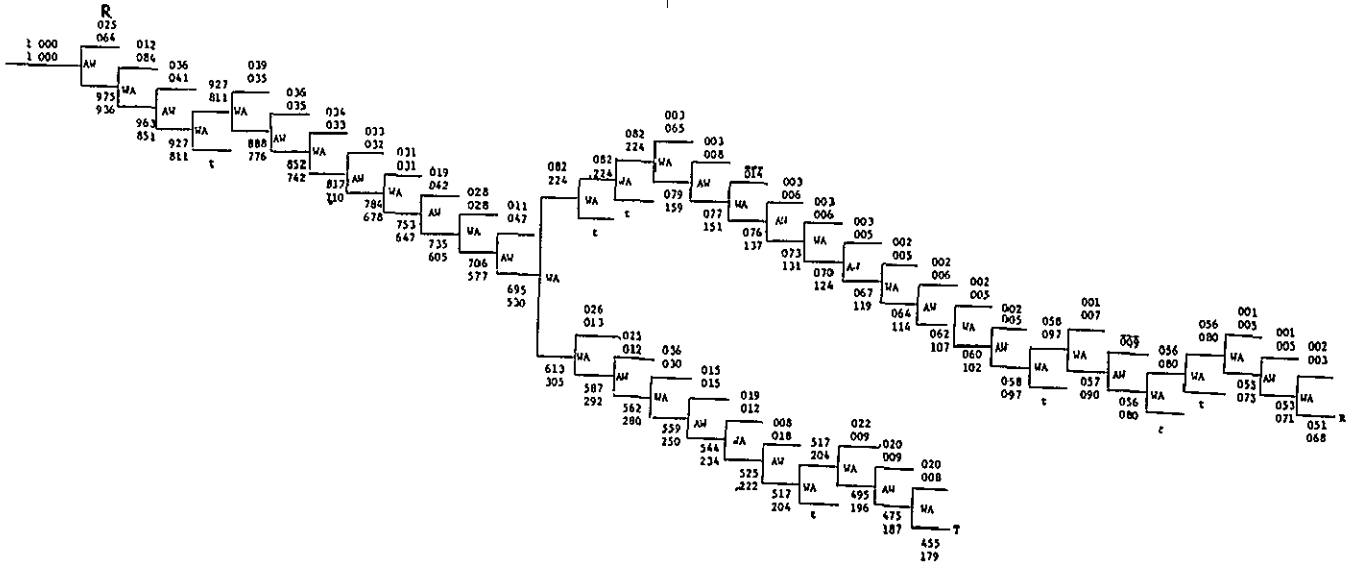

Table 3.3.1(C) The Values of the Reflected and Transmitted Intensity of the Ray at Each Interface of the Palisade Cells. The rays whose total intensity (reflected + transmitted) is less than 0.05 are not shown in the table. The optical mediums considered are cell wall, chloroplasts, cell sap and air. The pathway of light rays whose intensity is given in this table is shown by the solid lines of Figure 3.3.1.

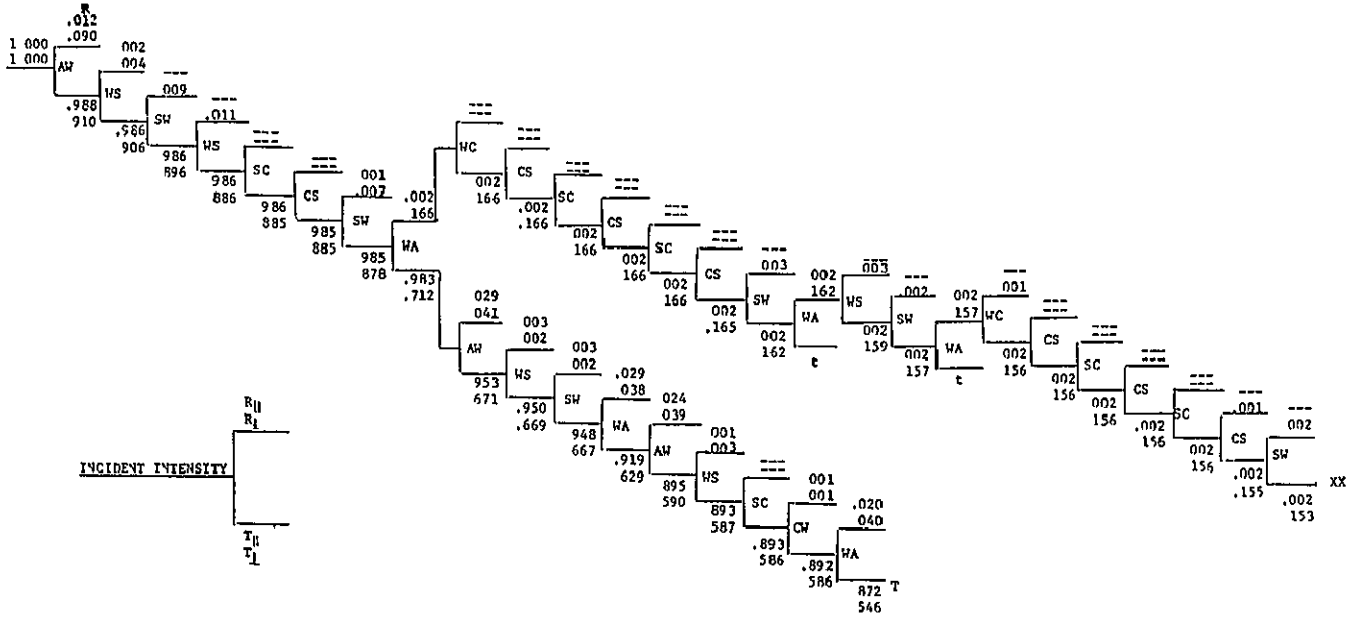

Table 3.3.1(D) The Values of the Reflected and Transmitted Intensity of the Ray at Each Interface of the Palisade Cells. The rays whose total intensity (reflected + transmitted) is less than 0.05 are not shown in the table. The optical mediums considered are cell wall and air. The pathway of light rays whose intensity is given in this table is shown by the dotted lines of Figure 3.3.1.

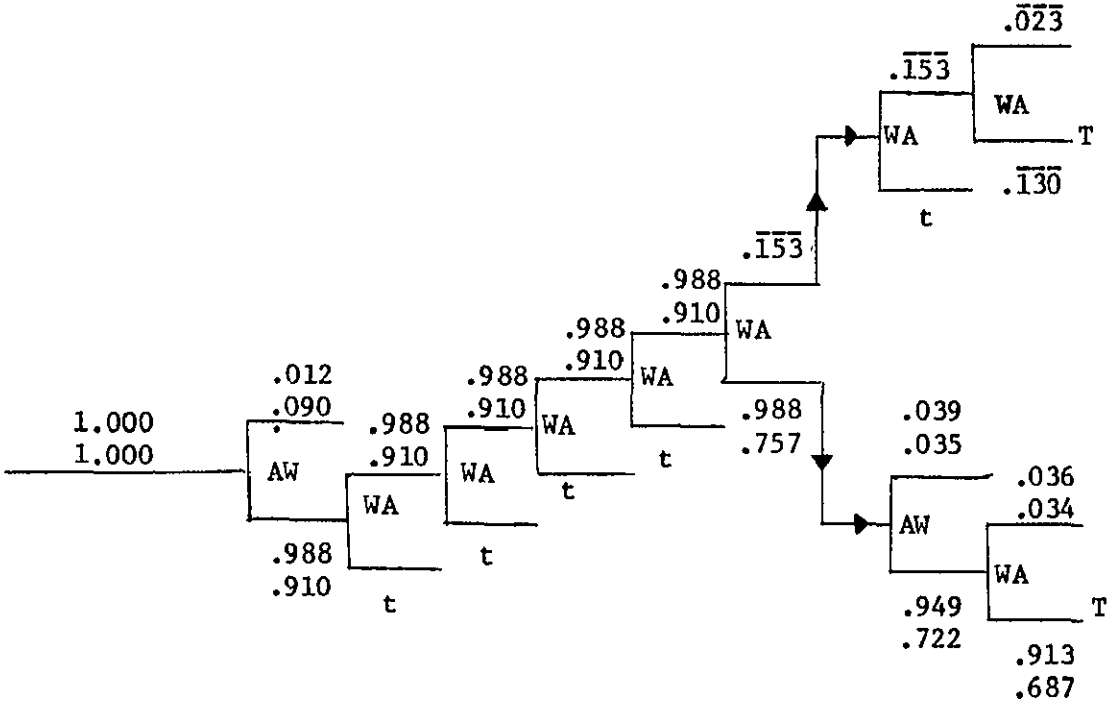

It seems that the reflection of light in the near infrared wavelengths (0.7 - 1.3 μm) from a typical leaf is likely to be more diffuse than its reflection in the visible wavelengths. This is because the near infrared light rays are likely to pass through many more interfaces of the leaf (because of almost no absorption of light in the near infrared wavelengths) than the corresponding light rays of the visible wavelengths. Also, the transmission from a leaf in the visible as well as near infrared wavelengths is likely to be fairly diffuse because a typical light ray has to pass through a fairly large number of interfaces before it is transmitted. These qualitative conclusions support the experimental results of Breece and Holmes[12] on healthy green soybean and corn leaves.

(E) Experimental and Ray Tracing Results

The value of reflection found by Sinclair[85] using a Beckman DK-2A Spectroreflectometer on the same leaf, whose cross section is shown in Figure 3.1.2, in the 0.7 - 1.3 μm region, was 47%. Transmission = 100 - 47 = 53% (because absorption of a leaf is almost equal to zero in the 0.7 - 1.3 μm wavelength region).

Ray Tracing Results. Note: The values of (reflection + transmission) found were assumed to be 100%.

Reflection (using 8 interfaces mentioned in sec. 3.3(D)) = 45.6%

Transmission (using 8 interfaces mentioned in sec. 3.3(D)) = 54.4%

Reflection (using air - cell wall and cell wall - air interfaces) = 30.3%

Transmission (using air - cell wall and cell wall - air interfaces) = 69.7%

Experimental results of Woolley[109] on the soybean leaves strongly support these ray tracing results. Woolley found the reflectance of a soybean leaf in 0.7 - 1.3 μm wavelength region to be about 47 percent. But after the soybean leaf was vacuum infiltrated with oil of refractive index 1.48, which essentially eliminated the air to cell wall and cell

wall to air interfaces only, its reflectance dropped to about 15 percent. This experiment clearly shows that the reflectance caused by the discontinuities in the indices of refraction of the geometrical surfaces (of the dimensions much larger than the wavelength of light) is significantly more than the reflection caused due to Rayleigh and/or Mie scattering by the particles (of the order of wavelength of light or smaller) inside the leaf cells because the reflectance caused by scattering should essentially remain unchanged after the leaf is vacuum infiltrated with oils of different refractive indices. Furthermore, it seems to support the author's conclusion "optical interfaces other than the cell wall to air and air to cell wall can contribute significantly to the reflection from a leaf."

3.4 Conclusions

The preliminary conclusions, yet to be confirmed by further ray tracing, and experiments are: considering only cell wall - air and air - cell wall interfaces seems to underestimate the reflection and overestimate the transmission from a leaf significantly in this particular case. Considering all the eight interfaces mentioned in Section 3.3(D), ray tracing seems to give results very close to the experimental results. Furthermore, considering only cell wall - air and air - cell wall interfaces is likely to give less diffuse reflectance and transmittance than that given by considering all the eight interfaces. There is some contribution to the reflection from a leaf due to Rayleigh and Mie scattering caused by the particles (of the order of the wavelength of light or smaller) in the leaf cells but the reflection caused by the leaf constituents -- cell walls, cell sap, chloroplasts, and air -- as given by the geometrical optics, is probably more significant than the reflection caused by scattering. Gates[39] pointed out that whatever scattering does exist is probably more of the Mie type than the Rayleigh type because the scattering phenomena is not strongly wavelength dependent. The model presented here can also be applied to the visible wavelengths if the appropriate complex indices of refraction of the leaf constituents in the visible wavelengths are known. The author believes that the model of a leaf presented in this article is more complete and realistic than as proposed by Willstätter and Stoll. It supports the experimental results of Breece and Holmes,[12] and Woolley.[109]

CHAPTER IV

SIMPLIFIED THERMAL EMISSION MODEL OF A PLANT CANOPY

4.1 Formulation of the Problem

Consider a plant canopy consisting of leaves, stems etc. on a soil background. Let the thermal long wavelength (4 to 14 μm) radiation coming from the plant canopy which is received by the sensor of the aircraft or satellite, be in the direction having direction cosines s_1, s_2, s_3. Direction s_1, s_2, s_3 is called the direction of the sensor. The expression for radiant flux density emitted by a plant canopy of any given geometry (orientation and area of leaves, stems, etc.) in the direction of the sensor was derived by Kumar[61], pp. 62-71. A more simplified but reasonably accurate expression of the emitted radiant flux density by a plant canopy received by the sensor of the aircraft or satellite is derived here.

Assumptions

1. We are sensing in the wavelength region 4 to 14 μm. Thus, the solar radiation reflected by a typical natural target can be neglected as compared to the radiation emitted by it (Section 2.5(C)).
2. The transmission of leaves and stems is assumed to be zero in the long wavelength region (i.e., 4 to 14 μm). This is because of the strong water absorption bands in the infrared wavelength region[52].
3. Multiple reflections from the leaves are neglected. Reflection by a leaf in the wavelength region 4 to 14 μm is usually quite small-(Section 2.6 (C)) so that multiple reflections from leaves can be safely neglected. Similarly, the radiation reflected by the soil and further reflected by

the leaves is neglected.

4. Assume that the leaves and soil emit the radiation diffusely. This assumption may not be valid. Experiments need to be conducted to check the validity of this assumption. However, this assumption is made for mathematical simplicity.

4.2 Radiation Emitted by a Plant Canopy

(A) Radiation Emitted by Leaves

Radiation is reflected and emitted from the leaves. The expression for radiation flux emitted by the leaves reaching the sensor (of aircraft or satellite) is derived as follows.

Consider a small element of a leaf of area, δa_ℓ, whose normal makes an angle θ with the direction of the sensor. The radiant flux emitted by the leaf reaching the sensor in the limit $\delta a_\ell \to 0$ is given by

$$F_\ell = \int_{\substack{\text{visible} \\ \text{from the} \\ \text{sensor}}} \frac{\epsilon(\ell)\, \sigma T_\ell^4\, A_d \cos\theta\, da_\ell}{r^2} \qquad (4.2.1)$$

where

summation is carried over all the leaves visible from the sensor

T_ℓ = temperature of the leaf

$\epsilon(\ell)$ = emittance of the leaf at temperature T_ℓ

σ = Stefan-Boltzmann constant

r = distance of the differential element of the leaf, da_ℓ, from the sensor

A_d = projected area of the detector receiving radiation, normal to the direction of the sensor

A plant canopy can be considered to be consisting of two parts: sunlit and shaded (some shaded areas may not be completely shaded because of scattered solar radiation reaching in those areas). The temperature of a leaf may vary from one spot of the leaf to another (Section 5.4). Also, the temperature of the leaves of the plant canopy may vary from one leaf to another. However, for simplification of Equation (4.2.1), let us assume that the sunlit leaves are at a mean temperature of $T(\ell,S)$ and the shaded leaves are at a mean temperature of $T(\ell,s)$. Let the mean emittance of the leaves be $\bar{\epsilon}(\ell)$. Since the distance of the sensor from the plant canopy is much larger than the dimensions of the plant canopy,

r can be assumed to be a constant. Thus, F_ℓ of Equation (4.2.1) can be approximated as

$$F_\ell = K\bar{\varepsilon}(\ell)\ [T(\ell,S)^4\ A_{\ell S} + T(\ell,s)^4\ A_{\ell s}] \qquad (4.2.2)$$

where

$$K = \frac{\sigma A_d}{r^2} = \text{constant}$$

$A_{\ell S}$ = total projected area of the visible (from the sensor) sunlit leaves normal to the direction of the sensor

$A_{\ell s}$ = total projected area of the visible (from the sensor) shaded leaves normal to the direction of the sensor

(B) Radiation Emitted by Stems

Stems have been neglected by most authors in building the model of a plant canopy. However, stems could contribute significantly to the spectral properties of a plant canopy[61]. Consider the stem as a cylinder. Let the area of a small longitudinal section (the product of diameter and length) of the stem be denoted by δa^*. To obtain an expression for the emitted radiant flux density, F^*, by the stems, one can replace a_ℓ by a^* in Equation (4.2.1) obtaining an expression similar to Equation (4.2.2), i.e.,

$$F^* = K\bar{\varepsilon}^*\ [T^*(S)^4\ A_{*S} + T^*(s)^4\ A_{*s}] \qquad (4.2.3)$$

where

$*$ = denotes the quantities for the stem corresponding to the quantities for the leaves with subscript ℓ (see Equation (4.2.1))

A_{*S} = total projected longitudinal sectional area of the visible (from the sensor) sunlit stems normal to the direction of the sensor

A_{*s} = same as A_{*S} for shaded stems

(C) Radiation Emitted by Soil

The radiation emitted by the soil is given by an equation similar to Equation (4.2.2).

$$F_g = K\bar{\epsilon}(g)\ [T(g,S)^4\ A_{gS} + T(g,s)^4\ A_{gs}] \qquad (4.2.4)$$

where

g = denotes the quantities for the soil corresponding to the quantities for the leaves with subscript ℓ (see Equation (4.2.1))

4.3 Radiation Reflected from a Plant Canopy

The radiation incident on the plant canopy comes from sun, sky, atmosphere and surrounding objects (Section 2.5(B)). When the sky is clear (below -5° F), the solar radiation reflected from a natural target-say plant canopy - can be neglected as compared to the radiation emitted by it (Section 2.5(C)). The reflected radiant flux density from the plant canopy is likely to increase with the increase in percentage ground cover* because the emittance of a typical soil is generally less than the emittance of a typical plant leaf (Section 2.6). Also the reflected radiant flux density from the plant canopy is likely to increase with the increase in number of surrounding objects (especially if the surrounding objects are higher than the plant canopy).

To derive an expression for the radiant flux density reflected from the plant canopy for a given plant geometry is involved because of the complex geometry (orientation of leaves, stems etc.) of the plant canopy. Duncan et al.[26] (1967) has developed an elaborate theory for the penetration of the direct and diffuse sunlight through a foliage composed of many layers of leaves with known orientation, reflectance and transmittance characteristics. Anderson and Denmead[2] (1969) have described a method for the easy calculation of the radiant flux densities of direct and diffuse radiation on inclined leaves in model plant stands. Kumar[61] has done much literature review pertaining to the interaction of light with a plant canopy. Recently, Suits[90] (1972) has calculated the directional reflectance of a vegetative canopy. No attempt will be made in this Section to derive an expression for the radiant flux density reflected from the plant canopy. Although the equations in this Chapter have been derived for the wavelength range 4 to 14 μm, they are equally valid for the wavelength range 4 to 20 μm.

The total radiation reaching the detector of the aircraft and/or satellite is the sum of the emitted and reflected radiation. All the equations derived here for the wavelength range 4 to 14 μm are also valid on the spectral basis in the same wavelength region.

---

* Percent ground cover is the percentage of the area of the soil under the plant canopy which is directly visible from the sensor.

CHAPTER V

FIELD EXPERIMENTS WITH LONGWAVELENGTH SPECTRORADIOMETER

5.1 Description of the Exotech Model 20-C Spectroradiometer

(A) Overview

The Exotech Model 20-C Spectroradiometer is a rugged field instrument which has four circular-variable-filters to provide spectral resolution ($\frac{\Delta\lambda}{\lambda}$) of approximately 2 percent. Most part of this Section (Sec. 5.1) is reproduced from Silva et. al.[83] and Robinson et. al.[82] for the convenience of the readers. This instrument is ideally suited to the rigors of a field environment, embodying sealed circuits for protection against dust and condensation, modular construction modules for simplified maintenance, and operational features to reduce the time necessary to secure data[27]. The instrument may be operated as two separate units. The short wavelength (SWL) unit is responsive to radiation in the wavelength range 0.38 to 2.5 micrometers and the long wavelength unit (LWL) is responsive to radiation in the wavelength range 2.8 to 5.6 and 7.0 to 14 micrometers.

The chopper wheel in the instrument is made of polished aluminum coated with silicon monoxide. The radiation from the scene passes through the foreoptics of the spectroradiometer and is chopped by the filter wheel. The arrangement of the detectors is such that each detector looks alternately at the scene radiation and at an internal blackbody reference. A circular variable filter (C. V. F.) in conjunction with a slit and relay optics performs the dispersion and focusing functions in the instrument.

Figures 5.1.1 amd 5.1.2 illustrate the radiation sensing and gathering systems for the LWL unit. The combined gathering and sensing system is referred to as the optical head. The SWL and LWL optical heads are functionally identical, except for the inclusion of a solar

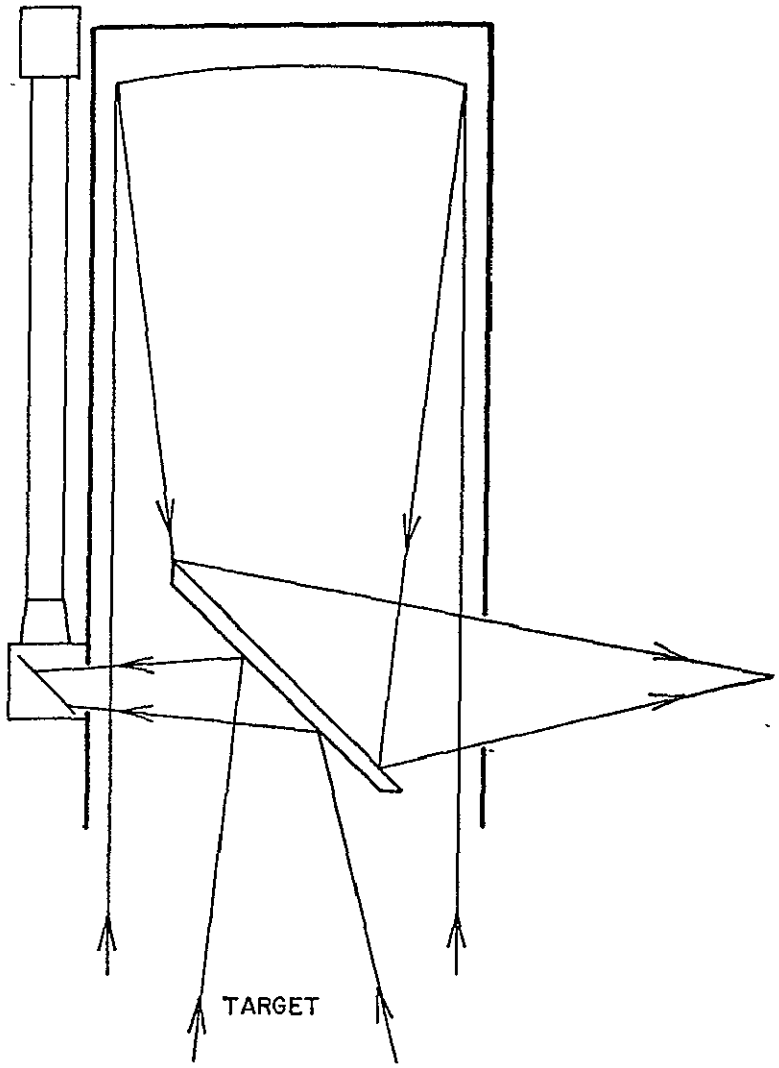

Figure 5.1.1 Schematic of Telescope Showing Viewing Arrangement in 3/4° F.O.V.

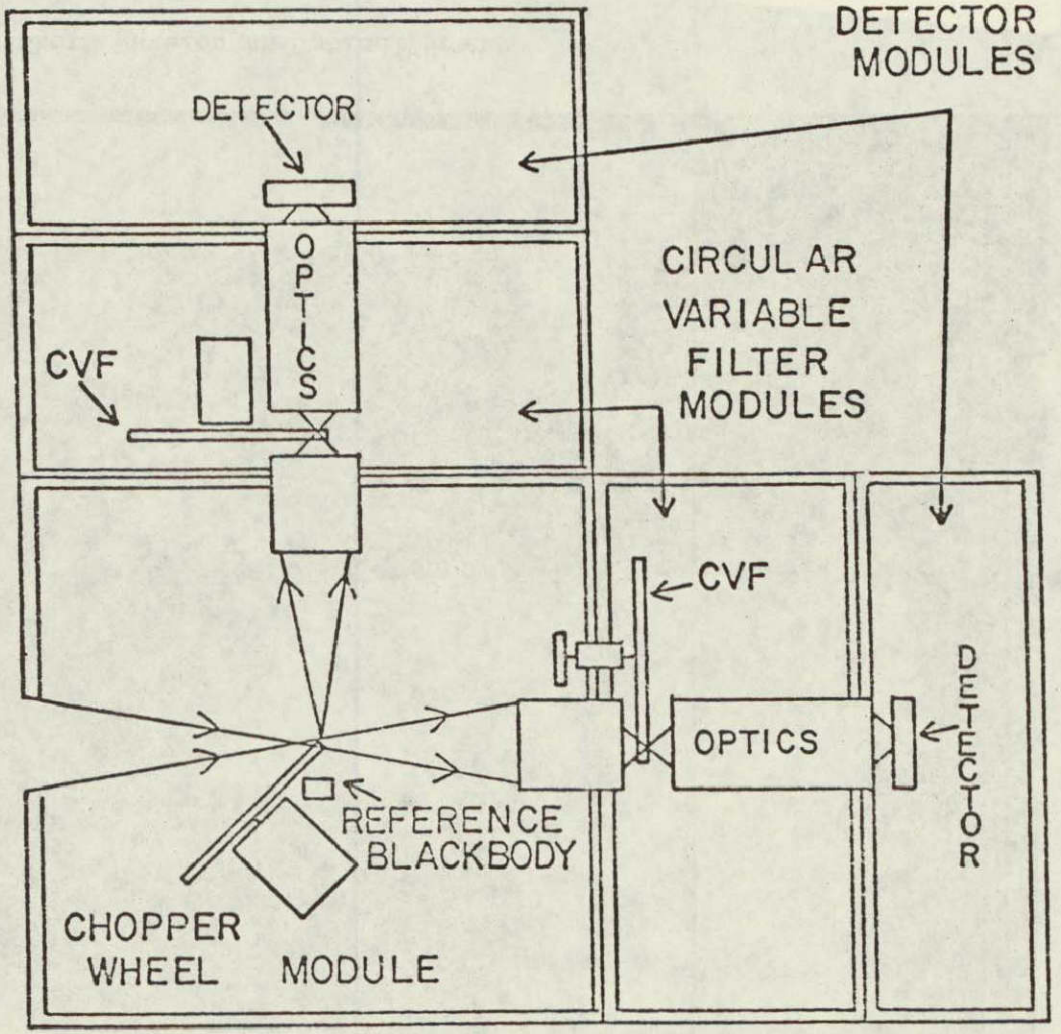

Figure 5.1.2 Radiation Sensing System for the Longwavelength Unit

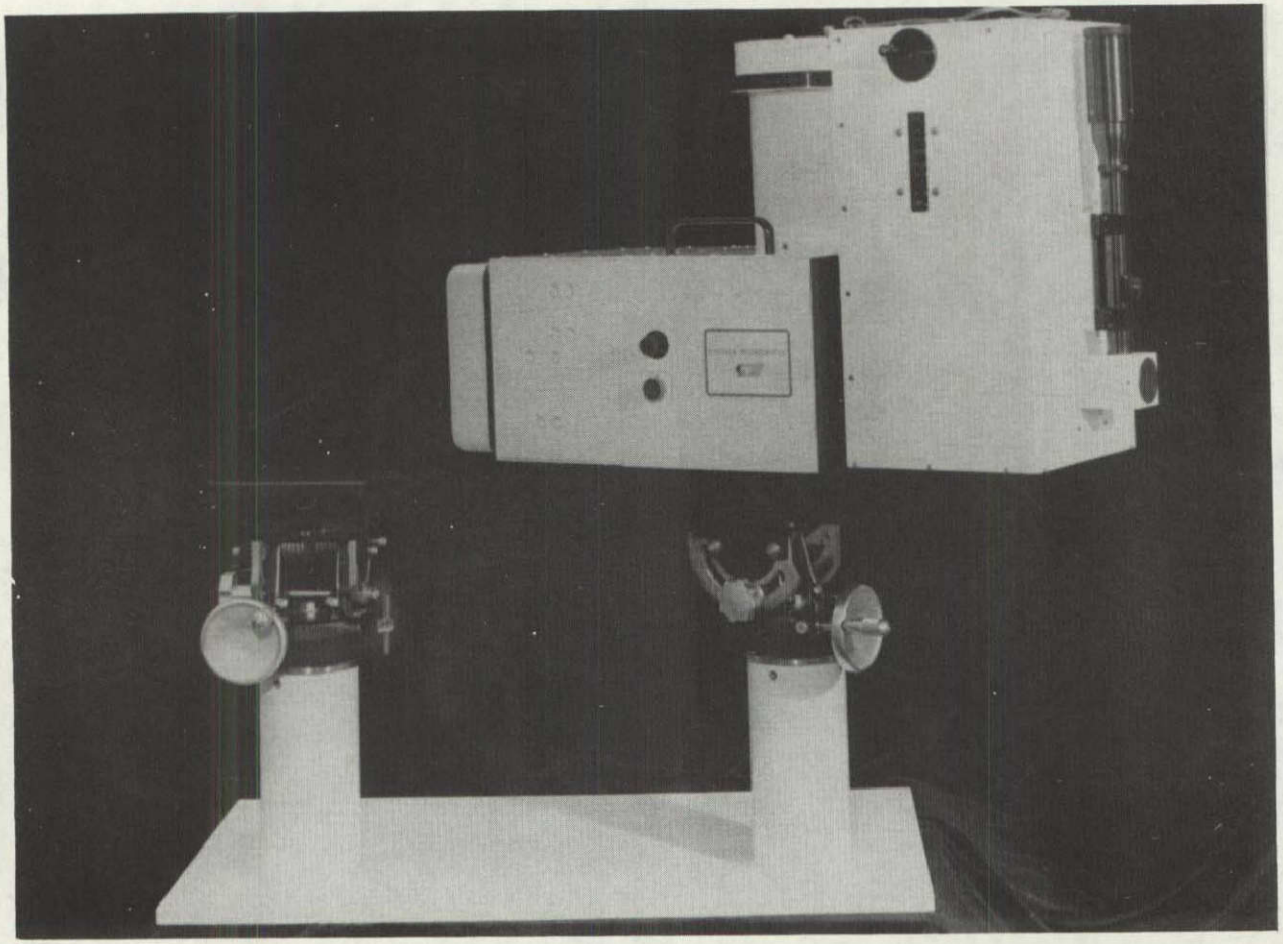

Figure 5.1.3 Short Wavelength Optical Head

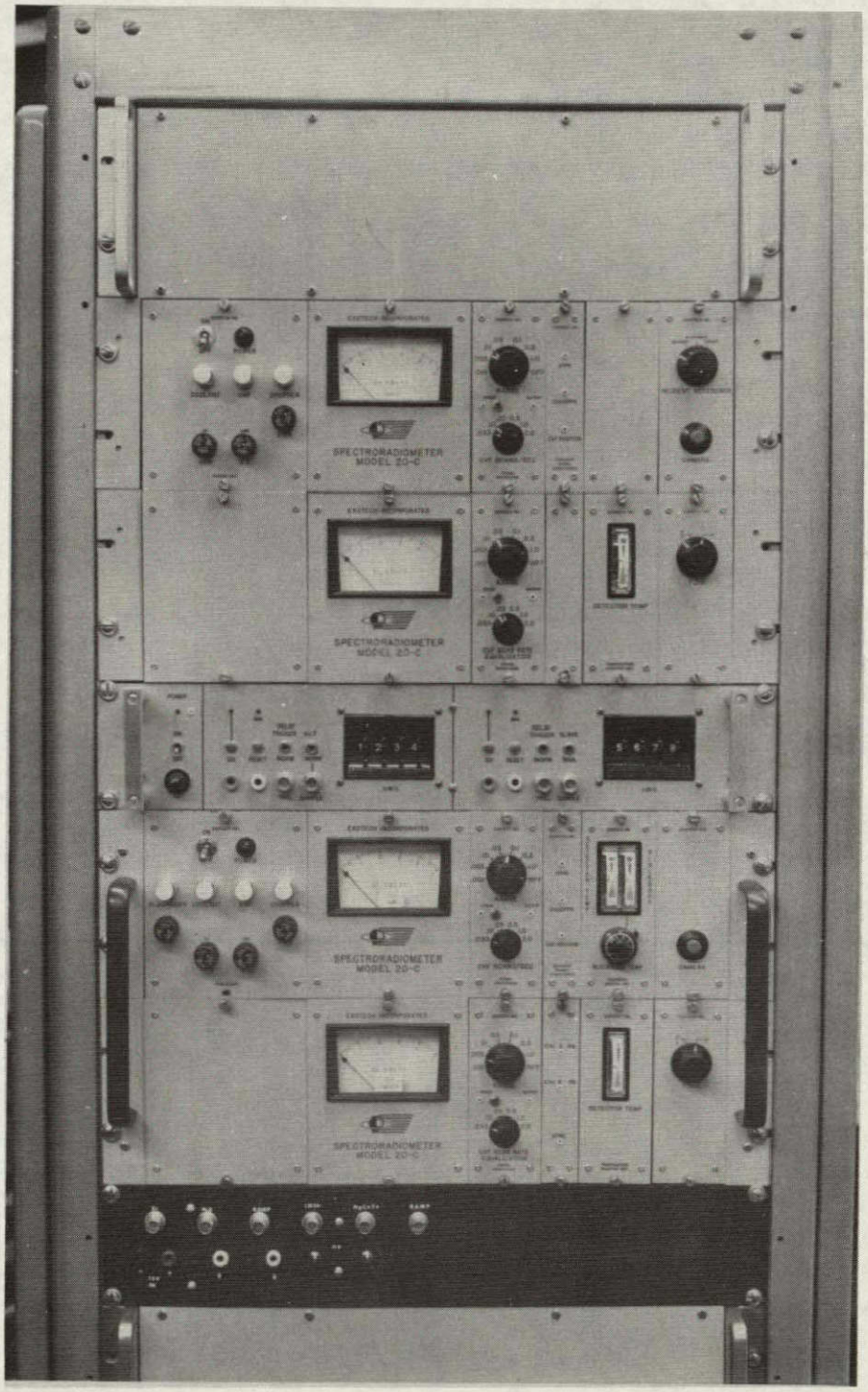

Figure 5.1.4 Panels for Electronic Processing and Control Circuitry

reference port on the SWL head. Figure 5.1.3 shows the SWL optical head. The cylinderical column behind the telescope is the solar reference port.

Figure 5.1.4 shows the panels for the electronic processing and control circuitry. The top two modules connect with the SWL optical head to control its operation and process the radiometric data and wavelength position signals. The bottom two modules perform a similar function for the LWL optical head. The module in the middle is the Data Acquisition Control Module, which provides the appropriate sequences of sample pulses for digitization of data at repeatable wavelengths.

(B) Important Specifications

Field of View (FOV) - 0.75° or 15° plane angle remotely selectable (Figure 5.1.5)

Spectral Region -

	CVF micrometers	Detector
Short Wavelength Unit	.38 - .72	Silicon
	.7 - 1.3	Lead Sulfide
	1.3 - 2.5	Lead Sulfide
Long Wavelength Unit	2.8 - 5.6	Indium Antinomide
	7.0 - 14.0	Mercury-Cadmium-Telluride

Spectral Scan Rate - Selectable 0.5, 1, 2, 4, 10 and 30 seconds per scan.

Spectral Resolution - Short Wavelength Unit 2.5%

Half Bandwidth 17 nanometers - visible

Half Bandwidth 32 nanometers - near infrared

Long Wavelength Unit 2%

Dynamic Range - Linear dynamic range of the system is at least 10^4.

Wavelength Accuracy - approximately ± .2% of the value

Power Requirements - 150 watts, 115 ± 20%, 60 Hz ± 1 Hz

(C) Description of Function

(1) Long Wavelength Unit

The radiation from the target scene is folded into the radiation processing system by the folding mirror either directly (15° FOV) or

from the primary mirror of the Newtonian telescope (3/4° FOV, see Figure 5.1.1). The folding mirror is rotated by a motor actuated by the FOV switch on the electronic processing and control circuitry front panel. A circular variable filter (CVF) design has been adopted because it is the best way to achieve a simple, rugged, field instrument with high radiometric efficiency[27].

A circular variable filter consists of a multilayer dielectric coating deposited on a circular substrate (circular substrate of short wavelength head and long wavelength head are germanium, and a composite material of glass and quartz respectively) in such a manner that coating thickness varies linearly with angle of rotation while remaining constant along a radius[27]. The spectral characteristics of such a filter at any particular angle are equivalent to a narrow bandpass filter having about 60 percent transmission with a bandwidth of 1 percent to 2 percent of the center wavelength. As the filter is rotated past a point illuminated by incident radiation, the center frequency changes so that an effective spectral scan is obtained. These characteristics are illustrated in Figure 5.1.5 which shows the transmission of the filter vs. angular rotation, with incident radiation from several sources.

When the folding mirror is in the 3/4° FOV position, the mirror on the back face of the folding mirror directs radiation from the target scene into the boresighting telescope for sighting and photography. Since the boresight uses radiation which would normally be lost due to the occulting of the folding mirror, this feature does not affect the efficiency of the radiometer.

The folded radiation enters the radiation processing system and is directed by the chopper wheel alternately to the two CVF wheels. Simultaneously, radiation from the heated reference blackbody whose temperature can be selected, is being directed alternately to the two CVF wheels (See Figure 5.1.2).

KRS-5 (thallium bromide-iodide) optics image the scene on the CVF wheels and refocus the stopped image onto the detector. KRS-5 is valuable because it transmits to very long wavelengths -- about 50 μm. The transmittance characteristics* of KRS-5, for a thickness of 2 mm, are given in Figure 5.1.6.

---

* R. D. Hudson, Jr., John Wiley & Sons, New York, p. 218, 1969.

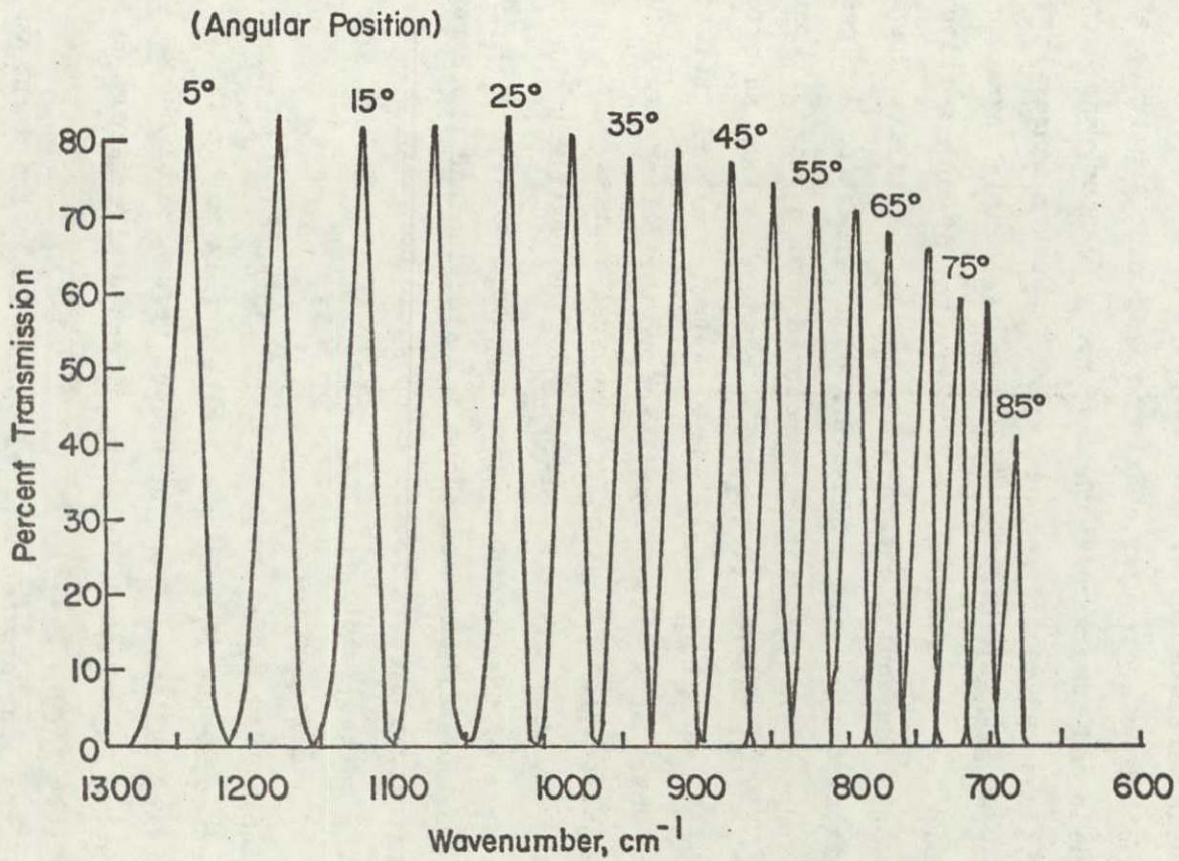

Figure 5.1.5 Transmission Characteristics of a Circular Variable Filter (Taken from Ref. [27])

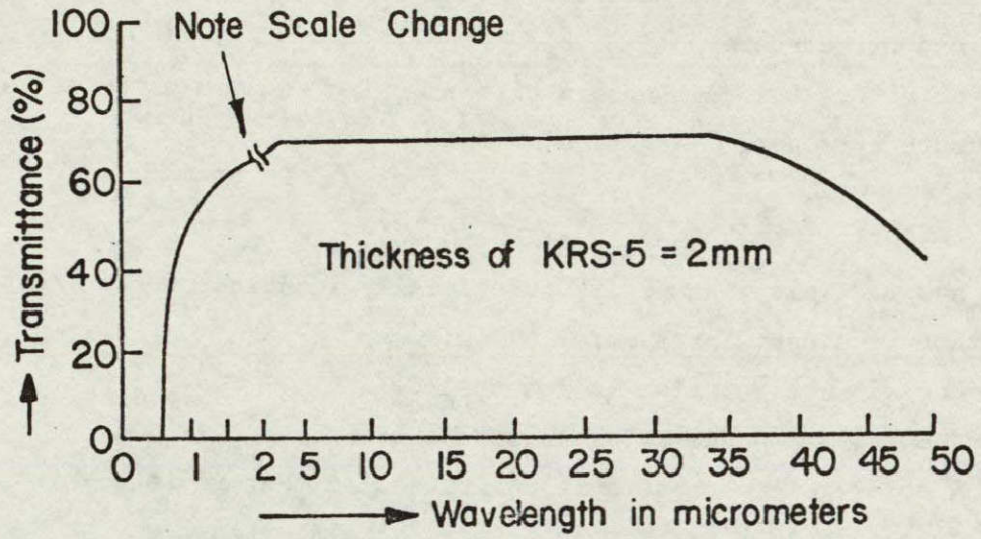

Figure 5.1.6 Transmittance of KRS-5 (Thallium Bromide-Iodide)*

*Taken from R. D. Hudson Jr., Infrared System Engineering, John Wiley & Sons, New York, p. 218, 1969.

One CVF wheel is turned at constant speed by a Siemens brushless DC motor and the shaft of the other CVF follows, being driven with a non-slip timing belt system. The speed of the DC motor is selectable on the front panel of the electronic processing and control circuitry. The CVF position is indicated by an optical shaft angle encoder which produces 1000 pulses per revolution. These pulses are the basis of the wavelength calibration scheme. These pulses are also integrated in the electronic processing and control circuitry module to produce a ramp suitable for driving X-Y plotters or recording CVF position information on strip chart recorders.

The detectors are each cooled with a Joule-Thompson cryostat using high pressure nitrogen.

(2) Short Wavelength Unit

The short wavelength unit is functionally identical to the long wavelength unit except for the following:

1. The silicon detector is not cooled.
2. The reference blackbody is not heated.
3. A solar reference port is positioned so that radiation from this diffusely translucent (Coors alumina) plate may be directed into the detectors by a mirror whose position is controlled by a knob on the front panel of the electronic processing and control module. This knob allows selection of the target scene, the solar port or an automatic mode which causes the instrument to alternate between the two, every two scans. Fused silica relay optics are used in place of the KRS-5.

The LARS Hi-Ranger mobile aerial tower is used to lift the optical heads to the desired position relative to the target scene (Figure 5.1.7). The optical heads may be lifted to a height of 15.3 m above the ground and may be suspended as far as 6.4 m from the edge of the Hi-Ranger at a height of 9.15 m. The control electronics, recording equipment, and other data recording instruments are located in the instrument van. A power unit towed behind the instrument van provides electrical power for both the instrument van and the spectroradiometer. Normally, a technician operates the equipment while the natural scientist directs the experiment. Further details of 'The LARS Extended Wavelength Spectroradiometer' are available in Robinson et. al.[82] .

Figure 5.1.7 Typical Setup of the Field Spectroradiometer System

5.2 Calibration of the Longwavelength Unit

(A) Basic Equations

The output signal, S, from the spectroradiometer at wavelength, λ, when exposed to a blackbody (see ref.[27], eq. (3.6)) at temperature, T, can be considered to be

$$S = K_1(\lambda)\,[\{L_{\lambda,b}(\lambda, T) + \delta L_{\lambda,\,b}\} - K_2(\lambda)\,\{L_{\lambda,\,b\ ref}(\lambda, T_r) + \delta L_{\lambda,\,b\ ref}\}] \qquad (5.2.1)$$

where

$K_1(\lambda)$ = instrument transfer function

$K_2(\lambda)$ = constant for the reference blackbody

T = temperature of the blackbody

T_r = temperature of the reference blackbody

$L_{\lambda,b}(\lambda,T)$ = blackbody spectral radiance at temperature, T, and wavelength λ.

$\delta L_{\lambda,b}$ = error in blackbody spectral radiance due to the stray radiation when the spectroradiometer is looking at the target blackbody

$L_{\lambda,b\ ref}(\lambda,T_r)$ = reference blackbody spectral radiance at temperature, T_r, and wavelength λ.

$\delta L_{\lambda,b\ ref}$ = error in reference blackbody spectral radiance due to stray radiation when the spectroradiometer is looking at the reference blackbody.

Stray radiation consists of:

(i) Radiation emitted by the parts of the spectroradiometer (chopper wheel, circular variable filter, lenses, etc.) reaching the detector. This depends on the temperature of these parts, which in turn depends on the instrument temperature. The instrument has been designed so that this stray radiation is small and can be neglected.

(ii) Small amount of reflected and emitted radiation from the unnatural

surroundings of the target (for example -- spectroradiometer, man, truck, etc.) is incident on the target and finally reaches the detector. This is quite small because the reflectance of the targets of our interest (i.e., plants, soils, etc.) in the wavelength range 7 - 14 μm is usually less than 15% (Section 2.6).

(iii) The radiation coming from the target and reaching the detector when the spectroradiometer is looking at the reference blackbody, and vice versa, is almost equal to zero and can be neglected (Section 5.1).

The spectroradiometer has been designed in such a way as to minimize the stray radiation. Hence, neglecting the stray radiation, Equation (5.2.1) reduces to

$$S = K_1(\lambda)\,[\{L_{\lambda,b}(\lambda,T)\} - K_2(\lambda)\,\{L_{\lambda,b\ ref}(\lambda,T_r)\}] \qquad (5.2.2)$$

If T_r (reference blackbody temperature) is kept constant, Equation (5.2.2) becomes the equation of a straight line for each value of the wavelength λ. In other words, it reduces to the form:

$$y = mx + c \qquad (5.2.3)$$

where

$S = y$, $K_1(\lambda) = m$ = slope of the straight line

$-K_1(\lambda)\,K_2(\lambda)L_{\lambda,b\ ref}(\lambda,T_r) = c$ = constant

The spectral blackbody radiance at temperature, T, and wavelength, λ, is given by Planck's Law with usual notations, as follows:

$$L_{\lambda,b}(\lambda,T) = \frac{2hc^2}{\lambda^5\,[\exp\,(hc/k\lambda T) - 1]} \qquad (5.2.4)$$

or

$$T = \frac{hc}{\lambda k\,\{\log_e\,(\,1 + \frac{2hc^2}{\lambda^5 L_{\lambda,b}(\lambda,T)}\,)\}} \qquad (5.2.5)$$

(B) Wavelength Calibration

The wavelength calibration for both the channels was done by finding the pulse number corresponding to the following strong, sharp and accurately known absorption bands of polystyrene, atmospheric carbon dioxide and methyl cyclohexane (liquid), in the infrared wavelength region (Figures 5.2.1 and 5.2.2).

It can be seen from the Figures 5.2.1 and 5.2.2 that pulse number vs. wavelength is almost a straight line. A straight line was fitted to these points for each channel by the least square fit, the results of which are given below.

(1) Indium Antimonide Channel

$$\text{Avg. } |\lambda - \lambda_p| = 0.014 \ \mu m, \quad \text{Max. } |\lambda - \lambda_p| = 0.027 \ \mu m \qquad (5.2.6)$$

where

Avg. = denotes the average value

λ_p = predicted value of the wavelength by a straight line least square fit

λ = experimentally determined value of the wavelength

Approximate Beginning of Wheel = Pulse 1

Pulse No.	Wavelength in Micrometers	Substance Used For Calibration
90	3.3033	Polystyrene, ref. [78]
116	3.4188	Polystyrene, ref. [78]
130	3.507	Polystyrene, ref. [78]
256	4.258	Carbon Dioxide, ref. [78]
398	5.143	Polystyrene, ref. [10]
435	5.3447	Polystyrene, ref. [10]

Approximate End of Wheel = Pulse 500

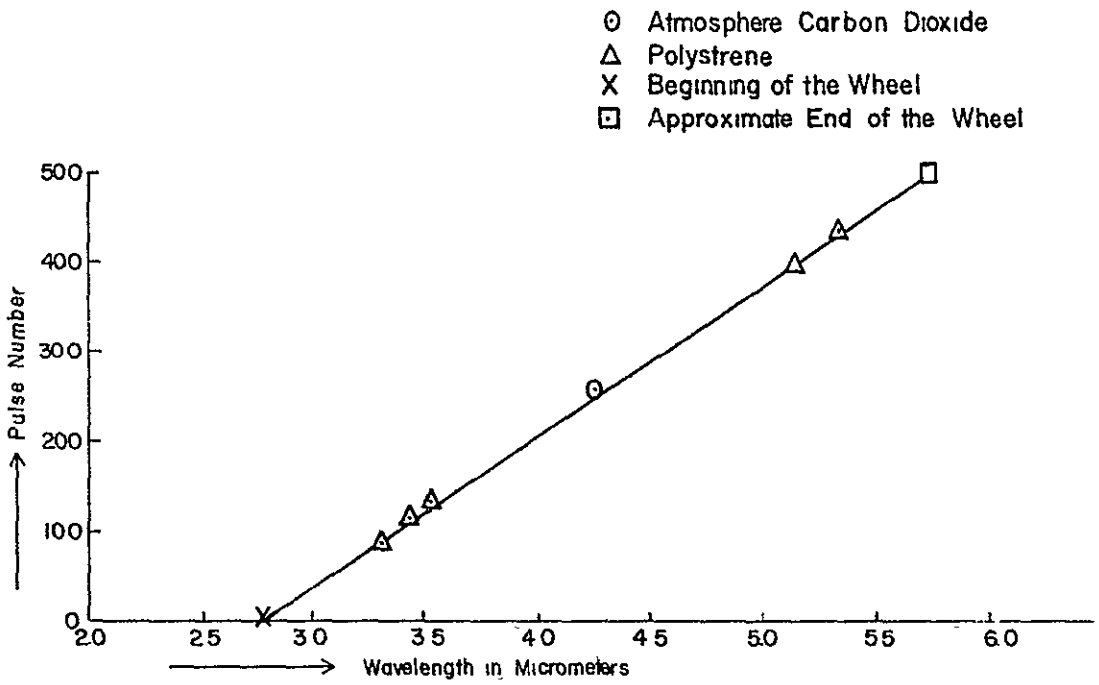

Figure 5.2.1 Wavelength Calibration for Indium Antimonide Channel

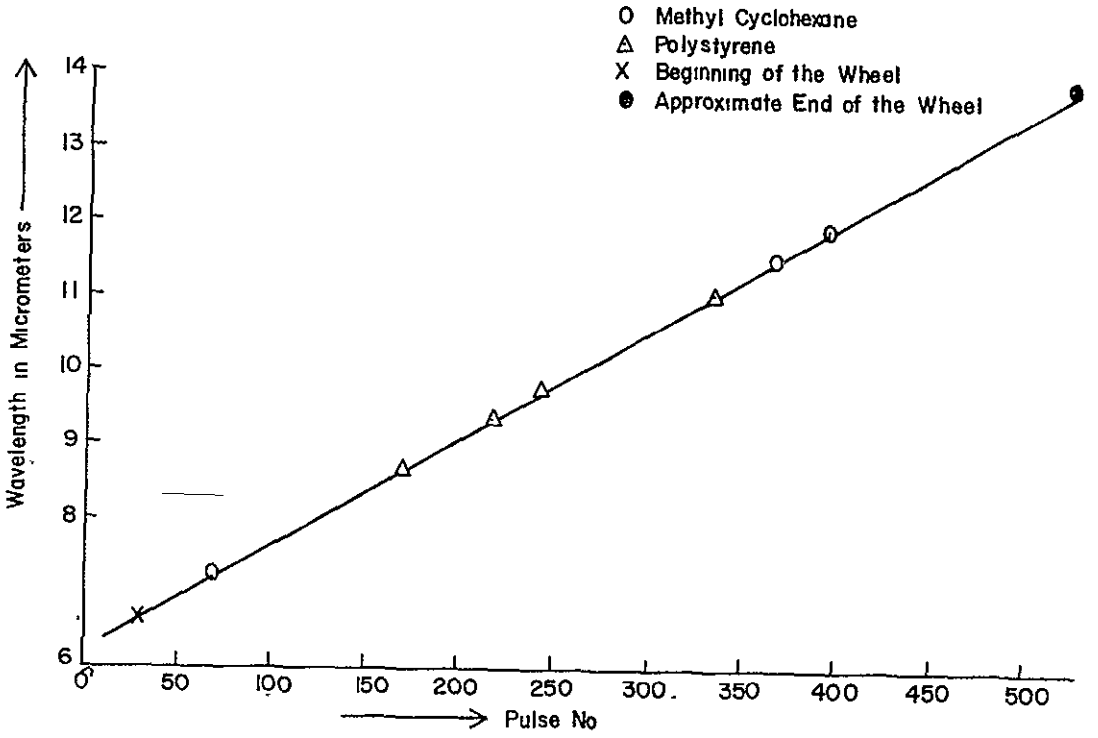

Figure 5.2.2 Wavelength Calibration for Murcury Cadmium Telluride Channel

(2) Mercury Cadmium Telluride Channel

Avg. $|\lambda - \lambda_p| = 0.007$ μm, Max. $|\lambda - \lambda_p| = 0.015$ μm

The nomenclature of Equations (5.2.6) and (5.2.7) is the same.

Approximate Beginning of Wheel = Pulse 30

Pulse No.	Wavelength in Micrometers	Substance Used For Calibration
68	7.268	Methyl Cyclohexane, ref. [78]
168	8.661	Polystyrene, ref.[10]and ref. [77]
216	9.3536	Polystyrene, ref. [10]
242	9.725	Polystyrene, ref. [10]
333	11.027	Polystyrene, ref. [10]
365	11.475	Methyl Cyclohexane, ref. [78]
393	11.862	Methyl Cyclohexane, ref. [10]

Approximate End of Wheel = Pulse 523

The pulse numbers for above mentioned absorption bands were checked from time to time in the summer of 1972 for indium antimonide channel and mercury cadmium telluride channel, and the maximum deviation of the pulse number from the originally found pulse number was ± 1 pulse number.

(C) Spectral Radiance Calibration

A uniformly closely controlled source having a high apparent spectral emittance of nearly one in the 2.8 to 5.6 μm range (indium antimonide channel) and in the 7 to 14 μm range (mercury cadmium telluride channel) is needed to serve as a blackbody for the spectral radiance calibration.

(1) Blackbody

A copper cone having an apex angle of 15° and diameter of about 6.5" was chosen as the blackbody. Copper was chosen because it is a good conductor of heat and thus can be maintained at an essentially uniform temperature. It was decided to paint the copper cone inside with such a paint so as to get the normal spectral emittance of the cone nearly to one in 2.8 - 5.6 μm and in 7 - 14 μm. The following paints were selected for conducting emittance tests on them, as these paints have been reported[94] as having high normal emittance.

1. Eppley - Parson's Optical Black Lacquer
2. Krylon Flat Black Enamel No. 1602
3. Krylon Glossy Black Enamel No. 1601
4. 3 M Velvet Black 101 - C 10

Comparative tests of apparent spectral emittance of these paints were conducted by painting each of these paints on a 6" x 6" area of a copper sheet. Each sample on the copper sheet was heated to 50° C (± 0.02° C) to insure that the emitted radiation by the sample would be much larger than the reflected radiation from it; and its spectral response was recorded in indium antimonide (InSb) channel as well as mercury cadmium telluride (HgCdTe) channel using 3/4° Field of View (FOV). These responses are shown in Figures 5.2.3 and 5.2.4 respectively. If the sample is not heated, it would behave nearly like a blackbody in a closed room for a closed room is nearly a blackbody cavity. Thus, the response of the sample paint in a closed room will be nearly the same irrespective of its emittance. This can be further explained by Figure 2.6.2 (Section 2.6) which shows that the error in experimentally determined emittance of a target with the radiometer decreases with the increase in temperature of the target. It is clear from Figures 5.2.3 and 5.2.4 that Parson's Optical Black Lacquer has the highest response and hence emittance at most of the wavelengths. In addition, the Eppley Laboratory confirmed the uniformity of the emittance of Parson's Black Lacquer with wavelength and it was found to be almost as good as gold black (heavy coat). In the British Meteorological Service, the emittance of the paint at 25° C (i.e., wavelength maximum of 10 μm) was established[51] at 0.98. For the

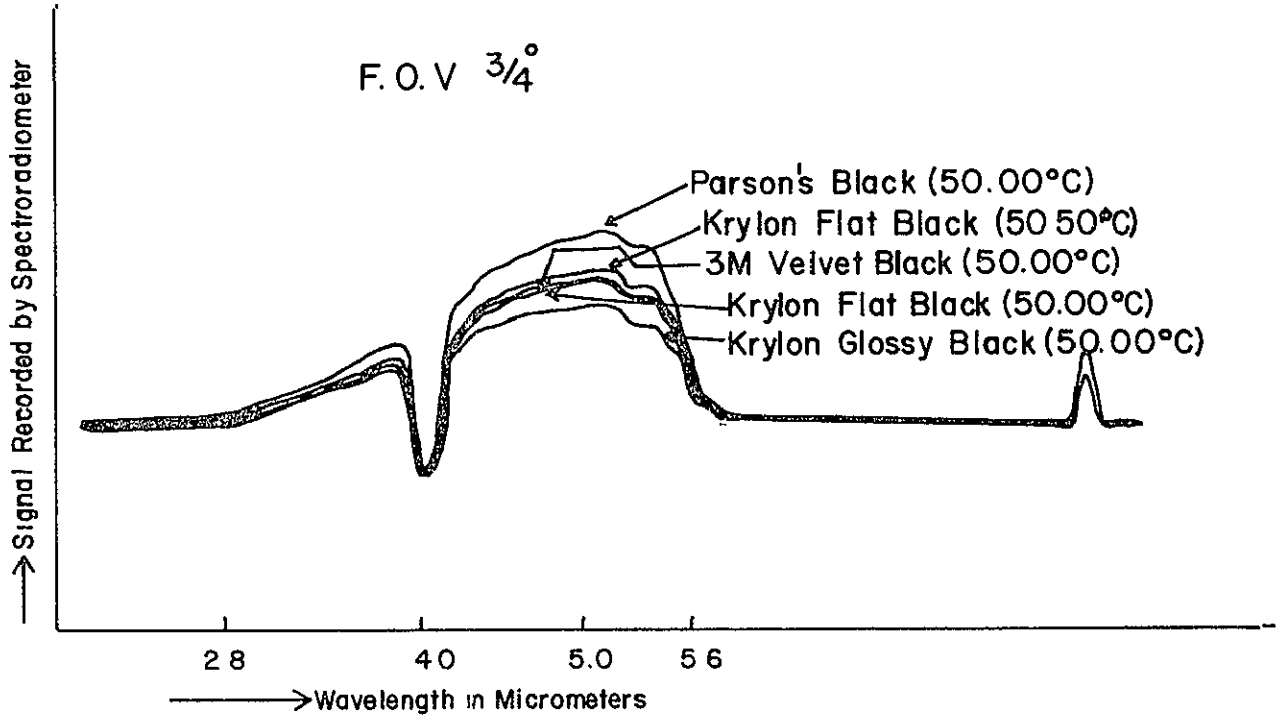

Figure 5.2.3 Comparison of the Emittance of Paints in Indium Antimonide Channel

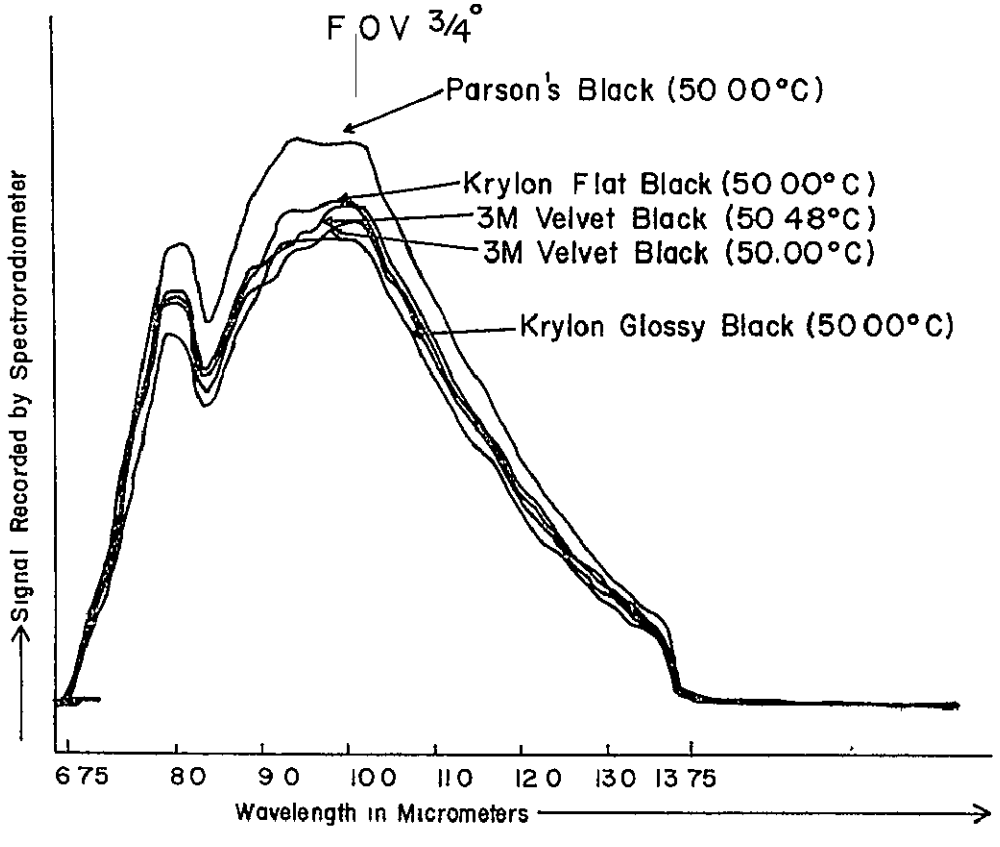

Figure 5.2.4 Comparison of Emittance of Paints in Mercury Cadmium Telluride Channel

value of emittance of paint = 0.98, the apparent emittance of the cone of 15° lies between about 0.995 and 1 (see reference 88).

The copper cone was painted with Parson's Optical Black Lacquer and fitted into a fiberglas covered foam box of dimensions about 16" length, 10" width and 14" height, as shown in Figure 5.2.5. The foam box was filled with water and the water was constantly stirred by a paint mixer driven by an electrical motor to maintain the water at a uniform temperature. The water was heated and cooled by a heater and ice, respectively till the cone attained the desired temperature. It was found that the cone could be kept at a uniform temperature (within 0.2° C) and held constant (the temperature of the cone dropped less than 1° C per hour with no attempt being made to control the temperature). Two such blackbodies were used in the field experiments, one to be kept at temperature well above the ambient temperature (called hot blackbody) and the other to be kept at temperature well below the ambient temperature (called cold blackbody).

(2) Method of Spectral Radiance Calibration

It can be seen from Equation (5.2.3) that the spectral radiance varies linearly with the signal for a given reference blackbody temperature at each wavelength. Calibration is accomplished in the field with the spectroradiometer mounted, ready for use, on the mobile aerial tower bucket[82] (Hi Ranger, see Figure 5.1.7). The hot blackbody temperature and the cold blackbody temperature are chosen 2 or 3° C above and 2 or 3° C below the highest and lowest expected temperatures of the targets (i.e., plants, soils, etc.), respectively. The cold blackbody is held snug against the opening of the optics of the spectroradiometer and the field of view of the spectroradiometer is set for 15°. The reference blackbody temperature is chosen so that the output from the spectroradiometer does not saturate during any portion of the scan, yet it is high enough to permit good resolution in the data. The reference blackbody temperature is kept constant throughout the experiment. Then a spectral scan of the blackbody is accomplished. The process is repeated for the hot blackbody. Data are recorded on the same analog tape as the experiment data and are later processed digitally. This process must be

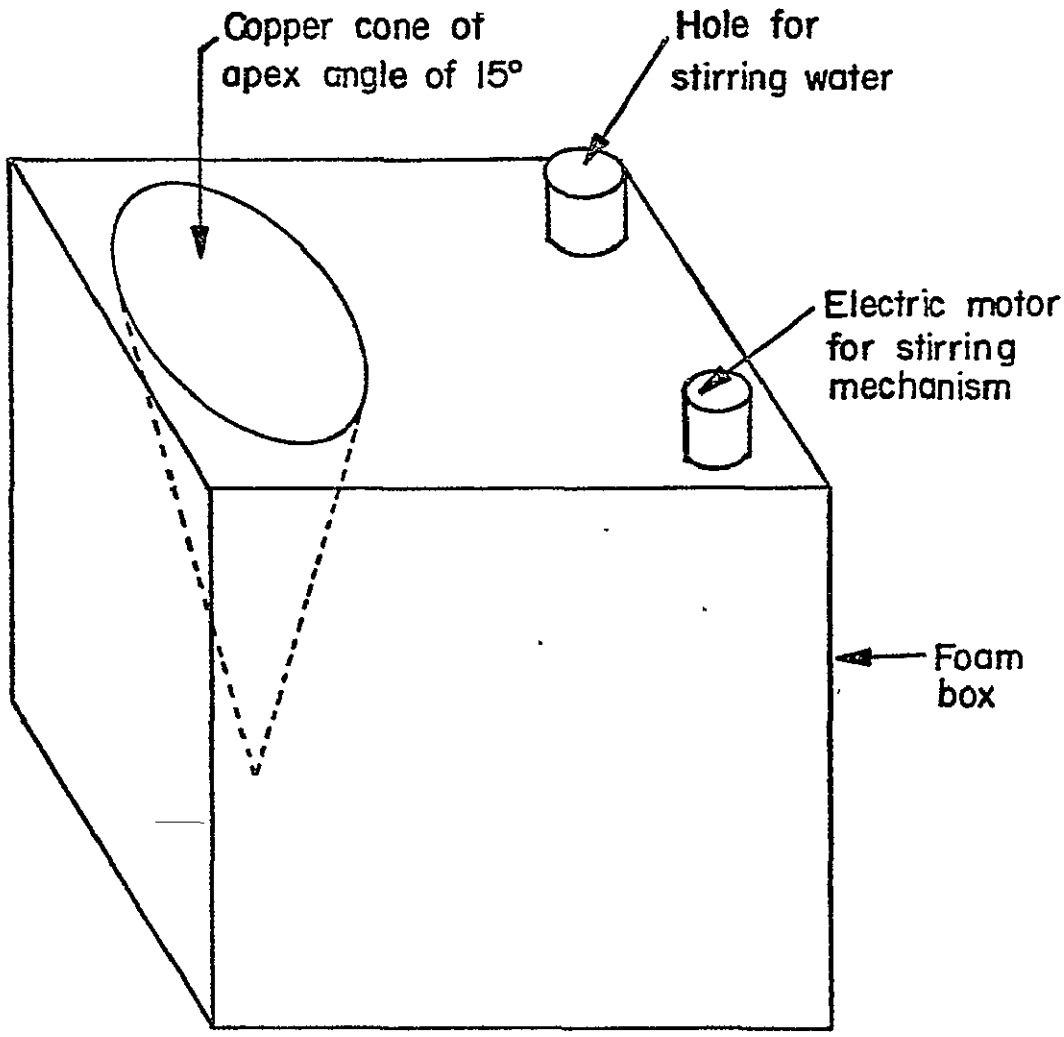

Figure 5.2.5 Blackbody

repeated if any parameter of the instrument is altered. The temperature of the target, T, was calculated by using Equations (5.2.3) to (5.2.5). To determine the accuracy of the calibration, a spectral scan of the blackbody was accomplished at temperatures of 17.5° C, 23.1° C and 37.6° C beside a corn field on the Purdue University Agronomy Farm. The blackbody at temperature 23.1° C was treated as a target at unknown temperature and its spectral radiance was computed by linear interpolation of the blackbody spectral radiance at 17.5° C and 37.6° C and this computed spectral radiance was used to calculate the corresponding temperature given by Equation (5.2.5). Figures 5.2.6 and 5.2.7 compare the theoretical (i.e., blackbody radiance at 23.1° C given by Planck's Law - Equation (5.2.4) and computed values of the spectral radiance and temperature of the target in indium antimonide and mercury cadmium telluride channels respectively. The characters 1 and 2 indicate the theoretical and computed values of the spectral radiance respectively. The characters 3 and 4 indicate the actual and computed values of the temperature respectively. The asterisk indicates agreement to within 0.5 per cent of the full scale value. It can be seen from Figures 5.2.6 and 5.2.7 that except for the wavelengths range 2.7 to 3.4 μm, the temperature usually computes to within ± 1° C and the spectral radiance usually computes to within ± 1 per cent of the full scale value. The high departure from theory in the wavelength range 2.7 to 3.4 μm is due to the relatively small values of spectral radiance (less than 100 microwatts/sq. cm./steradian/micrometer) and hence, low signal to noise ratio in this wavelength region.

Considering the fact that there are errors involved in this calculation like tape recorder noise (the signal was recorded on the tape), error in measurement of temperature, error in wavelength calibration, etc., the Figures 5.2.6 and 5.2.7 show that the assumption of linearity of the signal with spectral radiance at each wavelength, for a given reference blackbody temperature, is quite good for our purposes in both Indium Antimonide and Mercury Cadmium Telluride Channel. Hence, the use of Equation (5.2.3) is justified.

Further work was done to establish the linearity of the signal with the spectral radiance following the same procedure described above. The

Response Radiometric Units (Microwatts/Sq. Cm./Steradian/Micrometer)

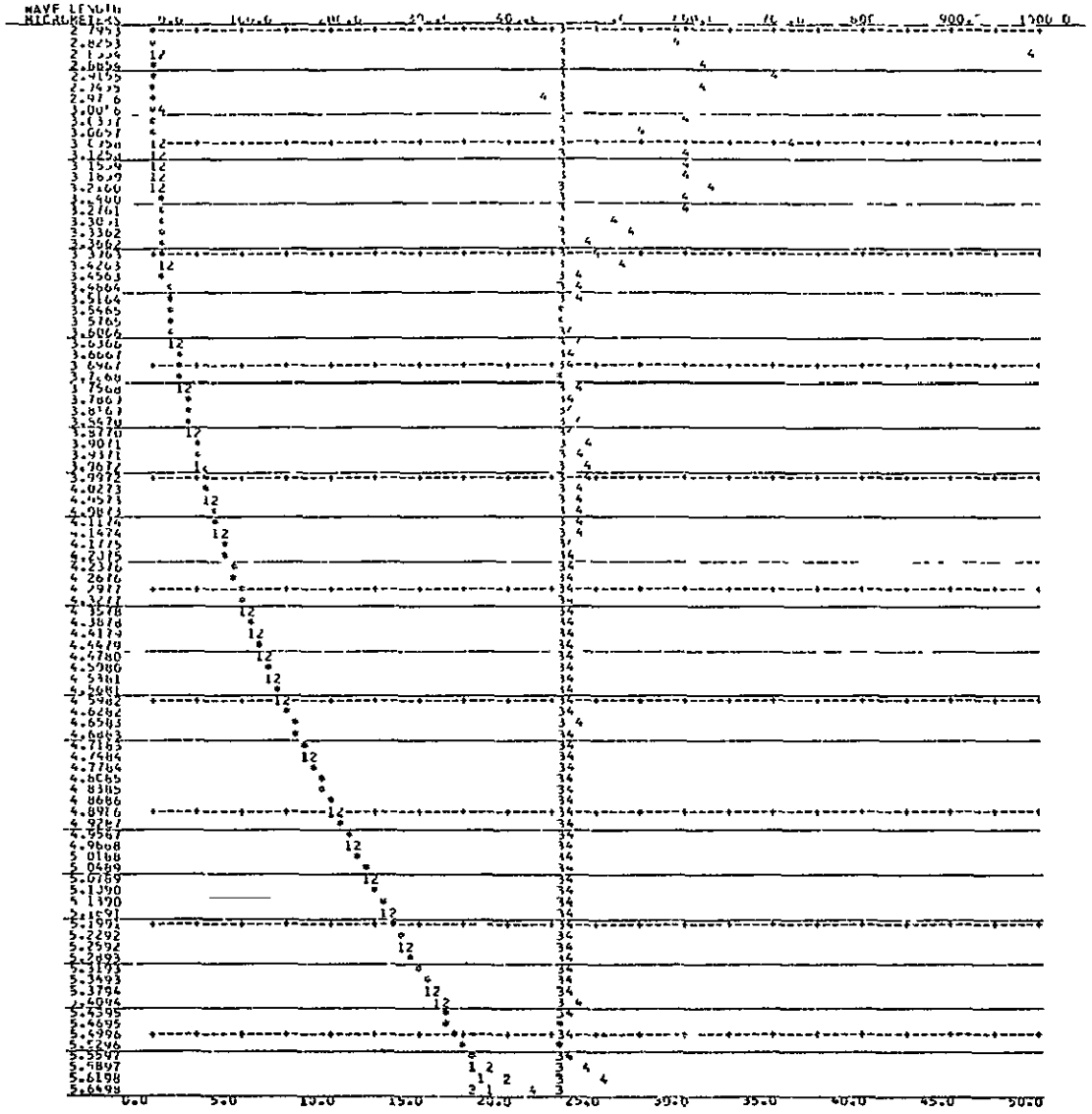

Figure 5.2.6 Theoretical and Computed Values of the Spectral Radiance and Temperature in Indium Antimonide Channel. The characters 1 and 2 indicate theoretical and computed values of the spectral radiance respectively. The characters 3 and 4 indicate the actual and computed values of the temperature respectively.

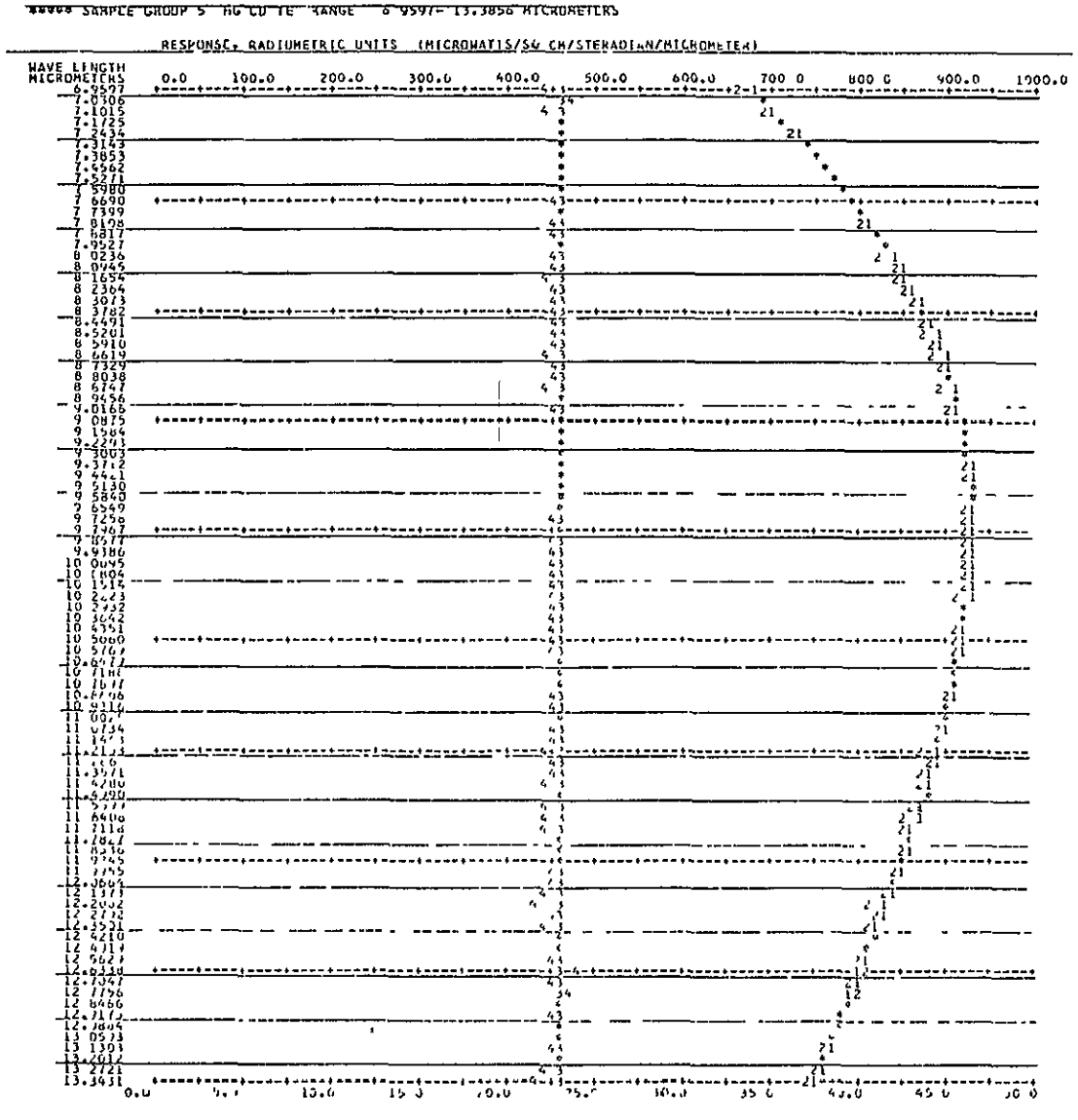

Figure 5.2.7 Theoretical and Computed Values of the Spectral Radiance and Temperature in Mercury Cadmium Telluride Channel. The characters 1 and 2 indicate theoretical and computed values of the spectral radiance respectively. The characters 3 and 4 indicate the actual and computed values of the temperature respectively.

spectral scan of the blackbody was accomplished at temperatures of 18.54° C, 23.37° C, 27.32° C, 31.97° C and 35.63° C in the mercury cadmium telluride channel (Figure 5.2.8). The blackbody at each of temperatures 23.37° C, 27.32° C and 31.97° C was treated as a target at unknown temperature and its spectral radiance was computed by linear interpolation of the blackbody spectral radiance at temperatures of 18.54° C and 35.63° C and this computed spectral radiance was used to calculate the corresponding temperature given by Equation (5.2.5). Table 5.2.1 shows the difference between the real and computed temperatures at 8 μm, 9 μm, 10 μm, 11 μm, 12 μm and 13 μm.

Table 5.2.1 Difference between Real and Computed Temperatures at Certain Wavelengths

Wavelength in Micrometers	Error in °C		
	Real Temperature 23.37° C	Real Temperature 27.32° C	Real Temperature 31.97° C
8	-0.13	+0.18	+0.30
9	-0.14	-0.33	-0.32
10	+0.16	+0.24	+0.25
11	+0.16	+0.06	-0.01
12	+0.22	+0.14	+0.17
13	+0.12	-0.11	+0.06

Table 5.2.1 shows that the maximum absolute error in computed temperature is 0.33° C, which is accurate enough for our purposes.

The spectral scan of the blackbody was accomplished at temperatures of 17.65° C, 17.88° C, 18.05° C and 18.46° C in the mercury cadmium telluride channel (Figure 5.2.9). It can be seen from Figure 5.2.9 that the minimum differentiable temperature difference of a blackbody visually from spectroradiometer scans is about 0.15° C.

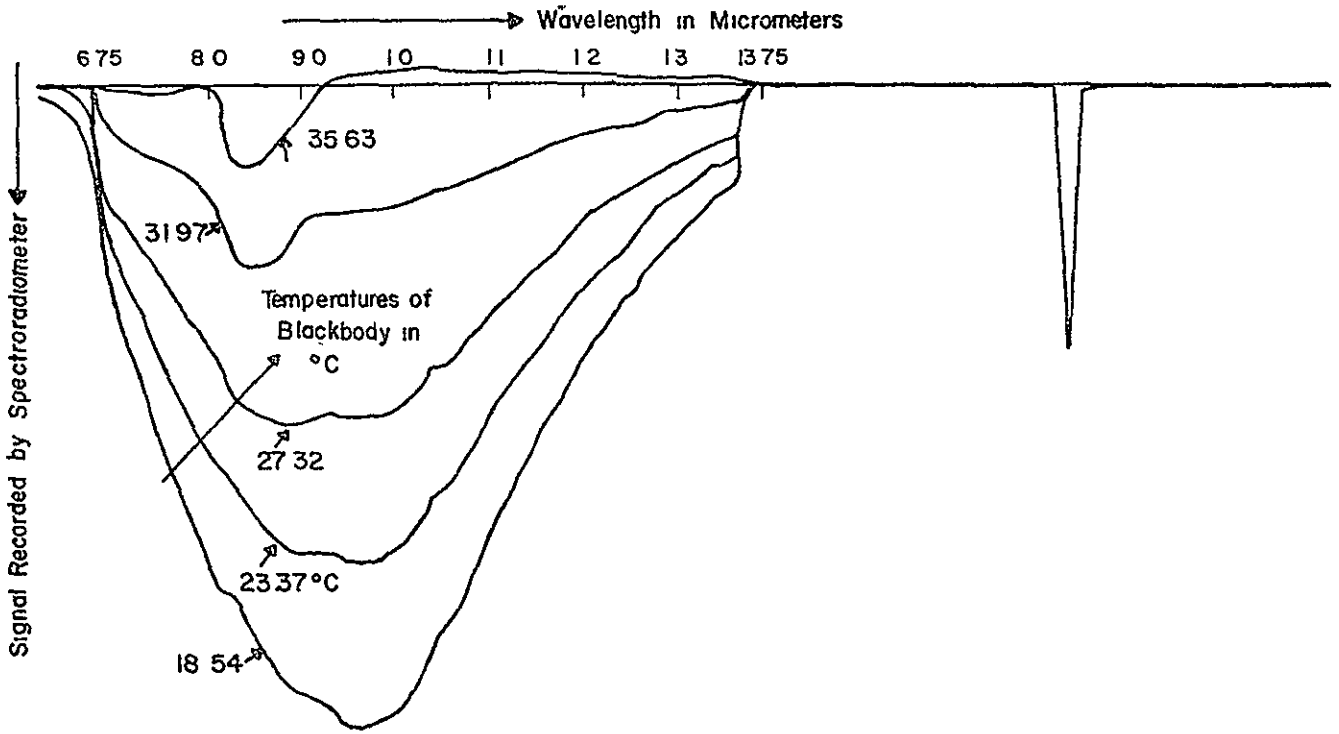

Figure 5.2.8 Scan of the Blackbody at Various Temperatures in Mercury Cadmium Telluride Channel

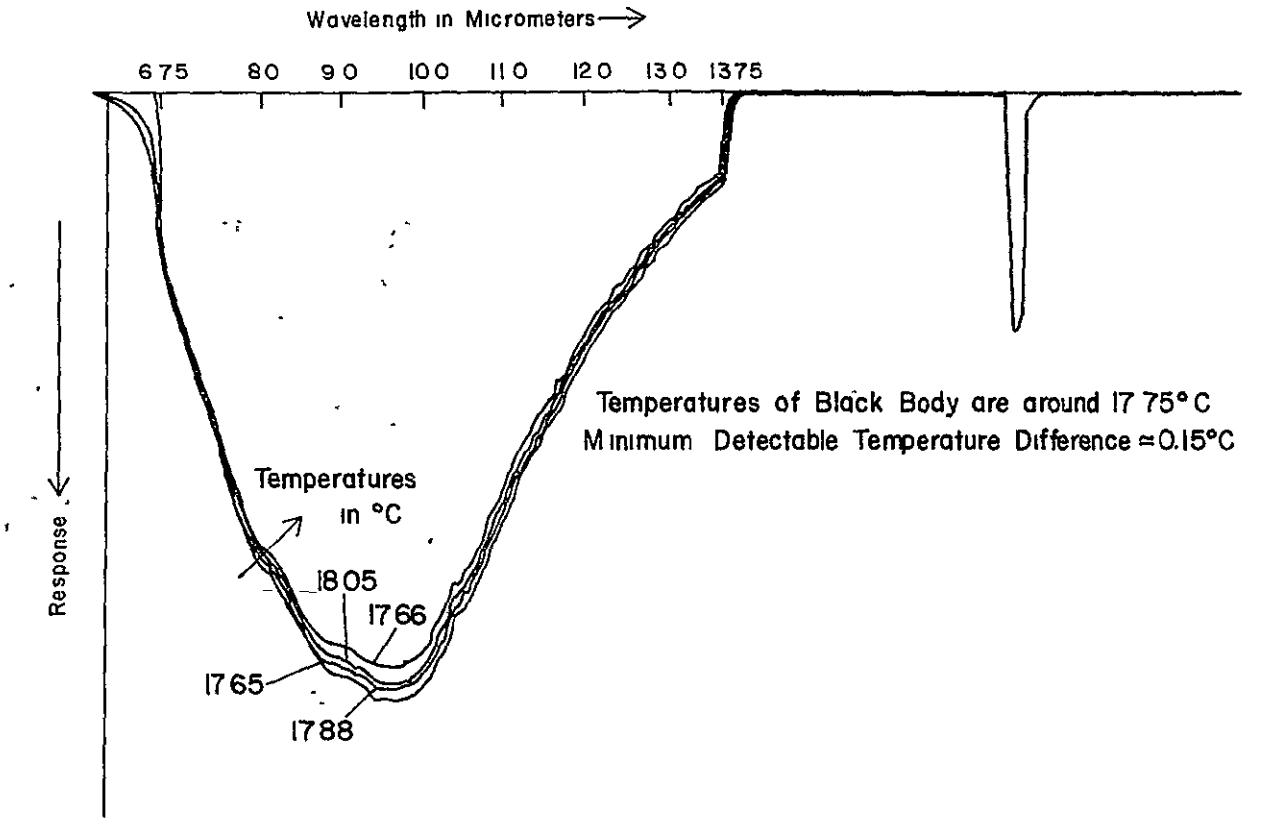

Figure 5.2.9 Minimum Differentiable Temperature Difference of a Blackbody in Mercury Cadmium Telluride Channel

5.3 Calibration of Precision Thermistor Thermometer Probes and the PRT-5 Portable Radiation Thermometer

(A) Calibration of Precision Thermistor Thermometer Probes

The thermistor thermometer is used for ground observations in field experiments and general-purpose temperature measurements[81]. The thermometer features digital display, battery operation and 0.1° C accuracy. For the convenience of the user, the thermometer is transported in a water-tight case which is safe and easy to handle under field conditions (Figure 5.3.1). In addition to protecting the instrument from bumps and dirt, the loaded case will float in fresh water. The instrument meets its accuracy specification from 15° C to 40° C. Thus, the instrument is ideally suited for measurement of contact temperatures of the natural targets (for example, soils, plant leaves, etc.) in a field environment, air temperature, temperature of water in a river, etc. Further details of the instrument are available[81].

Precision thermistor thermometer probes are used with the digital multimeter and 'temperature to voltage converter' to determine the temperature of a target. Probe types 709 and 705, manufactured by Yellow Springs Instruments, shown in Figure 5.3.2, were used for measuring the contact temperatures of soil and air respectively. Further details of the instrument are available[81].

Four thermistor probes, used with the Precision Thermistor Thermometers, were calibrated against Taylor Permafused precision thermometers, from 5° C to 50° C at an interval of 0.5° C. The probes and thermometers were immersed in a water bath, with thermometer positioned approximately in the center of four probes. The water bath had a stirring mechanism so that the water could be kept at nearly uniform temperature. The temperature of the water in the water bath was increased above the ambient temperature by the heating mechanism in the water bath, and decreased below the ambient temperature by adding cold water or ice.

The probes were numbered as follows:

Probe No. 1: Yellow Springs Instruments Company, Inc. Part No. 709 (color of connecting wire--dark tan, used with digital multimeter

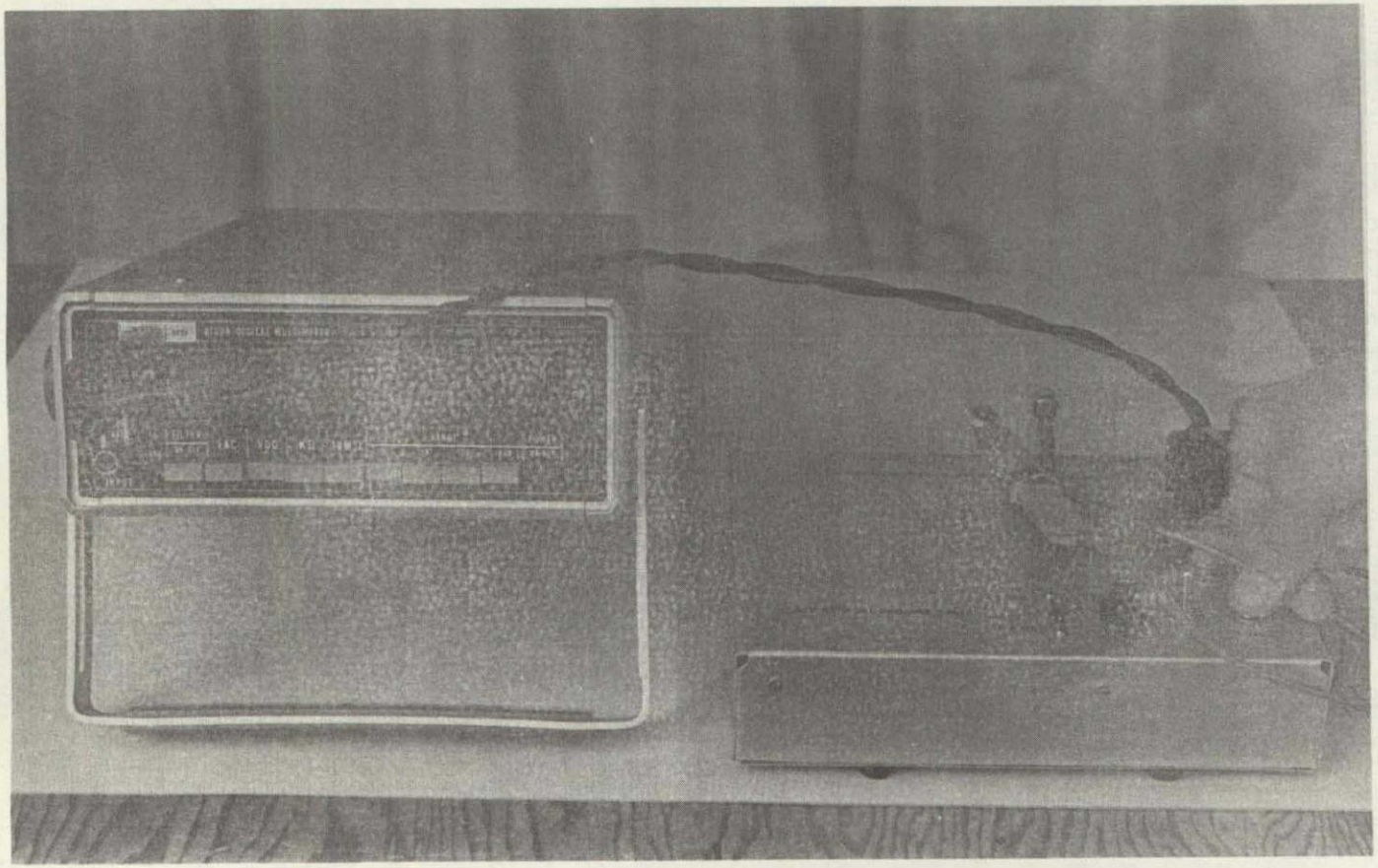

Figure 5.3.1 Precision Thermistor Thermometer

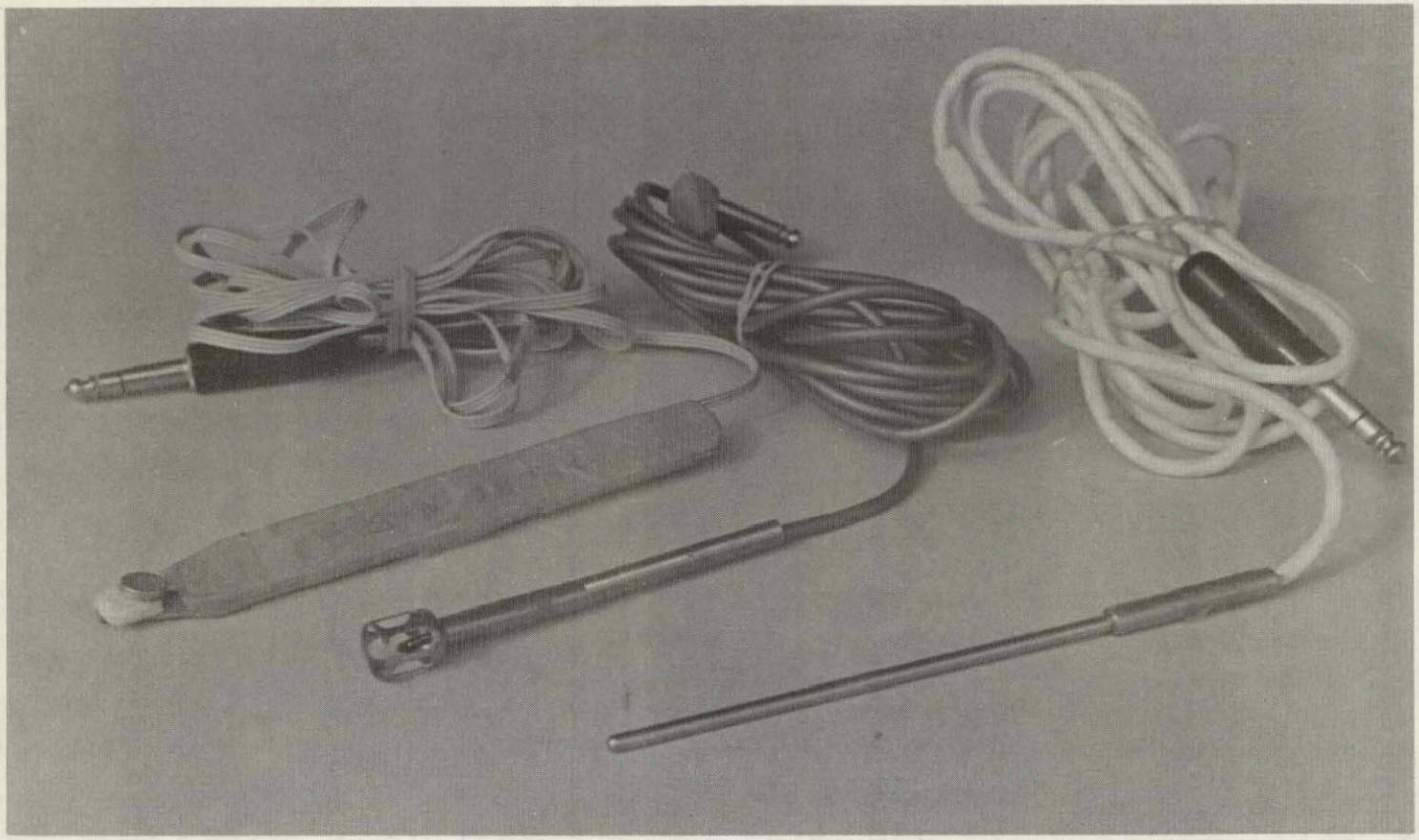

Figure 5.3.2 Precision Thermistor Thermometer Probe Types 709, 705 and 703
(From left to right probe types 709, 705 and 703)

No. 783 and temperature to voltage converter No. 1).

Probe No. 2: Yellow Springs Instrument Company, Inc. Part No. 703 (color of connecting wire--white, used with digital multimeter No. 783 and temperature to voltage converter No. 2).

Probe No. 3: Yellow Springs Instrument Company, Inc. Part No. 709 (color of connecting wire--light tan, used with digital multimeter No. 4174 and temperature to voltage converter No. 1).

Probe No. 4: Yellow Springs Instrument Company, Inc. Part No. 703 (color of connecting wire--gray, used with digital multimeter No. 4174 and temperature to voltage converter No. 2).

(B) Description of the PRT-5 Portable Radiation Thermometer

The model PRT-5 Portable Radiation Thermometer is a portable, battery-powered instrument for determining the effective radiance temperature (also called radiant temperature) of the objects[6] . It consists of a hand-held optical head and a separate solid-state electronics unit (Figure 5.3.3). The instrument is filtered to make measurements in the wavelength range of 8 to 14 micrometers because the atmosphere is nearly transparent in this wavelength region. An in-line temperature-controlled cavity containing the detector and the collecting optics lies directly behind a gold plated reflecting chopper. In this way, the detector "sees" the cavity as a reference by reflection when the chopper is closed. The instrument is powered by rechargeable, self-contained batteries. Measurements of targets which fill the field of view are independent of distance. The focus range of the optics is one foot to infinity. An open sight shows the pointing direction.

Important Brief Specifications:

Temperature Range of Operation = -20° C to +75° C

Accuracy = ±0.5° C

Reference Cavity Temperature = 45° C

(C) Field of View of PRT-5

The field of view (F.O.V.) of PRT-5 was determined as follows. The

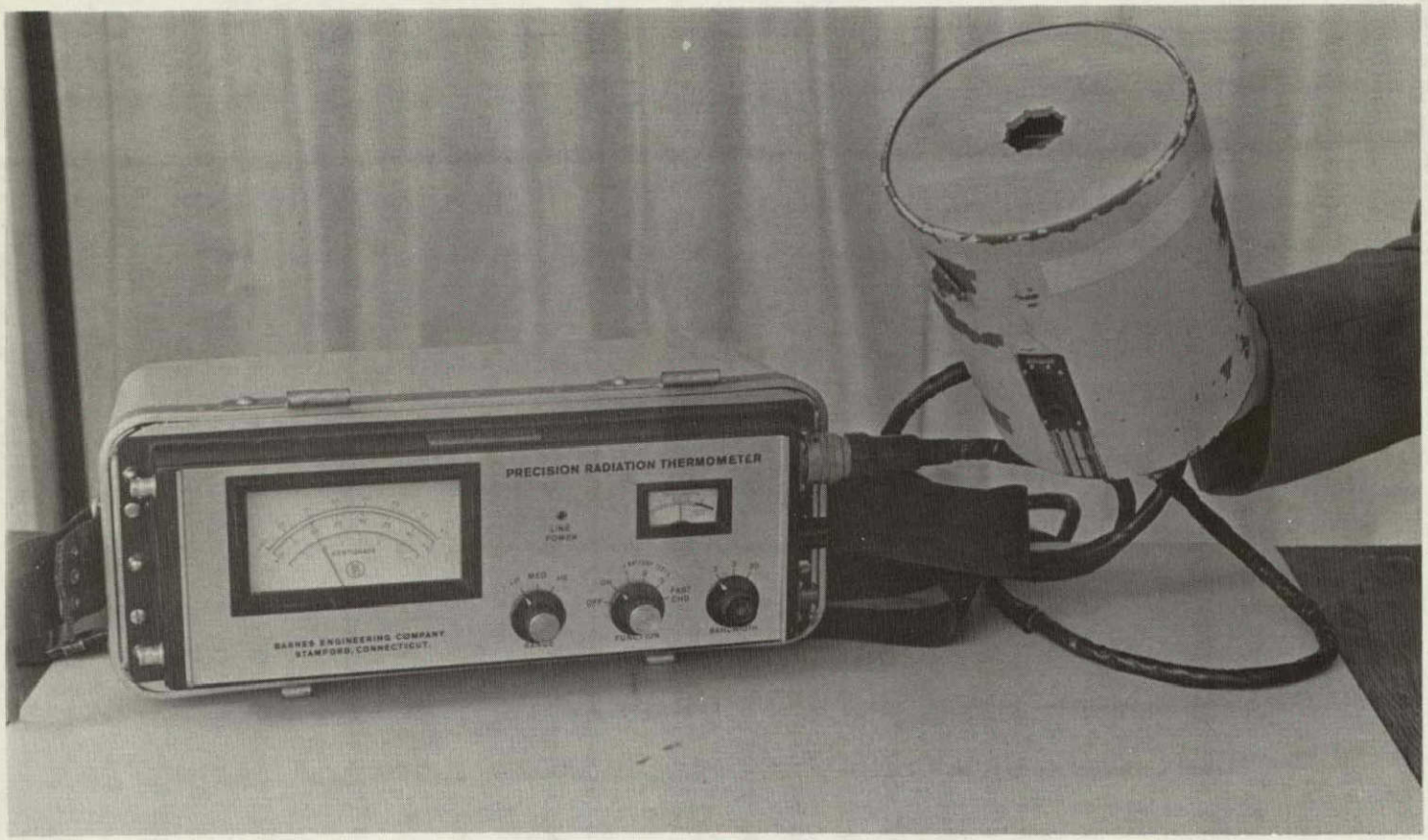

Figure 5.3.3 PRT-5 Portable Radiation Thermometer

PRT-5 was mounted on a stand so that it was looking vertically downward on to a graph paper. A soldering iron was moved from outside its F.O.V. to inside its F.O.V., on the graph paper. The points at which the PRT-5 showed an increase in response were taken to be boundary points of the F.O.V. These points, as joined by a smooth curve, are shown in Figure 5.3.4.

The F.O.V. and solid angle of the instrument were calculated as follows.

$$\text{F.O.V. in degrees} = \frac{2\ (\text{Area of the graph paper seen by PRT-5})^{1/2}}{(\text{Distance of the graph paper from PRT-5})\ (\pi)^{1/2}} \frac{180}{\pi}$$

or

$$\text{F.O.V.} = \frac{2 \times \sqrt{56.5}}{51.5\ (\pi)^{1/2}} \frac{180}{\pi} = 9.4^{\circ} \text{ plane angle}$$

The solid angle subtended by the target at the PRT-5 is given by :

$$\text{solid angle} = \frac{\text{Area of the graph paper seen by PRT-5}}{(\text{Distance of the graph paper from PRT-5})^2}$$

or

$$\text{solid angle} = \frac{56.5}{(51.5)^2} = 0.0212 \text{ steradian}$$

(D) Calibration of PRT-5

The calibration of PRT-5 was done using a conical blackbody (Figure 5.2.5), over a temperature range of about 5° C to about 50° C. The PRT-5 was set up vertically, aimed at the blackbody directly below it. The temperature of the blackbody was varied from about 5° C to about 50° C at temperature intervals of about 1 to 2° C. The blackbody was kept at a uniform temperature by a constant stirring mechanism (see Section 5.2 (C)). The results of the calibration are given below in Table 5.3.1.

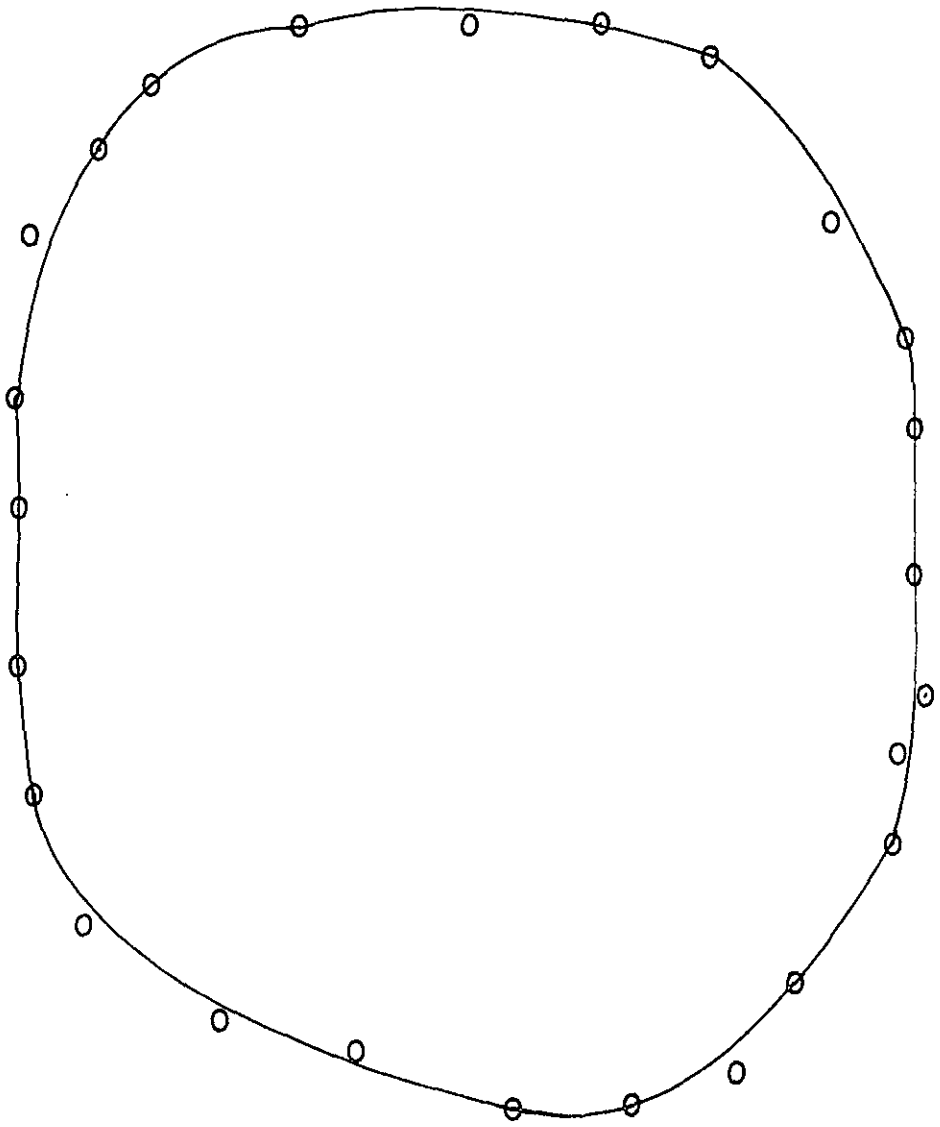

Area Seen by PRT-5= 56 5 sq. inches
Height of the Paper from PRT-5 =51.5 inches

Figure 5.3.4 Field of View of PRT-5 Portable Radiation Thermometer

Table 5.3.1 Temperature of the Blackbody vs. Temperature Indicated by the PRT-5

Temperature of the Blackbody in °C	Temperature Indicated by the PRT-5 in °C
49.91	50.60
48.56	49.30
46.30	47.05
45.28	46.00
43.32	43.50 M Scale
	44.00 H Scale
42.01	42.10 M Scale
	42.60 H Scale
40.39	40.60 M Scale
	41.10 H Scale
39.08	39.45
37.44	37.85
35.64	36.25
34.04	34.90
32.13	33.00
31.20	32.10
29.52	30.60
27.56	28.90
26.38	27.80
24.35	26.00
23.93	25.05
23.01	24.50
22.08	23.45
20.36	21.70
18.76	20.40
16.91	19.10
15.89	18.30
15.20	17.50
13.88	15.70
12.63	15.00

Table 5.3.1 cont.

Temperature of the Blackbody in °C	Temperature Indicated by the PRT-5 in °C
10.96	13.40
10.13	12.95
8.32	11.10
7.00	9.50
6.06	8.90

Note: L-Scale and M-Scale gave the same readings from 10 to 15° C.

5.4 Ground Truth for Experiments with Long Wavelength Spectroradiometer

The purpose of the ground truth is to help interpret the data produced by the spectroradiometer properly and to help find the causes of spectral variability within and between the targets of interest. Hoffer[45] has given the importance of ground truth data in remote sensing. The word 'spectroradiometer' has been used in this and the subsequent Sections to mean 'Long Wavelength (LWL) spectroradiometer' (i.e., Indium Antimonide Channel: 2.8 to 5.6 μm and Mercury Cadmium Telluride Channel: 7 to 14 μm). Measurement of ground truth variables like radiant sky and cloud temperature, air temperature, cloud temperature, leaf area index, etc. is helpful for proper interpretation of the results obtained from analysis of the spectroradiometric data.

(A) Radiance Sky and Cloud Temperature

The values of the sky radiance temperature (also called radiant temperature) and cloud radiance temperature were determined with PRT-5. If the temperature of the sky and/or cloud was not uniform over the whole sky and/or cloud, both maximum and minimum values of the radiance temperatures were recorded. Percentage of cloud cover was roughly estimated by looking at the sky. The minimum and maximum values of the radiance temperature of the clear sky were found to be about 'well below -20° C' (PRT-5 cannot measure radiance temperatures below -20° C) and -10° C respectively. The radiance temperature of the clouds were usually found to lie between about -5° C to about 20° C depending upon the type of clouds.

(B) Soil and Air Temperature

The contact temperatures of soil and air were measured using portable precision thermistor thermometer (Section 5.3(A)). Probe types 709 and 705 , manufactured by Yellow Springs Instruments, were used for measuring the contact temperatures of soil and air respectively. These probes, prior to their use, were calibrated against Taylor Permafused Precision Thermometers from 5° C to 50° C, as described in Section 5.3(A).

There are a number of errors involved in the measurement of the

contact temperature of a target by thermistors, thermocouples etc.[19] Their material usually has different emittance than the target (leaf, soil etc.) and thus experiences a different radiant energy exchange regime. In addition, they have different heat dissipation mechanisms than the target (leaf, soil etc.), having wire leads to carry, but no evaporating surface.

Soil and air temperature measurements were made on the soil on which spectroradiometric data was recorded. For each spectral scan of the target by the spectroradiometer, the temperatures were measured in the following order:

(i) Sunlit soil temperature was measured at two spots, about 3 to 4 feet apart. The spots were selected at random.

Temperature of the soil varies from one spot of the soil to another, in general. A meaningful temperature of the soil can be defined as the average temperature of the soil, average being taken over the area of the soil (Section 2.2). It is questionable if the measurement of the temperature of two spots of sunlit soil is nearly equal to the average temperature of the sunlit soil. The temperature measurements were made at only two spots of the soil because these measurements had to be made efficiently with each scan of the spectroradiometer. If the target did not have any sunlit soil, the temperature of the shaded soil was measured at four spots instead of two.

(ii) Air temperature near the target was measured in the shade.

(iii) Same as (i) except that the measurements were made on the shaded soil.

(iv) Air temperature around the target was measured in the shade.

Unfortunately, the soil and air temperatures could not be measured with the spectroradiometer scans of some of the targets because of the shortage of personnel. At least two persons are needed to measure the soil and air temperatures accurately with each scan of the spectroradiometer.

(C) Temperature of the Plant Leaves

It is very difficult to measure a meaningful temperature of a plant leaf accurately and efficiently. The effect of environmental variables

on the plant leaf temperatures was given in Section 2.4. The change in environmental variables causes a change in the temperature of a leaf (Section 2.3(A)). The temperature of a leaf in a field environment changes rapidly because of a rapid change in the environmental variables. In general, the temperature of a leaf varies very rapidly when the wind is blowing. Thus, if possible, the field experiments with long wavelength spectroradiometer should be conducted at a time when the wind is relatively steady.

The temperature of a leaf also varies from one spot of the leaf to another (Section 2.4(B)). A meaningful temperature of a leaf can be defined as the average temperature of the leaf over its entire area(Section 2.2). Similarly, a meaningful temperature of a plant canopy can be defined as the average temperature of its leaves.

Most part of the radiant flux density of emitted radiation coming from a plant canopy, received by the spectroradiometer, comes from the leaves and the soil directly visible from the spectroradiometer (see Chapter IV). Thus, to help interpret the data of the long wavelength spectroradiometer, it is adequate to measure the temperature of only those leaves which are directly seen by the spectroradiometer. However, in actual practice, it is quite tedious and impractical to measure the temperature of each small portion of the leaf and average it over the leaves directly seen by the spectroradiometer. Hence, the temperature of the leaves was not measured.

(D) Estimation of Other Variables of Ground Truth

Other variables like solar radiation, net radiation, minutes of sunshine, wind direction, wind velocity, relative humidity, evaporation rate etc. are recorded constantly (i.e., 24 hours a day) by the weather station at the Purdue Agronomy Farm and can be used, if needed. The values of these variables can be assumed to be the same at our experiment site as at the Weather Station since the experiment site was located quite close (within a mile) to the Weather Station. It should be pointed out that the scan of the targets was accomplished by both short wavelength and long wavelength spectroradiometer. The ground

truth taken for analyzing the data of short wavelength spectroradiometer, given in Appendix B can also be used if needed.

(E) Recommendations and Concluding Remarks

The spectroradiometer can record the data as fast as one second per spectral scan. In order to collect the ground truth at a time as close as possible to the time of accomplishing scan of the target with spectroradiometer, only the necessary variables of the ground truth should be be measured in a most expedient manner.

With each scan by the spectroradiometer, the soil temperature should be measured at a number of spots of the soil to get true and meaningful temperature of the soil. If the soil is partly sunlit and partly shaded, temperature measurements should be made on the sunlit as well as on the shaded soil. If the value of any ground truth variable -- say soil temperature varies rapidly, both minimum and maximum values of the variable should be recorded. Probe for the soil temperature measurement should be kept in the shade and it should come well in contact with the soil.

5.5 Evaluation of a Spectroradiometric Method for Determining Temperature and Spectral Emittance of a Natural Target

(A) Introduction

It is quite important to know the temperature of the natural target -- say plants -- to detect the subtle changes in their temperature caused due to stresses by insects, plant diseases, physiological disorders, nutrient deficiency and adverse environment effects. Optimum temperature exists for certain biological activity in the organisms. For example, soil temperatures too hot or too cold inhibit seed germination[8] . It is also necessary to know the temperature of a target for energy balance calculations.

Nutter[74] (1972) has given an excellent review of the radiation thermometery. Some authors of the technical literature have given the plot of spectral radiance temperature (see Section 2.2 for definition of spectral radiance temperature) vs. wavelength of some natural targets in a certain wavelength range but they have not attempted to find a reasonably accurate approximation to the temperature of the target from the data of spectral radiance temperature. For example, the plot of spectral radiance temperature vs. wavelength from a number of field scenes in the wavelength range of 5 to 15 μm is given on pp. 47-51 of the LARS Annual Report[63] . It will be shown that the spectral radiance temperature of a target can be considerably less than the target temperature.

(B) Spectral Radiance Temperature and Average Temperature of a Target

It was pointed out in Section 2.2 that if the temperature of a natural target is not constant over the whole target, its meaningful temperature can be defined as the average temperature of the target over its entire area. An example is given below to show that the spectral radiance temperature of a typical natural target having nonuniform temperature distribution, as measured by a spectroradiometer, is close to its average temperature for all practical purposes.

Consider a target divided into five parts equal in area. Let the temperature of the five equal parts be 20° C, 22° C, 24° C, 26° C and 28° C respectively. The average temperature of the target, T_{AVG} = 24° C. Let the target fill the field of view of the spectroradiometer. Let $T_s(\lambda)$ be the spectral radiance temperature of the target, as given by the spectroradiometer, assuming emittance of the target equal to one and neglecting the experimental errors involved. A plot of $T_{AVG} - T_s(\lambda)$ vs. wavelength is shown in Figure 5.5.1. Figure 5.5.1 shows that $T_{AVG} - T_s(\lambda)$ is less than 0.15° C in the wavelength interval 4 to 14 μm, which is within the accuracy of measurement of spectral radiance temperature by the Exotech Model 20C Spectroradiometer (Section 5.2).

(C) Definition of Temperature of a Nonblack Target for Applications to Spectroradiometric Measurements

In general, the temperature of a natural target is not uniform over the whole target. Consider a natural target whose temperature need not be uniform.

Let a spectroradiometer whose radiance and wavelength scales have been calibrated record the spectral radiance coming from the natural target at wavelengths λ_1, λ_2 ... λ_N. Let the target be opaque (i.e., transmission = 0) in the wavelength region λ_1 to λ_N. Throughout this section, i will refer to integers 1, 2, ... N; j and k will refer to integers lying between 1 and N. Let $\rho(\lambda_i)$ be the spectral hemispherical directional reflectance[67] of the natural target in the direction of the sensor.

$$\varepsilon(\lambda_i) = 1 - \rho(\lambda_i) \qquad \text{(using Kirchhoff's Law)} \qquad (5.5.1)$$

where

$\varepsilon(\lambda_i)$ = spectral directional emittance of the target in the direction of the sensor

The basic assumption made in this analysis is that the reflected radiation from the target is negligible as compared to the radiation emitted from it. If the sky is clear, this is true for most natural targets

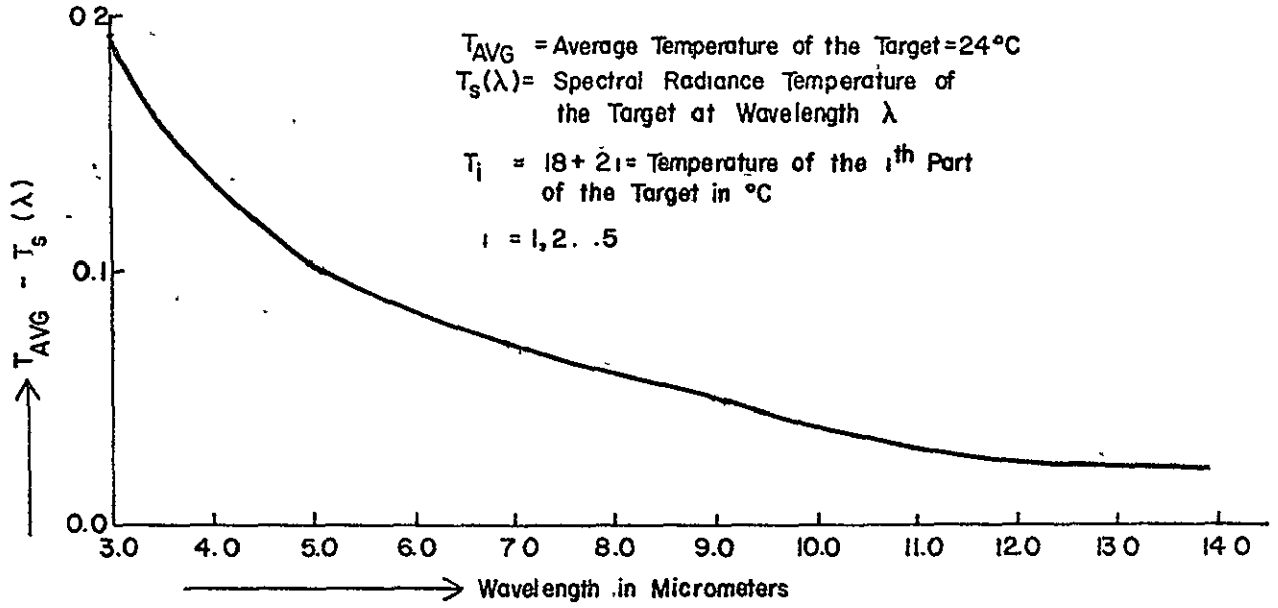

Figure 5.5.1 Difference Between Average Temperature and Spectral Radiance Temperature of a Target vs. Wavelength

for wavelengths longer than approximately 4 μm (Section 2.5(C)).

Neglecting the reflected radiation from the target, as explained above, and neglecting the scattering, absorption and emission by the atmosphere [64], one gets, using Planck's Law with usual notations.

$$T_s(\lambda_i) = \frac{hc}{k\lambda_i} \frac{1}{\log_e \{1 + \frac{2hc^2}{\lambda_i^5 L_{\lambda_i}}\}} \qquad (5.5.2)$$

$i = 1, 2, \ldots N$

where

$T_s(\lambda_i)$ = spectral radiance temperature at wavelength λ_i

L_{λ_i} = spectral radiance of radiation coming from the target at wavelength λ_i

or

L_{λ_i} ≃ spectral radiance of radiation emitted by the target at wavelength λ_i

The temperature of a target, for applications to spectroradiometric measurements, is defined using Planck's Law, as follows.

$$T = \frac{hc}{k\lambda_i} \frac{1}{\log_e \left[1 + \{\frac{2hc^2\,\varepsilon(\lambda_i)}{\lambda^5 L_{\lambda_i}}\}\right]} \qquad (5.5.3)$$

It should be pointed out that in actual practice, the values of temperature, T, at the wavelengths λ_1, λ_2 ... λ_N may not be equal because of the experimental errors involved. Throughout this Section the word "temperature" of a natural target will be used to mean temperature, T, defined by Equation (5.5.3).

(D) Determination of Temperature and Spectral Emittance of a Natural Target

There are N equations in Equation (5.5.2) and N unknowns, $T_s(\lambda_i)$, which can be determined.

$$L_{\lambda_i,b}(T_s(\lambda_i)) = L_{\lambda_i}(T) = \varepsilon(\lambda_i)\, L_{\lambda_i,b}(T) \qquad (5.5.4)$$

where

$L_{\lambda_i,b}(T_s(\lambda_i))$ = blackbody spectral radiance at wavelength λ_i and temperature $T_s(\lambda_i)$

$\varepsilon(\lambda_i)$ = spectral emittance of the target at wavelength λ_i

From Equations (5.5.3) and (5.5.4), one obtains

$$T_s(\lambda_i) \leq T,\ T_s(\lambda_i) = T \text{ if and only if } \varepsilon(\lambda_i) = 1 \qquad (5.5.5)$$

There are N equations in (5.5.4) and N+1 unknowns -- $\varepsilon(\lambda_i)$, i = 1, 2, ... N, and T. Therefore, Equation (5.5.4) cannot be solved, in general, i.e., the temperature, T, of the target cannot be determined without any knowledge about its spectral emittance.

The variables of Equation (5.5.4) are plotted vs. wavelength in Figures 5.5.2 to 5.5.7. Although the wavelength range in these Figures is taken to be 0.5 to 14 μm for illustrative purposes, we are concerned only with the wavelength range about 4 to 14 μm in this Section.

Figures 5.5.2 and 5.5.3 show that the difference between the temperature, T, and spectral radiance temperature, $T_s(\lambda)$, increases almost linearly as the wavelength increases for a given value of spectral emittance. Figure 5.5.7 shows that $[T - T_s(\lambda)]/\lambda$ vs. wavelength is almost a constant for a given value of spectral emittance of about 0.8 to 1. To find a good approximation of T, one minimizes $[T - T_s(\lambda)]$ over the wavelength range of the spectroradiometer. If the target were a gray body (i.e., spectral emittance is independent of wavelength), min $[T - T_s(\lambda)]$

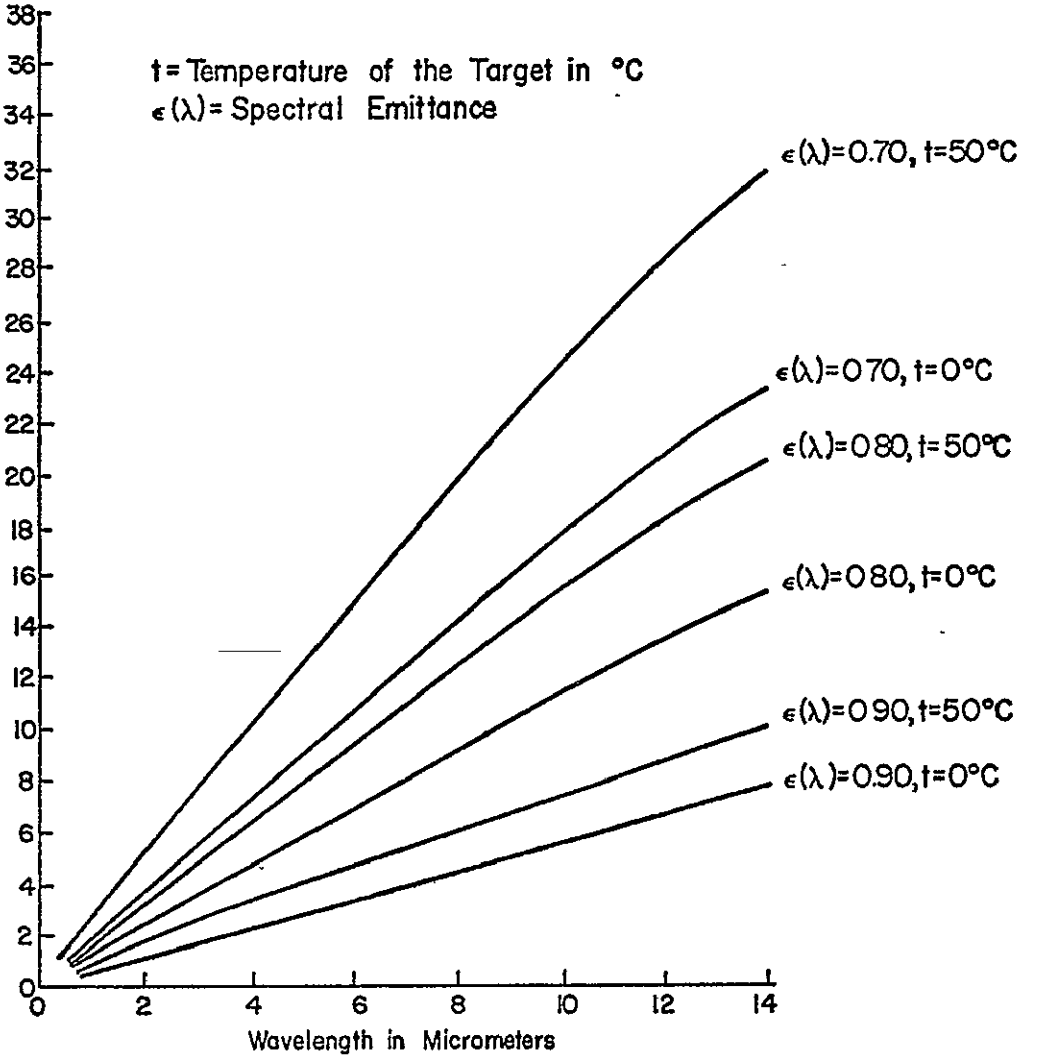

Figure 5.5.2 Difference Between Temperature and Spectral Radiance Temperature vs. Wavelength

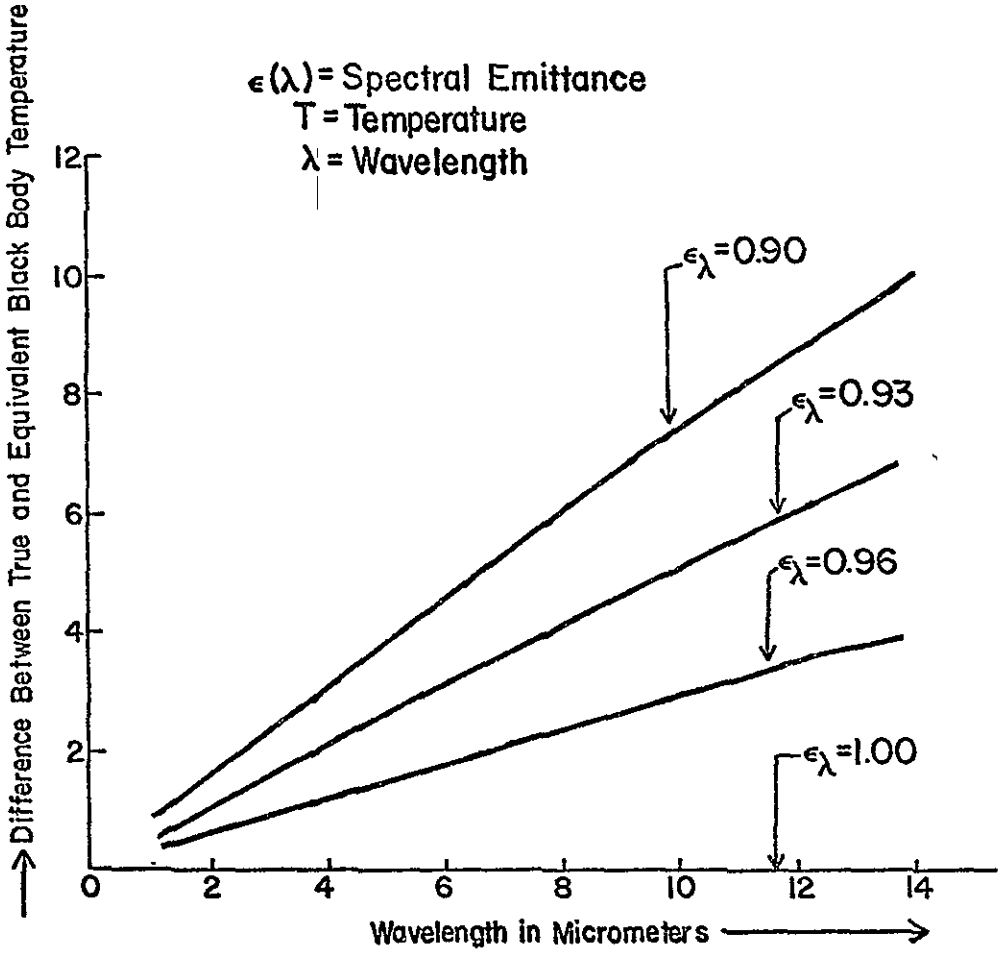

Figure 5.5.3 Difference Between Temperature and Spectral Radiance Temperature vs. Wavelength

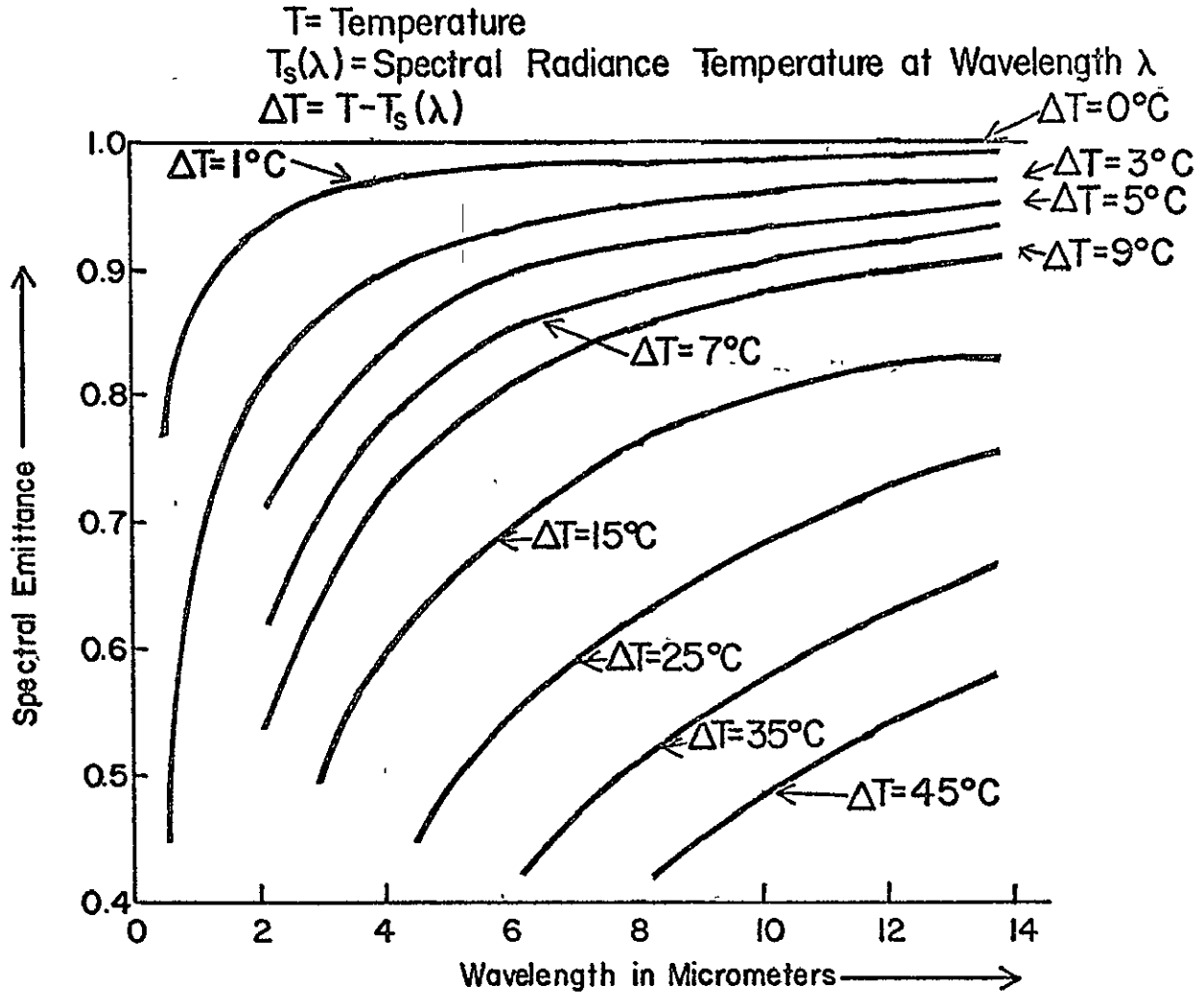

Figure 5.5.4 Spectral Emittance vs. Wavelength

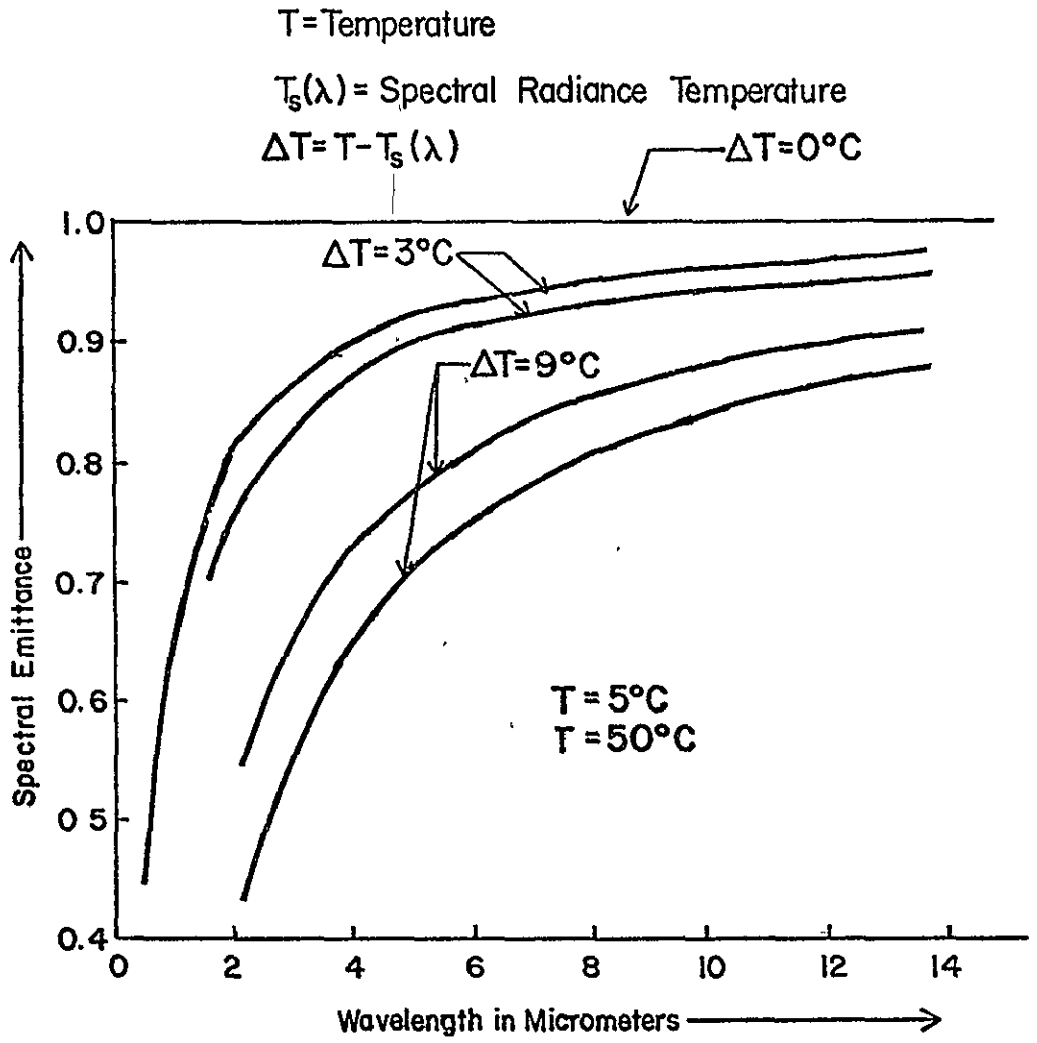

Figure 5.5.5 Spectral Emittance vs. Wavelength

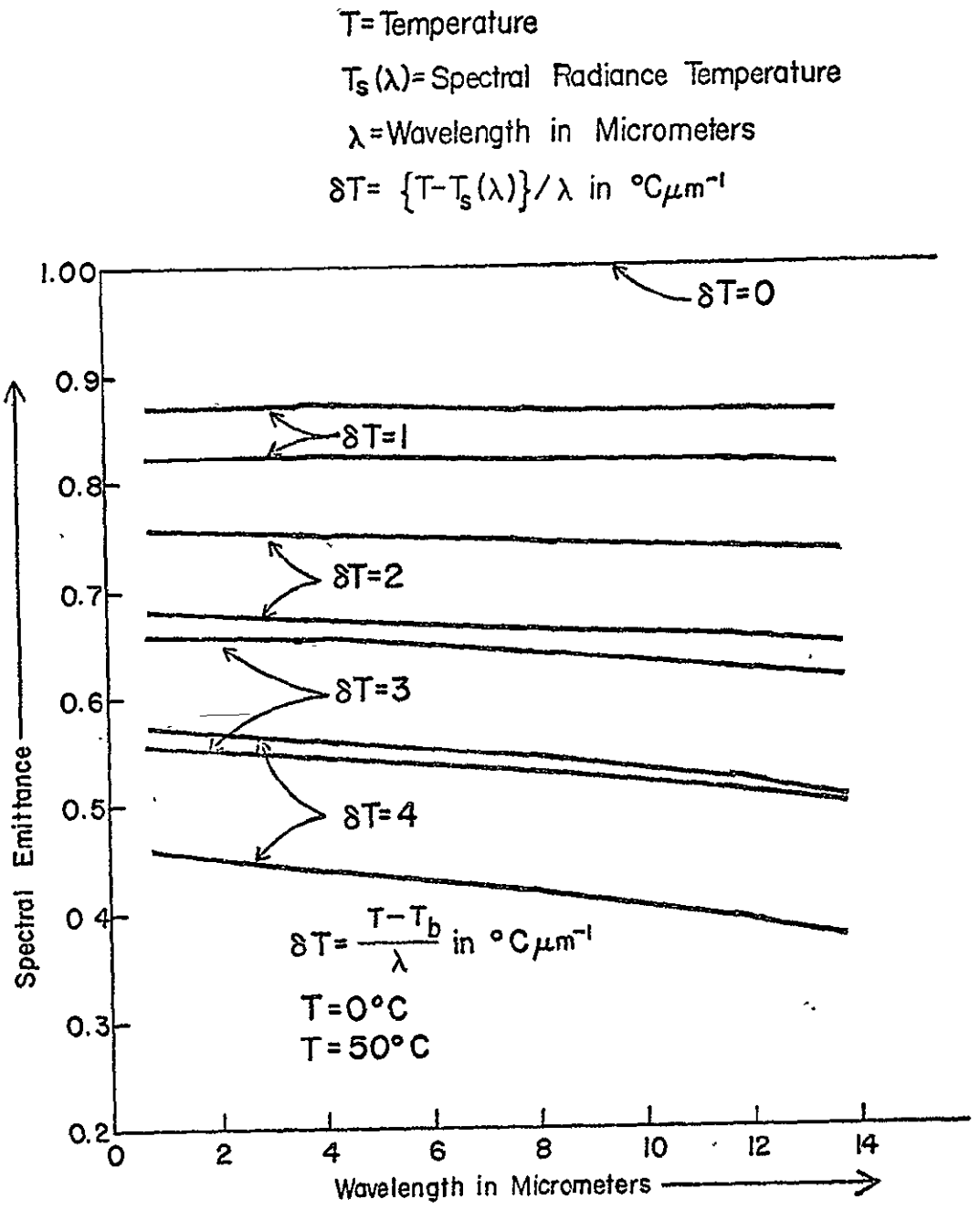

Figure 5.5.6 Spectral Emittance vs. Wavelength

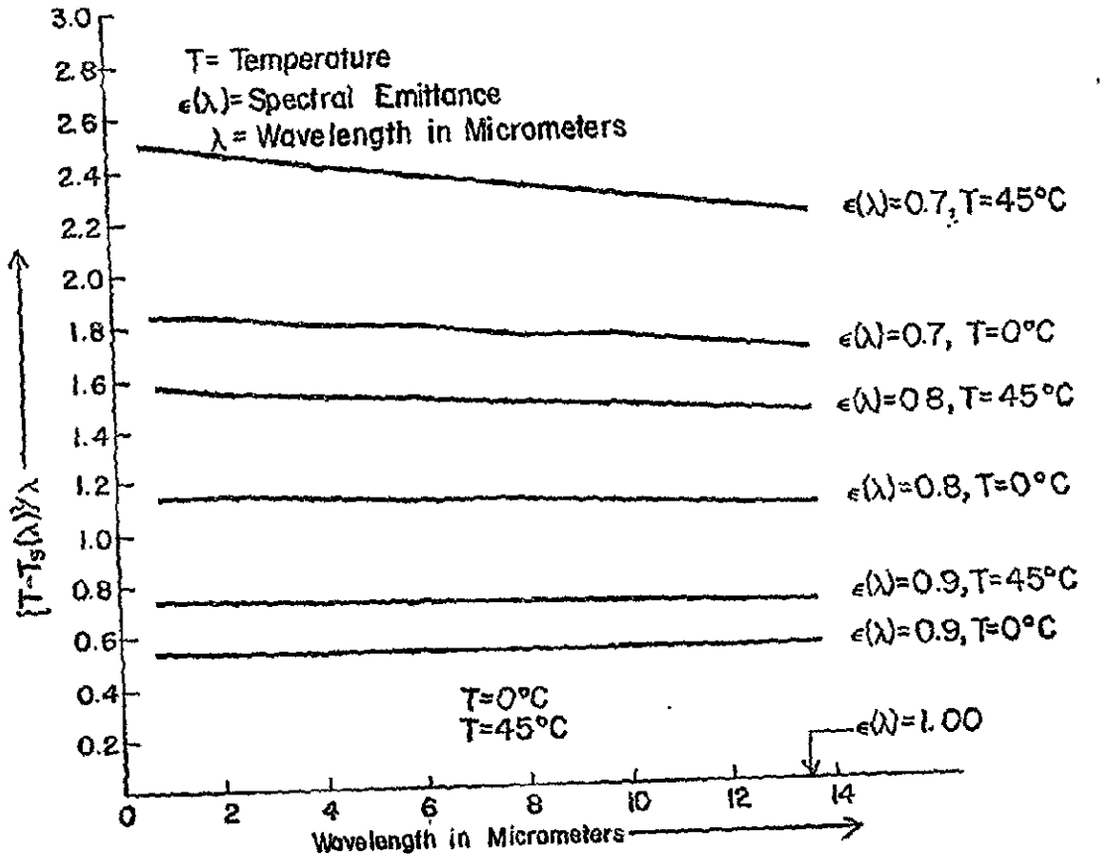

Figure 5.5.7 Plot of $\frac{T - T_s(\lambda)}{\lambda}$ vs. λ

will be found at the shortest wavelength of the wavelength range of the spectroradiometer -- λ_1. In actual practice, however, the natural target may not be a gray body [40,47,46] in the wavelength range 4 to 14 μm. Therefore, in general, min $[T - T_s(\lambda)]$ can lie anywhere between λ_1 and λ_N depending on spectral emittance and spectral radiance temperature of the target. Figures 5.5.4 and 5.5.5 show respectively, that the accuracy of experimentally determined spectral emittance of a target using a spectroradiometer, increases with increasing wavelengths; and the accuracy is weakly dependent upon the temperature of the target. As pointed out earlier, Equation (5.5.4) cannot be solved in general. However, the solutions of some of the special cases of Equation (5.5.4) are discussed as follows.

(a) If the target is a blackbody at one or more wavelengths λ_j, $1 \leq j \leq N$, one gets

$$T = T_s(\lambda_j) = \max_{\lambda_i} [T_s(\lambda_i)],\ i = 1, 2, \ldots N \qquad (5.5.6)$$

(b) The spectral emittance at some wavelength λ_j is a known function of the spectral emittance at some other wavelength λ_k, i.e.,

$$\varepsilon(\lambda_j) = f[\varepsilon(\lambda_k)] \qquad (5.5.7)$$

Equations (5.5.4) and (5.5.7) have (N+1) equations and (N+1) unknowns -- $\varepsilon(\lambda_i)$, $i = 1, 2, \ldots N$ and T. Thus, unknowns can be calculated.

It should be pointed out that if $T_s(\lambda) = T' =$ constant (i.e., independent of wavelength), it does not imply that the target is a blackbody, for its spectral emittance, $\varepsilon(\lambda)$, could be given by

$$(e^{hc/\lambda kT} - 1) \,/\, (e^{hc/\lambda kT'} - 1) \qquad (5.5.8)$$

In actual practice, however, it is very unlikely that the spectral emittance of a natural target is given by Equation (5.5.8). In actual practice, if $T_s(\lambda) =$ constant ± e, in the wavelength range about 7 to

14 μm, one could say that the target is probably almost a blackbody with spectral emittance greater than approximately 0.98; where e = average of absolute value of the error involved in determination of $T_s(\lambda)$ (Figure 5.5.3). A typical value of e is 0.5° C.

(c) Let the upper and/or lower bounds on the spectral emittance of the target be known in some known wavelength intervals $\lambda_j \leq \lambda \leq \lambda_k$. These bounds may be determined from the available data of spectral emittance in the literature and/or researcher's own experience and knowledge.

(i) Upper Bounds

$$\text{min. } \varepsilon(\lambda_i) \leq m_1, \text{ max. } \varepsilon(\lambda_i) \leq m_2 \tag{5.5.9}$$

Let

$$\text{max. } T_s(\lambda_i) = T_1 \text{ (found from spectroradiometric data)} \tag{5.5.10}$$

or $\text{max. } T_s(\lambda_i) = T_1$ (known value)

$$T \geq T_1 \quad \text{(Equation (5.5.5))} \tag{5.5.11}$$

Let { } denote the assumed value. Assume $\{T\}_1 = T_1$ and determine values of $\{\varepsilon(\lambda_i)\}_1$ using Equation (5.5.4) and check if min. $\varepsilon(\lambda_i) \leq m_1$. If not, then continue taking $\{T\}_2 = T_1 + \Delta T$, $\{T\}_3 = T_1 + 2\Delta T$ ... until at some $\{T\}_\ell = T_2$, min. $\varepsilon(\lambda_i) = m_1$ within certain prechosen suitable accuracy. Here ΔT is some suitable increment in temperature. For example, one can take ΔT as the average of absolute error involved in the determination of spectral radiance temperature by spectroradiometer. Similarly, one can determine T_3 corresponding to the condition max. $\varepsilon(\lambda_i) = m_2$. Let

$$\text{max. } [T_1, T_2, T_3] = T_{\text{h.l.b.}} \tag{5.5.12}$$

where

$T_{h.l.b.}$ = high lower bound of the temperature T.

If any other lower bound on T is known, it should also be included in Equation (5.5.12) to determine $T_{h.l.b.}$.

$$\varepsilon(\lambda_i)_{l.u.b.} = \frac{L_{\lambda_i,b}(\lambda_i, T_s)}{L_{\lambda_i,b}(\lambda_i, T_{h.l.b.})} \qquad (5.5.13)$$

where

$\varepsilon(\lambda_i)_{l.u.b.}$ = low upper bound on the spectral emittance $\varepsilon(\lambda_i)$

(ii) Lower Bounds

The same procedure used in "Upper Bounds" (Section D(c)(i)) can be followed to determine $T_{l.u.b.}$ and $\varepsilon(\lambda_i)_{h.l.b.}$ from the known lower bounds on spectral emittance.

Let the wavelengths at which min. $[\varepsilon(\lambda_i)_{l.u.b.}]$, min. $[\varepsilon(\lambda_i)_{h.l.b.}]$, max. $[\varepsilon(\lambda_i)_{l.u.b.}]$ and max. $[\varepsilon(\lambda_i)_{h.l.b.}]$, minimized/maximized over the wavelength range λ_1 to λ_N occur be λ_a, λ_b, λ_c and λ_d, respectively. Then min. $[\varepsilon(\lambda_i)]$ lies between λ_a and λ_b and max. $[\varepsilon(\lambda_i)]$ lies between λ_c and λ_d respectively. If $T_s(\lambda_j) \geq T_s(\lambda_k)$ for all $\lambda_j \geq \lambda_k$, where $1 \leq j \leq N$, $1 \leq k \leq N$, it implies that min. $\varepsilon(\lambda_i)$ and max. $\varepsilon(\lambda_i)$ would occur at wavelengths $\lambda_a = \lambda_b$, and $\lambda_c = \lambda_d$, respectively.

The author emphasizes that for most of the plant canopies with good ground cover (say, ground cover > 0.70), one can take $T_{h.l.b.}$ as the approximation to the temperature, T, of the plant defined by Equation (5.5.3) because the spectral emittance of most plant canopies with good ground cover probably lies between about 0.95 and 1.00 in 7 to 14 μm wavelength range (Section 2.6). If no more information on the spectral emittance of the target is available other than upper and/or lower bounds of its spectral emittance, which have been used to calculate $T_{h.l.b.}$ and $T_{l.u.b.}$ respectively, one can take

T (estimated) = $(T_{h.l.b.} + T_{l.u.b.})/2$.

One practical way of determining the temperature of a natural target

-- say a plant canopy is to take spectroradiometric data on the plant canopy at two different times when the sky is clear (cloud free) so that the reflected radiation from the target is negligible as compared to the radiation emitted by it (Section 2.5(C)). These times should be selected close enough so that the geometry (orientation of the leaves, stems, etc. percent ground cover) of the plant canopy can be assumed to be practically the same at both times. Wind should be steady at both of these times so that the wind does not change the geometry of the plant. Also, these two times should be such that the temperature of the plant at one time is likely to be significantly (at least 2° C) different from its temperature at the other time. This can be approximately checked by making a few measurements of contact temperature of the leaves directly visible from the spectroradiometer by thermistor. Now, an assumption can be made that the emittance of the plant canopy is equal at both of these times since its geometry is practically the same at both times. This gives one additional equation - Equation (5.5.7), and hence, temperature, T, of the plant canopy can be determined (Section 5.5D(b)). However, if the temperature of the plant canopy at one time is close to its temperature at another time within the experimental accuracy, then the spectral radiance of the plant canopy recorded by spectroradiometer will be equal at two times within experimental accuracy, i.e., two equations of Equation (5.5.4) are the same within experimental accuracy. So, there are only N independent equations in (5.5.4) and N+1 unknowns -- $\varepsilon(\lambda_i)$, i = 1, 2, ... N, and T. Temperature, T, cannot be determined without any knowledge of the spectral emittance of the target.

The same procedure can be followed to determine the temperature of a plant canopy by taking spectroradiometric data on two plant canopies of the same crop, maturity, geometry (orientation of leaves, stems, etc.) soil background, percent ground cover etc. These plant canopies can be assumed to have equal spectral emittance in the wavelength range of the spectroradiometer.

5.6 Ground Cover Experiment

(A) Description

The amount of vegetative ground present in an agricultural field or scene is one of the dominant factors influencing its spectral response[9]. Still, little quantitative information is now available to aid in understanding the interactive effects of the crop canopy and the soil background on the spectral characteristics of agricultural fields. The objective of this experiment is to determine the effect of amount of ground cover on the spectral response of corn in the long wavelength thermal infrared region as influenced by the soil background[9]. Russell silt loam soil was chosen as it is one of the common soils of Indiana. This experiment was designed by Dr. M. Bauer and Dr. J. Cipra of the Laboratory for Applications of Remote Sensing, Purdue University, and this description of the experiment has been written with their help.

The experiment was conducted on the Purdue University Agronomy Farm in the summer of 1972. Corn (Zea mays L.) were grown in the plots 6-76 cm rows, 4.6 meters long on May 25, 1972. Fertilizer and herbicides were applied prior to planting. The rows were marked by tractor and planting was done by hand in order to obtain uniform spacing between the rows. Plots with varying amounts of ground cover were established by having five different plant populations: 0, 15, 30, 60 and 90 thousand plants per hectare, each plant population being replicated twice (Figure 5.6.1).

Spectroradiometric scan of each of the plot numbers one to ten (Figure 5.6.1) was accomplished in the Indium Antimonide Channel (2.8 to 5.6 μm) with the Exotech Model 20C spectroradiometer (Secs. 5.1 and 5.2) on August 18, 1972, which was a relatively cloud free day (sky radiant temperature was less than -5°C). Unfortunately, Murcury Cadmium Telluride Channel (7 to 14 μm) was not in working order on that particular day and hence, no data could be taken in the Murcury Cadmium Telluride Channel.

(B) Materials and Methods

The spectral radiance and spectral radiance temperature of the target (Plot no. 1 to 10) was calculated at wavelength interval of about

6-76 cm rows of corn, 4.6 meters long
Soil: Russell silt loam

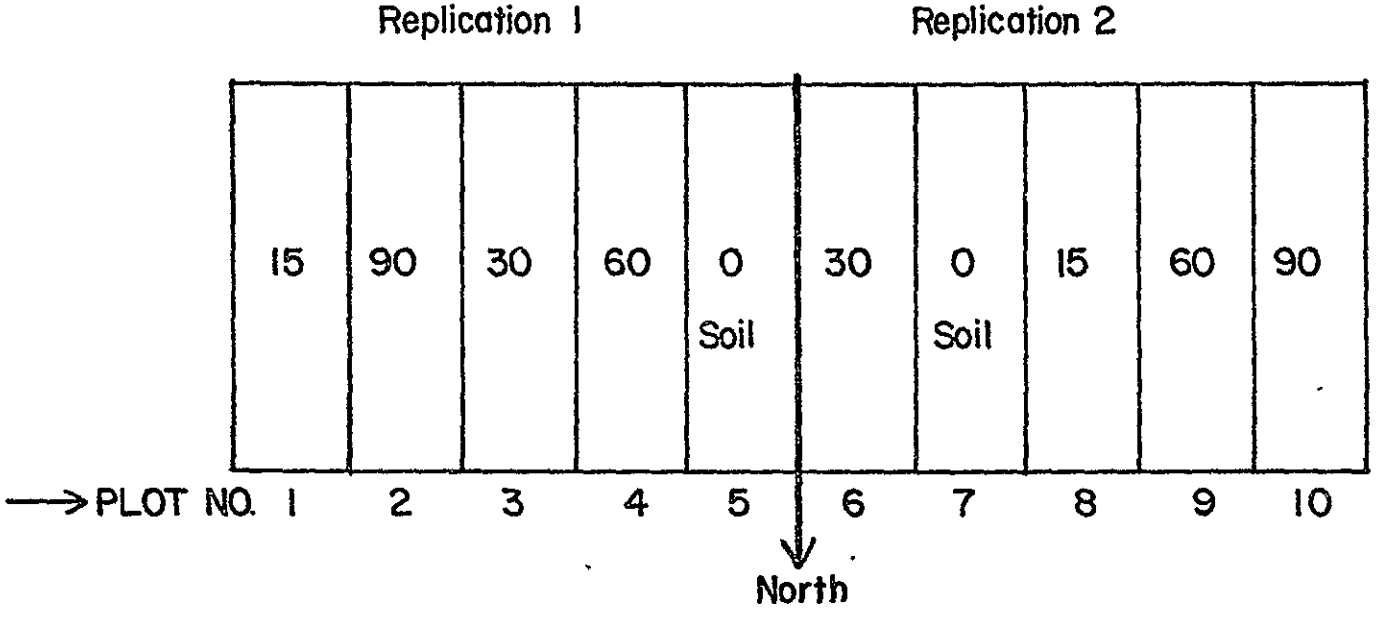

The numbers inside the plots denote plant population in thousands of plants per hectare.

Figure 5.6.1 Design for Ground Cover Experiment

0.03 μm in Indium Antimonide Channel (2.8 to 5.6 μm, see Section 5.2). The Indium Antimonide Channel was divided into the following five wavelength bands for analyzing the data.

1. 3.6 to 3.9 μm
2. 3.9 to 4.15 μm
3. 4.50 to 4.80 μm
4. 4.80 to 5.10 μm
5. 5.10 to 5.40 μm

The data in the wavelength region 2.6 to 3.6 μm were not analyzed because the value of the spectral radiance of the most natural targets--plants, soils etc. is relatively small (less than 100 microwatts/sq. cm./steradian/micrometer) in 2.6 to 3.6 μm; which results in low signal to noise ratio in this wavelength region (Sec. 5.2). The data in the wavelength region 4.15 to 4.50 μm were not analyzed because of strong absorption by atmospheric carbon dioxide (Section 2.5(A)) in this wavelength region (The data was taken from a height of about 30 ft. from the ground). The data in the wavelength region 5.40 to 5.60 μm were not analyzed because of low signal to noise ratio in this wavelength region because this wavelength region is near the wavelength 5.6 μm, which corresponds to the end of the circular variable filter wheel (Section 5.1 & 5.2) and the signal starts dropping near the end of the wheel.

The spectral radiance temperature calculated at wavelength interval of about 0.03 μm in Indium Antimonide Channel was averaged over each of the wavelength regions mentioned above, and is denoted by $T_s(\lambda)_{AVG}$.

(C) Results and Discussion

Bartlett's Test[76] was used to test for the homogeneity of the variances of the calculated values of the average spectral radiance temperature of the four plant populations (15, 30, 60 and 90 thousand plants per hectare) in each of the five wavelength regions mentioned above individually. No evidence was found to reject the hypothesis of homogeneous variances for α level of 0.05; hence the means of average spectral radiance temperatures of the four plant populations could be compared on the same basis. Soil plots (plant population = 0) were not included in the statistical analysis because the spectral radiance

temperature of the soil throughout 3.60 to 5.40μm was much different from the spectral radiance temperature of the other plant populations (Table 5.6.1).

The analysis of variance[76] was used to test the homogeneity of the means of the calculated values of $T_s(\lambda)_{AVG}$ for four plant populations (15, 30, 60, and 90 thousand plants per hectare) in each of the above mentioned five wavelength regions individually. Means of $T_s(\lambda)_{AVG}$ for the four plant populations were found to be statistically significantly different for an α level of 0.05. The values of the means of $T_s(\lambda)_{AVG}$ for each of the five plant populations (including soil) in each of the five wavelength regions are given in the following Table 5.6.1.

Table 5.6.1 Results of the Ground Cover Experiment

Wavelength Region	Plant Population (plants per hectare)	Percentage Ground Cover	Average Spectral Radiance Temperature
3.6 to 3.90 μm	0 (soil)	0 (soil)	43.80
" " "	15,000	30	37.07
" " "	30,000	50	34.95
" " "	60,000	75	34.47
" " "	90,000	90	34.97
3.90 to 4.15 μm	0 (soil)	0 (soil)	38.62
" " "	15,000	30	35.52
" " "	30,000	50	33.82
" " "	60,000	75	33.10
" " "	90,000	90	33.82
4.50 to 4.80 μm	0 (soil)	0 (soil)	36.17
" " "	15,000	30	34.25
" " "	30,000	50	33.12
" " "	60,000	75	32.90
" " "	90,000	90	32.87

Wavelength Region	Plant Population (plants per hectare)	Percentage Ground Cover	Average Spectral Radiance Temperature
4.80 to 5.10 μm	0 (soil)	0 (soil)	36.32
" " " "	15,000	30	34.22
" " " "	30,000	50	32.97
" " " "	60,000	75	32.97
" " " "	90,000	90	32.95
5.10 to 5.40 μm	0 (soil)	0 (soil)	36.05
" " " "	15,000	30	34.00
" " " "	30,000	50	33.05
" " " "	60,000	75	33.02
" " " "	90,000	90	33.52

The variables which can cause differences in the spectral radiance temperature of one plant population and another plant population are given in Table 5.8.3 (although Table 5.8.3 is given for corn blight, it can be applied to the ground cover experiment). The temperature (contact temperature) measurements of the sunlit soil and the shaded soil were made in the summer of 1972 (Section 5.4) at the time of taking spectroradiometric scans. The temperature of the sunlit bare soil was found to be about 8 to 12°C higher than the temperature of the shaded soil under the plant. The temperature of the sunlit soil and the shaded soil under the plant canopy consistantly decreased as the author went from the plant population 0 to 15,000 to 30,000 to 60,000 to 90,000 plants per hectare. This is because the solar radiant flux density reaching the soil under the plant decreases as the plant population increases. Also, most of the soil under the plants of population 30,000 and 60,000 plants per hectare was shaded. There was no sunlit soil under the plants of population 90,000 plants per hectare.

Table 5.6.1 shows:

(1) Average spectral radiance temperature of the soil is much different from the average spectral radiance temperature of the rest of the plant populations (0, 15,000, 30,000, 60,000, and 90,000 plants per hectare).

(2) The average spectral radiance temperature of the plants decreases consistently as we go from the plant population zero (soil) to the plant population 30,000 plants per hectare in all the wavelength regions given in Table 5.6.1. In the wavelength regions 4.80 to 5.10 μm and 5.10 to 5.40 μm, the average spectral radiance temperatures of the plant populations 15,000 and 30,000 plants per hectare are equal. The average spectral radiance temperature of the plants increases in the wavelength regions 3.60 to 3.90 μm, 3.90 to 4.15 μm and 5.10 to 5.40 μm as we go from a plant population of 60,000 plants per hectare to a plant population of 90,000 plants per hectare. Some of the differences in the trend of the average spectral radiance temperature vs. plant population in different wavelength regions may be because of the plant and/or soil emittance being different in different wavelength regions.

5.7 Temperature and Emittance of Healthy and Non-Sytemic Stressed Corn Leaves

(A) Temperature of Healthy vs. Non-Systemic Stressed Corn Leaves

Temperature measurements of the healthy spot of the corn leaf, blighted spot of the same corn leaf and the air temperature were made consecutively on the blighted corn plants grown in the Agronomy Farm of Purdue University on a relatively dry day when the sky was clear (sky radiant temperature -- below 5° C). Measurements were made on the blighted corn leaves because corn blight is representative of the problems of non-systemic stresses. Fifty readings of the temperature of the healthy spot of the leaf (T_H), blighted spot of the leaf (T_B) and air temperature near the leaf (T_A) were taken. The temperature of the healthy spot and the blighted spot was measured with a calibrated precision thermistor used with the digital meter (Section 5.3). The precision thermistor was a small thermistor having a resistance of 3000 ohms at 25° C and time constant (time required to indicate 63% of a new impressed temperature) of one second. A small thermistor was chosen so that its effect on the temperature of the leaf is negligible.

The temperature measurements were made on a day with relatively low wind velocity because the temperature of a leaf usually varies rapidly when the wind is blowing (Section 5.4(C)). When the temperature of the spot of a leaf and/or air was varying, both maximum and minimum values of the temperature were recorded and the average of the maximum and the minimum temperature was taken. The author found it difficult to get a good contact of the thermistor with a blighted spot because a blighted spot tends to break when brought in good contact with the thermistor. From these measurements, the temperature of healthy spot of a leaf minus air temperature ($T_H - T_A$) and the temperature of blighted spot of a leaf minus air temperature ($T_B - T_A$) were computed and are given in Table 5.7.1.

Table 5.7.1 Temperature of Healthy and Blighted Spots of Leaves Minus Air Temperature

No.	$T_H - T_A$	$T_B - T_A$
01	0.27	0.62
02	0.23	0.55
03	0.16	0.78
04	0.35	0.60
05	0.33	1.00
06	0.42	0.38
07	0.25	0.18
08	0.35	0.22
09	0.58	-0.34
10	0.36	0.40
11	-0.19	0.01
12	0.13	0.03
13	-0.31	0.21
14	0.20	0.10
15	-0.09	0.06
16	0.13	0.04
17	0.37	0.54
18	-0.21	-0.17
19	0.52	0.41
20	0.01	0.31
21	-0.02	0.02
22	0.01	0.21
23	0.17	0.10
24	-0.18	-0.12
25	0.24	0.28
26	0.09	0.21
27	0.29	0.18
28	0.08	0.19
29	0.17	0.10

Table 5.7.1 cont.

No.	$T_H - T_A$	$T_B - T_A$
30	-0.16	-0.23
31	0.02	-0.04
32	0.18	0.29
33	0.11	0.13
34	0.33	0.21
35	0.02	0.10
36	0.06	0.11
37	0.29	0.20
38	0.16	0.23
39	0.23	0.18
40	0.08	0.17
41	0.08	0.05
42	0.09	0.03
43	-0.09	0.00
44	-0.06	0.11
45	0.13	0.11
46	-0.09	0.13
47	0.31	0.25
48	-0.15	0.03
49	0.12	0.16
50	-0.04	0.03

The mean and the variance of the values of $(T_H - T_A)$ and $(T_B - T_A)$ were calculated and are given as follows.

	$T_H - T_A$	$T_B - T_A$
Mean	0.127	0.187
Variance	0.038	0.058

Bartlett's Test[76] was used to test for the homogeneity of the variances

of the data values of $(T_H - T_A)$ and $(T_B - T_A)$. No evidence was found to reject the hypothesis of homogeneous variances for α level of 0.05; hence, the means of $(T_H - T_A)$ and $(T_B - T_A)$ could be compared on the same basis. The Analysis of Variance [76] was used to test for the homogeneity of means of $(T_H - T_A)$ and $(T_B - T_A)$. No evidence was found to reject the hypothesis of homogeneous means for α level of 0.10. The mean of

$$(T_H - T_A) - (T_B - T_A) \approx 0.06 \qquad (5.7.1)$$

It should be pointed out that a difference of 0.06° C between the temperature of the blighted spots and the healthy spots of corn leaves is within the experimental accuracy of measurement of temperature by the precision thermistor (accuracy of temperature measurement of precision thermistor ≈ 0.1° C). A very preliminary conclusion, based on the results of this experiment, yet to be confirmed by further experiments, is that there is no significant difference of temperature between the blighted spots and healthy spots of corn leaves.

(B) Emittance of Blighted Corn Leaves

Completely blighted leaves were plucked from the corn plants on a clear day (sky radiant temperature below -20° C) and taken to an open space, where there were no objects near by. Thus, the surrounding radiation reflected by a blighted leaf was negligible as compared to the radiation emitted by it (Section 2.5(C)). The contact temperatures and the band radiance temperatures (see Section 2.2 for definition of band radiance temperature) in the wavelength range 8 to 14 μm, of a leaf were measured alternately with a precision thermisor and the PRT-5 radiation thermometer respectively. The measurements were made on ten blighted leaves. The emittance, $\varepsilon(8 - 14\ \mu m)$, of a leaf in the wavelength spectrum sensed by the PRT-5 (8 - 14 μm), was calculated as follows.

$$\varepsilon(8 - 14\ \mu m) = \frac{[T_s\ (8 - 14\ \mu m)]^4}{[T]^4} \qquad (5.7.2)$$

where

$T_s(8 - 14\ \mu m)$ = radiance temperature in the wavelength range 8 to 14 μm, as sensed by PRT-5

T = contact temperature as measured by precision thermistor

$\varepsilon(8 - 14\ \mu m)$ = emittance in the wavelength range 8 to 14 μm

The $\varepsilon(8 - 14\ \mu m)$ of the blighted leaves was found to lie between about 0.86 to 0.97. It should be pointed out that these results are very preliminary because these are based on a relatively few observations and a number of errors are involved in the measurement of contact and band radiance temperatures (Sections 5.7(A) and 5.4(C)). The range of $\varepsilon(8 - 14\ \mu m)$ of blighted leaves -- 0.86 to 0.97, is about the same as the range of emittance of healthy leaves (Section 2.6(C)). Thus, very careful and precise experiments need to be conducted to distinguish the subtle differences, if any, between the emittance of healthy and blighted leaves.

5.8 Experiment on Non-Systemic Stressed Corn Plants

(A) Description

The purpose of this experiment was to study the effect of non-systemic stresses on the spectral response of corn plants in the long wavelength thermal infrared wavelength region. The experiment was done for the southern corn leaf blight because corn blight is representative of the problems of non-systemic stresses.

The field experiments were conducted on the Purdue University Agronomy Farm in the summer of 1972. Corn plants of row width 76 cm, plant population 52500 plants per hectare, were grown on May 18 on the chalmers soil having a smooth surface and of silty clay loam texture.

The experimental design is shown in Figure 5.8.1. The experiment was designed by Dr. M. Bauer and Dr. J. Cipra of the Laboratory for Applications of Remote Sensing, Purdue University.

Southern corn leaf blight (SCLB) is caused by the fungus Helminthosporium maydis. The disease has been known for many years and is wide spread in corn-growing tropical areas of the world[67] . Symptoms of SCLB are the appearance of brown lesions on the lower leaves; the lesions grow in size and spread to upper leaves until the entire plant is prematurely killed (Figure 6.1.1). The corn fields were rated from blight level 0 (healthy corn) to blight level 5 (very severe blight) based on the amount of leaf damage[67] (Figure 6.1.2).

Two hybrids Pioneer 3306 and Pioneer 3571 were chosen for growing corn. One of the objectives of the experiment was to determine if there was any statistically significant difference in the spectral radiance temperature of the Pioneer 3306 (a type of hybrid) corn and Pioneer 3571 corn. Texas male-sterile cytoplasm (TMS) and normal cytoplasm versions of Pioneer 3306 corn and Pioneer 3571 corn were grown (Figure 5.8.1). Helminthosporium maydis (H. maydis) causes relatively mild infection on corn of normal (N) cytoplasm, but it attacks corn in TMS cytoplasm with unusual virulence which causes southern corn leaf blight. The TMS corn plots 3, 5, 10 and 14 were inoculated with H. maydis on June 28; whereas TMS corn plots 4, 6, 9 and 13 were inoculated with H. maydis on July

Row width: 76 cm
Plant population: 52500 plants per hectare
Soil: Chalmers silty clay loam

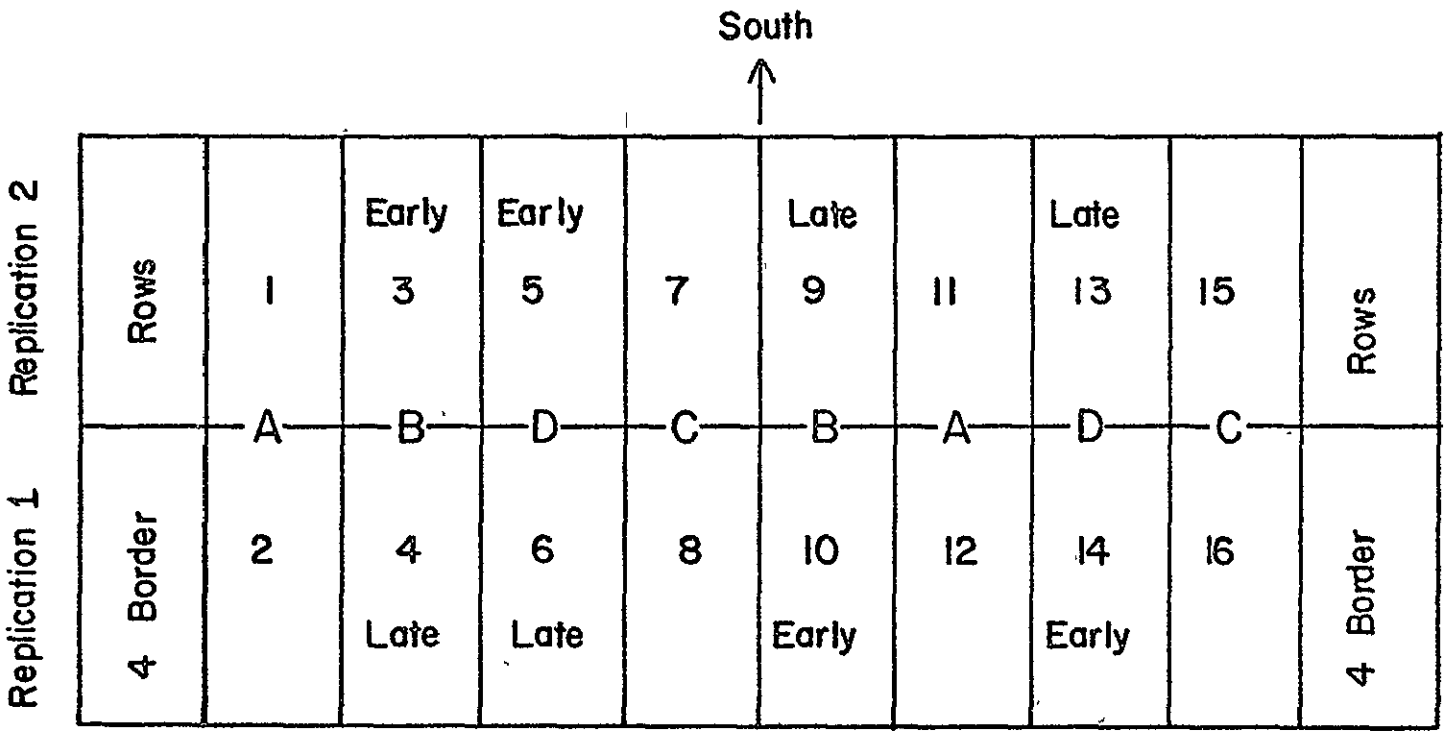

E = denotes that the plants were inoculated with SCLB on June 28
L = denotes that the plants were inoculated with SCLB on July 14
A = Pioneer 3306 - N Cytoplasm, Healthy
B = Pioneer 3306 - TMS Cytoplasm, Blighted
C = Pioneer 3571 - N Cytoplasm, Healthy
D = Pioneer 3571 - TMS Cytoplasm, Blighted
TMS = denotes Texas male-sterile N = denotes normal

Figure 5.8.1 Design of the Corn Blight Experiment

14 (Table 5.8.1).

Spectroradiometric scan in each of the Indium Antimonide Channel (2.8 to 5.6 μm) and Mercury Cadmium Telluride Channel was accomplished with Exotech Model 20C Spectroradiometer (Sections 5.1 and 5.2) on the plot numbers 2, 4, 6, 8, 10, 12, 14, 16, 13, 9, 5 and 3 on August 9, 1972, which was a relatively cloud free day (sky radiant temperature less than -5° C). The same experiment was repeated on August 17, 1972, which was also a relatively cloud free (sky radiant temperature less than 0° C) day. The experimental design can be illustrated by the following table

Table 5.8.1 Experimental Design of Corn Blight Experiment

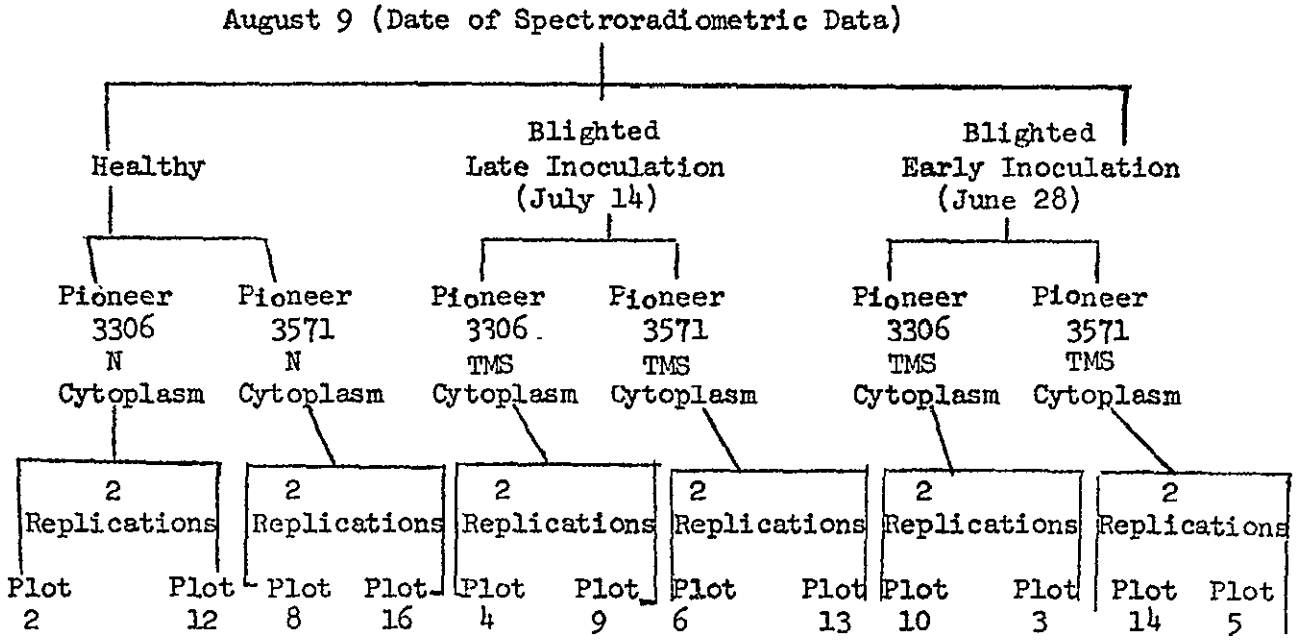

N = denotes normal

T = denotes Texas male-sterile

Plot numbers refer to the plots shown in Figure 6.8.1.

The experimental design for August 17 (date of taking the spectroradiometric data) is the same as the experimental design for August 9 given above.

(B) Materials and Methods

The spectral radiance and the spectral radiance temperature of the target was calculated at wavelength interval of about 0.03 μm in Indium Antimonide Channel (Section 5.2). The Indium Antimonide Channel (InSb) was divided into the following five wavelength bands for analyzing the data:

1. 3.6 to 3.9 μm
2. 3.9 to 4.15 μm
3. 4.50 to 4.80 μm
4. 4.80 to 5.10 μm
5. 5.10 to 5.40 μm

The reasons for not analyzing the data in the wavelength regions 2.6 to 3.6 μm, 4.15 to 4.50 μm and 5.40 to 5.60 μm are given in Section 5.6 (B).

Similarly, Mercury Cadmium Telluride (HgCdTe) Channel (7 to 14 μm) was divided into the following seven wavelength regions for analyzing the data:

1. 7.50 to 8.2 μm
2. 8.20 to 8.90 μm
3. 8.90 to 9.60 μm
4. 9.60 to 10.30 μm
5. 10.30 to 11.00 μm
6. 11.00 to 11.70 μm
7. 11.70 to 12.40 μm

The data in the wavelength regions 7.0 to 7.5 μm and 12.40 to 14.00 μm were not analyzed because the signal to noise ratio can be low in these wavelength regions as these correspond to near the start and near the end of the circular variable filter wheel respectively.

The spectral radiance and the spectral radiance temperature of the target was calculated at wavelength interval of about 0.07 μm in the Mercury Cadmium Telluride Channel (see Section 5.2).

(C) Results and Discussion

Let the average spectral radiance temperature of a corn plot in a certain wavelength region be defined as the average of the spectral radiance temperature (calculated at a wavelength interval of about 0.03 μm in Indium Antimonide Channel and 0.07 μm in Cadmium Telluride Channel) of the plot averaged over that wavelength region. Let average spectral radiance temperature of the healthy corn in a certain wavelength region be defined as the mean of the average spectral radiance temperature of the healthy corn plots (plot numbers 2, 8, 12 and 16), on which the spectroradiometric data was collected, in that wavelength region (Figure 5.8.1). The average spectral radiance temperature of the blighted corn (early inoculated with SCLB) and blighted corn (late inoculated with SCLB) can be defined similarly, the average being taken over the plots 10, 14, 3, 5, and the plots 4, 6, 13, 9 respectively.

Bartlett's Test[76] was used to test for the homogeneity of the variances of the calculated values of the average spectral radiance temperature of the healthy, early inoculated (June 28) with SCLB, and late inoculated (July 14) with SCLB, corn in each of the wavelength regions of the Indium Antimonide (InSb) Channel and Mercury Cadmium Telluride (HgCdTe) Channel, mentioned above. No evidence was found to reject the hypothesis of homogeneous variances for an α level of 0.05. Data of both dates (August 9 and August 17) were included in the analysis. Analysis of Variance for factorial design[89] was used to test for the homogeneity of the means of the average spectral radiance temperature of the healthy, early inoculated (June 28) with SCLB, and late inoculated (July 14) with SCLB corn in each of the wavelength regions of InSb and HgCdTe Channels mentioned above individually. The following conclusions were obtained:

1.) No evidence was found to reject the hypothesis of homogeneous means of the average spectral radiance temperature of corn Pioneer 3306 and corn Pioneer 3571 for an α lvel of 0.05 in each of the wavelength regions of In Sb Channel and HgCdTe Channel, mentioned above, i.e., the average spectral radiance temperature of the corn Pioneer 3306 was not found to

be statistically significantly different from the average spectral radiance temperature of the corn Pioneer 3571 for an α level of 0.05. This means that although the experiment was conducted for only two hybrids of corn -- Pioneer 3306 and Pioneer 3571; the results obtained from this analysis may well be applicable to many other corn hybrids.

2.) The average spectral radiance temperatures of the healthy corn, blighted corn inoculated on July 14 (average blight level* = 1.40) and blighted corn inoculated on June 28 (average blight level* = 3.4) were found to be statistically significantly different for an α level of 0.05.

3.) The average spectral radiance temperature of the corn (healthy and blighted) on August 9 was found to be statistically significantly different from the average spectral radiance temperature of the corn on August 17 for an α level of 0.05.

4.) The average spectral radiance temperature of the healthy, late inoculated (July 14) and early inoculated (June 28) blighted corn is given in the following Table 5.8.2.

Table 5.8.2 Average Spectral Radiance Temperature of Healthy vs. Blighted Corn

Wavelength Band	Average Spectral Radiance Temperature in ° C		
	Healthy Corn	Blighted Corn (inoculated July 14, average blight level = 1.4)	Blighted Corn (inoculated June 28, average blight level = 3.4)
	Indium Antimonide Channel		
3.60 to 3.9 μm	30.45	31.60	32.70
3.90 to 4.15 μm	29.31	30.53	31.49
4.50 to 4.80 μm	28.56	29.81	30.49
4.80 to 5.10 μm	28.31	29.59	30.31
5.10 to 5.40 μm	28.21	29.31	30.06

* Average blight level of the blighted corn inoculated on July 14 is defined as the average of the blight levels of all the plots (plot number 4, 6, 13 and 9) inoculated on July 14 on which the spectroradiometric data was taken. The average blight level of the blighted corn inoculated on June 28 is defined similarly.

Table 5.8.2 cont.

Wavelength Band	Average Spectral Radiance Temperature in ° C		
	Healthy Corn	Blighted Corn (inoculated July 14, average blight level = 1.4)	Blighted Corn (inoculated June 28, average blight level = 3.4)
	Mercury Cadmium Telluride Channel		
7.5 to 8.2 μm	28.86	30.24	31.22
8.2 to 8.9 μm	28.67	30.20	31.33
8.9 to 9.6 μm	28.42	29.95	30.97
9.6 to 10.3 μm	28.23	29.73	30.88
10.3 to 11.00 μm	28.32	29.75	30.74
11.00 to 11.70 μm	28.24	29.89	30.88
11.70 to 12.40 μm	28.52	30.05	31.00

Table 5.8.2 shows that the average spectral radiance temperature of the corn increases as the blight severity increases in each of the wavelength regions given in the Table. It also shows that for healthy corn as well as blighted (early inoculated as well as late inoculated) corn, the average spectral radiance temperature decreases as the wavelength increases in InSb Channel. In HgCdTe Channel also, the average spectral radiance temperature of the healthy as well as blighted corn generally decreases as the wavelength increases.

In this experiment, the variables which can cause differences in the average spectral radiance temperature of the healthy corn and the blighted corn are given in the following Table 5.8.3 (see Chapter IV).

Table 5.8.3 Variables that Can Cause Differences in the Average Spectral Radiance Temperature of the Healthy and Blighted Corn

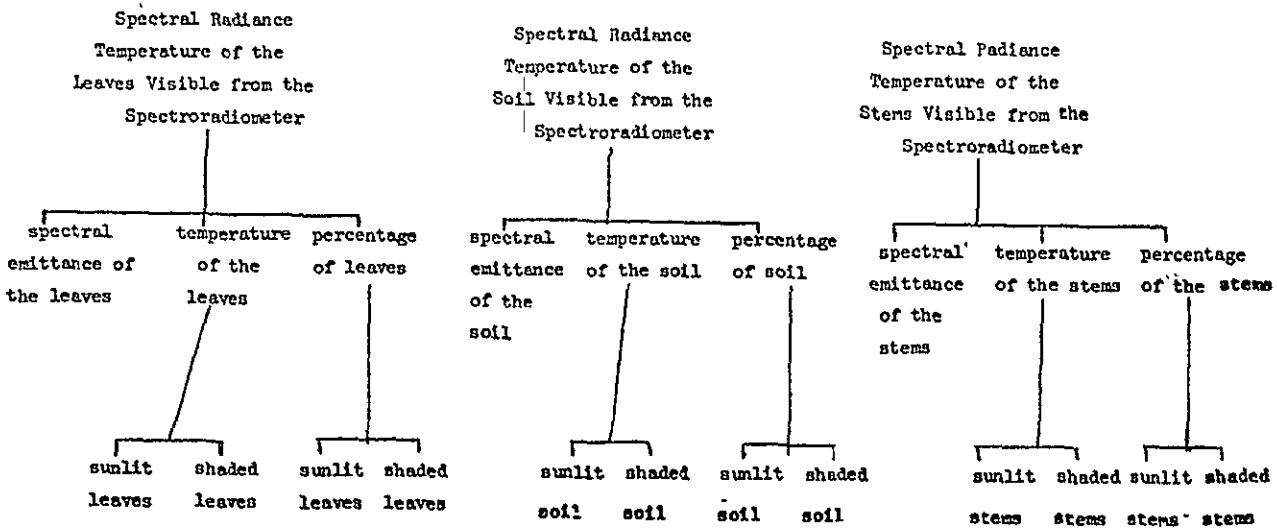

The important variables of Table 5.8.3 are discussed briefly as follows. Average spectral radiance temperature of the stems is not expected to be a predominant factor causing differences in the average spectral radiance temperature of the healthy and blighted corn. Hence, spectral radiance temperature of the stems is not discussed.

Based on a very limited number of observations, it was concluded in Section 5.7 that the band emittance of the blighted leaves in the wavelength range 8 to 14 μm was found to lie betweeen about 0.86 and 0.97, which is about the same as the range of emittance of the healthy leaves (Section 2.6(C)). Thus, there are perhaps subtle differences, if any, between the emittance of the healthy and blighted corn leaves. Hence, a very preliminary conclusion, yet to be confirmed by further experiments, is that the difference between the spectral emittance of the blighted and healthy corn leaves is not the predominant factor causing difference between the average spectral radiance temperature of the healthy and blighted corn plants.

It was reported in Section 5.7 that there was no statistically significant difference between the blighted and the healthy spots of the corn leaves. Hence a preliminary conclusion, yet to be confirmed by further experiments, is that the temperature differences, if any, between the leaves of the healthy and blighted corn plants do not contribute significantly to the difference between the average spectral radiance temperature of the healthy and blighted corn plants.

It should be pointed out that the blighted leaf is essentially dead. Its steady state temperature can be found by substituting Q_{CHEM} (net heat added to the leaf per unit time by chemical processes taking place in the leaf) = 0 and $Q_{TRANS} = 0$ in Equation (2.3.3). On a very hot sunny day, a healthy corn leaf can curl to reduce solar radiant energy per unit time incident on the leaf to prevent or at least delay wilting; whereas, a blighted leaf being essentially dead, cannot change its orientation to reduce the solar radiant energy per unit time incident on it. Hence, on a very hot sunny day, the temperature of the blighted leaf might be significantly higher than the temperature of a healthy leaf which would probably result in the difference between average spectral radiance

temperature of the blighted plants and healthy plants significantly greater than what is reported in this Section.

Healthy and blighted leaves were grown on the same soil. Hence, the spectral emittance of the soil of healthy and blighted corn plants is expected to be the same.

The percentage ground cover of a corn plant decreases as the blight level increases[9]. Also, it was reported in Section 5.6(C) that the temperature of the shaded as well as sunlit soil decreases as the percentage ground cover increases. The author believes, yet to be confirmed by further experiments, that the percentage of the soil, especially the sunlit soil, visible from the spectroradiometer, is perhaps the predominant factor causing the differences in average spectral radiance temperature of the healthy and blighted corn plants. The average spectral radiance temperature of the blighted corn plants was found to be higher than the average spectral temperature of the healthy corn plants because there was relatively more percentage of the soil visible from the blighted plants than from the healthy plants and the average spectral radiance temperature of the soil was higher than that of the leaves. This is supported by the following conclusions:

1.) The average spectral radiance temperature of the bare soil was much higher than the average spectral radiance temperature of the corn plants of population 15,000, 30,000, 60,000 and 90,000 plants per hectare (Section 5.6).

2.) The average spectral radiance temperatures of the four plant populations (15,000, 30,000, 60,000 and 90,000 plants per hectare) were found to be statistically significantly different and the average spectral radiance temperature generally decreased with an increase in plant population (Section 5.6).

5.9 Experiment on Systemic Stressed Corn Plants

(A) Description

The purpose of this experiment was to study the effect of systemic stresses on the spectral response of corn plants in the long wavelength thermal infrared wavelength region. The experiment was done for the nitrogen deficient plants because nitrogen deficiency is representative of the problems of systemic stresses.

Nitrogen is a vitally important plant nutrient, the supply of which can be controlled by man[93]. This element, to be absorbed by most plants (legumes excepted), must be in a form other than the elemental nitrogen. The forms most commonly assimilated by plants are: the nitrate (NO_3^-) and the ammonium (NH_4^+) ions. When the nitrogen fertilizers are used in conjunction with other plant nutrients in a sound crop management program, they greatly increase crop yields.

Carbon, hydrogen, oxygen, nitrogen, phosphorus and sulfur of which proteins and hence protoplasm are composed[93]. In addition to these six, there are fourteen other elements which are essential to the growth of some plant or plants: calcium, magnesium, potassium, iron, manganese, molybdenum, copper, boron, zinc, chlorine, sodium, cobalt, vanadium and silicon. Not all are required for all plants but all have been found to be essential to some.

When the plants are deficient in nitrogen, they become stunted and yellow in appearance[93]. This yellowing, or chlorosis, usually appears first on the lower leaves; the upper leaves remain green. In cases of severe nitrogen shortage, the leaves turn brown and die.

The field experiments were conducted on the Purdue University Agronomy Farm where long term fertility experiments are available. These are replicated experiments with varying rates of nutrient application. Corn plants of row width 71 cm, plant population 54,500 plants per hectare, were grown on May 18, 1972, on the chalmers soil having a smooth surface and a silty clay loam texture. The experimental design is shown in Figure 5.9.1. The experiment was conducted on three rates of nitrogen application: (the nitrogen application was given in the form of ammonium nitrate in spring) 0 kg/hectare, 67 kg/hectare and 201 kg/hectare (healthy).

corn plants of row width = 71 cm
plant population = 54500 plants per hectare
soil: chalmers silty clay loam

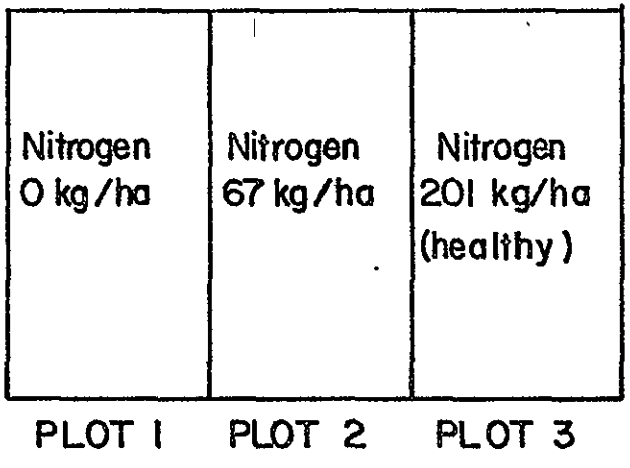

Figure 5.9.1 Experimental Design of Nitrogen Deficiency Experiment

The spectroradiometric scan of two different spots of each of the plot numbers - one to three (Figure 5.9.1) was accomplished in the Indium Antimonide Channel (2.8 to 5.6 μm) with the Exotech Model 20C Spectroradiometer (Sections 5.1 and 5.2) on August 18, which was a relatively cloud free day (sky radiant temperature was less than 0° C). Unfortunately, the Mercury Cadmium Telluride Channel (7 to 14 μm) was not in working order on that particular day and hence, no data could be taken in the Mercury Cadmium Telluride Channel.

(B) Materials and Methods

The spectral radiance and the spectral radiance temperature of the target (Plot no. 1 to 3) was calculated at a wavelength interval of about 0.03 μm in Indium Antimonide Channel (2.8 to 5.6 μm, see Section 5.2). The Indium Antimonide Channel was divided into the following four wavelength bands for analyzing the data:

1. 3.6 to 3.9 μm
2. 3.9 to 4.15 μm
3. 4.50 to 4.80 μm
4. 4.80 to 5.10 μm

The data in the wavelength region 5.10 to 5.40 μm was not analyzed because for some of the spectroradiometric scans, the signal started dropping in this wavelength region. The reasons for not analyzing the data in the wavelength regions 2.6 to 3.6 μm, 4.15 to 4.50 μm, and 5.40 to 5.60 μm are given in Section 5.6(B).

(C) Results and Discussion

Two different spots of the same plot were treated as replications for statistical analysis of the data. Bartlett's Test[76] was used to test for the homogeneity of the variances of the calculated values of the average spectral radiance temperature of the three plots (0 kg/hectare, 67 kg/hectare and 201 kg/hectare, see Figure 5.9.1) in each of the four wavelength regions mentioned above individually. No evidence was found to reject the hypothesis of homogeneous variances for an α level of 0.05; hence the means of average spectral radiance temperatures of the three corn plots could be compared on the same basis.

The analysis of variance[76] was used to test for the homogeneity of the means of the calculated values of $T_s(\lambda)_{AVG}$ of the three corn plots (0, 67, and 201kg/hectare) in each of the above mentioned four wavelength regions individually. Means of $T_s(\lambda)_{AVG}$ for the three nitrogen applications were found to be statistically significantly different for an α level of 0.05 and are given in Table 5.9.1 on the following page. Variables of ground truth (see Section 5.4) -- air temperature, sunlit soil temperature and shaded soil temperature are also given in Table 5.9.1.

Table 5.9.1 shows:

1.) As the nitrogen deficiency increases, the sunlit and shaded soil temperature increases. This is because the percentage ground cover decreases as the nitrogen deficiency increases (see Section 5.6). This trend was also found in the ground cover experiment (Section 5.6), i.e., the temperature of the sunlit soil and the shaded soil decreases as the percentage ground cover increases.

2.) $T_s(\lambda)_{AVG}$ of the plot no. 1 (nitrogen application 0kg/hectare) is lower than $T_s(\lambda)_{AVG}$ of the plot no.2 (nitrogen application 67kg/hectare); whereas, it is higher than the $T_s(\lambda)_{AVG}$ of the plot no. 3 (nitrogen application 201kg/hectare). A preliminary conclusion, yet to be confirmed by further experiments, is that the spectral radiance temperature of the plant in the long wavelength thermal infrared wavelength region is not necessarily higher for the more nitrogen deficient corn plant.

3.) The difference between the $T_s(\lambda)_{AVG}$ and the air temperature decreases as the nitrogen deficiency increases. This seems to support the results of Silva et al.[84] that nutritionally stressed plants are not always hotter than a control plant, but apparently are influenced more strongly by the environment.

The variables which can cause differences between the average spectral radiance temperature of the healthy plant and a stressed plant are given in Table 5.8.3 (although Table 5.8.3 is given for corn blight, it can also be applied to nitrogen deficient plants).

A tentative conclusion is that both percentage ground cover and the air temperature are important variables causing the differences in $T_s(\lambda)_{AVG}$ of the healthy and nitrogen deficient corn plants. Although the experiment was done on nitrogen deficient plants only, the results

Table 5.9.1 Results of the Nitrogen Deficiency Experiment

Wavelength Region	Nitrogen Application (kg/hectare)	Percent Ground Cover	Air Temperature in °C	Sunlit Soil Temperature in °C	Shaded Soil Temperature in °C	Average Spectral Radiance Temperature of plants in °C
3.60 to 3.90 µm	0	40	33.89	37.50	32.10	36.72
" " " "	67	50	34.13	37.38	31.72	36.95
" " " "	201 (healthy)	80	32.25	36.60	29.95	35.40
3.90 to 4.15 µm	0	40	33.89	37.50	32.10	35.42
" " " "	67	50	34.13	37.38	31.72	35.87
" " " "	201 (healthy)	80	32.25	36.60	29.95	34.47
4.50 to 4.80 µm	0	40	33.89	37.50	32.10	34.75
" " " "	67	50	34.13	37.38	31.72	34.77
" " " "	201 (healthy)	80	32.25	36.60	29.95	33.62
4.80 to 5.10 µm	0	40	33.89	37.50	32.10	34.60
" " " "	67	50	34.13	37.38	31.72	34.70
" " " "	201 (healthy)	80	32.25	36.60	29.95	33.52

obtained from it may well be applicable to the other systemic-stressed plants for nitrogen deficiency is representative of the problems of many systemic stresses.

CHAPTER VI

ANALYSIS OF MULTISPECTRAL SCANNER DATA OF NON-SYSTEMIC STRESSED CORN PLANTS IN SELECTED FLIGHTLINES

6.1 Introduction

The purpose of this study was to study mean response and determine the statistical separability of multispectral measurements from corn having varying levels of non-systemic stress severity. The analysis was done for southern corn leaf blight because corn blight is representative of the problems of many plant stresses, especially non-systemic stresses. The data were analyzed in one, two, three and four spectral channels for selected flightlines in the 1971 Corn Blight Watch Experiment (CBWE71). Multispectral scanner data in twelve spectral channels in the range 0.4 to 11.7 μm, collected with an optical-mechanical scanner at altitudes of 915 to 2135 meters were analyzed by applying automatic pattern recognition techniques. The key persons involved in the CBWE71 were consulted and ten flightlines were selected with their help (given in Appendix A), for analyzing the data. Only those flightlines were selected which had a fair or good number of fields of blighted corn. Furthermore, these flightlines were relatively free of the problems like fair percentage of cloud cover, lack of sufficient ground truth information, etc.

Southern corn leaf blight (SCLB) is caused by the fungus Helminthosporium maydis. The disease has been known for many years and is wide spread in corn-growing tropical areas of the world[67]. Symptoms of SCLB are the appearance of brown lesions on the lower leaves; the lesions grow in size and spread to upper leaves until the entire plant is prematurely

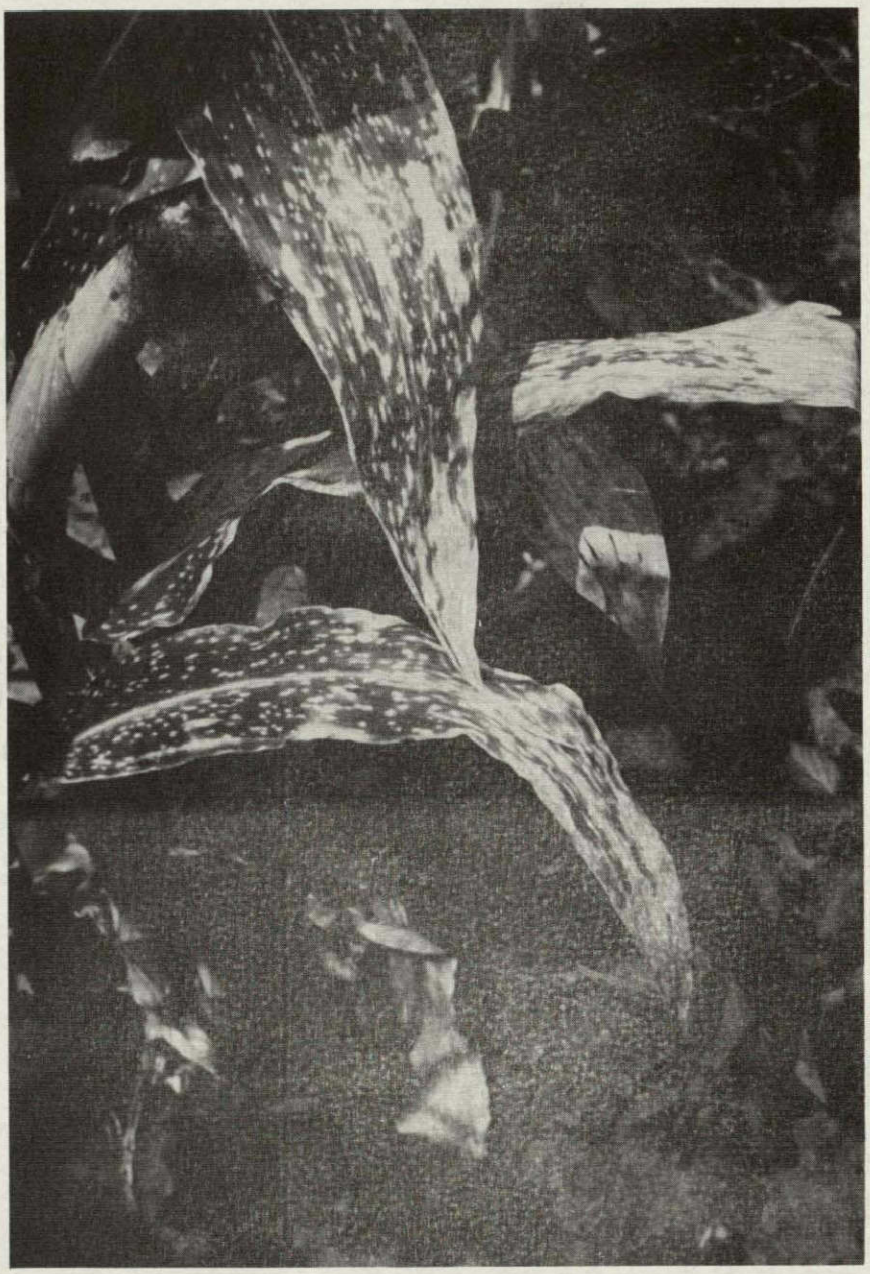

Figure 6.1.1 Southern Corn Leaf Blight. The disease is characterized by small, brown lesions which increase rapidly in size and number.

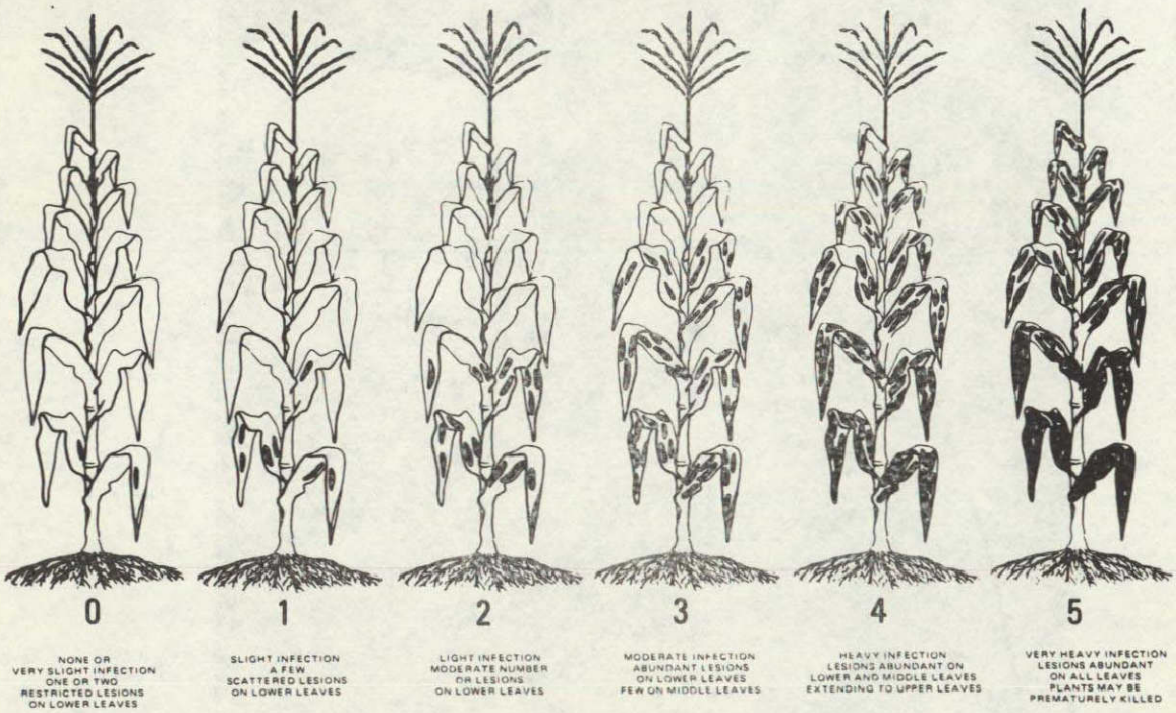

Figure 6.1.2 Scale for Estimating Southern Corn Leaf Blight Severity.

killed[67] (Figure 6.1.1). Only those corn fields were analyzed for which blight rating information from blight level 0 (healthy corn) to blight level 5 (very severe blight) based on the amount of leaf damage[67] were available (Figure 6.1.2). A total of 168 fields having 18804 sample points taken from ten flightlines were analyzed.

Black and white photography and gray scale printouts of spectral channels of the flightlines were used to aid in locating the boundaries of the corn fields on the LARS Digital Display.* The LARSYS Cluster Algorithm[91] was then used to find the spectrally distinct classes in six spectral channels. There could be more than one spectral class in one blight level but no more than one blight level was ever put in the same spectral class. A key assumption made in the cluster algorithm, statistics algorithm and feature selection algorithm is that the distributions of the classes are Gaussian. Histograms of the spectral classes defined above were used to check unimodality of the statistical distributions in individual channels. The spectral classes were re-defined to eliminate distinct multiple modes. This analysis was done by various analysts at the Laboratory for Applications of Remote Sensing in 1971. The author used the spectral classes defined by the analysts and checked the class unimodality. Further details of the 1971 Corn Blight Watch Experiment can be found in reference (67).

---

* The LARS Digital Display is a hardware system linked to an IBM 360/Model 67 using a cathode ray tube as the pictorial medium for gray scale multispectral imagery.

6.2 Mean Response of Corn Blight Levels in Each Spectral Channel

As discussed in the Introduction (Section 6.1), multispectral scanner data in twelve spectral channels in the wavelength range 0.4 to 11.7 μm were analyzed. The wavelength bands of each of the spectral channels are given below.

Table 6.2.1 Wavelength Bands of the Spectral Channels

Channel No.	Wavelength Band in Micrometers
1	0.46 - 0.49
2	0.48 - 0.51
3	0.50 - 0.54
4	0.52 - 0.57
5	0.54 - 0.60
6	0.58 - 0.65
7	0.61 - 0.70
8	0.72 - 0.92
9	1.00 - 1.40
10	1.50 - 1.80
11	2.00 - 2.60
12	9.30 - 11.70

Symptoms of Southern Corn Leaf Blight are the appearance of brown lesions on the lower leaves of the corn plant. Since in moderate blight (blight levels 1 and 2), the brown lesions are on the lower leaves (Figure 6.2.1), it makes it extremely hard to differentiate mildly blighted corn (blight levels 1 and 2) from healthy corn by remotely sensed aircraft data. As the blight progresses from blight level i ($i = 0, 1, 2, 3, 4$) to a blight level i+1, it is likely to cause only subtle changes in the reflection and emission of the corn plant. In general, there are variables other than the blight in corn plants having the same blight level -- soil variables, plant variables (percent ground cover is likely to be very important) and environmental variables --

which can cause significant differences in reflection and emission from a corn plant. Thus, it is extremely difficult to differentiate all the blight levels from remotely sensed aircraft data. Therefore, certain blight levels have been pooled (i.e., combined together to form a class) in this Section. The reasons for pooling certain blight levels together will be explained.

The statistics algorithm was used to find the mean response and standard deviation of each of the following corn blight classes in each of the twelve spectral channels for each of the ten flightlines given in Appendix A.

(a) Blight level 0
(b) Blight level 3
(c) Blight level 4
(d) Blight level 5
(e) Blight levels 0, 1 and 2 pooled together
(f) Blight levels 3, 4 and 5 pooled together
(g) Blight levels 0, 1, 2 and 3 pooled together
(h) Blight levels 4 and 5 pooled together

The corn blight severity was divided into two groups -- moderate blight and severe blight. This division was done in two ways as follows.

(i) Moderate blight consisted of blight levels 0, 1 and 2 pooled together and severe blight consisted of blight levels 3, 4 and 5 pooled together.
(ii) Moderate blight consisted of blight levels 0, 1, 2 and 3 pooled together and severe blight consisted of blight levels 4 and 5 pooled together.

The corn blight was divided into two groups -- moderate blight and severe blight on the assumption that the variables other than blight within and between the flightlines (i.e., soil variables, plant variables and environmental variables) can cause the same order of differences in reflection and emission from the corn plant as the differences in reflection and emission caused due to differences in blight severity <u>within</u> the moderate and <u>within</u> the severe blight.

The author compared the mean response of blight level 3 vs. blight

level 0; blight level 4 vs. blight level 0; blight level 5 vs. blight level 0; blight levels 3, 4, 5 pooled vs. blight levels 0, 1, 2 pooled; and blight levels 4, 5 pooled vs. blight levels 0, 1, 2, 3 pooled in each of the twelve spectral channels but could not find any regular pattern of the mean response of higher level/levels blighted corn vs. lower level/levels blighted corn in any of the spectral channels, i.e., for some of the flightlines, the mean response of the higher level/levels blighted corn was greater than the mean response of the lower level/levels blighted corn (including healthy corn -- blight level 0); whereas, for other flightlines, it was just the opposite. It is emphasised that the mean response of the blighted corn was not necessarily greater than the mean response of the healthy corn in the thermal channel (9.30 to 11.70 μm).

6.3 Statistical Separability of Spectral Classes of Blighted Corn

(A) Basic Equations

The method of obtaining spectral classes of blighted corn used in this analysis is given in Section 6.1. As pointed out in Section 6.1, a total of 168 fields having 18804 sample points taken from ten flight-lines were analyzed.

For a pair of Gaussian distribution patterns, the divergence in n channels C_1, C_2 ... C_n, for the case of normal variables with unequal covariance matrices is given[68] by

$$D(i,j \mid C_1, C_2 \ldots C_n) = 1/2 \text{ tr } [(\Sigma_i - \Sigma_j)(\Sigma_j^{-1} - \Sigma_i^{-1})] + 1/2 \text{ tr } [(\Sigma_i^{-1} + \Sigma_j^{-1})(U_i - U_j)(U_i - U_j)^T] \quad (6.3.1)$$

where

U and Σ represent the mean vector and covariance matrix, respectively;

tr[A] (trace A) is the sum of the diagonal elements of A.

A modified form of the divergence D_T, referred to as the "transformed divergence," has a behavior more like probability of correct classification[21] than D (Figure 6.3.1).

$$D_T = 2[1 - \exp(-D/8)] \quad (6.3.2)$$

Transformed divergence has been used throughout this study.

Let i and j denote the blight levels i and j. Let $W_{i_k j_\ell}$ denote the weight between k^{th} spectral class of blight level i and ℓth spectral class of blight level j, for computing the weighted average of transformed divergence over the pairs of spectral classes. Throughout this analysis, $W_{i_k j_\ell}$ was taken either = 0 or = 1. The weights which were taken = 0 and the weights which were taken = 1 shall be specified in

P_c = Probability of Correct Classification of a pair of classes

D = Divergence between a pair of classes

D_T = Transformed divergence between a pair of classes

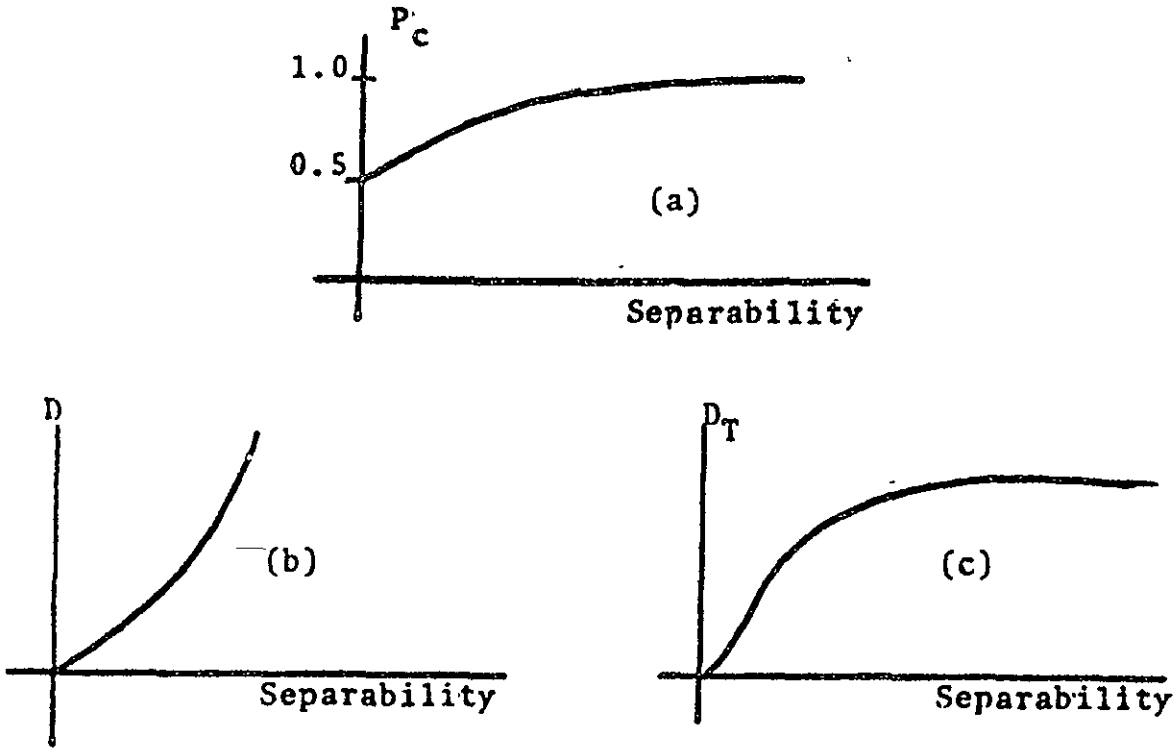

Figure 6.3.1 Relationship of Separability and (a) Probability of Correct Classification, (b) Divergence, (c) Transformed Divergence.

(Taken from Swain [91] (1972))

each individual case.

$$\text{Let } D^n_{TAVG} = \frac{1}{N} \sum_{i=0}^{5} \sum_{j=i}^{5} \sum_{k=1}^{n_i} \sum_{\ell=1}^{n_j} W_{i_k j_\ell} D^n_T (i_k, j_\ell \mid C_1, C_2 \ldots C_n) \quad (6.3.3)$$

where

n_i = no. of spectral classes in blight level i

n_j = no. of spectral classes in blight level j

N = total no. of spectral class pairs whose weights $W_{i_k j_\ell}$ were taken = 1.

$D^n_T (i_k, j_\ell \mid C_1, C_2 \ldots C_n)$ = transformed divergence between k^{th} spectral class of blight level i and ℓ^{th} spectral class of blight level j in n spectral channels - $C_1, C_2 \ldots C_n$.

Let D^n_{TMAVG} denote maximum of D^n_{TAVG}, maximized over a set of n spectral channels.

Throughout this analysis, $W_{i_k j_\ell} = 0$ when i=j and k=ℓ.

(B) Maximum Average Statistical Separability Between the Spectral Class Pairs of Mild, Intermediate and Severe Blight

The corn blight severity was divided into three groups - mild blight (blight levels 0 and 1), intermediate blight (blight levels 2 and 3) and very severe blight (blight levels 4 and 5).

The subset of each of one, two, three and four spectral channels which maximized the average transformed divergence given by Equation (6.3.3) was selected and the maximum average transformed divergence (maximized over a subset of channels) was tabulated. Let $\{D^n_{TMAVG}\}$ denote a vector whose p^{th} component (where p = 1, 2 ... 10) represents D^n_{TMAVG} in p^{th} flightline. Each of $\{D^1_{TMAVG}\}$, $\{D^2_{TMAVG}\}$, $\{D^3_{TMAVG}\}$ and $\{D^4_{TMAVG}\}$ was computed using Equation (6.3.3) for the following Sections 6.3(B)(1) to 6.3(B)(4). The values of $W_{i_k j_\ell}$ given below for Sections 6.3(B)(1) to 6.3(B)(4) hold true for all values of k and ℓ.

(1) Maximum Average Statistical Separability Between all Spectral Class Pairs

Spectral classes were found with the help of the LARSYS Cluster

Processor[91] (Sec. 6.1). Between all spectral class pairs, weights are set equal to one, i.e., $W_{i_k j_\ell} = 1$ for all i, j, k and ℓ. In all Sections 6.3(B)(2) to 6.3(B)(4) given below, $W_{i_k j_\ell} = 0$ for i=j, and the weights whose values are not specified are taken = 1.

(2) Maximum Average Statistical Separability Between All Spectral Class Pairs of Mild Blight (Blight Levels 0 and 1), Intermediate Blight (Blight Levels 2 and 3) and Very Severe Blight (Blight Levels 4 and 5)

Between all spectral class pairs of blight levels 0 and 1, blight levels 2 and 3, blight levels 4 and 5, weights are set equal to zero, i.e., $W_{0_k 1_\ell} = 0$, $W_{2_k 3_\ell} = 0$, $W_{4_k 5_\ell} = 0$.

(3) Maximum Average Statistical Separability Between the Spectral Class Pairs of Moderate (Blight Levels 0, 1 and 2) and Severe (Blight Levels 3, 4 and 5) Blight.

The southern corn leaf blight severity was divided into two groups--moderate blight (blight levels 0, 1 and 2) and severe blight (blight levels 3, 4 and 5). Between all spectral class pairs of blight levels 0, 1 and 2, weights are set equal to zero. Similarly, between all spectral class pairs of blight levels 3, 4 and 5, weights are set equal to zero, i.e., $W_{0_k 1_\ell} = 0$, $W_{0_k 2_\ell} = 0$, $W_{1_k 2_\ell} = 0$, $W_{3_k 4_\ell} = 0$, $W_{3_k 5_\ell} = 0$, $W_{4_k 5_\ell} = 0$.

(4) Maximum Average Statistical Separability Between Spectral Class Pairs of Mild Blight (Blight Levels 0 and 1) and Very Severe Blight (Blight Levels 4 and 5)

Between all spectral class pairs of blight levels 0 and 1, blight levels 4 and 5, weights are set equal to zero, i.e., $W_{0_k 1_\ell} = 0$, $W_{4_k 5_\ell} = 0$. Spectral classes of blight levels 2 and 3 were not included in the analysis.

Let $\{D^n_{TMAVG}\}_1$, $\{D^n_{TMAVG}\}_2$, $\{D^n_{TMAVG}\}_3$ and $\{D^n_{TMAVG}\}_4$ denote the values of $\{D^n_{TMAVG}\}$ in Sections 6.3(B)(1), 6.3(B)(2), 6.3(B)(3) and 6.3(B)(4). Bartlett's Test[76] was used to test for the homogeneity of variances of $\{D^1_{TMAVG}\}_1$, $\{D^1_{TMAVG}\}_2$, $\{D^1_{TMAVG}\}_3$ and $\{D^1_{TMAVG}\}_4$. No evidence was

found to reject the hypothesis of homogeneous variances for α level of 0.001; hence, means of $\{D^1_{TMAVG}\}_1$, $\{D^1_{TMAVG}\}_2$, $\{D^1_{TMAVG}\}_3$ and $\{D^1_{TMAVG}\}_4$ could be compared on the same basis. A low value of α was taken to guard against rejecting the hypothesis when it is actually true. The same analysis was done for each n (no. of spectral channels) = 2, 3 and 4, individually, and the same results were obtained as for n = 1. Let $\overline{D}^n_{TMAVG}$ denote the mean of the components (i.e., p = 1, 2 ... 10) of $\{D^n_{TMAVG}\}$. It was found that each of $\overline{D}^1_{TMAVG}$, $\overline{D}^2_{TMAVG}$, $\overline{D}^3_{TMAVG}$ and $\overline{D}^4_{TMAVG}$ individually, increased consistently as the author went from Section 6.3(A)(1) to Section 6.3(A)(2) .... to Section 6.3(A)(4), as shown in Figure 6.3.2. Also, this trend was generally found in most of the flightlines. Since the average transformed divergence between spectral class pairs is the measure of average separability between them, this trend shows that the greater the difference between the severity of spectral blight classes, the more separable they are.

(C) Maximum Average Statistical Separability Between the Spectral Class Pairs of All Possible Pairs of Blight Levels

A more detailed analysis of the statistical separability of spectral classes of blighted corn is done in this Section, than in Section 6.3(B) using the same data as in Section 6.3(B). A subset of each of one, two, three and four spectral channels which maximized the average transformed divergence given by Equation (6.3.4) was selected and the maximum average transformed divergence (maximized over a subset of channels) was tabulated.

$$\text{Let } D^n_{TAVG\ ij} = \left[\frac{1}{N} \sum_{k=1}^{n_i} \sum_{\ell=1}^{n_j} W_{i_k j_\ell} D^n_T (i_k, j_\ell \,|\, C_1, C_2 \ldots C_n) \right] \qquad (6.3.4)$$

where

$D^n_{TAVG\ ij}$ denotes average transformed divergence between spectral class pairs of blight level i and blight level j in n spectral channels $C_1, C_2 \ldots C_n$.

The rest of the notation is the same as in Equation (6.3.3).

No. of flightlines analyzed = 10

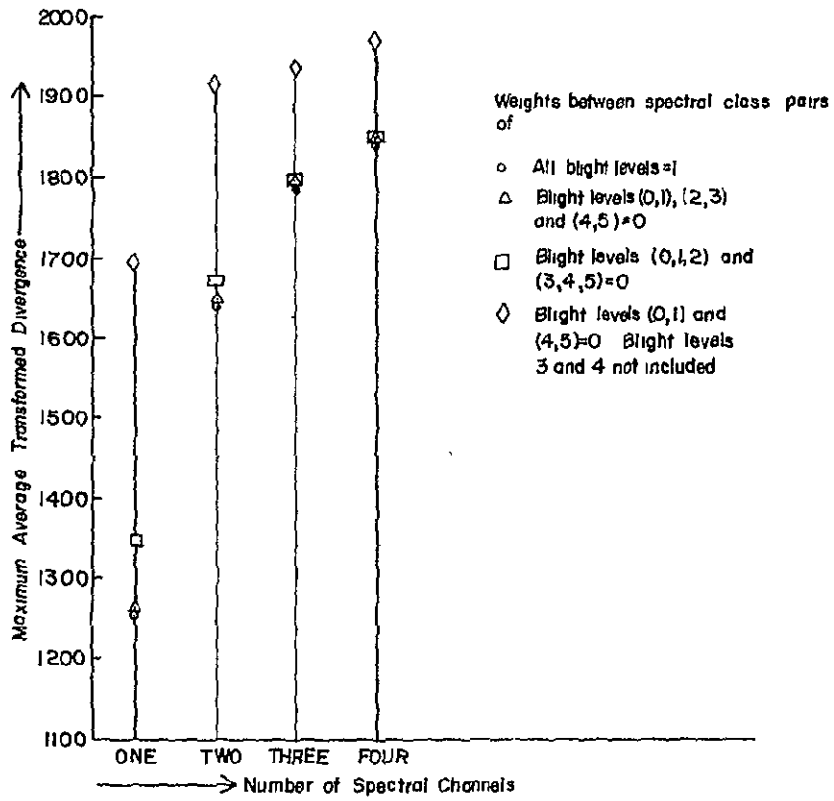

Figure 6.3.2 Statistical Separability Between the Spectral Class Pairs of Mild, Intermediate and Severe Blight

Let $D^n_{TMAVG\ ij}$ denote maximum of $D^n_{TAVG\ ij}$, maximized over a set of n spectral channels. Note that unlike Equation (6.3.3), summation over indices i and j (which denote the blight levels) is not done in Equation (6.3.4)

The maximum average transformed divergence between spectral class pairs of all possible pairs of blight levels, in n spectral channels of p^{th} flightline can be conveniently represented by a triangular matrix, as follows.

Let $[D^n_{TMAVG\ ij}]_p$, i = 0, 1 ... 4 and j = i+1, ... 5, denote a 5 × 5 triangular matrix with elements $D^n_{TMAVG\ ij}$ in p^{th} flightline. $[D^n_{TMAVG\ ij}]_p$ was computed for n = 1, 2, 3, 4 using Equation (6.3.4) with $W_{i_k j_\ell} = 1$ for all values of i, j, k and ℓ, in each of the ten flightlines individually (p = 1, 2 ... 10), i.e., maximum average transformed divergence between spectral class pairs of all possible pairs of blight levels in one, two, three and four spectral channels was calculated in each of ten flightlines individually.

Mean and variance of each of the elements of $[D^1_{TMAVG\ ij}]_p$ over all the flightlines (p = 1, 2 ... 10) were calculated. Bartlett's Test[76] was used to test for the homogeneity of variances of the elements of $[D^1_{TMAVG\ ij}]$ found above. No evidence was found to reject the hypothesis of homogeneous variances for α level of 0.001; hence, the means of elements of $[D^1_{TMAVG\ ij}]_p$, p = 1, 2 ... 10, could be compared on the same basis. The same analysis was done on the elements of $[D^n_{TMAVG\ ij}]_p$ for each of n = 2, 3 and 4, individually, and the same results were found as for n = 1.

Let the elements of $[\bar{D}^n_{TMAVG\ ij}]$ denote the average of the corresponding elements of $[D^n_{TMAVG\ ij}]_p$ over all flightlines. It was found that $\bar{D}^n_{TMAVG\ ij+1}$ was greater than (in most cases) or almost equal to (in some cases) $\bar{D}^n_{TMAVG\ ij}$, for i = 0, 1 ... 4 and j = i+1, ... 5 for each of n = 1, 2, 3 and 4 spectral channels individually, i.e., it means that the greater the difference between the blight levels, the greater the maximum average transformed divergence between their spectral class pairs, and, hence, more separable the blight levels are (Figure 6.3.3). This trend was also generally found in most of the flightlines (Figures 6.3.4 to 6.3.13).

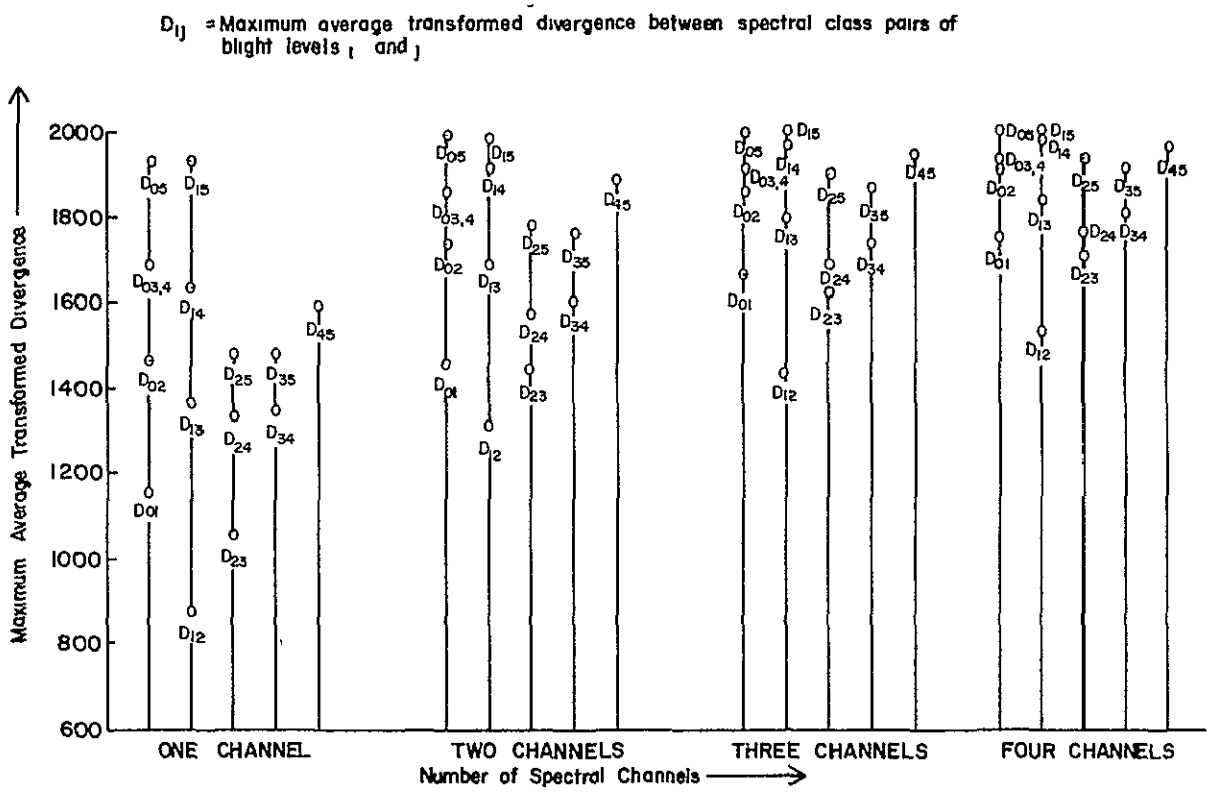

Figure 6.3.3 Statistical Separability Between the Spectral Class Pairs of All Possible Pairs of Blight Levels. All of the Ten Flightlines are Included.

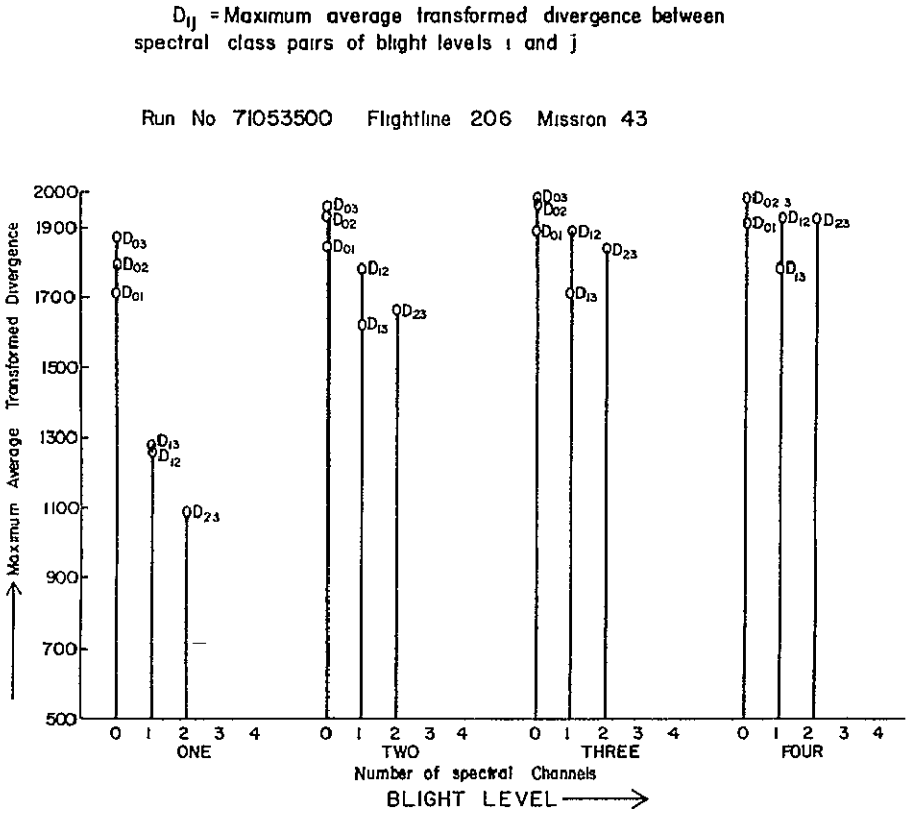

Figure 6.3.4 Statistical Separability Between the Spectral Class Pairs of All Possible Pairs of Blight Levels.
Flightline: 206 Mission: 43M

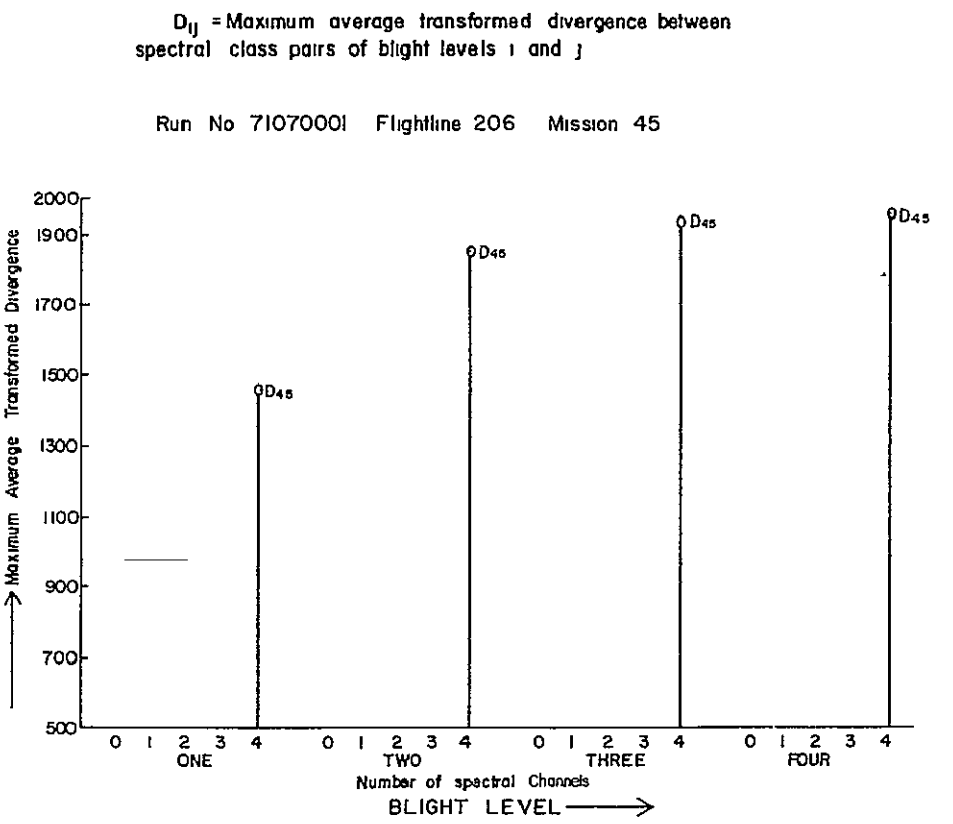

Figure 6.3.5 Statistical Separability Between the Spectral Class Pairs of All Possible Pairs of Blight Levels. Flightline: 206 Mission: 45M

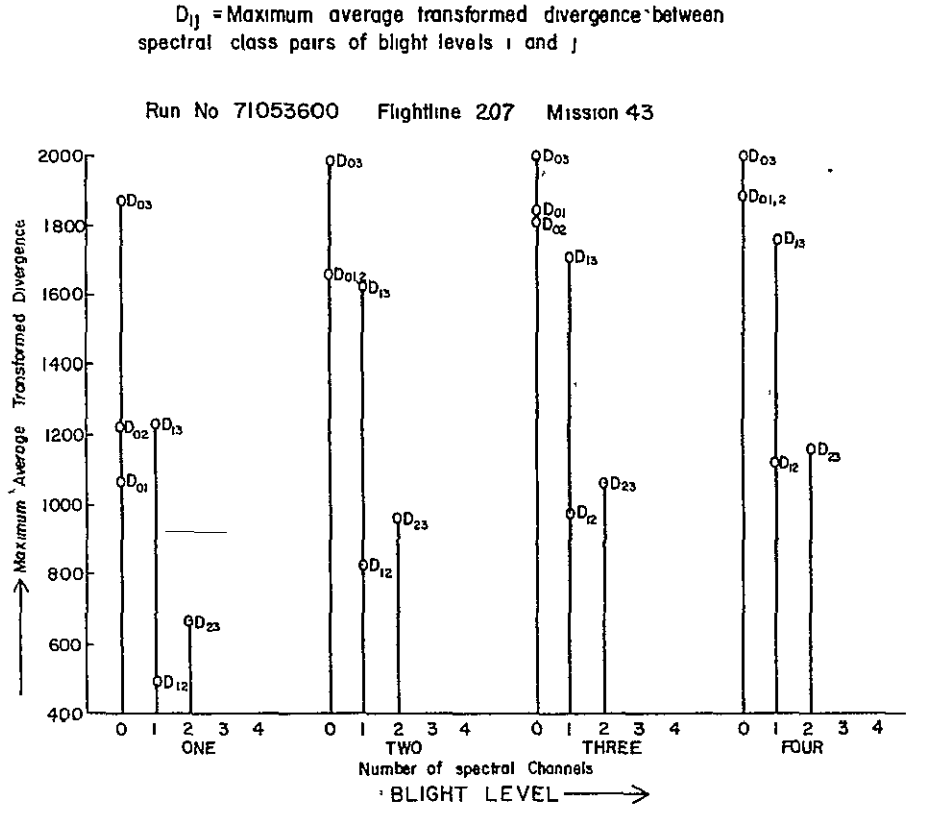

Figure 6.3.6 Statistical Separability Between the Spectral Class Pairs of All Possible Pairs of Blight Levels. Flightline: 207 Mission 43M

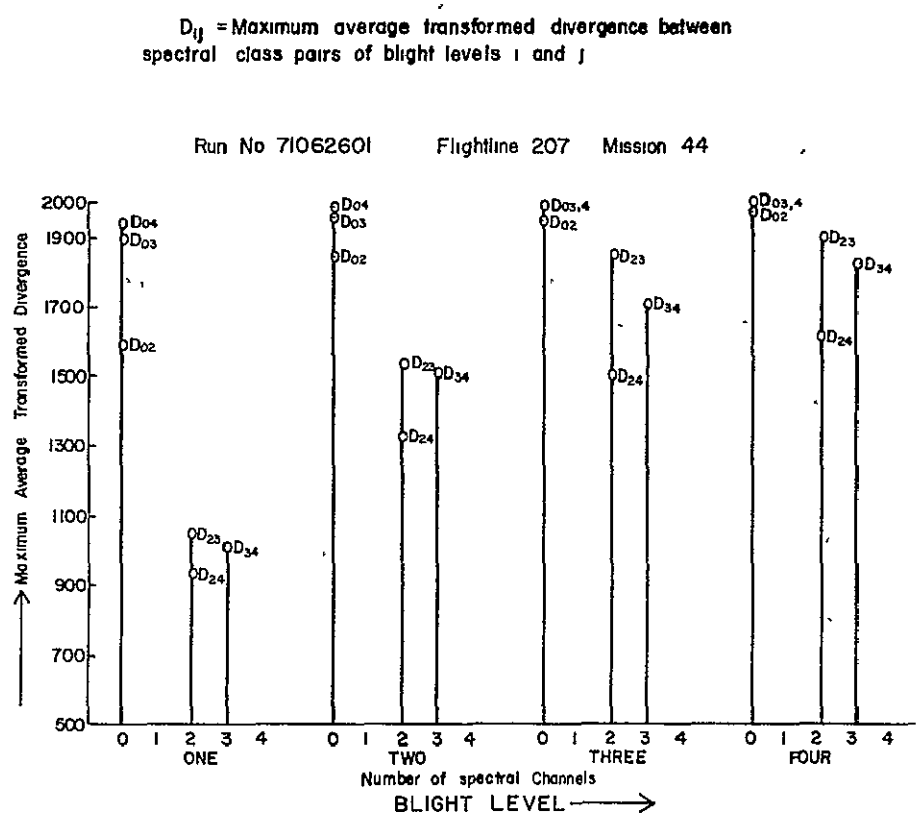

Figure 6.3.7 Statistical Separability Between the Spectral Class Pairs of All Possible Pairs of Blight Levels. Flightline: 207 Mission: 44M

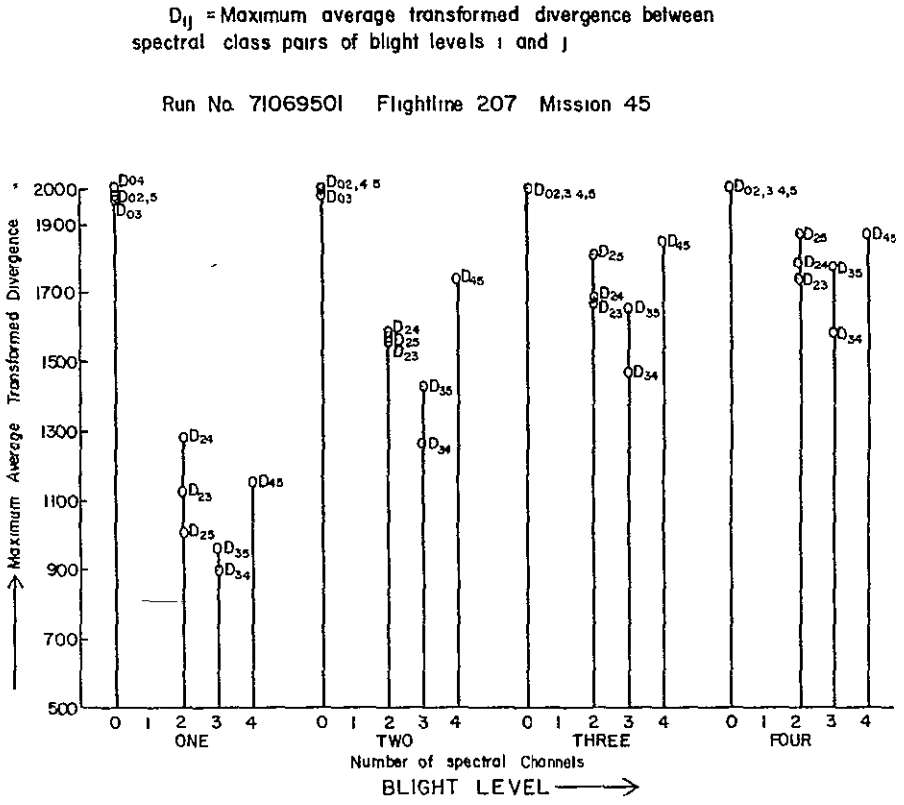

Figure 6.3.8 Statistical Separability Between the Spectral Class Pairs of All Possible Pairs of Blight Levels. Flightline: 207 Mission: 45M

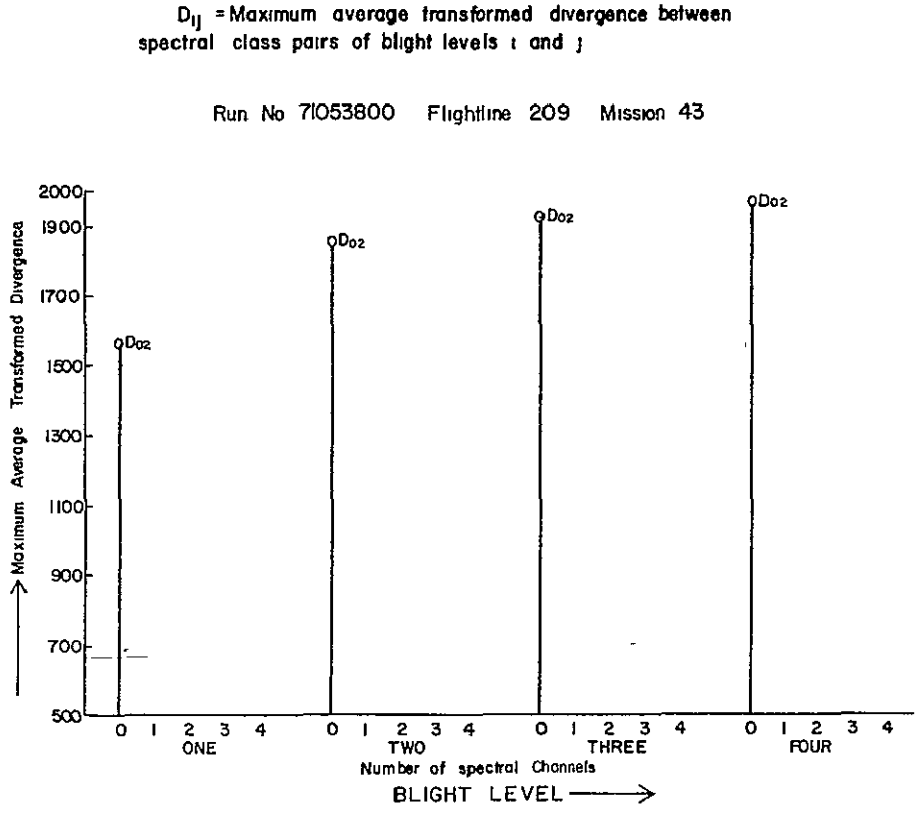

Figure 6.3.9 Statistical Separability Between the Spectral Class Pairs of All Possible Pairs of Blight Levels. Flightline: 209 Mission: 43M

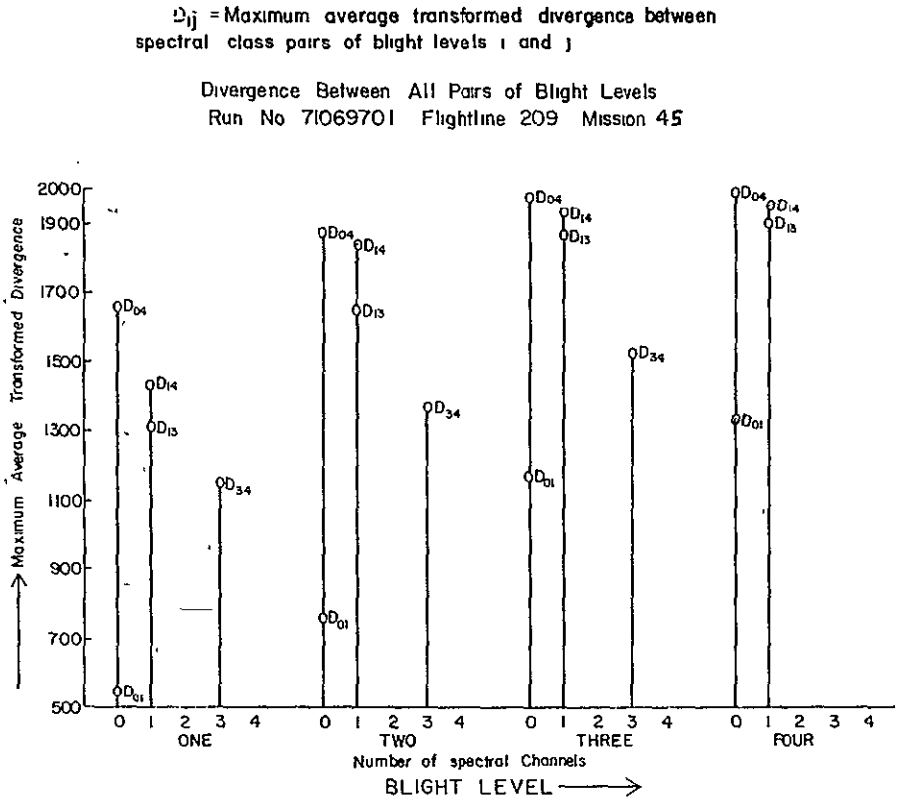

Figure 6.3.10 Statistical Separability Between the Spectral Class Pairs of All Possible Pairs of Blight Levels. Flightline 209 Mission: 45M

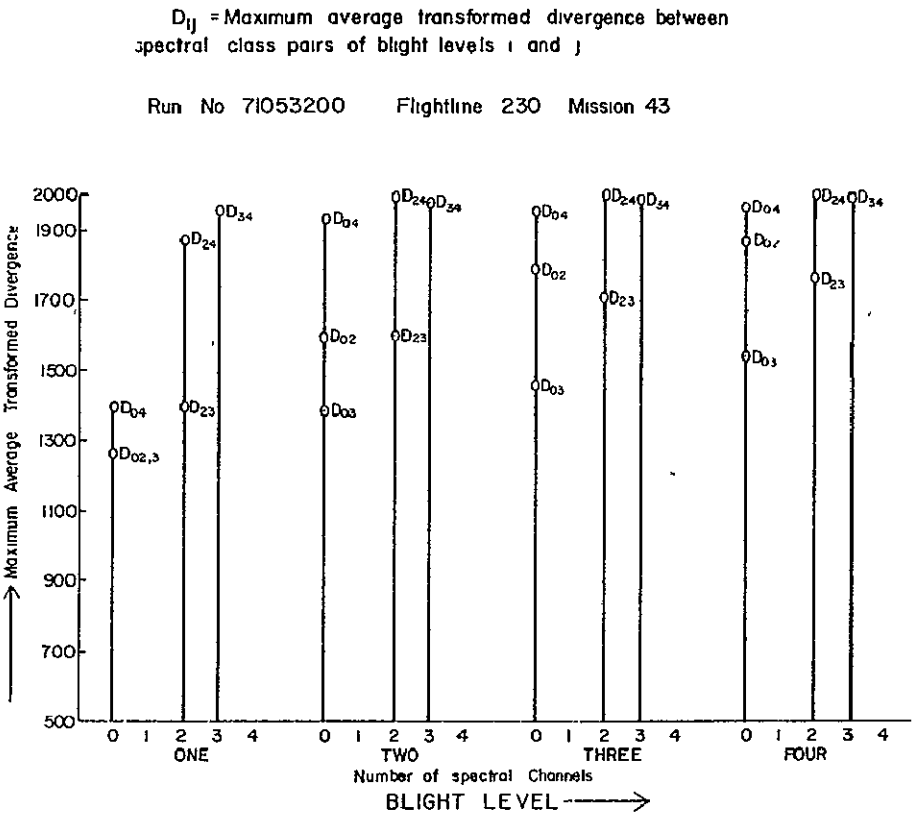

Figure 6.3.11 Statistical Separability Between the Spectral Class Pairs of All Possible Pairs of Blight Levels. Flightline: 230 Mission 43M

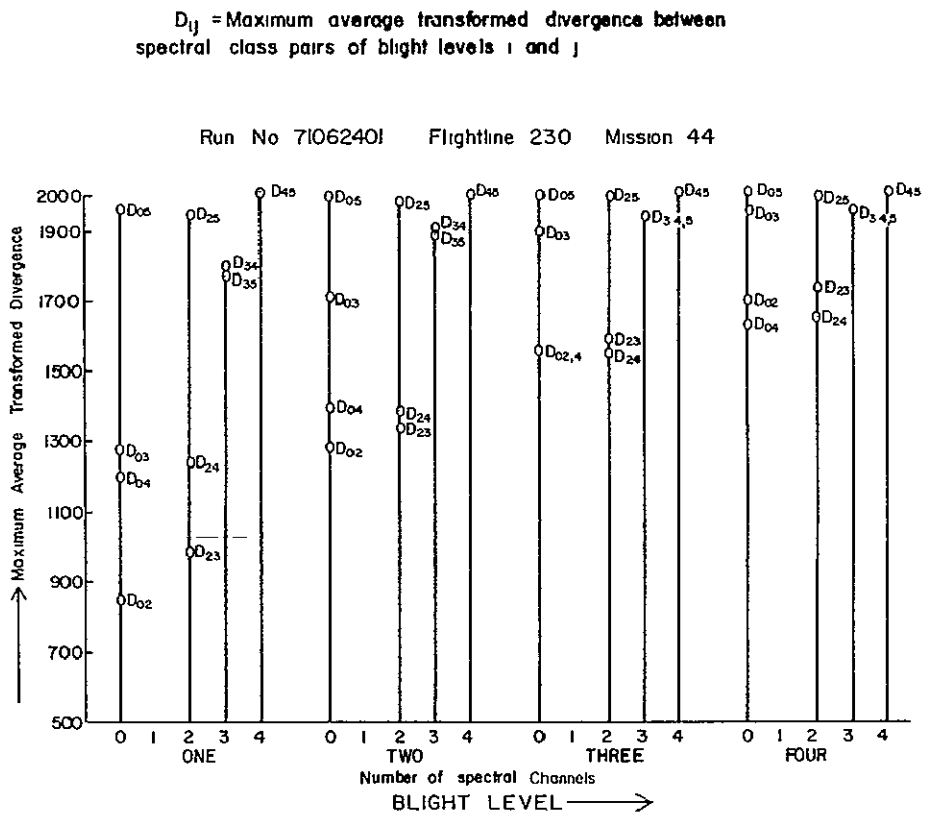

Figure 6.3.12 Statistical Separability Between the Spectral Class Pairs of All Possible Pairs of Blight Levels. Flightline: 230 Mission 44M

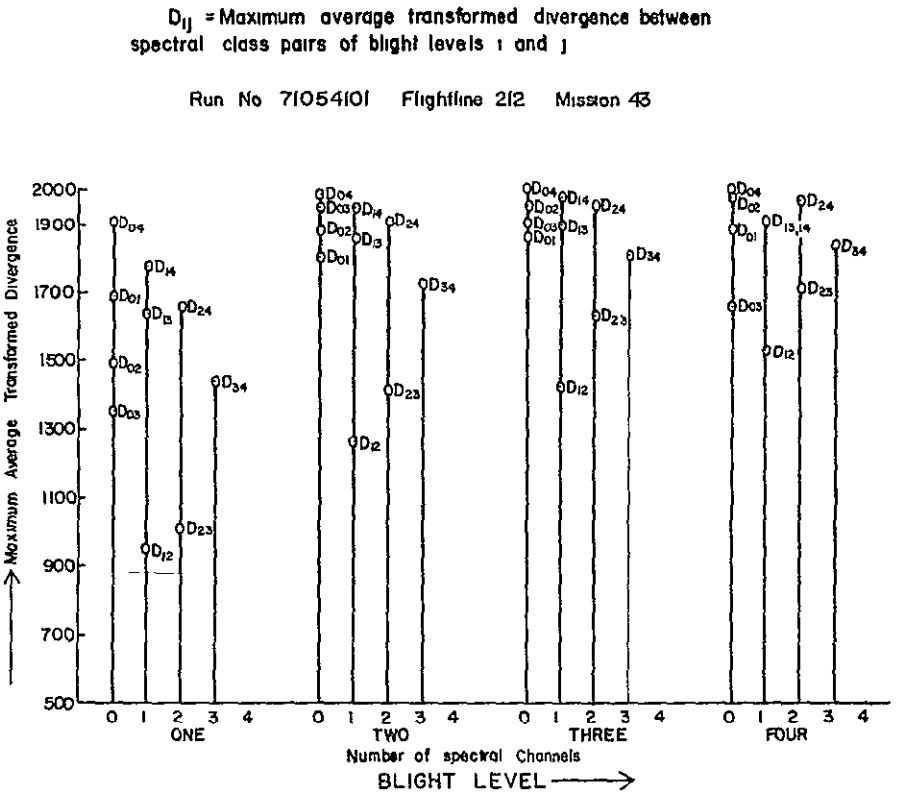

Figure 6.3.13 Statistical Separability Between the Spectral Class Pairs of All Possible Pairs of Blight Levels. Flightline: 212 Mission: 43M

(D) Conclusions

The conclusions based on the analysis of limited amount of data of ten flightlines are:

The greater the difference between blight levels, the more statistically separable they usually are. This result is encouraging considering the fact that there are other variables within and between the flightlines--soil variables, plant variables (percent ground cover is likely to be very important) and environmental variables -- which can cause significant differences in reflection and emission from the plant canopy (whereas blight levels 1 and 2 cause brown lesions on the lower leaves which is likely to cause only relatively subtle changes in the reflection and emission from the healthy plant canopy). In addition, a number of human decisions and errors are involved in this analysis. For example, errors in rating the blight level in ground observations, scanner errors (geometric distortion, detector and system noise, calibration uncertainty, etc.). The analysis presented here has much practical application for it gives the maximum average transformed divergence between the spectral class pairs of blight levels, from which hopefully in the near future, classification accuracy will be reasonably predicted.

The statistical separability of spectral classes of blighted corn has been presented here in much detail, data quantity (168 fields having 18804 sample points) and depth. Although the analysis was done for corn blight only, the conclusions obtained from this analysis may well be applicable to other crop stresses, because corn blight is representative of the problems of many plant stresses, especially non-systemic stresses.

6.4 Statistical Separability of Spectral Classes of Blighted Corn in Each Spectral Channel

The average transformed divergence (averaged over all possible pairs of all spectral classes), D^n_{TAVG}, was found in each of the twelve spectral channels given in Sec. 6.2 for each of ten flightlines given in Appendix A (see Sec 6.2). Bartlett's[76] test was used to test for the homogeneity of the variances of the values of the average transformed divergence for ten flightlines in the twelve spectral channels. No evidence was found to reject the hypothesis of homogeneous variances for α level of 0.05, and hence, the means fo the average transformed divergence in the spectral channels could be compared on the same basis. The average of D^n_{TAVG}, averaged over ten flightlines is shown in Figure 6.4.1. Figure 6.4.1 shows that D^n_{TAVG} is highest in spectral channel of wavelength range 1.00 to 1.40 μm. Since the average transformed divergence between the spectral class pairs is the measure of average separability between them. this trend shows that the spectral classes of corn (healthy and blighted) are most separable in the wavelength range 1.00 to 1.40 μm. This may be because the percentage of the soil visible from the sensor is a predominent factor causing the difference in the spectral response of the healthy and blighted plants and there is much contrast between the reflectance of the soil and the corn plant leaves in the wavelength range 1.00 to 1.40 μm (the reflectance of the leaves is much higher than the soil).

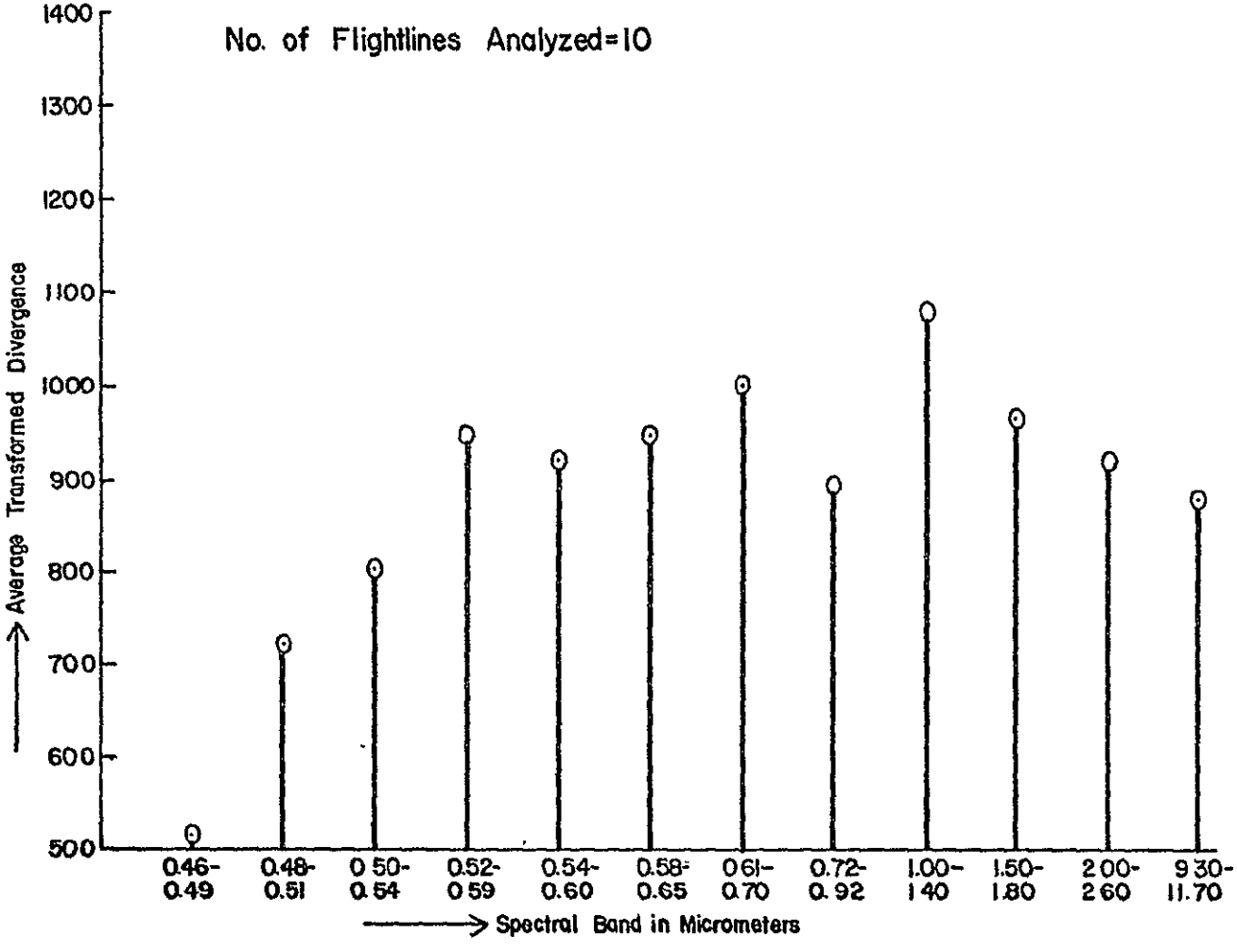

Figure 6.4.1 Statistical Separability Between the Spectral Class Pairs of Blighted Corn in Each Spectral Channel

CHAPTER VII
RECOMMENDATIONS AND CONCLUDING REMARKS

The spectral emittance of a wide variety of leaves and soils should be measured in the natural environment in which the plants grow. There may be more differences in the spectral emittance of the natural targets -- leaves, soils etc. in the wavelength region 2.8 to 5.6 μm (Indium Antimonide Channel of Exotech Model 20C Spectroradiometer, see Section 5.1) than in the wavelength region 7 to 14 μm (Mercury Cadmium Telluride Channel) (Section 2.6). For measuring reflectance of the target, one should use a source of radiation whose output beam is chopped so that the surrounding radiation has no effect on the measured reflectance. Knowing the spectral reflectance, spectral emittance can be determined using Kirchhoff's Law (Section 2.2).

Field temperature measurements should be taken in the most expedient way possible because temperature of the leaves, soil, air etc. (especially leaves) changes quite rapidly depending on the environmental conditions. To determine the effect of air temperature on the temperature of the natural target of interest (leaves, soil etc, under field conditions), one should record the temperature of the target and the air w.r.t. time consecutively. For proper interpretation of the long wavelength spectroradiometric data, it will be helpful to record, in addition to the other variables of ground truth given in Section 5.4, the percentage of sunlit soil (visible from the spectroradiometer), percentage of shaded soil, percentage of sunlit leaves and percentage of shaded leaves.

Further experiments need to be conducted to confirm the preliminary conclusions of Sections 5.6 to 5.9, obtained from the experiments conducted with the long wavelength spectroradiometer. These experiments should be conducted in a variety of environmental conditions (for example: when sky is relatively clear, when sky is overcast with clouds, at night etc.).

In conclusion, it should be said that the spectroradiometric data on the targets on which multispectral scanner data (aircraft and/or satellite) is collected, will prove to be helpful in interpreting the multispectral scanner data properly. In addition, it will help explain causes of spectral variability within and between the targets of interest.

LIST OF REFERENCES

1. Allen, W. A., Gausman, H. W., Richardson, A. J., and Thomas, J. R., "Interaction of Isotropic Light with a Compact Plant Leaf," J. Opt. Soc. Am., 59, pp. 1376-1379, 1969.

2. Anderson, M. C. and Denmead, O. T., "Short Wave Radiation on Inclined Surfaces in Model Plant Communities," Agronomy Journal, 61, pp. 867-872, 1969.

3. Ansari, A. Q. and Loomis, W. E., "Leaf Temperatures," American Journal of Botany, 46, pp. 713-717, 1959.

4. Askenasy, E. "Ueber Die Temperature Welche Pflanzen im Sonnenlicht Annehmen," Bot. Zeit., 33, pp. 441-444, 1875.

5. Aston, A. R., Millington, R. J. and Peters, D. B., "Radiation Exchange in Controlling Leaf Temperature." Agronomy Journal, 61, pp. 797-800, 1969.

6. Barnes Engineering Company," Instruction Manual for Model PRT-5 Precision Radiation Thermometer," Stamford, Connecticut, Jan. 1967 (Rev. April 1968).

7. Barnes, R. B., "Thermography of the Human Body," Science, 140, pp. 870-877, 1963.

8. Bartholic, J. F., Namken, L. N., and Wiegand, C. L., "Aerial Thermal Scanner to Determine Temperatures of Soils and of Crop Canopies Differing in Water Stress", Agronomy Journal, 64, pp. 603-608, 1972.

9. Bauer, M. E., and Cipra, J. E., Personal Communication, Laboratory for Applications of Remote Sensing, W. Lafayette, Indiana.

10. Beckman's Instruments, Inc. Calibrated Polystyrene Film and/or Perkin-Elmer, Inc. (Instruments Division) Calibrated Polystyrene Film.

11. Birth, G. S., "Spectrophotometry of Biological Materials," Ph.D. Thesis, Purdue University Library, W. Lafayette, Indiana, June 1971.

12. Breece, H. T., III, and Holmes, R. A., "Bi-Directional Scattering Characteristics of Healthy Green Soybean and Corn Leaves in Vivo," Applied Optics, 10, pp. 119-127, 1971.

13. Buettner, K. J. K., Kern, Capt. C. D., and Cronin, J. F., "The Consequences of Terrestrial Surface Infrared Emissivity," Proceedings of the Third Symposium on Remote Sensing of Environment, University of Michigan, Ann Arbor, pp. 549-561, 1964.

14. Buettner, K. J. K., and Kern, C. D., "The Determination of Infrared Emissivities of Terrestrial Surfaces," J. Geophys. Res., 70, pp. 1329-1337, 1965.

15. Carlson, R. E., "Remote Detection of Moisture Stress: Field and Laboratory Experiments," An Abstract of Ph.D. Thesis, Iowa State University, Ames, Iowa, 1971.

16. Chapman, H. D., "Diagnostic Criteria for Plants and Soils," University of California, Division of Agricultural Sciences, p. 793, [ed.] 1966.

17. Charney, E. and Brackett, F. S., "Spectral Dependence of Scattering from a Spherical Alga and its Implications for the State of Organization of the Light-accepting Pigments," Arch. Biochem. Biophys., 92, pp. 1-12, 1961.

18. Clum, H. H., "The Effect of Transpiration and Environment Factors on Leaf Temperatures," American Journal of Botany, 13, pp. 194-230, 1926.

19. Conaway, J. and Van Bavel, C. H. M.,"Remote Measurement of Surface Temperature and its Applications to Energy Balance and Evaporation Studies of Bare Soil Surfaces," Technical Report Ecom. 2-67P-1, U.S.D.A., Phoenix, Arizona, 130p., Dec. 1966.

20. Conaway, J., and Van Bavel, C. H. M., "Evaporation from a Wet Soil Surface Calculated from Radiometrically Determined Surface Temperatures," J. Appl. Meteor., 6, pp. 650-655, 1967.

21. Cook, G. D., "Environmental Effects on Plant Leaf Temperature," M. S. Thesis, Purdue University, W. Lafayette, Indiana, 1963.

22. Cook, G. D., and Dixon, J. R., "Transpiration: Its Effects on Plant Leaf Temperature," Science, 144, pp. 546-547, 1964.

23. Cox, L. M., and Boersma, L., "Transpiration as a Function of Soil Temperature and Soil Water Stress," Plant Physiology, pp. 550-556, 1967.

24. Curtis, O. F., "Leaf Temperatures and the Cooling of Leaves by Radiation," Plant Physiology, 11, pp. 343-364, 1936.

25. Curtis, O. F., "Wallace and Clum, 'Leaf Temperatures': A Critical Analysis with Additional Data," American Journal of Botany, 25, pp. 761-771, 1938.

26. Duncan, W. G., Loomis, R. S., Williams, W. A., and Hanau, R., "A Model for Simulating Photosynthesis in Plant Communities," Hilgardia, 38(4), pp. 181-205, 1967.

27. Exotech Incorporated, "Technical Description of the Model 20 Extended Wavelength Spectrometer," Rockville, Maryland, August 1968.

28. Falckenberg, G., "Die Absorptionskonstanten Einiger Meteorologisch Wichtiger Korper Fur Infrarote Wellen," Met. Z., 45, pp. 334-337, 1928.

29. Fuchs, M., and Tanner, C. B., "Infrared Thermometry of Vegetation," Agronomy Journal, 58, pp. 597-601, 1966.

30. Fuchs, M., and Tanner, C. B., "Surface Temperature Measurements of Bare Soils," Journal of Applied Meteorology, 7, pp. 303-305, April 1968.

31. Gates, D. M., "The Energy Environment in Which We Live," American Scientist, 51, pp. 327-348, 1963.

32. Gates, D. M. "Leaf Temperature and Energy Exchange," Arch. Met. Geophys. Biokl., B12, p. 321, 1963.

33. Gates, D. M., "Leaf Temperature and Transpiration," Agronomy Journal, 56, pp. 273-277, 1964.

34. Gates, D. M., "Characteristics of Soil and Vegetated Surfaces to Reflected and Emitted Radiation," Proceedings of the Third Symposium on Remote Sensing of Environment, University of Michigan, Ann Arbor, pp. 573-600, 1964.

35. Gates, D. M., "Heat Transfer in Plants," Scientific American, 213, pp. 76-84, Dec. 1965.

36. Gates, D. M., "Sensing Biological Environments with a Portable Radiation Thermometer," Applied Optics, 7 (9), pp. 1803-1809, 1968.

37. Gates, D. M., "Energy Exchange and Ecology," Bioscience, p. 90, 1968.

38. Gates, D. M., "Remote Sensing with Special Reference to Agriculture and Forestry," National Academy of Sciences, Washington D. C., pp. 248-250, 1970.

39. Gates, D. M., Keegan, H. J., Schleter, J. C., and Weidner, V. R., "Spectral Properties of Plants," Applied Optics, 4, pp. 11-20, 1965.

40. Gates, D. M. and Tantraporn, W., "The Reflectivity of Deciduous Trees and Herbaceous Plants in the Infrared to 25 Microns," Science, 115, pp. 613-616, 1952.

41. Gausman, H. W., Allen, W. A., and Cardenas, R., "Reflectance of Cotton Leaves and Their Structure," Remote Sensing of Environment, 1, pp. 19-22, 1969.

42. Gausman, H. W., Allen, W. A., Cardenas, R., and Richardson, A. J., "Relation of Light Reflectance to Cotton Leaf Maturity," Proceedings of 6th Symposium on the Remote Sensing of Environment, pp. 1123-1141, University of Michigan Press, Ann Arbor, Michigan, 1969.

43. Gubareff, G. G., Janssen, J. E., and Torborg, R. H., "Thermal Radiation Properties Survey: A Review of the Literature", Honeywell Research Center, Minneapolis-Honeywell Regulator Company, Minneapolis, Minnesota, 1960.

44. Hagner, M., "Thermal Mapping of Conifer Seedlings - a Useful Method in Pathological and Physiological Research," Z. Pflanzenphysiol. Bd., 61. S., pp. 322-331, 1969.

45. Hoffer, R. M., "The Importance of 'Ground Truth' Data in Remote Sensing," Presented at the United Nations Panel Meeting on the Establishment and Implementation of Research Programs in Remote Sensing, National Institute for Space Research, São José dos Campos, S.P, Brazil, Nov. 29-Dec. 10, 1971 (LARS Print 120371, Purdue University, Indiana.)

46. Hovis, W. A., Jr., "Infrared Spectral Reflectance of Some Common Minerals," Applied Optics, 5, pp. 245-248, 1966.

47. Hovis, W. A., Jr., "Optimum Wavelength Intervals for Surface Temperature Radiometry," Applied Optics, 5, pp. 815-818, 1966.

48. Idso, S. B. and Jackson, R. D., "The Significance of Fluctuations in Sky Radiant Emittance for Infrared Thermometry," Agronomy Journal, 60, pp. 388-392, 1968.

49. Idso, S. B., Jackson, R. D., Ehrler, W. L., and Mitchell, S. T., "A Method for Determination of Infrared Emittance of Leaves," Ecology, 50(5), pp. 899-902, 1969.

50. International Commission on Illumination (CIE), "International Lighting Vocabulary", Publication CIE No. 17(E-1.1), 360p., 1970.

51. IGY Instruction Manual, Part VI, " Radiation Instruments and Measurements," Pergamon Press, New York, p. 436, 1958.

52. Irvine, W. M. and Pollack, J. B., "Infrared Optical Properties of Water and Ice Spheres," Icarus, 8, pp. 324-360, 1968.

53. Jackson, R. D., and Idso, S. B., "Ambient Temperature Effects in Infrared Thermometry," Agronomy Journal, 61, pp. 324-325, 1969.

54. Jensen, W. A., "Botanical Histochemistry--Principles and Practices," W. H. Freeman and Co., San Francisco, 1962.

55. Johannsen, C. J. "The Detection of Available Soil Moisture by Remote Sensing Techniques," Ph.D. Thesis, Purdue University, W. Lafayette, Indiana, 1969.

56. Knipling, E. B., "Physical and Physiological Basis for the Reflectance of Visible and Near-Infrared Radiation from Vegetation," Proceedings of the Symposium on Information Processing, Purdue University, W. Lafayette, Indiana, pp. 732-741, 1969.

57. Knoerr, K. R., and Gay, L. W., "Tree Energy Balance," Ecology, 46, pp. 17-24, 1965.

58. Kondrat'yev, K. Y., "Radiative Heat Exchange in the Atmosphere," Pergamon Press Ltd., London, 1965.

59. Kruse, P. W., McGlauchlin, L. D., and McQuistan, R. B., "Elements of Infrared Technology", John Wiley and Sons, New York, 1962.

60. Kryuchkov, V. V., "Leaf Temperature of Some Plants in the Khiban", Soviet P. Physiol., 8, pp. 502-504, 1961.

61. Kumar, R., "Radiation from Plants- Reflection and Emission: A Review", AA&ES72-2, Purdue University Library, W. Lafayette, Indiana, 88p., Feb. 1972.

62. Laboratory for Applications of Remote Sensing, "Remote Multispectral Sensing in Agriculture," Annual Report, Vol. 3, Purdue University, W. Lafayette, Indiana, 1968.

63. Laboratory for Applications of Remote Sensing, "Remote Multispectral Sensing in Agriculture," Annual Report, Vol. 3, Purdue University, W. Lafayette, Indiana, 1970.

64. Lenschow, D. H., and Dutton, J. A., "Surface Temperature Variations Measured from an Airplane over Several Surface Types," Journal of Applied Meteorology, 3, pp. 65-69, 1964.

65. Loomis, W. E., "Absorption of Radiant Energy by Leaves," Ecology, 46, pp. 14-24, 1965.

66. Lorenz, D., "The Effect of the Long-wave Reflectivity of Natural Surfaces on Surface Temperature Measurements Using Radiometers," Journal of Applied Meteorology, 5, pp. 421-430, 1966.

67. MacDonald, R. B., Bauer, M. E., Allen, R. D., Clifton, J. W., Erickson, J. D., and Landgrebe, D. A., "Results of the 1971 Corn Blight Watch Experiment," Eighth International Symposium on Remote Sensing of Environment, Ann Arbor, Michigan, pp. 157-190, Oct. 2-6, 1972.

68. Marill, T., and Green, D. M., "On the Effectiveness of Receptors in Recognition Systems," I.E.E.E. Trans. on Information Theory, vol. IT-9, pp. 11-17, Jan. 1963.

69. Miller, C. D., "An Airborne Spectral Radiometer," in Proceedings of the Second Symposium on Remote Sensing of Environment, pp. 359-373, University of Michigan, Ann Arbor, 1963.

70. Monteith, J. L., and Szeicz, G., "Radiative Temperature in the Heat Balance of Natural Surfaces," Quart. J. Roy. Met. Soc., 88, pp. 496-507, 1962.

71. Myers, V. I., and Allen, W. A., "Electrooptical Remote Sensing Methods as Nondestructive Testing and Measuring Techniques in Agriculture," Applied Optics, 7, pp. 1819-1838, 1968.

72. Myers, V. I., Carter, D. L., and Rippert, W. J., J. Irrigat. Drain. Div. Amer. Soc. Civil Eng., 92, p. 59, 1966.

73. Myers, V. I., Weigand, C. L., Heilman, M. D., and Thomas, J. R., "Remote Sensing in Soil and Water Conservation Research," Proceedings of the Fourth Symposium on Remote Sensing of Environment, University of Michigan Press, Ann Arbor, pp. 801-813, 1966.

74. Nutter, G. D., "Radiation Thermometry Part 1 - Recent Trends," Mechanical Engineering, pp. 16-23, July 1972.

75. Oppenheim, A. K., "Radiation Analysis by the Network Method," Trans. ASME, 78, pp. 725-735, 1956.

76. Ostle, B., "Statistics in Research," The Iowa State University Press, 1969.

77. Plyer, E. K., Blaine, L. R., and Nowak, Matthew, "Reference Wavelengths for Calibrating Prism Spectrometers," Journal of Research of the National Bureau of Standards, Vol. 58, No. 4, pp. 195-200, 1957.

78. Plyer, Earle K. and Peters, C. Wilbur, "Wavelengths for Calibration of Prism Spectrometers," Journal of Research of the National Bureau of Standards, Vol. 45(6), pp. 462-467, Dec. 1950.

79. Read, D. W. L., and Ashford, R., "Effect of Varying Levels of Soil and Fertilizer Phosphorous and Soil Temperature on the Growth and Nutrient Content of Bromegrass and Reed Canarygrass," Agronomy Journal, 60, pp. 680-682, 1968.

80. Renck, L. E., "Light Scatter in Biological Materials," M.S. Thesis, Purdue University Library, W. Lafayette, Indiana, 109p., 1972.

81. Robinson, B. F., and Silva, L. F., "Portable Precision Thermistor Thermometer," LARS Information Note 072470 (Revised), Laboratory for Applications of Remote Sensing, Purdue University, W. Lafayette, Indiana, 1970.

82. Robinson, B., Silva, L., Haselby, R., Kumar, R., Simmons, W., Bauer, M., and Cipra, J., "The LARS Extended Wavelength Spectroradiometer," LARS Information Note 040173, Laboratory for Applications of Remote Sensing, Purdue University, W. Lafayette, Indiana (In Preparation).

83. Silva, L., Hoffer, R., and Cipra, J., "Extended Wavelength Field Spectroradiometry," 7th Symposium on Remote Sensing of Environment, The University of Michigan, Ann Arbor, Michigan, May 1971.

84. Silva, L. F., and Staff, "Measurements Programs in Remote Sensing at Purdue University", LARS Information Note 012872, Laboratory for Applications of Remote Sensing, Purdue University, W. Lafayette, Indiana, 1972.

85. Sinclair, T. R., "Pathway of Solar Radiation Through Leaves," M.S. Thesis, Purdue University Library, W. Lafayette, Indiana, 1968.

86. Sinclair, T. R., Schreiber, M. M., and Hoffer, R. M., "A Diffuse Reflectance Hypothesis for the Patway of Solar Radiation Through Leaves," Agronomy Journal, 65, pp. 276-283, 1973.

87. Sparrow, E. M., and Cess, R. D., "Radiation Heat Transfer," Brooks/Cole Publishing Co., Belmont, California, 1966.

88. Sparrow, E. M., and Jonsson, V. K., "Radiant Emission Characteristics of Diffuse Conical Cavities," J. Opt. Soc. Am., 53, pp. 816-821, 1963.

89. Steel, R. G. D., and Torrie, J. H., "Principles and Procedures of Statistics with Special Reference to the Biological Sciences," McGraw-Hill Book Company, Inc., New York, 1960.

90. Suits, Gwynn H., "The Calculation of the Directional Reflectance of a Vegetative Canopy," Remote Sensing of Environment, 2, pp. 117-125, 1972.

91. Swain, P. H., "Pattern Recognition: A Basis for Remote Sensing Data Analysis," LARS Information Note 111572, Laboratory for Applications of Remote Sensing, Purdue University, W. Lafayette, Indiana, pp. 1-40, 1972.

92. Tanner, C. B., "Plant Temperatures," Agronomy Journal, 55, pp. 210-211, 1963.

93. Tisdale, S. L., and Nelson, W. L., "Soil Fertility and Fertilizers," The Macmillan Company, Collier-Macmillan Limited, London, 1966 (Second Edition).

94. Touloukian, Y. S., DeWitt, D. P., and Hernicz, R. S., "Thermal Radiative Properties - Coatings," Thermal Physical Properties of Matter, Vol. 9, Thermophysical Properties Research Centre, Purdue University, W. Lafayette, Indiana, 1972.

95. Turrell, F. M., and Austin, S. W., "Comparative Nocturnal Thermal Budgets of Large and Small Trees," Ecology, 46, pp. 25-34, 1965.

96. Ullstrup, A. J., "Corn Diseases in the United States and Their Control," U.S. Department of Agriculture Handbook No. 199, 1961.

97. U.S. Air Force, "Handbook of Geophysics and Space Environment," Edited by Shea L. Valley, Cambridge Research Laboratory, Washington, 1965.

98. U.S. Department of Navy, "Handbook of Military Infrared Technology," Edited by William L. Wolfe, Office of Naval Research, University of Michigan, Washington, D.C., 1965.

99. Viskanta, R., "Class Notes for Advanced Radiation Heat Transfer," Purdue University, W. Lafayette, Indiana, 1967.

100. Waggoner, P. E., and Shaw, R. H., "Temperature of Potato and Tomato Leaves," Plant Physiology, 27, pp. 710-724, 1951.

101. Wark, D. Q., Yamamoto, G., and Lienesch, J. H., "Method of Estimating Infrared Flux and Surface Temperature from Meteorological Satellites," J. Atmospheric Sci., 19, pp. 369-384, 1962.

102. Wear, J. F., "Remote Sensing Applications in Forestry, the Development of Spectro-Signature Indicators of Root Disease on Large Forest Areas," Pac. N.W. For. Range Exp. Sta., U.S. Dept. Agr., Ann. Prog. Rep., Sept., 1966.

103. Wear, J. F., Pope, R. B., and Orr, P. W., "Aerial Photographic Techniques for Estimating Damage by Insects in Western Forests," Pac. N.W. For. Range Exp. Sta., U.S. Dept. Agr., 1966.

104. Wendlandt, W. W., and Hecht, H. G., "Reflectance Spectroscopy," Interscience Publishers, New York, Chapter 2, 1966.

105. Wiegand, C. L., and Namken, L. N., "Influences of Plant Moisture Stress, Solar Radiation, and Air Temperature on Cotton Leaf Temperature, Agronomy Journal, 58, pp. 582-586, 1966.

106. Williamson, R. E., and Splinter, W. E., "Effects of Light Intensity, Temperature, and Root Gaseous Environment on Growth of Nicotiana Tabacum L.," Agronomy Journal, 61, pp. 285-288, 1969.

107. Willstätter, R., and Stoll, A., "Untersuchungen Uber Die Assimilation Der Kohlensäure," Springer, Berlin, 1918.

108. Wolpert, A., "Heat Transfer Analysis of Factors Affecting Plant Leaf Temperature," Plant Physiology, 37, pp. 113-120, 1962.

109. Woolley, J. T., "Reflectance and Transmittance of Light by Leaves," Plant Physiology, 47, pp. 656-662, 1971.

APPENDIX A

Flightlines Selected for Analyzing Multispectral Scanner Data of 1971 Corn Blight Watch Experiment

Flightline	Mission No.	Run No.
206	43M	71053500
206	45M	71070001
207	43M	71053600
207	44M	71062601
207	45M	71069501
209	43M	71053800
209	45M	71069701
230	43M	71053200
230	44M	71062401
212	43M	71054101

APPENDIX B

Ground Truth Variables Recorded with the Experiments with Short Wavelength Spectroradiometer

An example of the ground truth variables recorded with the experiments under field conditions with the short wavelength head of the Exotech Model 20C spectroradiometer is given on the following page. These variables were recorded by Dr. M. Bauer and Dr. J. Cipra of Laboratory of Applications of Remote Sensing, Purdue University. * denotes that the variables were not recorded in that particular experiment. Although these ground truth variables were recorded with experiments with short wavelength unit, these can also be used to interpret the data of longwavelength unit if needed.

RUN SEQUENCER	251	RUN NUMBER	72013600
EXPERIMENT NUMBER	7210020	OBSERVATION NUMBER	72916
DATE DATA COLLECTED (YYMMDD)	720729	DATE DATA COLLECTED	7/29/72
TIME DATA COLLECTED	2029	EXPERIMENT NAME	GROUND COVER
PRINCIPAL INVESTIGATOR	LAUER,MARVIN	SCENE TYPE	
LOCATION	AGRONOMY FARM	AIR TEMPERATURE	26.6
BAROMETRIC PRESSURE		RELATIVE HUMIDITY	
CLOUD COVER		WIND SPEED	
VISIBILITY		CLOUD TYPE AND ALTITUDE	
WIND DIRECTION		REFORMATTING DATE	5/31/73
REFORMATTING CALIBRATION CODE	3	SIDE ANGLE	00
SWING ANGLE	00	FORWARD DIRECTION	225
DISTANCE TO GROUND	30.00	FOCAL DISTANCE	
FIELD OF VIEW	15.00	LOCATION LATITUDE	0402813N
LOCATION LONGITUDE	0965927W	FLIGHT LINE	
PHOTOGRAPH SERIAL NO.		NUMBER OF SAMPLE GROUPS	3
TREATMENT CODE 1	1	TREATMENT CODE 2	3
TREATMENT CODE 3		TREATMENT CODE 4	
TREATMENT CODE 5		TREATMENT CODE 6	
FIELD NUMBER	15	REPLICATION NUMBER	2
PLOT NUMBER	6	SPECIES	CORN
VARIETY	PIO 3369 A	MATURITY	PRE-BLISTER
HEIGHT	2.08	ROW WIDTH	0.76
PLANT COUNT 22 THOUSANDTHS OF ROW		PERCENT GROUND COVER	30
LEAVES PER PLANT	12	LEAF AREA INDEX	2.14
MOISTURE STRESS		NUTRIENT DEFICIENCY	
WEEDY		DISEASE INFECTION	
INSECT INFECTION		HAIL OR WIND DAMAGE	
LODGING DAMAGE		LATEST ID UPDATE DATE	5/31/73
SERIES NAME	RUSSELL	PERCENT SAND CONTENT	
PERCENT SILT CONTENT		PERCENT CLAY CONTENT	
TEXTURE	SILT LOAM	MUNSELL COLOR	10.0YR /
MOISTURE (FIELD) CONTENT		MOISTURE (LABORATORY) CONTENT	
SURFACE CONDITION	SMOOTH	DRAINAGE CLASS	
HORIZON	A	NUMBER OF PHOTOGRAPHS	
PHOTOGRAPH FILM TYPE	A	TARGET TEMPERATURE	
TARGET LENGTH		TARGET WIDTH	
INSTRUMENT NAME	EXOTECH MOD 20C	SCAN RATE	0.25
CALIBRATION RUN NUMBER		IRRADIANCE CALIBRATION RUN	72032100
HIGH SQUARE WAVE LEVEL	5.005	LOW SQUARE WAVE LEVEL	0.001

PARALLEL CANOPY-SOIL

DETECTOR NAME	DETECTOR RANGE	DETECTOR EQUILIZATION	NUMBER OF SAMPLES	WAVE BAND COEFFICIENTS A	B	C	D	SAMPLE GROUP
SI	3.300	0.25	465	0.374	0.001	0.0	0.0	1
PB S	1.000	0.25	450	0.747	0.001	0.0	0.0	2
PB S	1.000	0.25	443	1.289	0.003	0.0	0.0	3